Functional and Mechanistic Analysis of Protein Degradation by Human Cytomegalovirus to Uncover Viral Immune Evasion Mechanisms

Alice Fletcher-Etherington

Department of Medicine
Cambridge Institute for Medical Research

Newnham College
University of Cambridge

This thesis is submitted for the degree of
Doctor of Philosophy

September 2021

Declaration

I hereby declare that this thesis is the result of my own work and includes nothing that is the outcome of work done in collaboration, except as declared in the acknowledgements and preface to each chapter, and specified in the text. The contents of this thesis are original and have not been submitted in whole or in part for any other degree or qualification at the University of Cambridge, or any other university. This thesis does not exceed the word limit of 70,000 words, excluding figures, tables, appendices and bibliography, as specified by the Clinical Medicine and Clinical Veterinary Medicine Degree Committee.

Alice Fletcher-Etherington

September 2021

Abstract

Alice Fletcher-Etherington

Functional and Mechanistic Analysis of Protein Degradation by Human Cytomegalovirus to Uncover Viral Immune Evasion Mechanisms

Human cytomegalovirus (HCMV) is a ubiquitous herpesvirus that represents a significant global health burden. In immunocompetent individuals, HCMV establishes a lifelong persistent and typically asymptomatic infection that is controlled by a multifaceted host immune response. However, immunocompromised patients, including transplant recipients and those with acquired immunodeficiency syndrome, are at a high risk of HCMV-associated morbidity and mortality. HCMV is also the most prevalent infectious cause of congenital disease, with the ability to cause neurodevelopmental complications.

Cell-intrinsic immune responses are the first line of defence against viruses, mediated by constitutively expressed host proteins and processes that respond directly to virus infection. As a result of virus-host coevolution, viruses often antagonise antiviral host proteins by driving their downregulation, mislocalisation or inactivation. A quantitative proteomic analysis of HCMV infection published by our group found that at least 133 proteins are likely targeted for degradation by HCMV during early infection. For the project presented in this thesis, seven of these candidate antiviral factors were screened for antiviral activity using a novel restriction assay system and plaque assays. Two proteins, mixed lineage kinase domain-like pseudokinase (MLKL) and DmX-like protein 1 (DMXL1), were then selected for further mechanistic and functional characterisation.

MLKL is the terminal effector of a form of cell death called necroptosis. Many herpesviruses suppress necroptotic signalling to evade cell death. However, the mechanism of HCMV-mediated inhibition of necroptosis has so far remained elusive. HCMV protein pUL36 was found to be necessary and sufficient for the downregulation of MLKL and the inhibition of necroptosis. pUL36 has previously been shown to inhibit another mode of cell death, apoptosis, making it a multifunctional cell death inhibitor.

DMXL1 interacts with the vacuolar-type H^+-ATPase to regulate endosomal acidification, with implications for endosomal trafficking, autophagy, immune signalling and many other cellular processes. The viral gene responsible for downregulation of DMXL1 was identified as pUS33A, which may recruit the E3 ligase Kip1 ubiquitination-promoting complex (KPC) to target DMXL1 for proteasomal degradation.

Therapeutics currently available for treating HCMV are associated with significant toxicity and drug resistance. Characterisation of the protein-protein interactions underlying the viral evasion of cell-

intrinsic immune responses may permit the development of small molecule therapeutics that disrupt these interactions and facilitate endogenous inhibition of viral replication. As well as contributing to our understanding of how HCMV regulates cell death and endosomal acidification, this thesis also presents proteomic data that will enable the identification of additional antiviral host proteins and the characterisation of virus protein function.

Acknowledgements

There are a number of individuals that I would like to thank for their guidance and support, without whom this work would not have been possible. First and foremost, my supervisor, Dr. Mike Weekes. Mike has not only provided endless scientific advice and guidance, but has also been instrumental in my career development. I am particularly thankful for the way in which he has always valued my opinions and contributions, encouraged me to develop new skills by presenting at conferences and writing papers, and supported my transition out of academia. I feel lucky and grateful to have spent the last four years under his supervision.

This project would not exist without previous work conducted by others in the Weekes lab, particularly the degradation screens performed by Dr. Katie Nightingale and the HCMV interactome by Dr Luís Nobre. Other experiments performed by members of the lab, notably Katie, Dr. Lior Soday and Dr. Benjamin Ravenhill, are also described to provide context to my work. I am eternally thankful to Katie, who provided help and guidance through the entirety of the project. She is a wonderful teacher and scientist, and I am truly grateful for all the time she spent supervising me. I am also thankful to Luís, Katie, Ben and Dr. Kai-Min Lin, for providing me with some of the plasmids and cell lines used in this work.

Beyond the science, I would like to thank all members of the Weekes lab, both past and present, for all the support and laughs. You have been a complete joy to work with, true friends and the best work colleagues anyone could hope for. Thank you to Katie, who is a tremendous advocate for women in science; Luís, que no pare la fiesta; Dr. Colin Davies, who introduced me to the wonders of a New Zealand Sav; Lior, who is one of the kindest and friendliest souls I have ever met; Kai-Min, for coming out with the most hilarious one-liners when they were needed most; Leah Hunter, who is the biggest ray of sunshine and lifted us all during the pandemic; Ben, who would make a fantastic PI; and Dr. Cassie Zerbe, whose observations on ‘the English’ never fail to provide entertainment. I would like to give a special shout-out to Martin Potts, who started his PhD at the same time as me and has seen me at my best, my worst, and every state in between. Thank you for the endless reassurance, for answering every question I had no matter how stupid, and for being the best leopard-print-wearing partner-in-crime there ever was.

Next, I must thank all those at the Cambridge Institute for Medical Research (CIMR) who have contributed to and facilitated this work. I would particularly like to mention Dr. Robin Antrobus from the CIMR Proteomics Facility, for generating all of the mass spectrometry data detailed in this thesis, Dr. Jack Houghton, for proteomics and bioinformatics support, and Dr. Reiner Schulte and colleagues in the Flow Cytometry Core Facility. I am also grateful to Mark Smallwood and all of the operations

and support staff, who not only keep the CIMR afloat but also contribute substantially to the positive and welcoming environment that makes the CIMR such a wonderful place to work.

I would also like to acknowledge our collaborators, especially Dr. Rich Stanton and colleagues at Cardiff University for generating all of the recombinant viruses used in this work; Dr. Ceri Fielding (Cardiff University) for performing the infections for the plasma membrane block deletion virus screen; Dr. Pete Tomasec for work on the 48 h degradation screen; Professor Andrew Davison and Jenna Nichols at the University of Glasgow for sequencing the viruses; and Professor Steven Gygi at Harvard Medical School for providing access to the MassPike software for proteomics analysis. Too many people to note have provided feedback and advice on this work through lab meetings, conferences and email correspondences – thank you to you all. This research was supported by funding from the Medical Research Council and the Wellcome Trust.

Of course, I also have to thank my nearest and dearest for all the love and support over the last four years and previous. The Wantage crew, for being the best group of friends a girl could have growing up. We don't see each other often, but when we do it's like nothing has changed. I hope it never does. The Newnham girls, especially Lizzie, Nicole and Ankita. As if we're all going to be Dr.s! Thanks for getting me through the rough times and being with me during the best. To all of the people I've been lucky enough to call friends over the last seven years here in Cambridge (you know who you are), thank you. Robin, thank you for always being at the end of the phone, and for telling me to get a grip when it was needed. This thesis is the second best thing to come out of the last four years, you're the first.

Last but never least, to Mum and Dad. Mum, who always tells me that 'every problem can be sorted'. I'm slowly beginning to believe that you're right. Dad, who has read every single this word of this thesis. I never did learn my times tables, but I think this makes up for it. I will never be able to express how grateful I am to both of you for your love, encouragement and support.

Table of Contents

List of Figures

Introduction

Chapter 3

Chapter 4

Chapter 5

Chapter 6

Appendices

List of Tables

Introduction

Materials and Methods

Chapter 3

Chapter 5

Chapter 6

Appendices

Abbreviations

4HB	Four-helix bundle
A	
AcN	Acetonitrile
AGC	Automatic gain control
AIDS	Acquired immunodeficiency syndrome
ANOVA	Analysis of variance
ARF	Antiviral restriction factor
Arg	Arginine
ARHGAP35	Rho GTPase-activating protein 35
ATP	Adenosine triphosphate
ATP6V0C	ATPase H^+-transporting V_0 subunit C
B	
BAX	BCL2-associated X
BSR	Blasticidin resistance
C	
CDKN1B	Cyclin-dependent kinase inhibitor 1B
cDNA	Complementary DNA
CRISPR	Clustered regularly interspaced short palindromic repeats
CST	Cell Signalling Technology
CUL1	Cullin 1
Cys	Cysteine
D	
DAVID	Database for Annotation, Visualization and Integrated Discovery
DAXX	Death domain-associated protein 6
DC	Dendritic cell
DDX	DExD/H-box helicase
DHCR24	24-dehydrocholesterol reductase
DMEM	Dulbecco's Modified Eagle's Medium
DMSO	Dimethyl sulfoxide
DMXL	DmX-like
DNA	Deoxyribonucleic acid
dNTP	Deoxynucleoside triphosphate
DRM	Detergent-resistant membrane
DTT	Dithiothreitol
E	
E. coli	*Escherichia coli*
EBV	Epstein-Barr virus
EDTA	Ethylenediaminetetraacetic acid
ER	Endoplasmic reticulum

F

FA	Formic acid
FBS	Fetal bovine serum
FBXO3	F-box protein 3
FC	Fold change
FRMD6	FERM domain-containing protein 6

G

GAPDH	Glyceraldehyde 3-phosphate dehydrogenase
GFP	Green fluorescent protein
GGGS	Glycine-glycine-glycine-serine
gRNA	Guide RNA

H

HA	Hemagglutinin
HCD	Higher-energy collision dissociation
HCMV	Human cytomegalovirus
HECT	Homologous to E6AP C-terminus
HEK293	Human embryonic kidney 293 cells
HEK293T	HEK293 cells immortalised with SV40 large T antigen
HERC5	HECT domain and RCC1-like domain-containing protein 5
HFFF	Human fetal foreskin fibroblast
HFFF-TERT	Human fetal foreskin fibroblast cells immortalised with human telomerase
HIV	Human immunodeficiency virus
HLA	Human leucocyte antigen
HLTF	Helicase-like transcription factor
HPLC	High-performance liquid chromatography
HSCT	Hematopoietic stem cell transplant
HSV	Herpes simplex virus
HUWE1	HECT, UBA and WWE domain-containing E3 ubiquitin protein ligase 1

I

ICP	Infected cell protein
IE	Immediate-early
IFIT	Interferon-induced protein with tetratricopeptide repeats
IFN	Interferon
IL	Interleukin
IP	Immunoprecipitation
iRFP	Near-infrared fluorescent protein
ISG	Interferon-stimulated gene

K

KPC	Kip1 ubiquitination-promoting complex

L

LC	Liquid chromatography
LC3B	Microtubule-associated protein light chain 3B
LDH	Lactate dehydrogenase
LFQ	Label-free quantification
LMAN2L	Lectin mannose-binding 2-like
Lys	Lysine

M

m/z	Mass-to-charge ratio
MCLB	Mammalian cell lysis buffer
MCMV	Murine cytomegalovirus
MEF	Mouse embryonic fibroblast
MHC	Major histocompatibility complex
MIEP	Major IE enhancer and promoter
MLKL	Mixed lineage kinase domain-like pseudokinase
MOI	Multiplicity of infection
MS	Mass spectrometry

N

NaCl	Sodium chloride
NB	Nuclear body
NEB	New England Biolabs
NFW	Nuclease-free water
NF-κB	Nuclear factor-kappa B
NK	Natural killer
NRP	Neuropilin
NSA	Necrosulfonamide

O

ORF	Open reading frame
*ori*Lyt	Origin of lytic DNA replication

P

PAGE	Polyacrylamide gel electrophoresis
PAMP	Pathogen-associated molecular pattern
PBS	Phosphate-buffered saline
PCDHGB5	Protocadherin gamma subfamily B5
PCR	Polymerase chain reaction
PDGFRα	Platelet-derived growth factor receptor alpha
PLXN	Plexin
PM	Plasma membrane
PML	Promyelocytic leukemia
PMP	Plasma membrane profiling
PRR	Pattern recognition receptors
PsKD	Pseudokinase domain
PSM	Peptide spectral match
puroR	Puromycin resistance

Q

qPCR	Quantitative PCR
QTV	Quantitative temporal viromics

R

RBBP7	Retinoblastoma-binding protein 7
RCMV	Recombinant cytomegalovirus
RHIM	RIP homotypic interaction motif
RhoA	Ras homolog family member A

RIG-I	Retinoic acid-inducible gene I
RING	Really interesting new gene
RIP	Receptor-interacting serine/threonine-protein kinase
RIPA	Radioimmunoprecipitation assay buffer
RNA	Ribonucleic acid
RNA-seq	RNA sequencing
RNF123	RING finger protein 123
RT	Reverse transcription

S

S:N	Signal-to-noise
SA	Serine-alanine
SCF	(Skp1)-CUL1-F-box
SDS	Sodium dodecyl sulphate
SEM	Standard error of the mean
SEMA	Semaphorin
Ser	Serine
sgRNA	Single guide RNA
shRNA	Short hairpin RNA
Sigma	Sigma-Aldrich
SILAC	Stable isotope labelling by amino acids in cell culture
siRNA	Small interfering RNA
Skp1	S-phase kinase-associated protein 1
SOT	Solid organ transplant
Sp100	Speckled protein of 100 kDa
SUGP2	SURP and G-Patch domain-containing 2

T

TBZ	TNFα + BV-6 + Z-VAD-fmk
Tet	Tetracycline
Thermo	Thermo Fisher Scientific
Thr	Threonine
TLR	Toll-like receptor
TMT	Tandem mass tag
TNF	Tumour necrosis factor
Tp	Temporal protein profile
Tyr	Tyrosine

U

UBAC1	Ubiquitin-associated domain-containing 1
UBR5	Ubiquitin protein ligase E3 component N-recognin 5
UPS	Ubiquitin-proteasome system

V

VAC	Viral assembly compartment
VACV	Vaccinia virus
V-ATPase	Vacuolar-type H^+-ATPase
vICA	viral inhibitor of caspase-8 activation

W

WCL	Whole cell lysate
WDR7	WD repeat-containing protein 7
WT	Wild type

Z

ZBED1	Zinc finger BED-type-containing 1
Z-VAD-fmk	Z-VAD(OMe)-fluoromethyl ketone

Units

× g	times gravity
°C	degree Celsius
µg	Microgram
µl	Microlitre
µm	Micrometre
µM	Micromolar
bp	Base pair
cm	Centimetre
h	Hour
hpi	Hours post-infection
kDa	Kilodalton
M	Molar
mg	Milligram
min	Minute
ml	Millilitre
mm	Millimetre
mM	Millimolar
ms	Millisecond
ng	Nanogram
nl	Nanolitre
nm	Nanometre
nmol	Nanomole
pmol	Picomole
ppm	Parts per million
rpm	Revolutions per minute
s	Second
Th	Thomson
U	Enzyme unit
V	Volt
v/v	Volume per volume
w/v	Weight per volume

Publications

Fletcher-Etherington A, Nobre L, Nightingale K,… Weekes MP. Human cytomegalovirus protein pUL36: A dual cell death pathway inhibitor. *Proc Natl Acad Sci U S A* 2020; **117**: 18771-18779

Fletcher-Etherington A, Weekes MP. Quantitative temporal viromics. *Annu Rev Virol* 2021; **8**: 159-181

Nightingale K, Lin KM, Ravenhill BJ, Davies C, Nobre L, Fielding CA, Ruckova E, **Fletcher-Etherington A**,… Weekes MP. High-definition analysis of host protein stability during human cytomegalovirus infection reveals antiviral factors and viral evasion mechanisms. *Cell Host Microbe* 2018; **24**: 1–14

(In press) Nightingale K, Potts M, Hunter L, Fielding CA, Zerbe CM, **Fletcher-Etherington A**,… Weekes MP. Human cytomegalovirus protein RL1 degrades the antiviral factor SLFN11 via recruitment of the CRL4 E3 ubiquitin ligase complex. *Proc Natl Acad Sci U S A* 2022

(In review) Depierreux DM, Altenburg AF, Soday L, **Fletcher-Etherington A**,… Weekes MP, Smith GL. Selective modulation of cell surface proteins during vaccinia infection: implications for immune evasion strategies. *bioRxiv* 2021

Chapter 1: Introduction

1.1 An introduction to human cytomegalovirus

1.1.1 Phylogeny

Human cytomegalovirus (HCMV) is a member of the family *Herpesviridae*, an evolutionarily ancient group of enveloped viruses with double-stranded deoxyribonucleic acid (DNA) genomes. The *Herpesviridae* family consists of at least 107 virus species, which infect a wide range of mammalian, avian and reptilian species [1]. The *Herpesviridae* belong to the order *Herpesvirales*, which also includes a family of piscine and amphibian herpesviruses, the *Alloherpesviridae*, and a family of two invertebrate herpesviruses, the *Malacoherpesviridae* **(Figure 1.1)** [1]. Defining herpesvirus characteristics have arisen from long-term coevolution with their host species, notably the ability to reach a high prevalence within a population and cause lifelong and typically asymptomatic infections [2]. The *Herpesviridae* are divided into three subfamilies: the *Alpha*, *Beta* and *Gammaherpesvirinae*, all of which encompass human viruses **(Table 1.1)** [1]. HCMV belongs to the *Betaherpesvirinae*, a family of mammalian-tropic viruses that are distinguished by their ability to establish latent infection in leukocytes, lengthy replication cycles, cell-associated infection and their relative inability to cross host species barriers [3].

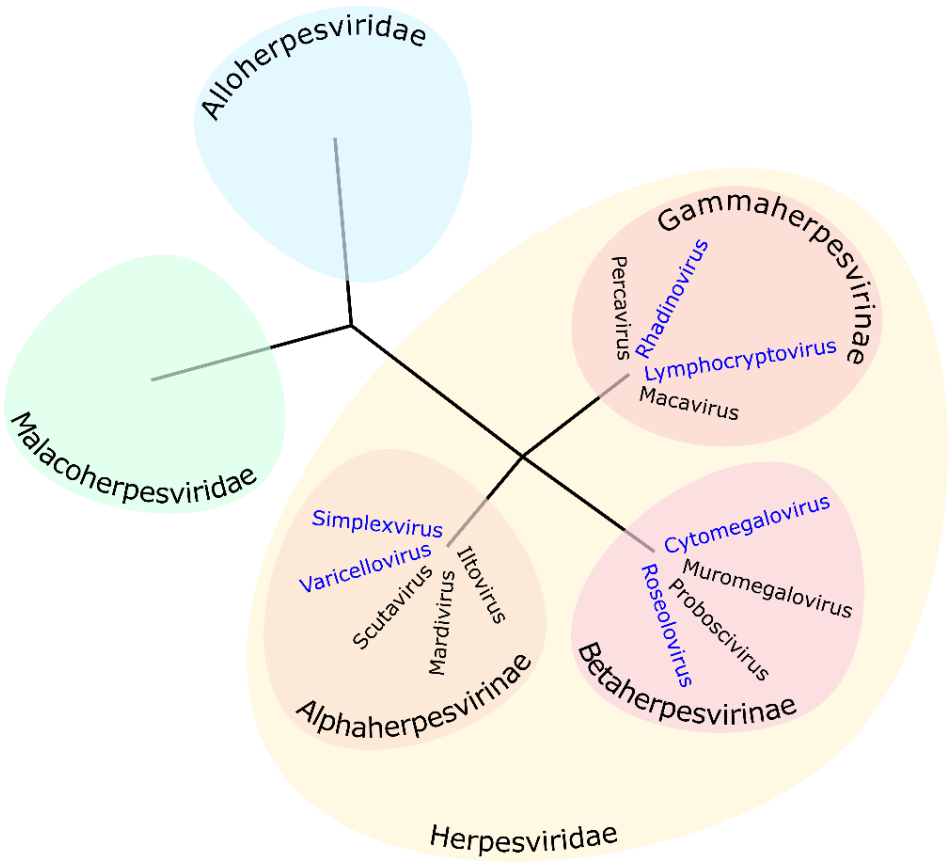

Figure 1.1: The *Herpesvirales.*

The *Herpesvirales* order consists of three families: the *Herpesviridae*, the *Alloherpesviridae*, and the *Malacoherpesviridae*. Genera within the *Alpha-*, *Beta-* and *Gammaherpesvirinae* that contain human viruses are highlighted in blue. Taxonomy shown is as defined by the International Committee on Taxonomy of Viruses [1].

Name of virus	*Alternative names*
Herpesviridae	
Alphaherpesvirinae	
Simplexvirus	
Herpes simplex virus type 1	HSV-1
Herpes simplex virus type 2	HSV-2
Varicellovirus	
Varicella-zoster virus	VZV
Betaherpesvirinae	
Cytomegalovirus	
Human cytomegalovirus	HCMV
Roseolovirus	
Human herpesvirus 6A	HHV-6A
Human herpesvirus 6B	HHV-6B
Human herpesvirus 7	HHV-7
Gammaherpesvirinae	
Lymphocryptovirus	
Epstein-Barr virus	EBV
Rhadinovirus	
Human herpesvirus 8	HHV-8, Kaposi's sarcoma-associated herpesvirus, KSHV

Table 1.1: The human herpesviruses.
There are nine human herpesviruses, here listed under their family, subfamily and genus.

1.1.2 Epidemiology, transmission and clinical features

HCMV is a ubiquitous pathogen, with 60% seropositivity in the Global North and up to 100% seropositivity in the Global South, varying according to geographic location and socio-economic status [4]. Infection can occur at any stage of life, but most commonly during childhood. Horizontal transmission of HCMV occurs through exposure to infected saliva, tears, urine, stool, breast milk, semen or other body fluids. HCMV can remain stable for up to six hours on certain surfaces, meaning there is also possibility for transmission via fomites [5]. Vertical transmission is also common, occurring in around 0.2-2% of pregnancies [3,6]. Transmission to the fetus occurs via the placenta [7], and can result in severe hearing and neurodevelopmental impairments (see **1.1.2.3**).

As with all herpesviruses, primary infection with HCMV leads to the establishment of a latent reservoir, which is maintained throughout the lifetime of the host. In immunocompetent people, HCMV infection

is largely asymptomatic, although primary infection can occasionally present as a mononucleosis-like syndrome. In rare cases, primary infection or reactivation of HCMV in otherwise healthy individuals has been attributed to diseases of the gastrointestinal tract (colitis), central nervous system (meningitis, encephalitis, myelitis), cardiovascular and haematological system (haemolytic anaemia, thrombocytopenia), eyes (uveitis) or lungs (pneumonitis) [8]. These infections are typically self-limiting and can be controlled by the host immune system. More common and severe are the diseases seen in immunocompromised patients, caused by either reactivation of HCMV from a latent reservoir or acquisition of a primary infection. These include more severe forms of the clinical manifestations listed above, as well as hepatitis, retinitis and graft rejection (in transplant recipients). Immunocompromised patients at risk of HCMV-associated disease include acquired immunodeficiency syndrome (AIDS) patients, solid organ transplant (SOT) recipients and allogeneic hematopoietic stem cell transplant (HSCT) recipients. HCMV can also infect the developing fetus, and is the most common infectious cause of congenital disease [9].

1.1.2.1 HCMV in AIDS patients

The most common clinical manifestation of HCMV infection in AIDS patients is HCMV retinitis, accounting for 85% of all HCMV-related complications, followed by colitis, neurological disorders, pneumonitis, hepatitis and adrenalitis [10]. Although the use of anti-retroviral therapy (ART) reduces the incidence of HCMV-associated disease in AIDS patients, HCMV can still cause significant morbidity and mortality in patients with low $CD4^+$ T cell counts at the onset of therapy and in resource-limited settings where ART is less widely available [10,11].

1.1.2.2 HCMV in transplant recipients

HCMV-associated disease in transplant recipients can occur when:

a. A seronegative recipient under immunosuppressive therapy receives a transplant from a seropositive donor. Approximately 78% of these cases result in a primary infection [12].
b. A seropositive recipient receives immunosuppressive therapy. In around 40% of these cases, the patient's own latent HCMV reservoirs reactivate to cause productive and symptomatic disease [12].
c. A seropositive recipient receives a transplant from a seropositive donor, resulting in re-infection with a different strain of HCMV.

HCMV disease in SOT recipients manifests as fever, malaise, leukopenia, thrombocytopenia, and liver dysfunction, and in both SOT and HSCT recipients as end-organ disease most commonly involving the gastrointestinal and respiratory tracts. HCMV infection can also be associated with acute rejection, graft dysfunction, graft vs host disease after HSCT, other opportunistic infections and mortality [13].

1.1.2.3 Congenital HCMV infection

The prevalence of congenital HCMV infection is thought to be between 0.2 and 2% of live births, making it the most significant infectious cause of congenital disease [3,6]. Prevalence varies according to characteristics of the maternal population (age, race and economic status) [6]. Congenital HCMV infection can be acquired when:

a. A seronegative mother becomes infected during pregnancy. In around 32% of such cases the virus transmits across the placenta [14].

b. A seropositive mother becomes reinfected with a new strain of HCMV [15].

c. There is reactivation of latent maternal HCMV reservoirs [15,16].

Around 1% of infants from mothers who are seropositive prior to conception acquire a congenital HCMV infection [12]. Due to the high prevalence of seropositivity, the majority of HCMV-infected infants are born to mothers who first acquired HCMV before pregnancy. Intrauterine transmission to the developing fetus can result in a number of clinical manifestations, including fetal loss. 8-10% of infants with congenital infection will exhibit neurodevelopmental abnormalities, the most common of which is hearing loss [6]. It has been estimated that the overall birth prevalence of symptomatic congenital HCMV infection worldwide is 0.07% [14].

1.1.2.4 Links to other diseases

HCMV infection has been linked to the pathogenesis of atherosclerosis (AS), with sero-epidemiological and molecular biological evidence showing an increased incidence of HCMV infection in AS groups [17]. Given the role of activated immune cells in the development of vascular AS, it is thought that an HCMV-induced inflammatory response could drive the expansion of atherosclerotic plaques [18]. However, epidemiological studies show no statistically significant association, and a mechanism behind the link is unclear.

Causative links with autoimmune diseases including systemic lupus erythematosus, systemic sclerosis, diabetes mellitus type I and rheumatoid arthritis have also been reported in the literature, although clear associations between disease and HCMV seroprevalence have not been established [19]. In particular, HCMV reactivation is common in individuals with ulcerative colitis, although it is unclear whether this is a cause or effect relationship [20].

HCMV disease is also common in patients with leukaemia, lymphoma and other malignancies, especially those undergoing immunosuppressive treatment [21]. In particular, HCMV infection has been implicated in the pathogenesis of glioblastoma, with preliminary studies indicating that anti-HCMV immunotherapy results in improved overall survival [22–24]. However, significant controversy surrounds the detection of HCMV in glioblastoma samples and the role of HCMV in glioblastoma oncogenesis [22].

Finally, latent HCMV infection is thought to contribute to the age-associated deterioration of the immune system [25–27]. A common method used to study this effect is to measure the effect of HCMV on the immune response to influenza vaccination. However, while some studies have reported a negative association between HCMV infection and the response to influenza vaccination [28,29], others have shown no significant effects [30]. Recently, a systematic review and meta-analysis concluded that there is 'no unequivocal evidence' that latent HCMV infection affects the antibody response to influenza vaccination [31]. As highlighted in later sections **(1.2.3)**, HCMV infection has a profound and lasting impact on innate and adaptive immune cell populations, including the inflation of memory $CD4^+$ and $CD8^+$ T cell populations [32]. It has been postulated that this 'memory inflation' reduces T cell diversity and weakens host immunity [33,34], which may explain the observed immunosenescence in seropositive individuals. However, in contradiction to this hypothesis, other studies have shown that T cell receptor and B cell receptor repertoires are intact in seropositive individuals [35,36]. Understanding of the mechanism of HCMV-induced immunosenescence therefore remains limited.

1.1.3 Therapeutics and prophylaxis

Currently, there are six antiviral treatments for HCMV licensed for use in the UK. These are the nucleoside analogues ganciclovir (GCV), valganciclovir (VGCV) and valaciclovir, the pyrophosphate analogue foscarnet, the monophosphate nucleotide analogue cidofovir, and most recently, letermovir. The first five of these agents reduce viremia and viral shedding by targeting the DNA polymerase, but are each associated with significant toxicity and drug resistance [3,37]. HCMV acquires resistance to these drugs through the selection of mutations in the gene encoding the pUL54 DNA polymerase subunit, and in the case of GCV and VGCV, also the gene encoding the viral kinase pUL97 [38]. Letermovir utilises a different mechanism, inhibiting the HCMV terminase complex, and has been shown to be the best drug for prophylaxis after HSCT in terms of preventing HCMV infection and safety [39]. A number of other promising anti-HCMV therapeutics are in development, including maribavir, which targets pUL97 and shows reduced haematotoxicity and nephrotoxicity compared to GCV and VGCV [40]. However, due to the ability of HCMV to acquire resistance through the rapid selection of mutations in genes UL54 and UL97, novel therapeutics with distinct mechanisms of action are desperately needed. Furthermore, not all licensed drugs are suitable for all HCMV-associated diseases. For example, none of the drugs described have been approved for use in pregnant women due to their teratogenic or embryotoxic effects in animal studies [41], making congenital HCMV infection an important area of unmet clinical need.

Strategies for the development of new antivirals include the disruption of interactions between antiviral host proteins and their viral antagonists, to promote endogenous antiviral activity **(1.2.1)**; genetic screening for viral or host proteins that are required for virus replication and therefore represent potential drug targets [42–44]; and, chemogenomic screening of compounds to identify those with antiviral activity [45–48].

Other therapeutic strategies include the adoptive transfer of donor lymphocytes (for allo-HSCTs from a seropositive donor) and passive immunisation with HCMV immunoglobulin (for SOT patients) [49]. All current anti-HCMV therapies target the lytic viral replication cycle, but there is increasing interest in targeting latent HCMV reservoirs to prevent disease caused by HCMV reactivation. These include the 'kick and kill' strategy, where treatment induces partial reactivation from latency, allowing circulating $CD8^+$ cytotoxic T cells to detect and kill infected cells [50].

In 2004, the US National Vaccine Advisory Committee ranked a vaccine to prevent CMV disease as highest priority on the basis of economic benefits and years of healthy life gained [51]. However, there is still no licensed vaccine. Difficulties in developing an efficacious vaccine indicate that protection against primary infection likely requires a multifaceted, strong and specific immune response. The lack of complete understanding of the immune correlates of protection to HCMV is therefore a significant challenge facing future vaccine development. Despite this, there have been some positive clinical trial data, with two vaccines in particular recently or currently being evaluated in phase III trials. DNA vaccine ASP0113, encoding pp65 and gB, was well tolerated and showed promising efficacy results in a phase II clinical trial in seropositive recipients undergoing allo-HSCT [52]. However, a recently concluded phase III trial (NCT01877655) did not demonstrate a significant improvement in overall survival or reduction of end-organ disease. Moderna has recently launched a phase III trial (NCT05085366) of its messenger RNA vaccine mRNA-1647, encoding gB and the pentameric protein complex [52]. The trial will evaluate efficacy of the vaccine against primary HCMV infection in women of childbearing age, after phase I and II studies showed that the vaccine induced functional antigen-specific responses [52].

1.1.4 Virion structure

Historically, herpesviruses were assigned based on their distinctive virion architecture; the genomic DNA is packed inside an icosahedral (T = 16) protein capsid, which is surrounded by a less structured tegument layer and encased by an envelope derived from host cell endomembranes **(Figure 1.2)**. The HCMV capsid is composed of five core proteins: the major capsid protein pUL86, the minor capsid protein pUL46, the minor capsid protein binding protein pUL85, pUL48A and the portal protein pUL104 [53].

The capsid is surrounded by an proteinaceous layer called the tegument, which contains over half of the 71 proteins found within infectious virions, along with a number of cellular proteins and viral and cellular ribonucleic acids (RNAs) [55,56]. Tegument proteins are released into the cell upon entry of the virus, and play a number of essential roles at the start of the lytic cycle prior to gene expression [57]. The most abundant tegument proteins are the large tegument protein pUL48, which associates directly with the capsid, the lower matrix protein pp65/pUL83, the upper matrix protein pp71/pUL82 and the large matrix phosphoprotein pp150/pUL32 [53].

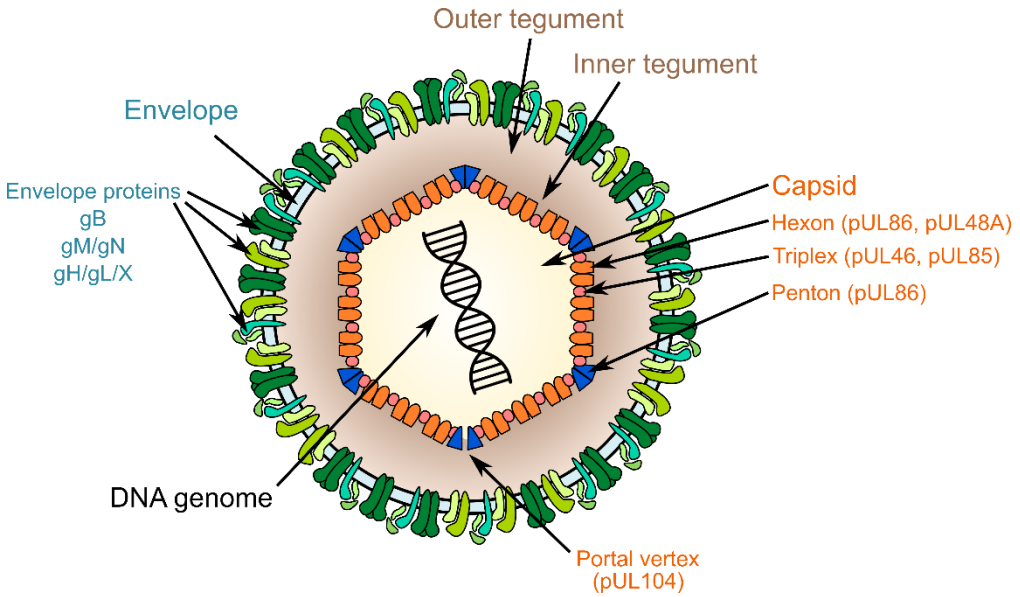

Figure 1.2: The structure of HCMV.

The major structural proteins of the HCMV virion are labelled. gH/gL/X highlights that gH:gL can either form a pentameric complex with pUL128, pUL130 and pUL131 to permit infection of epithelial and endothelial cells, or a trimeric complex with gO which allows infection of all cell types [54].

The viral envelope is acquired during secondary envelopment as the viral capsid buds through cellular endomembranes making up the viral assembly compartment (VAC) **(1.1.8.5)**. The envelope contains a number of viral and host cell proteins, the most abundant of which are gB, gH, gL, gM and gN.

1.1.5 Genome: structure, organisation and gene products

HCMV has a double-stranded linear DNA genome of 235 kilobases [58]. A defining feature of the herpesviruses is a genome that contains direct or inverted repeats of greater than 100 base pairs (bp), which appear to have arisen independently at multiple points in herpesvirus evolution [59]. There are six classes (A-F) of herpesvirus genomes based on the orientation and organisation of the repeats [60] **(Figure 1.3)**. The canonical HCMV genome based on laboratory HCMV strains exhibits the most complex structure, class E, which is shared with members of the *Simplexvirus* genus of *Alphaherpesviruses*. The class E architecture exhibits two unique regions (U_L and U_S) each flanked by terminal (TR_L and TR_S) and internal (IR_L and IR_S) inverted repeats, and a sequence of a few 100 bp (*a* sequence) that is repeated directly at the genome termini and inversely at the IR_L-IR_S junction. The *a* sequences can recombine with one another, generating four genome isomers, although the functional consequence of this isomerisation is not well understood **(Figure 1.3)**. The HCMV genome contains several *cis*-acting elements that instruct DNA replication, transcription and packaging: the origin of replication, *oriLyt*, the genome packaging elements *pac1* and *pac2*, and a number of transcriptional promoters and enhancers including the major immediate-early (IE) promoter [61].

Transcriptional analysis shows that the HCMV genome encodes at least 170 canonical protein-coding genes [58]. Approximately one third of these coding regions contain splice sites, although the extent to which this affects the protein complement of HCMV is so far unclear. In addition, ribosomal footprinting and proteomics have identified a substantial number of additional non-canonical open reading frames (ORFs) that may encode functional proteins [62,63]. Other gene products include four polyadenylated long non-coding RNAs (RNA2.7, RNA1.2, RNA4.9 and RNA5.0), polyadenylated anti-sense transcripts and several non-polyadenylated RNAs such as microRNAs [64].

Forty-five core HCMV gene products are conserved across the herpesviruses, 78% of which are essential for growth in fibroblasts [65]. Genes are named according to their location in the genome, with a prefix of either RL, UL, US or TRS depending on whether they are located in unique or repeat regions **(Figure 1.3)**. Protein names are often given as the gene name preceded by a 'p' (protein) or 'gp' (glycoprotein), or as a unique name based on its function. For example, gene UL36 encodes the protein 'pUL36', otherwise known as the viral inhibitor of caspase-8 activation, 'vICA'.

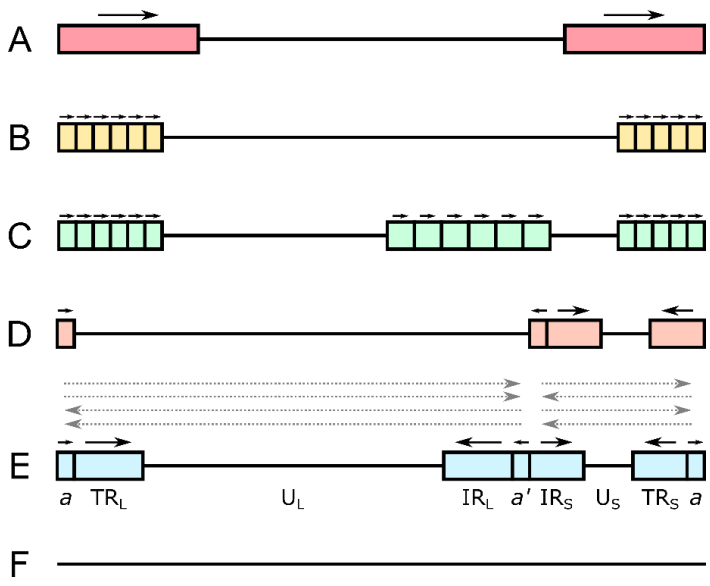

Figure 1.3: Herpesvirus genomes.

Six classes of herpesvirus genomes were defined by Roizman and Pellett [60]. Unique and repeat regions are shown as lines and boxes, respectively. The dotted arrows show the orientation of the long and short regions in the four different isomers of the class E genomes. Clinical strains of HCMV, which are increasingly being used for laboratory-based studies, including in this thesis, have a considerably different genome organisation that is more similar to the class D architecture.

1.1.6 Strains

Historically, research into HCMV predominantly utilised two laboratory strains, AD169 and Towne, both of which have undergone multiple serial passages in fibroblasts [66]. Characterisation of the genome of these strains revealed that extensive passage had favoured the accumulation of multiple mutations, including a deletion in the U_L/*b'* region and a compensatory duplication of the terminal repeat TR_L/IR_L. In the AD169 genome, ORFs UL133-UL151 belonging to U_L/*b'* are replaced by a duplication of ORFs RL1-14 [61] **(Figure 1.4)**. As a result, these strains are unlikely to adequately represent clinical HCMV, especially in terms of immune evasion and virulence functions that are selected for *in vivo* but are redundant *in vitro*. For example, the U_L/*b'* region that is missing in strain AD169 contains genes involved in modulation of inflammatory responses and natural killer (NK) cell function [67].

A study of the genome modifications acquired by clinical viruses cultured *in vitro* showed that this problem also extends to low-passage strains, with rapid selection of mutations occurring in a reproducible manner [68]. Mutation of RL13, UL36 and the UL128-UL131A region occurs within a few replications and in some cases is followed by loss of U_L/*b'*. In order to overcome the problem of genetic instability, the genome of a clinical strain called Merlin was cloned as a bacterial artificial chromosome (BAC) [67]. Sequencing of the prototype Merlin BAC clone (RCMV1111) identified mutations in RL13 and UL128 that had been selected during an early passage [67]. Restoration of the viral sequence to that in the original clinical sample resulted in impaired growth, meaning stable propagation could only be achieved by placing both regions under control of a tetracycline repressor, followed by growth of the virus (RCMV1502) in human fetal foreskin fibroblasts expressing tetracycline [67]. All HCMV strain Merlin viruses used for experiments in this thesis are based on either RCMV1111 or RCMV1502 **(2.11.1)**.

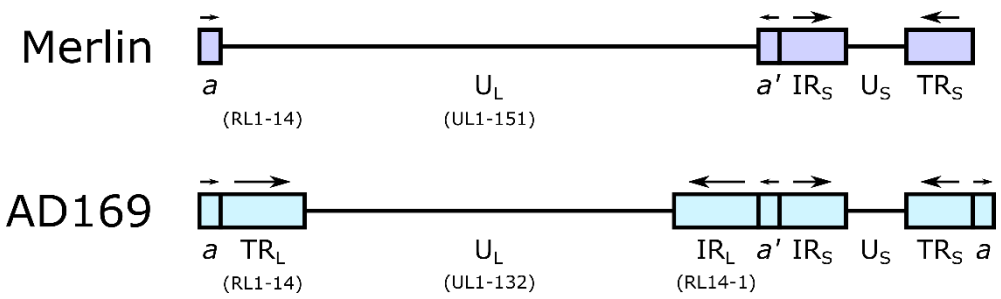

Figure 1.4: The genomes of clinical and laboratory strains of HCMV vary significantly.
A comparison of the genome architecture of one clinical strain of HCMV, Merlin, and one highly passaged laboratory strain, AD169. As well as the duplication-deletion event affecting the U_L/*b'* region, AD169 also has mutations in RL5A, RL13, UL36 and UL131A. Both of these strains of virus are used in experiments throughout this thesis.

1.1.7 Cell tropism

Despite being tightly restricted to human cell types, HCMV exhibits a broad cellular tropism within the human host. Infection of epithelial cells permits inter-host transmission; infection of endothelial cells and hematopoietic cells facilitates intra-host spread, with cells of the myeloid lineage also allowing long-term carriage and persistence of the virus by supporting latent infection; and infection of fibroblasts and smooth muscle cells promotes efficient proliferation [69].

1.1.8 Lytic replication cycle

The lytic replication cycle of HCMV is long, with progeny release beginning at 48 to 72 hours post-infection (hpi) and maximal virus release at 72 to 96 hpi. Infected cells can continue to release virus for several days, dependent on the cell death suppression machinery expressed by the strain [53].

1.1.8.1 Entry

The highly conserved HCMV envelope glycoprotein gB forms homotrimers that mediate membrane fusion during viral entry. Several host cell proteins have been identified as receptors for gB, including the epidermal growth factor receptor (EGFR), the platelet-derived growth factor receptor alpha (PDGFRα) and integrins [70–72]. However, more recent studies have indicated that gB likely mediates fusion without binding cellular receptors [73]. The second major HCMV glycoprotein complex is the gM/gN heterodimer, which has an essential role in mediating attachment to cells, likely via interactions with heparan sulphate proteoglycans [74]. Finally, the gH/gL heterodimer forms two mutually exclusive complexes that regulate cell tropism. The gH/gL/gO trimer is required for the infectivity of cell-free virions, and is thought to bind PDGFRα [75,76]. The gH/gL/gpUL128/gpUL130/gpUL131 pentamer is required for the infection of leukocytes, dendritic cells (DCs), epithelial and endothelial cells and uses neuropilin-2 (NRP2) as a receptor [77,78]. It is generally assumed that, upon recognition of the corresponding receptor, gH/gL complexes activate gB-mediated fusion. gH/gL/gO-dependent entry is pH- and clathrin-independent, and is thought to occur via plasma membrane (PM) fusion or macropinocytosis [79,80]. Contrarily, pentamer-dependent entry into epithelial and endothelial cells occurs via endocytosis followed by low pH-dependent fusion with endosomal membranes [81]. Extended propagation of HCMV in fibroblasts results in a 100- to 1000-fold reduction in endothelial cell tropism [82,83]. This transition was found to be caused by mutations in the UL128-131 region that are picked up quickly during passage (**1.1.6**, [77]).

After being released into the cytoplasm, the viral nucleocapsid hijacks cellular microtubules to facilitate transport to the nucleus. Here, the DNA is released and enters the nucleus through nuclear pores. These processes are thought to rely on the action of tegument proteins that remain closely associated with the nucleocapsid, including pUL47/pUL48 and pp150 [57,84,85].

1.1.8.2 Gene expression and DNA replication

HCMV gene expression is temporally regulated, and has historically been categorised into three distinct phases of expression based on the effects of inhibitors of protein synthesis and viral DNA replication: immediate-early (IE), early (E) and late (L). More recently, examination of the temporal expression profiles of HCMV proteins using quantitative temporal viromics established that there are at least five distinct temporal protein profiles (Tp), Tp1-5 [86] **(1.4.4)**. Transcription of viral genes is performed by the host RNA polymerase II, and is tightly regulated by a range of viral and cellular genetic, epigenetic and environmental factors [87]. IE (Tp1) expression occurs within half an hour of viral entry, independent of *de novo* protein expression and DNA replication. The most studied IE (Tp1) genes are the major IE proteins IE1-p72 and IE2-p86, the expression of which is controlled by the major IE enhancer and promoter (MIEP). IE1-p72 and IE2-p86 control all subsequent early and late events in HCMV replication through transcriptional transactivation, as well as inhibiting a number of antiviral cell-intrinsic and innate immune responses.

From six hpi, following expression of the major IE genes, early (Tp2) gene expression ensues. Early gene products include a number of proteins required for DNA replication, as well as proteins involved in modulation of the host cell and immune evasion.

Viral DNA replication begins around 24 hpi and is thought to be stimulated by transcriptional activation of a region close to the *ori*Lyt, allowing unwinding of the DNA and loading of the replication fork proteins. DNA replication is dependent on a core set of HCMV proteins forming the replication fork machinery, including the UL54-encoded polymerase catalytic subunit; the UL44-encoded polymerase processivity subunit; the UL57-encoded single-stranded DNA binding protein; and the helicase primase complex consisting of proteins encoded by UL105, UL70 and UL102 [53]. In addition to these six core replication proteins, amplification of HCMV DNA from the *ori*Lyt is also dependent on pUL84, pIE2 and, in some cell types, the UL36-UL38 gene locus [88–90].

Late genes (Tp3-5) typically encode structural proteins or proteins that control maturation and egress. They can be divided into two broad classes based on their dependence on viral DNA replication, or three classes (Tp3-5) based on their temporal profiles of expression [86].

1.1.8.3 Capsid assembly and DNA encapsidation

After their synthesis in the cytoplasm, HCMV structural proteins are shuttled to the nucleus. A protein scaffold composed of the assembly protease pUL80a and the assembly protein precursor pUL80.5 is formed and directs oligomerisation of the major capsid protein [91] **(1.1.4)**. This is followed by the addition of the small capsid protein and the triplexes, which stabilise the nucleocapsid. At the portal vertex, the portal protein pUL104 interacts with the terminase complex (pUL89, pUL56 and pUL51). As the assembly protease disassembles the scaffold, the virus genome is threaded through the portal vertex into the capsid [91]. The terminase then cleaves the genome concatemer at the *pac-1* and *pac-2*

sequences, allowing packaging of one complete genome per capsid. Encapsidation is a complex process, requiring a number of other HCMV proteins [53].

1.1.8.4 Host cell modification

Cellular processes manipulated by HCMV include cellular metabolism, cellular signal transduction, the cell cycle and host cell stress responses [92–95]. Of particular relevance to this thesis is the modulation of immune responses and cell death responses, which are covered in detail in later sections (**1.2** and **Chapter 5**, respectively).

There are multiple phases of host cell modulation. First is the stimulation of innate immune signalling upon viral entry, which HCMV manipulates in order to maintain the effects of this response that are beneficial to virus replication [such as nuclear factor-kappa B (NF-κB)-mediated activation of the MIEP [96]] while inhibiting detrimental effects such as the release of interferon (IFN). Early viral gene expression is followed by the dysregulation of cell cycle progression, maintaining cells in the G0/G1 phase and creating an environment that is optimal for viral gene expression and DNA synthesis [94]. By the late phase of infection, the host cell has undergone substantial modification and reorganisation, with the formation of a large nuclear replication compartment and the perinuclear VAC.

1.1.8.5 Egress and release

HCMV virions exit the cell via a two-stage envelopment and egress process. Firstly, the virions pass through the nuclear envelope by primary envelopment at the inner nuclear membrane followed by deenvelopment at the outer membrane **(Figure 1.5)**. Budding through the inner membrane is dependent on destabilisation of the nuclear lamina, a function performed by HCMV proteins pUL50 and pUL53, which form the nuclear egress complex (NEC) [84,97].

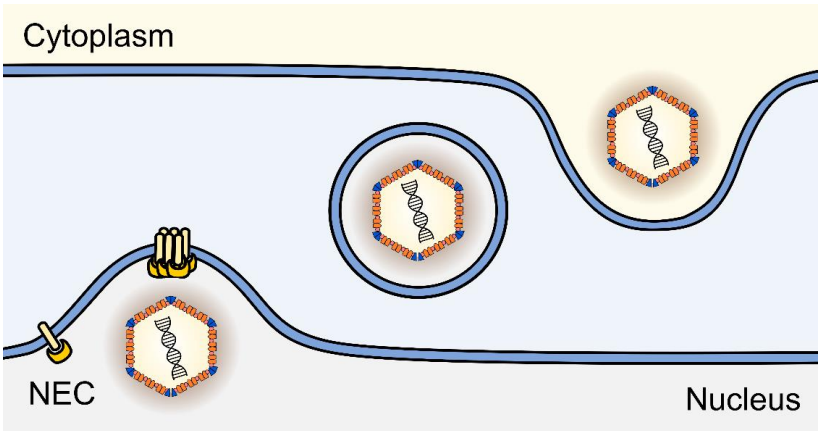

Figure 1.5: Nuclear egress.
NEC, nuclear egress complex.

The post-nuclear stages of egress occur in the VAC, and involve tegumentation, secondary envelopment and transport to the PM. The VAC is a juxtanuclear compartment that results from extensive remodelling of the secretory apparatus [98]. It is made up of layers of organelle-specific vesicles that exhibit markers of the Golgi apparatus, trans-Golgi network, early endosomes, late endosomes and lysosomes [99]. The distinct layers of the VAC contain specific sets of structural and tegument viral proteins. Although tegumentation begins in the nucleus with addition of the inner tegument proteins, the majority of the tegument is acquired as capsids traverse through the VAC [98]. Transport through the VAC is thought to utilise microtubules that radiate from the microtubule organising centre around which the VAC is arranged [100]. Nascent particles undergo secondary envelopment shortly after entrance into a region occupied by vesicles that exhibit markers of early and recycling endosomes [91]. Proteins in the tegument layer facilitate interactions with additional tegument and envelope proteins associated with the membranes of these vesicles, followed by budding into the vesicle lumen in a process that is believed to be dependent on the host endosomal sorting complex required for transport (ESCRT) machinery [91]. The resulting fully mature virions are then exported out of the cell via cellular secretory pathways.

1.1.9 Latency

After primary infection, the virus establishes a latent infection in cells of the early myeloid lineage, including $CD14^+$ monocytes and their $CD34^+$ progenitors. Latency involves the maintenance of the viral genome in the absence of IE gene expression and infectious virion production. Initially thought to be a quiescent state, two recent studies have shown that latency is associated with low-level expression of a broad range of viral genes, mirroring the expression programme observed late in the lytic replication cycle [101,102]. Although the latency-specific functions of very few viral proteins have been characterised, gene expression during latency has been associated with immune evasion, cell survival and genome maintenance.

Latency and reactivation are tightly controlled by regulation of the MIEP by a range of cellular and viral factors [103]. Upon infection of myeloid cells, expression of IE proteins is inhibited by the presence of repressive chromatin structures around the MIEP. This repression is released upon the differentiation of latently infected progenitor cells into macrophages or DCs, activating the phased pattern of gene expression associated with lytic infection.

1.2 The immune response to HCMV and viral immune evasion mechanisms

A healthy immune system is able to elicit a broad, strong and durable response upon infection with HCMV. The importance of the host immune response is highlighted by the severe HCMV-associated disease observed in immunocompromised hosts, as well as the breadth of immune evasion mechanisms encoded by the virus. HCMV has coevolved with the human host over millions of years, during which

its large coding capacity has been utilised to counteract each antiviral strategy developed by the host, enabling its characteristic ability to persist lifelong.

1.2.1 Cell-intrinsic immune responses and antiviral restriction factors

The first line of defence against HCMV upon cellular infection is mediated by constitutive IFN-independent cell-intrinsic responses. These include chemical barriers, antimicrobial peptides, cell death **(1.6.1)** and autophagy **(1.3.2)**, as well as an abundance of antiviral mechanisms mediated by constitutively expressed host proteins that have evolved specifically to function as antiviral restriction factors (ARFs).

While there is not a single universally accepted definition of an ARF, they typically exhibit a number of common characteristics [104–106]. First, they are able to inhibit virus replication and provide an immediate and direct defence against virus infection, prior to the onset of the IFN response and induction of the innate and adaptive immune responses [106]. Second, although ARFs are constitutively expressed, and therefore able to inhibit virus replication immediately following viral entry, their expression tends to be amplified by IFN or virus infection. Although the majority of ARFs are induced by IFN, the IFN-independent activation of ARF activity in the early stages of HCMV infection prior to induction of the IFN response is thought to be important for achieving early virus control [107]. Importantly, a key defining feature of these proteins is that they are able to mediate viral restriction independently of IFN production and signalling [108], distinguishing them from proteins involved in innate immunity.

Evolutionary pressure for both host survival and virus replication drives the selection of favourable mutations in host and viral genomes that enable constitutively expressed host proteins to develop antiviral activity and equip viruses with a range of powerful countermeasures. As a result of this evolutionary ‘arms race’, ARFs often display genetic features of positive evolutionary selection, such as an atypical high ratio of the non-synonymous mutation rate (dN) to the synonymous mutation rate (dS) [104]. Viruses evolve faster than their hosts, conferring another defining feature of ARFs: the presence of corresponding viral antagonists employed by the virus to counteract ARF activity. ARFs that have been shown to target HCMV, along with their viral antagonists, are listed in **Table 1.2**.

It is thought that the restriction factors encoded in the genome of the host, and the viral proteins that have evolved to counteract these defences, are key determinants of host susceptibility to disease. Viral antagonists utilise several different mechanisms for attenuating ARF activity. Generally, the virus protein hijacks host cell machinery to drive post-translational modification of the ARF (e.g., ubiquitination, SUMOylation or phosphorylation), leading to its degradation, displacement, mislocalisation or inactivation. Viral antagonism of ARFs presents an opportunity for their characterisation through the identification of proteins that are post-translationally modified, downregulated or mislocalised specifically during infection.

Importantly, disruption of interactions between ARFs and their viral antagonists has the potential to enable endogenous inhibition of viral replication, as shown, for example, by the use of small molecular compounds to disrupt the interaction between the ARF apolipoprotein B mRNA editing enzyme catalytic subunit 3G (APOBEC3G) and HIV protein viral infectivity factor (Vif) [109,110]. Identification of anti-HCMV restriction factors, and characterisation of the molecular interactions between these ARFs and their viral antagonists, could therefore provide opportunities for developing novel therapeutics.

Restriction factor		*Evidence of HCMV restriction*	*Upregulated by IFN?*	*Viral lifecycle stage inhibited*	*Viral antagonists*	*Mechanism of antagonism by HCMV antagonist*	*Evidence of positive selection?*
ATRX	Alpha thalassemia retardation syndrome X-linked	[111]	Unknown	All involved in epigenetic silencing of viral transcription from promyelocytic leukemia (PML)-nuclear bodies (PML-NBs)	**pp71 (HCMV)** BNRF1 (EBV) ORF75 (KSHV)	Displaces ATRX from PML-NBs [111]	No
DAXX	Death domain-associated protein 6	[112]	Yes		**pp71 (HCMV)** BNRF1 (EBV) E4 ORF3 (adenovirus)	Mediates DAXX degradation in a proteasome-dependent, ubiquitin-independent manner [113]	No
MORC3	Microorchidia 3	[114]	Yes		ICP0 (HSV-1)	Proteasomal degradation [62]. No HCMV antagonist identified.	No
PML	Promyelocytic leukemia	[115]	Yes		**IE1 (HCMV)** ICP0 (HSV-1) E4 ORF3 (adenovirus) ORF75c (murine gammaherpesvirus 68)	Inhibits SUMOylation of PML [116]	No
Sp100	Speckled protein of 100 kDa	[117]	Yes		**IE1 (HCMV)** ORF3 (herpesvirus saimiri)	Mediates loss of SUMOylated forms of Sp100 and degradation of Sp100, perhaps by acting as an E3 ligase [118]	No
APOBEC3A	Apolipoprotein B editing enzyme catalytic subunit 3A	Maternal-fetal interface [119]	Yes	Genome replication	Ribonucleotide reductase (alpha- and gammaherpesviruses)		Primates
BclAF1	Bcl-2-associated transcription factor 1	[120]	Unknown	Gene expression	**pp71, pUL35 (HCMV)** US3 (HSV-1)	Induce proteasomal degradation of BclAF1 [120]	No
CTCF	CCCTC-binding factor	[121]	No	Gene expression	None known		No

Gal-9	Galectin-9	[122]	Yes	Entry	None known		No
HLTF	Helicase-like transcription factor	[62]	No	Unknown	**pUL145 (HCMV)** Vpr (HIV-1)	Recruits the Cullin4 E3 ligase complex to target HLTF for degradation [62]	No
IFIT1	Interferon-induced protein with tetratricopeptide repeats 1	[123]	Yes	Translation, genome replication (?)	C9 (VACV)		Yes
MxB/Mx2	Myxovirus resistance B	[124]	Yes	Nuclear entry/uncoating	None known		Yes
SAMHD1	Sterile alpha motif and histidine-aspartate domain-containing protein 1	[125]	Yes	Reverse transcription, viral gene expression	**pUL97 (HCMV)**, and other conserved herpesvirus protein kinases Vpx (HIV-2, some SIVs) Vpr (some SIVs)	Phosphorylates and inactivates SAMHD1 [126]	Yes
SLFN11	Schlafen-11	[127]	Yes	Unknown	**RL1 (HCMV)**	Recruits the e Cullin4-RING E3 Ubiquitin Ligase (CRL4) complex to target SLFN11 for degradation [127].	Yes
SPOC1	Survival-time associated PHD protein in ovarian cancer-1	[128]	Unknown	Transcription	Vpr (HIV-1)		No
TRIMs	Tripartite motif protein (including PML – see above)	TRIM28 (KAP1) [129]	Unknown	Transcription	Rep (adeno-associated virus)		No
		TRIM43 [130]	No, but induced by infection	Transcription	None known		Vertebrates

Viperin	Virus inhibitory protein, endoplasmic reticulum-associated, interferon-inducible	Antiviral [131] and proviral [132]	Yes	Virion morphogenesis	None known		Yes
ZAP	Zinc finger antiviral protein	[133,134]	Yes	Viral protein translation	**IE1 (HCMV)**	CpG suppression in IE1 RNA	Yes

Table 1.2: Antiviral restriction factors that target HCMV.

Reviewed in [104,443–446]. SIV, simian immunodeficiency virus; VACV, vaccinia virus.

1.2.2 The innate immune response

In contrast to constitutive intrinsic responses, the innate immune response is an IFN-dependent response fulfilled by IFN-stimulated gene (ISG) products, which are induced in response to IFN secretion following the recognition of viruses by germline-encoded pattern recognition receptors (PRRs). PRRs include the Toll-like receptors (TLRs), nucleotide-binding and oligomerisation domain (NOD)-like receptors (NLRs), retinoic acid-inducible gene I (RIG-I)-like receptors (RLRs) and the cytosolic DNA sensors. Several PRRs are thought to recognise HCMV. Recognition of HCMV glycoproteins gB and gH by TLR2 results in induction of a NF-κB-dependent signalling pathway that leads to the expression and release of several inflammatory cytokines, including C-C motif chemokine ligand 5 (CCL5), interleukin 6 (IL6), IL7, IL8, and IL12 [135–137] **(Figure 1.6)**. The DNA sensor cyclic GMP-AMP synthase (cGAS) has been shown to be a key sensor of HCMV DNA in DCs and macrophages, leading to the activation of the stimulator of interferon response cGAMP interactor 1 (STING) pathway, which induces type I IFN production [138] **(Figure 1.6)**. Other PRRs implicated in HCMV recognition include TLR3 and TLR9, CD14, NLR family CARD domain-containing 5 (NLRC5), NOD1 and NOD2, IFN gamma inducible protein 16 (IFI16) and Z-DNA binding protein 1 (ZBP1) [137].

Together, type I IFNs and inflammatory cytokines limit viral replication at the site of infection, recruit phagocytic leukocytes, professional antigen presenting cells and NK cells, and activate adaptive immune responses [139]. Synthesis of type I IFN (IFNα/β) results in both the induction of antiviral ISGs belonging to the innate immune system and the amplification of the expression of a number of ARFs **(1.2.1) (Figure 1.6)**, meaning that there is substantial cross-talk between the intrinsic and innate arms of the immune response. Innate ISGs include signalling molecules [e.g. mitochondrial antiviral signalling protein (MAVS)], transcription factors [e.g. IFN regulatory factors (IRFs)], interferon-induced 15 kDa protein (ISG15) and PRRs [e.g. 2′–5′–oligoadenylate synthetase (OAS), protein kinase R (PKR), and IFI16].

The major IE proteins of HCMV, IE1-p72 and IE2-p86, play a key role in modulating the innate cytokine response. IE2-p86 inhibits induction of several inflammatory cytokines and chemokines through binding NF-κB, whereas IE1-p72 inhibits the downstream action of type I IFN by interfering with Janus kinase (JAK)/signal transducer and activator of transcription (STAT) signalling **(Figure 1.6)** [140]. Another major effector of the anti-IFN response is HCMV protein pp65, which either promotes the export of IRF3 from the nucleus, suppresses the induction of ISGs and/or inhibits cGAS/STING signalling [137].

A further key component of the anti-HCMV innate response is the induction of NK cells, highlighted by the susceptibility of NK cell-deficient individuals to HCMV-associated disease and the number of NK cell evasion mechanisms encoded by the virus [141]. NK cells inhibit HCMV inter-cell transmission via the production of IFN-γ and the stimulation of IFN-β production in target cells [142,143], and eliminate infected cells through cytotoxicity. NK cells can also mediate antigen-specific memory

responses towards HCMV infection via the modulation of adaptive immune cells. HCMV encodes several mechanisms to prevent NK cell activation, either by encoding or upregulating ligands for inhibitory NK cell receptors [such as human leucocyte antigen (HLA) E and pUL18] or preventing activating NK cell receptor signalling [144–146].

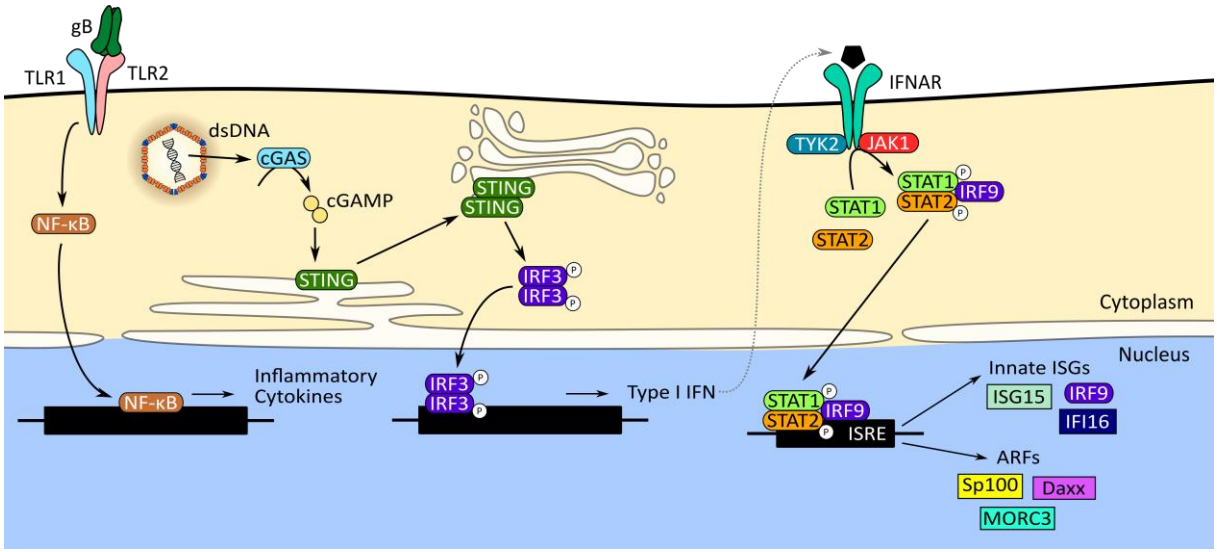

Figure 1.6: The synthesis and action of type I IFN.
Recognition of viral pathogen-associated molecular patterns (PAMPs) by PRRs results in the induction of type I IFN and inflammatory cytokines via pathways involving the transcriptional regulators IRF3 and NF-κB, respectively. The nascent IFN can act in an autocrine or paracrine manner to initiate the activation of the JAK/STAT signal cascade. This in turn induces the expression of innate IFN-stimulated genes (ISGs) and the upregulation of ARF expression, which establishes an antiviral state within the cell. ISRE, IFN-stimulated response element.

1.2.3 The adaptive immune response

Adaptive immunity plays a key role in controlling both primary HCMV infection and the balance between latency and reactivation. Primary infection elicits the production of antibodies against a range of HCMV proteins, including pp65, pp150, gB, IE1, UL123 and the pentameric gH/gL complex [144,147]. The importance of the humoral response to HCMV is highlighted by the fact that women with pre-existing anti-HCMV antibodies from primary infection prior to conception are at lower risk of vertical transmission of HCMV to the fetus [148].

HCMV elicits one of the strongest cell-mediated adaptive immune responses recorded, with around 10% of the $CD4^+$ and $CD8^+$ memory T cell repertoire of HCMV seropositive individuals specific to HCMV epitopes [149]. The cytotoxic $CD8^+$ T cell response is thought to be particularly protective during

primary infection and reactivation, with adoptive transfer of HCMV-specific $CD8^+$ T cells being used therapeutically to alleviate post-transplantation HCMV-related complications [150]. The anti-HCMV effect of $CD4^+$ T cells, exerted through cytolysis and IFNγ secretion, is also important, with a lack of these responses associated with HCMV-related complications [148,151]. The HCMV-specific αβ T cell response to primary infection is thought to involve phases of expansion, contraction and the formation of long-term effector and central memory pools, which prevent clinical disease following periodic reactivation of the virus throughout the lifetime of the host. In addition to conventional αβ T cell responses, other immune cell subsets, including γδ T cells and induced regulatory T cells also modulate the immune response to HCMV [148,152].

HCMV is a paradigm of adaptive immune evasion, employing a number of mechanisms to interfere with MHC class I processing and presentation pathways in order to evade recognition by $CD8^+$ T cells. These mechanisms are encoded by genes of the US2-11 gene block: pUS2 and pUS11 direct the degradation of MHC class I molecules, pUS3 retains MHC class I-peptide complexes in the endoplasmic reticulum (ER), and pUS6 prevents peptide translocation into the ER [153–156]. $CD4^+$ T cell responses are also suppressed via disruption of MHC class II antigen presentation through repression of JAK1 and class II transactivator (CIITA) expression [144].

Despite the strength of the immune response against HCMV, the infection is never cleared, and the virus is able to establish a latent infection. T cell responses to latency-associated antigens have been documented, with $CD4^+$ T cells specific for UL138 being able to recognise latently infected cells [157]. pUL111A (vIL-10), a viral protein expressed during latency, downregulates the expression of MHC class I and II molecules, suppressing both allogeneic and autologous recognition by $CD4^+$ cells and allowing latently infected cells to evade the $CD4^+$ T cell response [144,158].

1.3 Protein degradation in virus-host warfare

One strategy utilised by viruses to evade cell-intrinsic, innate and adaptive immunity and to create a cellular environment that is conducive to virus replication is the modulation of host protein abundance. This can be achieved via the regulation of host transcription, messenger RNA stability, translation, protein stability, or, of particular relevance to this thesis, the subversion of cellular protein degradation machinery to target host proteins for degradation. Two major pathways of intracellular protein degradation, the ubiquitin-proteasome system (UPS) and lysosomal proteolysis, are briefly introduced below.

1.3.1 Ubiquitination and the ubiquitin-proteasome system

During cellular homeostasis, the UPS is responsible for the regulation of many fundamental cellular processes through altering the abundance of key regulatory proteins, as well as being the primary mechanism of protein quality control by degrading misfolded or damaged proteins [159,160]. In this

pathway, proteins are marked for degradation through post-translational covalent conjugation of linear chains of ubiquitin molecules to one or more of the protein's lysine, cysteine, serine or threonine residues. This is performed in a sequential manner by a series of enzymes, classified as E1, E2 or E3 [159]. The ubiquitin-activating E1 enzyme first activates the C-terminal glycine residue of ubiquitin via adenosine triphosphate (ATP) hydrolysis, and transfers it to the ubiquitin-conjugating E2 enzyme. The E2 then cooperates with the E3 ubiquitin ligase to attach it to the substrate. While most cells express one or two E1 enzymes, there are approximately 40 E2 enzymes and more than 600 E3 enzymes that exhibit cell-type- and organelle-specific expression patterns [160]. E3 ligases are categorised into three classes: the homologous to E6-AP carboxyl terminus (HECT) E3 ligases, the really interesting new gene (RING) E3 ligases and the RING-between-RING (RBR) E3 ligases [161]. Distinct E2:E3 pairings enable specific recognition of thousands of substrates.

In addition to protein degradation, ubiquitination is increasingly implicated in the regulation of many other cellular processes, by inducing changes in protein conformation, protein-protein interactions and protein localisation. The exact fate of a ubiquitinated protein depends on the number of ubiquitin molecules attached and the manner in which the ubiquitin molecules are linked. Ubiquitin itself contains seven lysine residues. In the most well-characterised form of ubiquitination, Lys-48 of ubiquitin is further conjugated to additional ubiquitin molecules to form a polyubiquitin chain. Lys-48-linked chains are the canonical signal for protein degradation, enabling recognition by the 26S proteasome: a catalytic, ATP-dependent multisubunit protease. Lys-11-linked chains and monoubiquitination can also mediate proteasomal degradation of normally-folded proteins, while Lys-48 and Lys-63 linkages are involved in the degradation of misfolded proteins through the UPS or autophagy [162,163]. Examples of non-proteolytic functions of ubiquitination include the regulation of DNA repair, autophagy and immune responses (Lys-63-linked ubiquitin chains), and the epigenetic control of gene expression, cytoskeletal rearrangements and receptor internalisation (monoubiquitination) [162–164].

Proteolytic and non-proteolytic forms of ubiquitination are employed by the host cell to regulate antiviral defences, and exploited by viruses for their replication and immune evasion [165]. Viruses manipulate the host ubiquitin system by encoding proteins that exhibit E3-like ligase activity or deubiquitinase activity, act as adapter proteins that alter the substrates recognised by host E2 and E3 enzymes, or manipulate the abundance or activity of cellular E3 ligases [166]. HCMV employs all of these mechanisms, enabling the virus to evade cell death, regulate the cell cycle, evade cell-intrinsic immunity, inhibit IFN induction and signalling, and prevent recognition of infected cells by T cells and NK cells [167].

1.3.2 Lysosomal proteolysis

Lysosomes are the terminal degradative compartment of the secretory, endocytic, autophagic and phagocytic pathways [168]. These single-membrane bound organelles contain a myriad of proteases,

nucleases, glycosidases, lipases, phospholipases and phosphatases that are optimally active in an acid environment [169]. The characteristic low pH of lysosomes is maintained by action of the vacuolar-type H^+-ATPase (V-ATPase). One of the pathways of lysosomal proteolysis is macroautophagy (hereinafter referred to as autophagy), which involves the engulfment of cytoplasmic material and intracellular organelles into double-membrane vesicles, termed autophagosomes [170]. Autophagosomes subsequently fuse with lysosomes, resulting in degradation of the captured material by lysosomal hydrolases.

In addition to utilising the host UPS for mediating the degradation of antiviral proteins, viruses can also harness pathways of lysosomal proteolysis. Endolysosomal degradation in particular represents an opportunity for regulating the abundance of PM proteins. For example, HCMV proteins pUS18 and pUS20 can act independently or in concert to divert two NK cell activation ligands into lysosomal degradation pathways [145,146].

The endolysosomal and autophagy-lysosomal pathways are part of the cell-intrinsic arsenal that can respond to and restrict virus infection through degradation of virus particles and proteins **(1.2.1)**. However, these pathways are often subverted and harnessed by viruses, not only to evade degradation and regulate the abundance of host and viral proteins, but also for cell entry, replication and cell exit [171]. The regulation of these pathways during infection can be complex. This is especially true for the interaction between HCMV and the autophagy-lysosome pathway. As viral inhibition of autophagy has been shown to be essential for virus replication, and agonists of autophagy decrease virus production, it could be assumed that autophagy acts solely to restrict infection [172,173]. However, HCMV has also been shown to stimulate autophagy during early infection, which is thought to provide a source of intracellular membranes for viral assembly [174,175]. Although these interactions are not yet fully elucidated, it appears that HCMV regulates autophagy in a highly cell type-specific and time-dependent manner.

1.4 Quantitative proteomics as a tool to study virus-host interactions

Due to recent advances in mass spectrometry (MS) instrumentation, quantitation and multiplexing capacity, quantitative MS has become an important tool for the study of virus-host interactions through time and space. Our group (laboratory of Dr. Michael Weekes at the Cambridge Institute for Medical Research [176]) has recently published a number of proteomic screens designed to improve our understanding of changes in the cellular and viral proteomes that occur over the time course of HCMV infection. These screens utilise the ‘bottom-up’ proteomics approach with isobaric tandem mass tags (TMTs) and/or stable isotope labelling by amino acids in cell culture (SILAC) to enable relative quantitation of protein abundance across multiple conditions. Data from these screens are presented

repeatedly throughout this thesis, and so a detailed explanation of the methodology and each of the studies is given below.

1.4.1 Bottom-up proteomics

'Bottom-up' proteomics refers to the characterisation and quantitation of proteins by proteolytic digestion followed by analysis of the resulting peptide mixture by liquid chromatography tandem mass spectrometry (LC-MS/MS) [177]. After separation by LC, peptides are ionised and separated according to their mass-to-charge ratio (m/z) (MS1 scan). Precursor ions of a particular m/z are selected and fragmented into smaller fragment ions (e.g. by collision-induced dissociation) and then separated again by their m/z ratio to create a spectrum (MS2). Characterisation of the precursor peptides is typically performed following the MS run, using algorithms that match the observed tandem mass spectra derived from peptide fragmentation to the theoretical spectra generated from *in silico* digestion of a protein database. Fractionation of peptides prior to LC-MS/MS, for example by strong cation exchange chromatography or high pH reversed-phase liquid chromatography (HpRP), increases both the analytical dynamic range and proteome coverage [178].

1.4.2 Quantitation strategies

The method of protein quantitation determines how protein abundance will be measured, as well as having implications for the number of proteins that can be quantified, the number of conditions that can be studied simultaneously, and the precision of comparative measures of protein abundance [179].

1.4.2.1 Label-free methods

Label-free quantification (LFQ) is based on the comparison of MS spectra from samples that are analysed by independent MS runs. Protein abundance is measured by calculating the area under the curve of the chromatographic peak of the peptide precursor ions, or by counting the number of fragment-ion spectra corresponding to a particular protein (spectral counting). As samples are analysed separately, experiments based on LFQ are susceptible to sources of variation introduced during LC-MS/MS, such as sample injection and the differential selection of precursor ions for fragmentation. However, recent advances in data-independent acquisition approaches are enabling more reliable quantitation [180,181], while avoiding the expense and additional sample preparation steps required for label-based methods.

1.4.2.2 Label-based methods

Label-based methods allow samples from the same experiment to be analysed and differentiated in the same MS run, enabling precise quantitation and reducing run times. Two of the most common labelling strategies are the metabolic labelling of proteins prior to cell lysis (e.g. SILAC), and the chemical labelling of peptides with isobaric tags (e.g. TMTs) following protein digestion.

SILAC involves the addition of amino acids labelled with different stable isotopes into the cell culture medium of living cells [182]. The stable isotopes are gradually incorporated into nascent proteins, introducing small mass differences to otherwise identical peptides that enable differentiation by MS. Samples can be combined prior to protein digestion, minimising variation introduced during parallel processing of samples. However, due to the small number of isotopically distinct amino acids, SILAC experiments are generally limited to the comparison of three conditions.

TMTs are isobaric labels, composed of an amine-reactive N-hydroxysuccinimide-ester group, a spacer arm for mass-normalisation and a reporter group **(Figure 1.7A)**. Each tag has an identical overall mass but different mass deviations in the reporter and balancer regions of the molecule due to the incorporation of different numbers and combinations of stable ^{13}C and ^{15}N isotopes [183]. After labelling the peptides from each sample with a different TMT reagent, the samples are combined and assessed in a single LC-MS/MS or LC-MS3 analysis **(Figure 1.7B)**. For LC-MS/MS, reporter ions are released from the labels during the peptide fragmentation step of the MS2 scan. However, with this approach, near-isobaric MS1 peptide ions can be coisolated and fragmented together with the target ions, skewing the reporter ion intensities and limiting the accuracy and precision of the data [184]. Performing an additional isolation and fragmentation event (MS3 scan) eliminates this interference effect **(Figure 1.7C)**. The most intense fragment ion from the MS2 scan is selected, and the attached isobaric tags cleaved by higher-energy collision dissociation (HCD) to release the reporter group. The reporter ions are identified according to their distinct m/z, and comparison of the reporter ion intensities allows relative peptide abundance across each of the samples to be measured.

Although use of SILAC can enable more precise measurements of relative abundance and increase proteome coverage [179], the multiplexing capacity of TMT is superior to that of the three-plex SILAC system, currently allowing concomitant comparison of up to 16 samples [185].

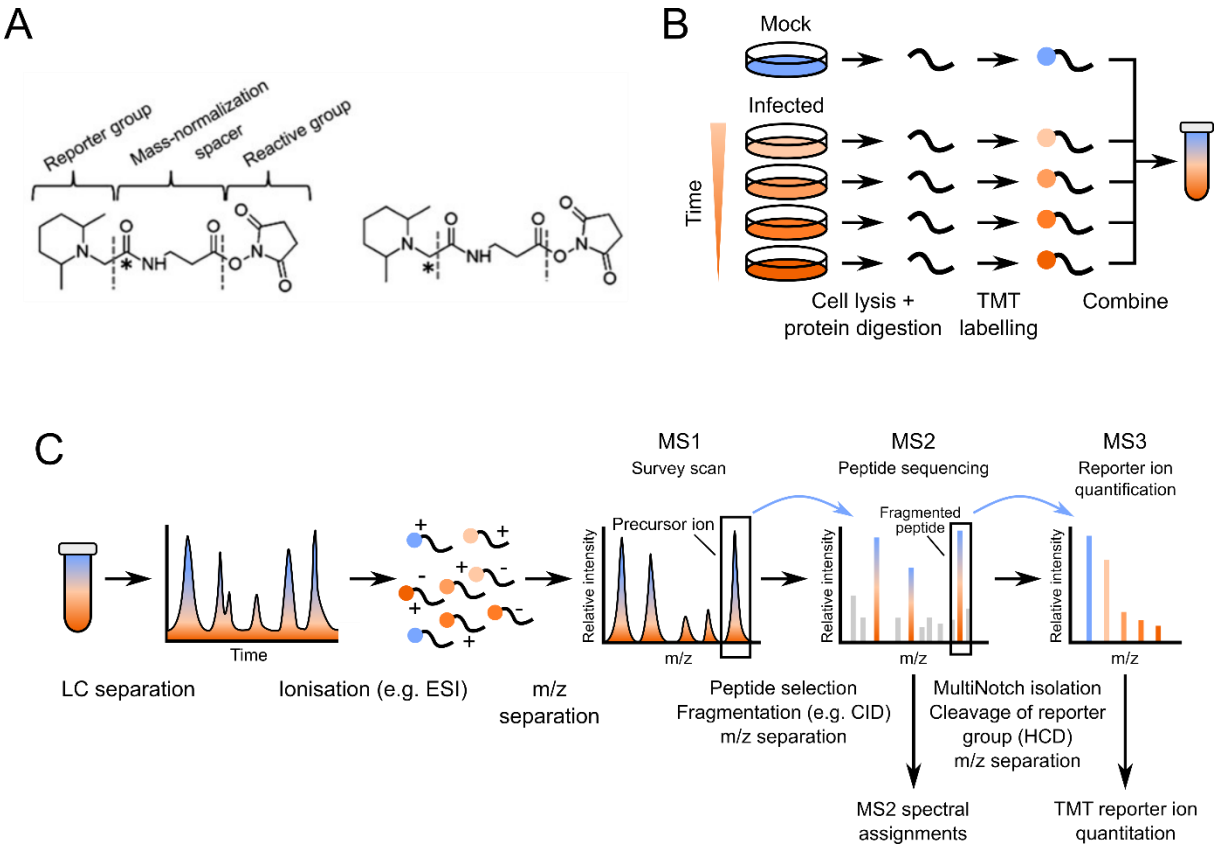

Figure 1.7: TMT-based quantitative proteomics.

(A) Chemical structure of two TMT reagents, with the position of stable isotopes marked with an asterisk. This figure was reproduced from Jia *et al.* (2019) [186] (published under an open access Creative Commons CC-BY license). **(B)** Illustration of a quantitative temporal viromics (QTV) experiment using TMT-based quantitation. Cell lines are infected and lysed at different times post-infection. Proteins are then digested, and the peptides from each sample labelled with a different TMT reagent. Samples are combined, and often fractionated, before analysing by LC-MS/MS or LC-MS3. **(C)** LC-MS3 workflow, as described in 1.4.2.2. CID, collision-induced dissociation; ESI, electrospray ionisation; HCD, high-energy collision dissociation; LC, liquid chromatography; m/z, mass-to-charge ratio; TMT, tandem mass tag.

1.4.3 Plasma membrane profiling

The PM is the site of first contact between a host cell and invading virus and provides an interface between the infected cell and the host's immune system. A number of viruses have been shown to downregulate the expression of proteins at the PM, including HIV-1 and HCMV [187,188]. Identifying changes that occur at the cell surface is therefore key to understanding the virus lifecycle and viral immune evasion. However, examination of PM proteins through MS analysis of whole cell lysates (WCLs) can be challenging, as PM proteins are typically hydrophobic and low in abundance, and are therefore underrepresented in proteomic samples. Moreover, the presence of proteins in the secretory pathway, prior to or following their emergence at the PM, can obscure information about the abundance of the protein specifically at the PM. As such, a variety of methods can be used to enrich for PM proteins prior to MS. These methods include those that separate PM proteins based on their physicochemical properties (size, charge or hydrophobicity), make use of affinity interaction with a lectin or antibody, or chemically couple a tag to the side groups of exposed surface proteins prior to affinity purification [189].

Plasma membrane profiling (PMP), first described in 2012, applies the selective oxidation and aminooxy-biotinylation of sialylated PM glycoproteins, followed by affinity purification with high capacity streptavidin [190,191] **(Figure 1.8)**. This technique has been used to study changes at the cell surface over time during HCMV, EBV, HSV-1 and HIV infection [86,187,192–194]. In addition to identifying host proteins that are up or downregulated at the PM, PMP can also be used to identify viral PM proteins with high confidence [86,193].

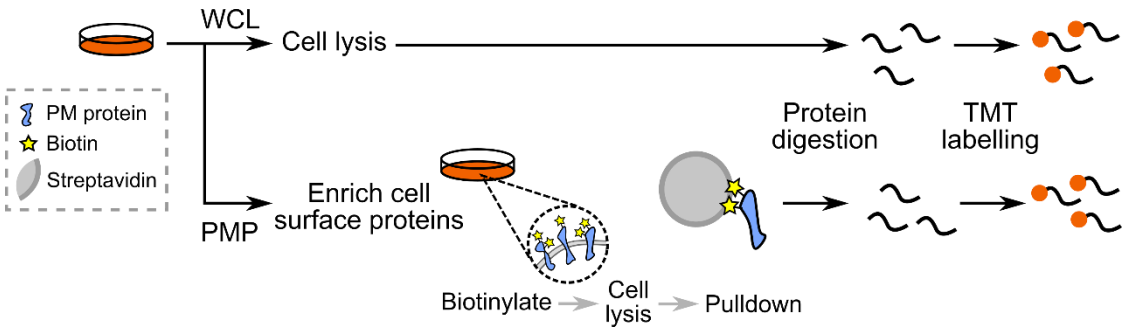

Figure 1.8: Plasma membrane profiling.

PMP, plasma membrane profiling; TMT, tandem mass tag; WCL, whole cell lysate.

1.4.4 Key study 1: Quantitative temporal viromics

Weekes MP, Tomasec P, Huttlin EL, *et al.* Quantitative temporal viromics: an approach to investigate host-pathogen interaction. *Cell* 2014; **157**: 1460-1472

Quantitative temporal viromics (QTV) utilises the multiplexing capacity of TMT to facilitate MS-based relative quantitation of protein abundance across multiple time points of infection [179]. In a study published in 2014, QTV was used to analyse changes at the whole cell level upon HCMV infection, and additionally combined with PMP to reveal the temporal effects of infection on the cell surface [86]. HFFFs were infected with HCMV strain Merlin or mock-infected, and lysed at seven time points from 6 to 96 hpi. Over 8,000 proteins were quantified, including 1,184 PM proteins, 139 canonical HCMV proteins and 14 noncanonical HCMV ORFs. The study identified several candidate anti-HCMV restriction factors, based on their immediate upregulation and subsequent downregulation, including tripartite motif protein (TRIM) 5, 16, 22 and 38, sterile alpha motif and histidine-aspartate domain-containing protein 1 (SAMHD1), zinc finger antiviral protein (ZAP) and Schlafen-11 (SLFN11). SAMHD1, ZAP and SLFN11 have since been shown to exhibit specific antiviral activity against HCMV [125,127,133,134]. The inclusion of a PM-enriched fraction enabled identification of NK and T cell ligands that were modulated over the course of infection, while also revealing the downregulation of a number of cell surface proteins with unknown infection-specific functions. These included eight protocadherins and several members of the semaphorin-plexin signalling pathway. Finally, temporal quantitation of HCMV proteins allowed classification of viral proteins based on their temporal profiles **(1.1.8.2)**.

Between 2014 and 2021, our group has applied QTV to the study of EBV, BK polyomavirus, VACV, HSV-1 and influenza A virus [192–197]. Elsewhere, other groups have utilised a variety of different proteomic quantitation methods, including LFQ, SILAC, TMT and isobaric tags for relative and absolute quantitation (iTRAQ), to study changes in host and viral proteomes through a time course of viral infection [179]. As well as investigating changes in protein abundance, QTV can be combined with other methods to study protein localisation, post-translational modifications and protein-protein interactions in a temporal manner [179].

1.4.5 Key study 2: Degradation screens

Nightingale K, Lin K-M, Ravenhill BJ, *et al.* High-definition analysis of host protein stability during human cytomegalovirus infection reveals antiviral factors and viral evasion mechanisms. *Cell Host Microbe* 2018; **24**: 1-14

Lin K-M, Nightingale K, Soday L, *et al.* Rapid degradation pathways of host proteins during HCMV infection revealed by quantitative proteomics. *Front Cell Infect Microbiol* 2020; **10**: 578259

As already described, ARFs can be identified based on the presence of viral antagonists that inhibit their activity **(1.2.1)**. One mechanism of viral antagonism is targeted protein degradation. To identify proteins that are degraded during the early stages of infection, our group developed three orthogonal proteomic screens that combine QTV with the application of proteasomal and lysosomal inhibitors, transcriptomics and SILAC.

In the first screen, changes in protein abundance occurring in the early phase of infection (0-24 h) were measured in the presence or absence of inhibitors of the proteasome (MG132) or lysosome (leupeptin), to identify proteins targeted for degradation via these pathways **(Figure 1.9A)**.

The second screen utilised pulsed SILAC (pSILAC) to compare the rates of protein degradation during HCMV and mock infection up to 18 hpi **(Figure 1.9B)**. Here, cells were cultured in media containing 'medium' SILAC amino acids prior to infection, and the media switched to that containing 'heavy' SILAC amino acids at the point of infection. Samples harvested at different time points were then labelled with different TMT reagents. Medium-labelled peptides were synthesised prior to infection, and so changes in abundance of these peptides represented degradation during infection. Heavy-labelled peptides were synthesised during infection and therefore represented synthesis. By comparing rates of degradation in mock and HCMV-infected cells, this screen enabled identification of proteins that were degraded beyond normal turnover.

With the third screen, changes in protein abundance were compared with changes in transcript levels to distinguish between degraded and transcriptionally regulated proteins **(Figure 1.9C)**. RNA was extracted from infected HFFFs at different time points post-infection and analysed by RNA-sequencing (RNA-seq). The data were then compared to the WCL proteomic data from the QTV study [86]. Where a decrease in abundance was accompanied by transcript upregulation, it is likely that the protein is actively degraded.

To identify the proteins most likely to be degraded during infection, data from all three screens were combined. A 'medium confidence' shortlist contained 133 proteins that were degraded in at least one of the three screens, as judged by stringent criteria, and degraded in at least one other of the screens judged by sensitive criteria (detailed in **Figure 1.10**). A 'high-confidence' shortlist identified 35 proteins degraded in at least 2/3 screens using stringent criteria.

The majority of the 133 proteins degraded with medium confidence were rescued by the addition of MG132. MG132 is a broad, non-selective inhibitor that can also inhibit lysosomal cathepsins and calpains in addition to the proteasome [198]. In order to extend this analysis and to further define the mechanisms of virus-mediated protein degradation, another screen was performed using the selective proteasome inhibitor bortezomib [199]. This study found that the majority of proteins downregulated at 12 hpi and rescued by MG132 treatment are also rescued by bortezomib [199], suggesting that the predominant mechanism of degradation is via the proteasome.

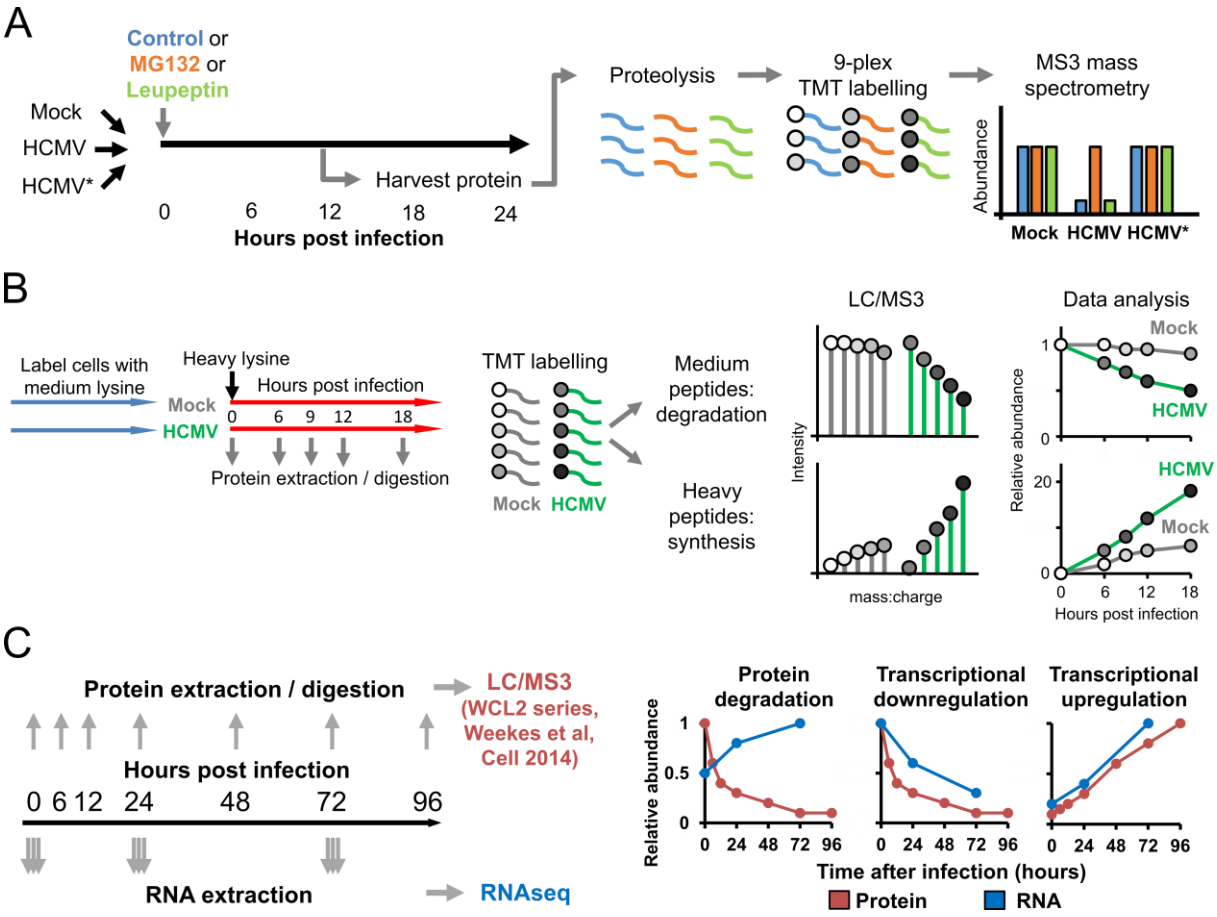

Figure 1.9: Proteomic screens used to identify proteins degraded by HCMV.

These figures have been reproduced from Nightingale, Lin *et al.* (2018) [62] (published under an open access Creative Commons CC-BY license). **(A)** Proteasome/lysosome screen. HFFF-TERTs were infected with either HCMV, irradiated HCMV (HCMV*) or mock-infected, and incubated in the presence of the proteasome inhibitor MG132 or the lysosomal protease inhibitor leupeptin. Proteins were harvested at 12, 18 or 24 hpi and quantified by TMT-based LC-MS3. **(B)** pSILAC screen. HFFF-TERTs were labelled with medium lysine prior to infection and heavy lysine following infection. Proteins harvested at different times after infection were labelled with different TMT reagents. **(C)** Transcriptome/proteome screen. RNA was extracted from HFFFs at different time points and analysed by RNA-seq. These data were then compared to the WCL proteomic data from the QTV study [86].

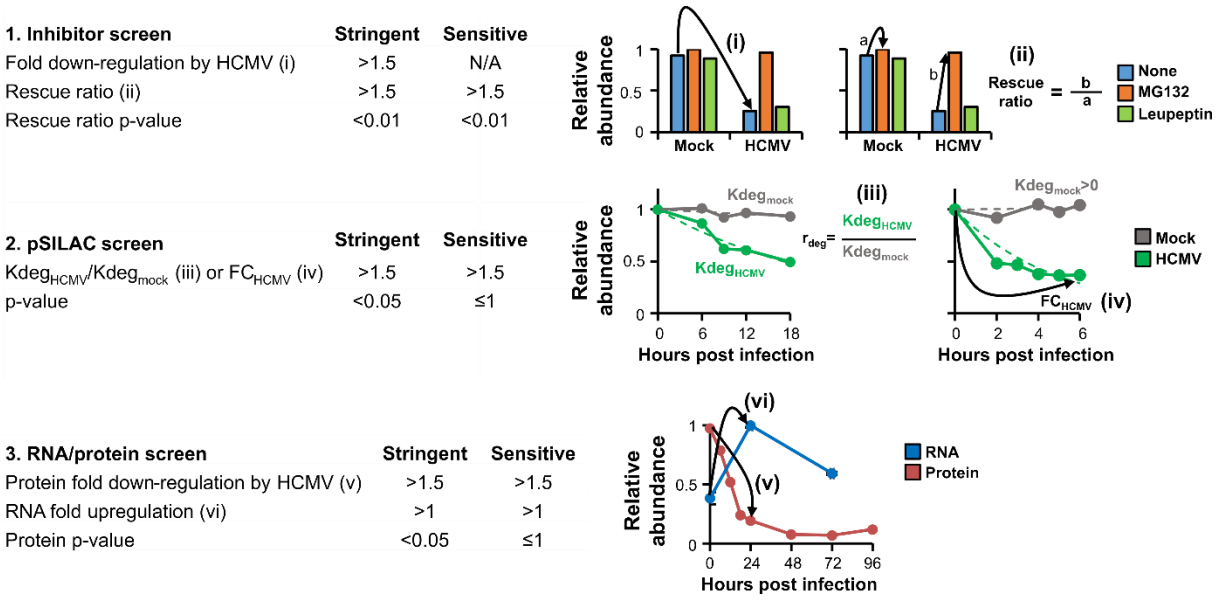

Figure 1.10: The 'sensitive' and 'stringent' criteria used to define putative degraded proteins.
This figure has been adapted from Nightingale, Lin *et al.* (2018) [62] (published under an open access Creative Commons CC-BY license).

1.4.6 Key study 3: The HCMV gene block deletion virus screen

Nightingale K, Lin K-M, Ravenhill BJ, *et al.* High-definition analysis of host protein stability during human cytomegalovirus infection reveals antiviral factors and viral evasion mechanisms. *Cell Host Microbe* 2018; **24**: 1-14

Nightingale K, Fielding CA, Zerbe C, *et al.* Human cytomegalovirus protein RL1 degrades the antiviral factor SLFN11 via recruitment of the CRL4 E3 ubiquitin ligase complex. *bioRxiv* 2021

The utility of QTV can be extended via the use of viral mutants to characterise the function of individual proteins or for unbiased screening of virus protein function. In Nightingale, Lin *et al.* (2018), 10 recombinant HCMV viruses, each lacking a block of nonessential genes, were used to identify gene blocks responsible for the observed effects on the cellular proteome [62]. Following identification of a block of genes responsible for downregulation of a specific protein, single-gene-deletion viruses covering genes in the block can then be screened. Data from the gene block deletion screen were reanalysed along with proteomic data generated for **Chapter 6** of this thesis to enable an extended and comparative analysis.

1.4.7 Key study 4: The HCMV interactome

Nobre L V, Nightingale K, Ravenhill BJ, *et al.* Human cytomegalovirus interactome analysis identifies degradation hubs, domain associations and viral protein functions. *Elife* 2019; **8**: e49894

Approaches that can be used alongside quantitative proteomics for the study of protein-protein interactions include immunoprecipitation (IP), yeast two-hybrid methods, hydrogen/deuterium exchange, and chemical cross-linking [179]. The HCMV interactome is based upon an IP-MS analysis of 169 exogenously expressed V5-tagged HCMV strain Merlin proteins in infected cells. This analysis identified >3,400 high confidence virus-host and >150 virus-virus protein interactions. Amongst many other findings, the study identified viral interactors of 31/133 host proteins shown to be degraded in the Nightingale, Lin *et al.* (2018) study. Furthermore, 51 viral proteins were identified as interactors of at least one E3 ligase, identifying potential mechanisms by which the virus manipulates the host UPS.

1.5 Original project aims

The overarching aim of the project described in this thesis was to identify novel ARFs from a shortlist of proteins degraded by HCMV. Once identified, the antiviral mechanism of the host proteins and mechanism of virus-mediated degradation would be characterised using a combination of functional assays, proteomics and classical biochemical techniques. Seven candidate ARFs were selected based on:

1. Evidence of protein degradation during infection, from the Nightingale, Lin *et al.* (2018) early degradation screens **(1.4.5)** [62];
2. Evidence of IFN-stimulation, based on unpublished data evaluating IFN-stimulated changes in the proteome and/or data from the interferome [200];
3. The literature, and/or;
4. QTV analysis of other virus infections, including VACV, HSV-1, EBV and KSHV.

The proteins selected for follow-up were ARHGAP35, DHCR24, DMXL1, FRMD6, IFIT2, LMAN2L, and MLKL. Full names and alternative names of the genes/proteins are listed in **Table 1.3**. ARHGAP35, DHCR24, DMXL1 and MLKL fell within the ‘high confidence’ shortlist of proteins degraded by HCMV, and LMAN2L within the ‘medium confidence’ shortlist [62]. FRMD6 and IFIT2 did not fall into either category but were degraded based on less-strict criteria and chosen due to other characteristics, detailed below.

Gene Symbol	*Description*	*Alternative names*
ARHGAP35	Rho GTPase-activating protein 35	GRF1 GRLF1 KIAA1722 P190A P190ARHGAP Glucocorticoid receptor DNA-binding factor 1 Glucocorticoid receptor repression factor 1 Rho GAP p190A
DHCR24	24-dehydrocholesterol reductase	KIAA0018 Δ^{24}-sterol reductase 24-dehydrocholesterol reductase 3-beta-hydroxysterol Delta-24-reductase Diminuto/dwarf1 homolog Seladin-1
DMXL1	DmX-like protein 1	
FRMD6	FERM domain-containing protein 6	C14orf31 Willin
IFIT2	Interferon-induced protein with tetratricopeptide repeats 2	ISG54 IFI54 ISG-54 K Interferon-induced 54 kDa protein
LMAN2L	Lectin mannose-binding 2 (LMAN2)-like	VIPL VIP36-like protein
MLKL	Mixed lineage kinase domain-like pseudokinase	

Table 1.3: Full and alternative names of the candidate ARFs.

Both the gene and protein will be referred to in this thesis using the gene symbol.

1.6 The seven candidate antiviral restriction factors

1.6.1 MLKL

Mixed lineage kinase domain-like pseudokinase (MLKL) is the non-enzymatic terminal effector of necroptosis, a form of programmed cell death (PCD) [201]. In multicellular organisms, PCD represents an integral cell-intrinsic antiviral defence mechanism. Necroptosis, along with other forms of PCD including apoptosis and pyroptosis, are activated in response to virus infection and/or signatures of the innate immune response. Cell death has the consequence of limiting virus replication and spread to uninfected neighbouring cells, while promoting or regulating the inflammatory and innate immune responses that serve to shape widespread antiviral defence.

There is significant intracellular cross talk between apoptotic and necroptotic pathways. Ligation of death receptors including tumour necrosis factor receptor 1 (TNFR1), TNF-related apoptosis-inducing ligand receptor 1 and 2 (TRAILR1/2) and Fas leads to apoptotic cell death that is dependent on the cleavage of procaspase-8 into its active form [202]. Active caspase-8 suppresses the necroptotic pathway, with inhibition of caspase-8 releasing this suppression and switching the pathway towards necroptosis [203,204]. Necroptosis relies on interactions between receptor-interacting serine/threonine-protein kinases 1 and 3 (RIP1/3) mediated by their RIP homotypic interaction motif (RHIM) domains [205] **(Figure 1.11)**. Oligomerisation of RIP1 and RIP3 results in the autophosphorylation of RIP3, which can then interact with and phosphorylate MLKL. Phosphorylation of MLKL releases it from an auto-inhibitory state, after which it oligomerises and interacts with the PM to cause cell swelling and membrane rupture [206–208]. Other RHIM domain-containing proteins, including ZBP1 and TIR domain-containing adapter molecule 1 (TRIF), a key propagator of the TLR3/4 signalling pathway, can also facilitate activation of the pathway via RIP3 **(Figure 1.11)**.

In order to suppress death receptor-stimulated extrinsic apoptosis, HCMV protein pUL36, or viral inhibitor of caspase-8 activation (vICA), directly interacts with procaspase-8 to prevent cleavage into its active form [209]. However, as inhibition of caspase-8 activity has the side effect of triggering necroptosis, HCMV would need to encode a separate mechanism to suppress necroptosis in order to evade cell death entirely.

A number of herpesviruses inhibit necroptotic signalling through the activity of viral RHIM-domain-containing proteins that can compete with host RHIM-domain adaptor proteins for binding to RIP3 [210–212]. However, HCMV does not encode any RHIM-domain proteins, and is instead thought to employ an early, pIE1-regulated protein to block necroptosis at a stage following MLKL phosphorylation [213].

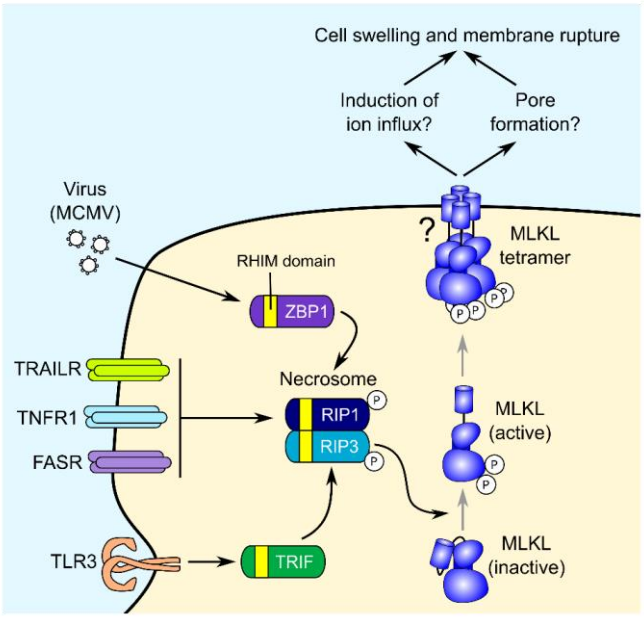

Figure 1.11: Simplified schematic of the necroptotic signalling pathway.
Necroptosis can be activated by death receptor stimulation, the cytoplasmic sensing of MCMV DNA by ZBP1, or the detection of PAMPs by TLR3/4. These three pathways converge with the assembly of a RIP1:RIP3 oligomeric complex termed the necrosome. This results in RIP3-dependent phosphorylation and activation of MLKL, which then interacts with the PM to cause cell swelling and loss of PM integrity. The nature of the interaction between MLKL and the PM, and the mechanism of membrane rupture, remains uncharacterised [201]. This figure was adapted from Fletcher-Etherington *et al.* (2020) [214].

MLKL was degraded, according to stringent scoring criteria **(Figure 1.10)**, in both the proteasome/lysosome screen and pSILAC screen **(Figure 1.12A and B)**. MLKL abundance was upregulated in cells infected with irradiated HCMV (HCMV*), indicating that HCMV infection stimulates or stabilises MLKL in the absence of gene expression, and/or that a product of viral gene expression is necessary to downregulate MLKL levels during infection **(Figure 1.12A)**. MLKL transcription was significantly upregulated in the early stages of infection (< 24 h), which may explain the upregulation of MLKL protein levels upon infection with HCMV* **(Figure 1.12C)**. Another screen observing proteomic changes in HFFF-TERTs upon IFN stimulation showed that MLKL is upregulated around two-fold by IFN (unpublished, results not shown).

The increase in MLKL transcripts at 24 hpi also indicates that the observed downregulation of MLKL protein occurs via a post-transcriptional mechanism. MLKL levels were also rescued by treatment with bortezomib, a specific proteasomal inhibitor, suggesting that inhibition of the proteasome is sufficient to inhibit MLKL downregulation **(Figure 1.12D)**.

Infection with HCMV strain AD169, in comparison to strain Merlin, rescued levels of MLKL **(Figure 1.12E)**. AD169 contains a deletion in the U_L/b' region of the genome, as well as mutations in genes RL5A, RL13, UL36 and UL131A. U_L/b' contains 20 putative ORFs which are often lost after passage in cell culture and therefore may represent viral functions necessary for latent infection and/or immune evasion *in vivo* [215].

QTV studies of other herpesviruses (HSV-1, EBV and KSHV) have not identified any downregulation of MLKL, with MLKL actually being upregulated around two-fold during EBV infection [192,194,216].

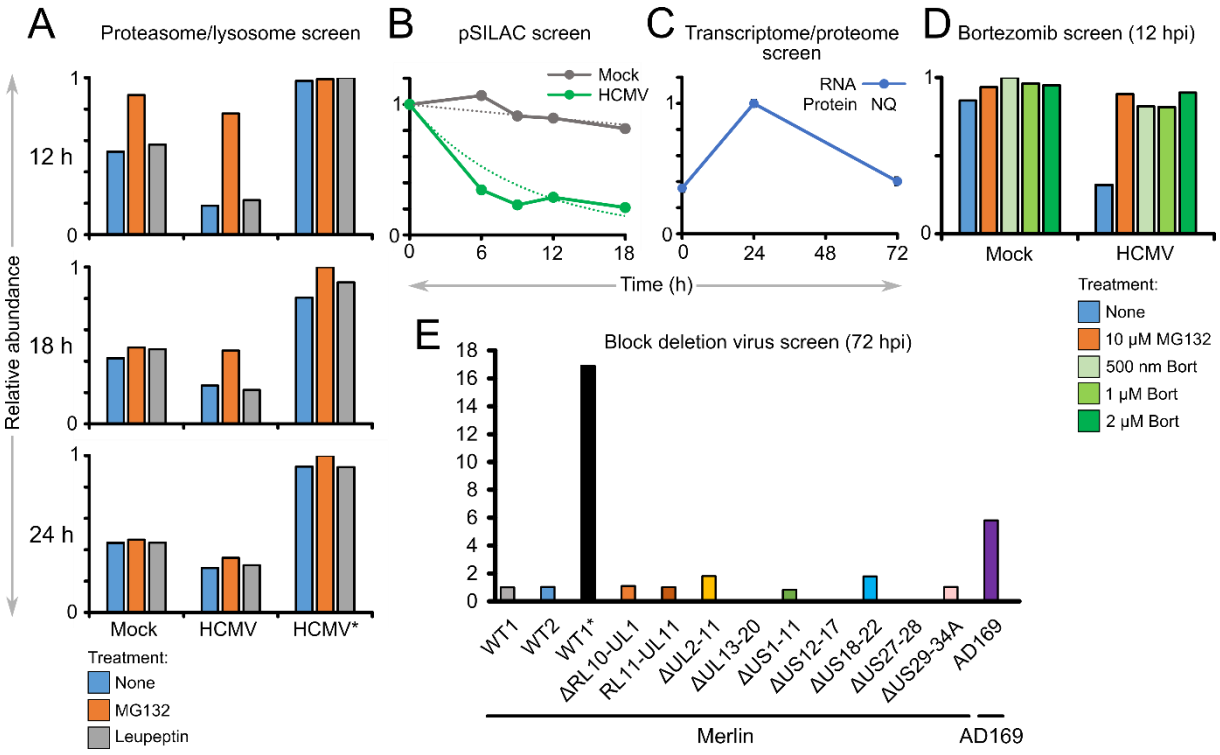

Figure 1.12: Evidence for the degradation of MLKL during HCMV infection.

(A-C) Figures generated from data published in Nightingale, Lin *et al.* (2018) [62] under a Creative Commons CC-BY license, relating to screens described in 1.4.5. **(D)** Figure generated from data published in Lin, Nightingale *et al.* (2021) [199] under a Creative Commons CC-BY license, relating to a screen described in 1.4.5 (MOI: 5, 12 h infection) **(E)** Figure generated from data published in Nightingale, Lin *et al.* (2018) based on a screen described in 1.4.6. HFFFs were infected with strain Merlin (WT1), WT1 that lacked UL16 and UL18 (WT2), one of nine block deletion viruses derived from WT1 or WT2, irradiated WT1 (WT1*) or strain AD169 (MOI: 10, 72 h infection). All y-axes show abundance relative the amount of protein/RNA in the sample with the highest abundance. NQ, not quantified; bort, bortezomib.

1.6.2 DMXL1

DmX-like protein 1 (DMXL1) was first identified as an evolutionarily-conserved homologue of the *Drosophila melanogaster* gene DmX, which encodes a large WD repeat protein [217]. Although poorly characterised, DMXL1 has been implicated in the regulation of the V-ATPase [218]. DMXL1 interacts with the ATPase V_1 sector, and knockdown of DMXL1 inhibits V-ATPase-mediated intracellular vesicle re-acidification [219,220].

Interestingly, HCMV is already known to downregulate the function of the V-ATPase via miR-US25-1, a microRNA that targets ATPase H^+-transporting V_0 subunit C (ATP6V0C) [221]. However, knockdown of ATP6V0C, and inhibition of the V-ATPase, has been shown to inhibit the replication of HCMV [222]. This has been explained by evidence showing that disruption of endosomal acidification impedes the formation of the VAC [221,222]. The reason for viral suppression of the V-ATPase, which is important for VAC formation and viral replication, remains elusive. Given that the V-ATPase is involved in a range antiviral of cellular processes, including autophagy, MHC class II presentation and PRR signalling, HCMV may downregulate DMXL1 and ATP6V0C to evade cell-intrinsic, innate and/or adaptive immune responses, at the expense of inhibiting VAC formation.

DMXL1 was degraded in both the proteasome/lysosome screen and pSILAC screen, according to stringent scoring criteria **(Figure 1.13A and B)**. Although there was no observed induction of DMXL1 upon infection with HCMV* in the proteasome/lysosome screen at 12-24 hpi, some increase was observed in the block deletion virus screen at 72 hpi **(Figure 1.13A and E)**. DMXL1 transcript levels increased through infection, suggesting that DMXL1 expression may be induced by infection and that the mechanism of DMXL1 protein downregulation is post-transcriptional **(Figure 1.13C)**. Although there was little downregulation of DMXL1 in the bortezomib screen, the small amount of downregulation observed was rescued by addition of bortezomib, implying that the degradation is proteasomal **(Figure 1.13D)**. Deletion of the US29-34A block restored levels of DMXL1 in two independent experiments **(Figure 1.13E)**, indicating that a gene (or genes) in this block is responsible for the degradation of DMXL1. This block contains seven uncharacterised viral genes: US29, US30, US31, US32, US33A, US34 and US34A.

DMXL1 was downregulated by around 40% over a course of EBV infection, but not upon HSV-1 infection or KSHV reactivation [192,194,216].

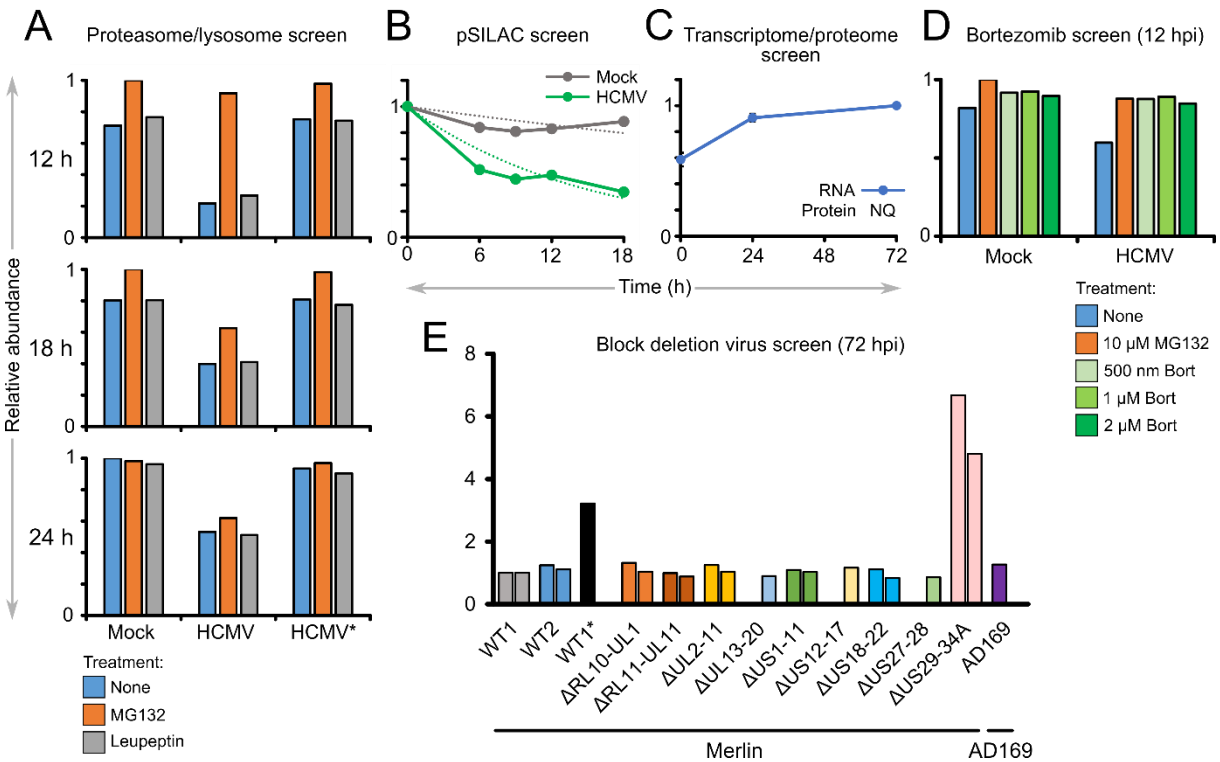

Figure 1.13: Evidence for the degradation of DMXL1 during HCMV infection.

As described in Figure 1.12.

1.6.3 ARHGAP35

Rho GTPase-activating protein 35 (ARHGAP35) was first characterised as a factor that associates with the promoter of the human glucocorticoid receptor (hGR) gene and represses its expression [223]. Glucocorticoids have been shown to increase transcription from the HCMV MIEP in a hGR-dependent manner, enhancing HCMV replication [224–226].

It was later discovered that ARHGAP35 has a second, seemingly unrelated function: stimulating the GTPase activity of Ras homolog family member A (RhoA) [227]. Inactivation of RhoA by converting RhoA-GTP to RhoA-GDP inhibits the formation of focal adhesions and stress fibres and promotes cell spreading, protrusion and polarity [227]. Interestingly, human papillomavirus protein E7 has been shown to suppress ARHGAP35 activity, negatively regulating cell spreading [228].

ARHGAP35 was degraded in all three of the early degradation screens, according to stringent criteria **(Figure 1.14A-C)**. Similarly to DMXL1, there was no observed induction of ARHGAP35 upon infection with HCMV* at the early time point **(Figure 1.14A)** but there was a significant seven-fold induction at 72 hpi **(Figure 1.14A and E)**. ARHGAP35 transcript levels increased very slightly by 24 hpi, at which point the amount of protein was already significantly reduced **(Figure 1.14C)**, indicating that the mechanism of downregulation is post-transcriptional. Again, a small amount of downregulation that was observed in the bortezomib screen was rescued upon addition of bortezomib, building confidence in the hypothesis that ARHGAP35 is proteasomally degraded. None of the genes covered by the gene block deletion viruses studied were shown to be necessary for ARHGAP35 downregulation **(Figure 1.14E)**, despite the fact that *de novo* viral gene expression is required for ARHGAP35 downregulation or to prevent ARHGAP35 induction, as indicated by the rescue of ARHGAP35 upon infection with HCMV*. This might be because ARHGAP35 is targeted by the redundant action of more than one viral protein, or because the viral gene(s) responsible do not lie within any of the gene blocks represented in this screen.

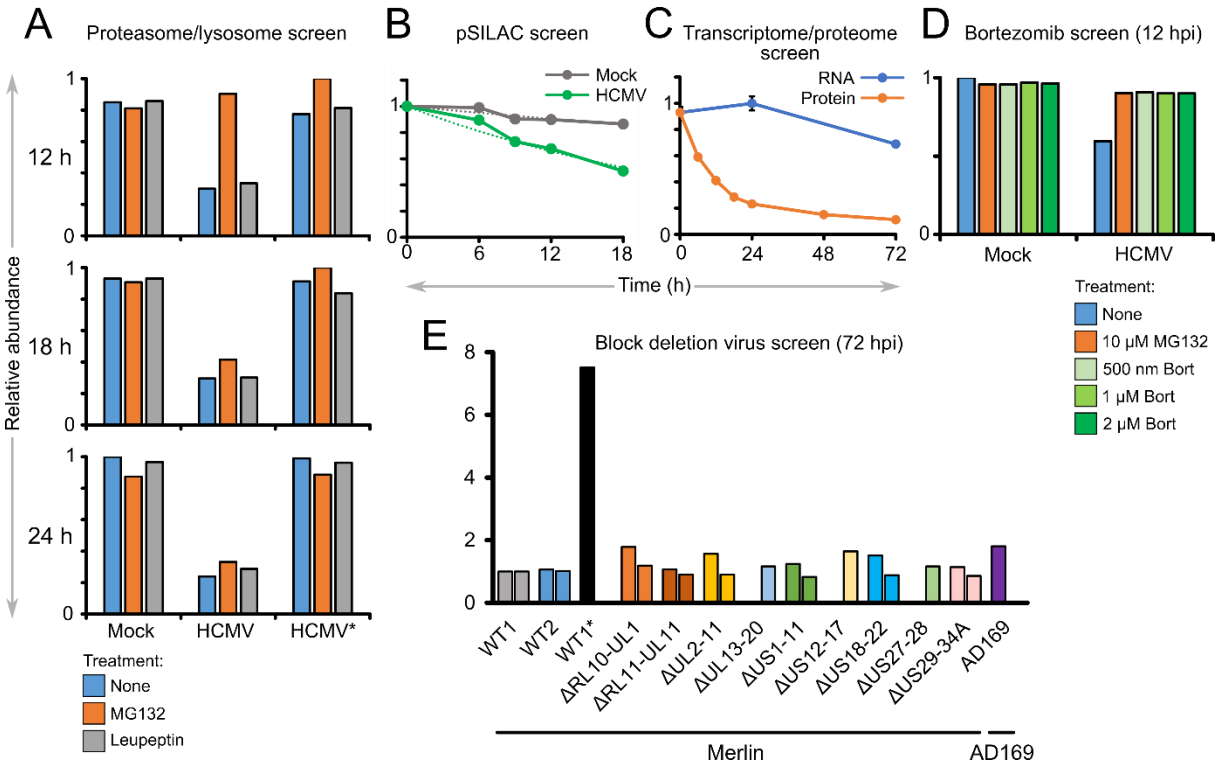

Figure 1.14: Evidence for the degradation of ARHGAP35 during HCMV infection.

As described in Figure 1.12.

1.6.4 DHCR24

24-dehydrocholesterol reductase (DHCR24) catalyses the last step in the Bloch pathway of cholesterol biosynthesis: the conversion of desmosterol to cholesterol [229,230]. DHCR24 has also been implicated in cell signalling, the formation of lipid rafts, cell stress responses, apoptosis and regulation of steroidogenesis [229,231]. Loss of DHCR24 is not lethal at the cellular level, as desmosterol can act as a surrogate for cholesterol in a number of functions [229]. However, desmosterol is unable to substitute for cholesterol in the formation of ordered membrane domains such as lipid rafts, which are involved in a number of signalling pathways [232,233]. Recently, hepatitis C virus (HCV) non-structural protein 3-4A has been shown to directly cleave DHCR24, resulting in increased levels of desmosterol and increased fluidity of the membranes where HCV replication occurs [234].

Despite downregulating DHCR24, HCMV infection is thought to cause an increase in cellular cholesterol levels, in part by downregulating the ATP binding cassette subfamily A member 1 (ABCA1) cholesterol efflux transporter [235] and increasing cholesterol esterification [236]. It is possible that downregulation of DHCR24 acts to regulate cellular cholesterol in a time- and location-specific manner without affecting global cholesterol levels.

DHCR24 was degraded in the proteasome/lysosome and pSILAC screens, according to stringent criteria, and the transcriptome/proteome screen as judged by sensitive criteria **(Figure 1.15A-C)**. DHCR24 levels were only rescued by MG132 at 12 hpi **(Figure 1.15A)** and this was not replicated in the bortezomib screen **(Figure 1.15D)**, so it remains to be seen whether DHCR24 downregulation is truly inhibited by MG132. DHCR24 transcript levels were slightly down at 24 hpi, and then increased significantly by 72 hpi **(Figure 1.15C)**. Although the mechanism of DHCR24 downregulation remains to be determined, it has been shown that HCMV protein pUS14 is necessary [146]. Deletion of the US12-17 block resulted in an increase in the amount of DHCR24 **(Figure 1.15E)**, and in a separate experiment, infection with ΔUS12-21 and ΔUS14 viruses restored levels of DHCR24 protein in comparison to cells infected with wild type (WT) HCMV at both the PM and WCL levels **(Figure 1.16)**. Deletion of genes US12-21 resulted in an increase in DHCR24 protein over the course of infection **(Figure 1.16A)**, which may be driven by host-mediated activation of transcription from 24-72 hpi **(Figure 1.15C)**.

DHCR24 is significantly downregulated upon reactivation of KSHV [216], upregulated during EBV infection [192], but remains constant during HSV-1 infection [194].

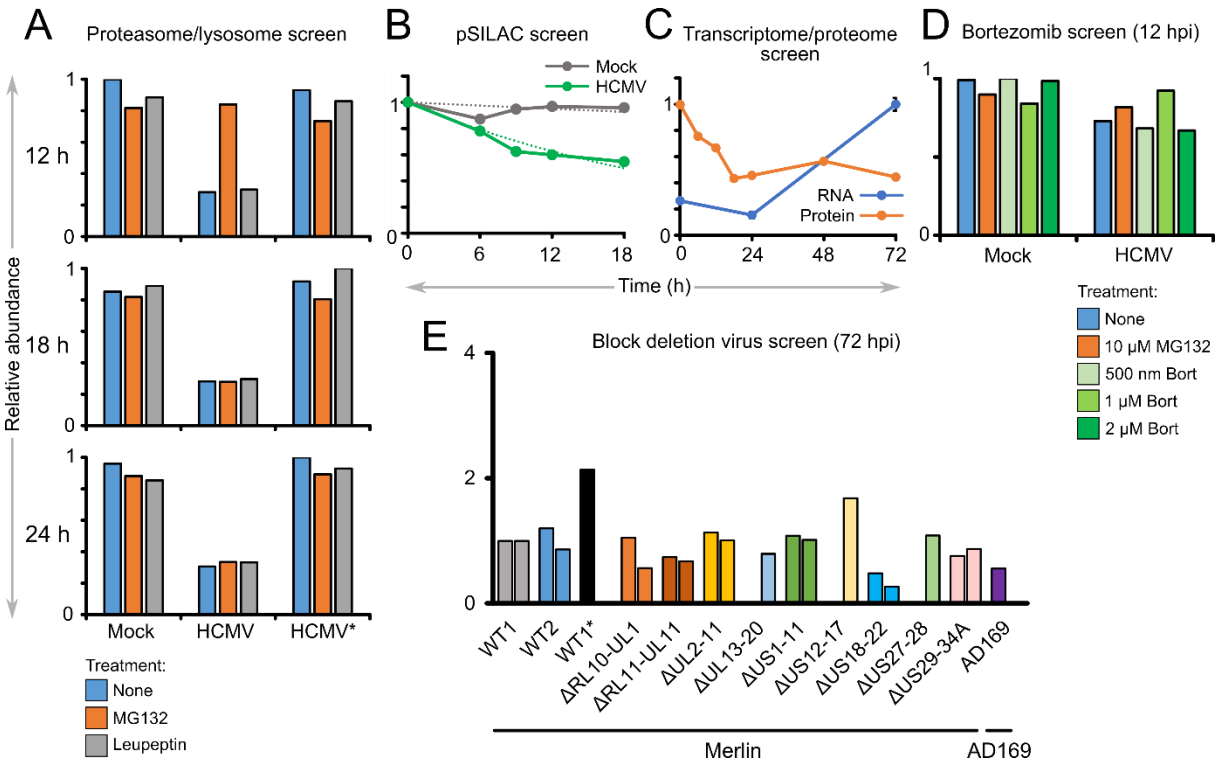

Figure 1.15: Evidence for the degradation of DHCR24 during HCMV infection.

As described in Figure 1.12.

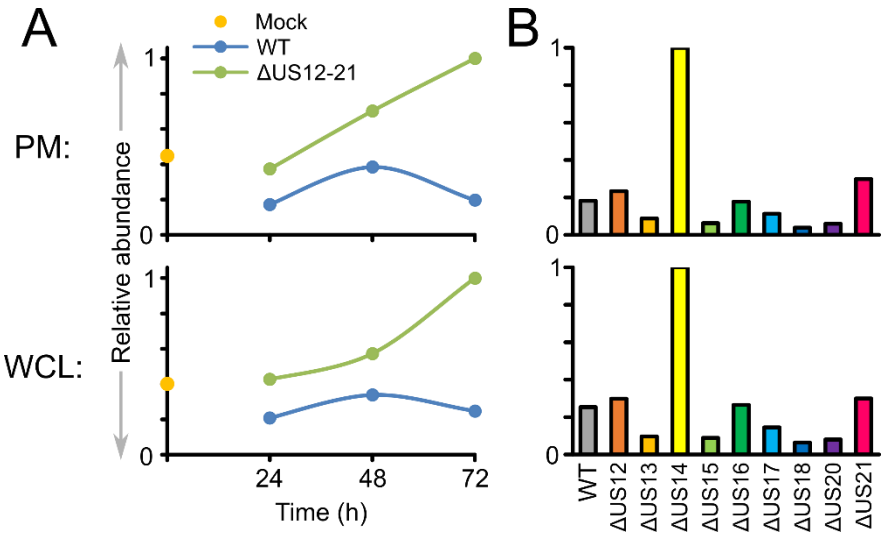

Figure 1.16: DHCR24 is downregulated by pUS14.

Both figures were generated from existing data published in Fielding *et al.* 2017 [146] under a Creative Commons CC-BY license. **(A)** HFFFs were infected with WT or ΔUS12-21 HCMV strain Merlin, or mock-infected (MOI: 10). WCLs and a PM-enriched fraction were prepared at different times post-infection and analysed by TMT-based LC-MS3. **(B)** HFFFs were infected with one of nine single-gene-deletion viruses or WT HCMV strain Merlin (MOI: 10). WCLs and a PM-enriched fraction were prepared at 72 hpi and analysed by TMT-based LC-MS3.

1.6.5 FRMD6

FERM domain-containing protein 6 (FRMD6) belongs to the 4.1 superfamily, members of which are characterised by their 4.1 ezrin radixin moasin (FERM) domains and their role in maintaining the submembrane actin cytoskeleton [237]. Although there has been conflicting evidence, FRMD6 expression has been shown to activate the Hippo pathway, increasing phosphorylation of multiple pathway components including YES1-associated transcriptional regulator (YAP) [238–241].

FRMD6 and the Hippo pathway have been implicated in several virus infections. FRMD6 is upregulated in response to stimuli that promote the lytic reactivation of the gammaherpesvirus EBV, indicating that downregulation of FRMD6 may promote latency [242]. Both hepatitis B virus (HBV) and KSHV upregulate YAP, which would presumably have a similar effect to downregulating FRMD6 [243,244].

FRMD6 was degraded in the proteasome/lysosome screen, according to stringent scoring criteria **(Figure 1.17A)**, and rescued by both MG132 and bortezomib at 12 hpi **(Figure 1.17A and D)**. In addition, MG132 led to upregulation of FRMD6 in mock-infected cells, suggesting that FRMD6 undergoes proteasome-dependent turnover under homeostatic conditions **(Figure 1.17A)**. FRMD6 transcript abundance decreased over the course of infection, indicating that FRMD6 levels may be regulated by both pre- and post-translational mechanisms **(Figure 1.17C)**. None of the genes covered by the gene block deletion viruses studied were shown to be necessary for FRMD6 downregulation **(Figure 1.17E)**.

FRMD6 was not on the high- or medium-confidence shortlists for degradation, but was selected for further investigation due to the fact that it was also significantly downregulated during both VACV and HSV-1 infection [194,196], indicating an important antiviral function.

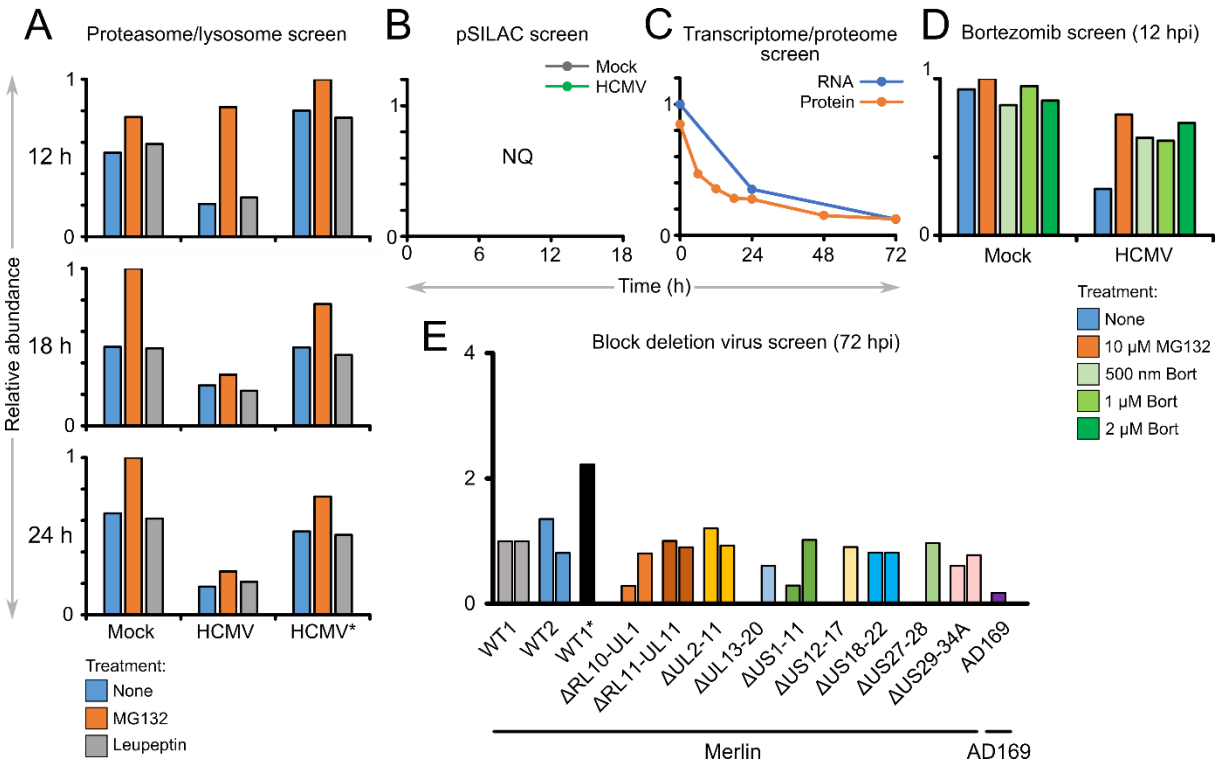

Figure 1.17: Evidence for the degradation of FRMD6 during HCMV infection.

As described in Figure 1.12.

1.6.6 IFIT2

Interferon-induced protein with tetratricopeptide repeats 2 (IFIT2) is one of four human IFITs, a family of proteins that are strongly induced by type I IFN, bind a diverse range of protein and nucleic acid ligands, and exhibit a number of antiviral functions [245]. Each IFIT has a range of binding partners, therefore having the potential to exhibit different antiviral effects. For example, IFIT2 has been shown to bind AU-rich double-stranded RNA [246] and eukaryotic translation initiation factor 3 (eIF3) subunits c and e to inhibit translation initiation [247].

IFIT2 was shown to restrict HBV replication [248], but at the start of this PhD project there was no evidence for a direct effect on viruses with DNA genomes. However, in 2019 it was shown that VACV protein C9 can target IFIT1, 2 and 3 for degradation via the UPS [249]. In the absence of C9, the IFIT proteins prevented genome uncoating and replication of VACV. Furthermore, individual depletion of IFIT1, 2 and 3 has been shown to increase KSHV virion production [250].

Observations of IFIT2 degradation were confounded by the large induction of IFIT2 at 12 hpi. As well as being stimulated by IFN, there is evidence for HCMV-induced selective activation of IFIT2 expression independent of the canonical IFNα/β signalling pathway [251–254]. However, the increase in IFIT2 levels in cells infected with HCMV* and upon MG132 and bortezomib treatment indicates that HCMV acts to limit the virus-induced increase in IFIT2 expression in a manner that is dependent on viral protein expression and the proteasome **(Figure 1.18A, D and E)**. IFIT2 protein abundance started to decrease by 18 hpi, while transcript levels remained high until 24 hpi, indicating that the mechanism of IFIT2 downregulation is post-transcriptional **(Figure 1.18C)**. None of the genes covered by the gene block deletion viruses studied were shown to be necessary for IFIT2 downregulation **(Figure 1.18E).**

QTV has shown that IFIT2 is downregulated during infection with VACV [196], and exhibits a gradual decline in EBV-infected cells following its initial upregulation [192].

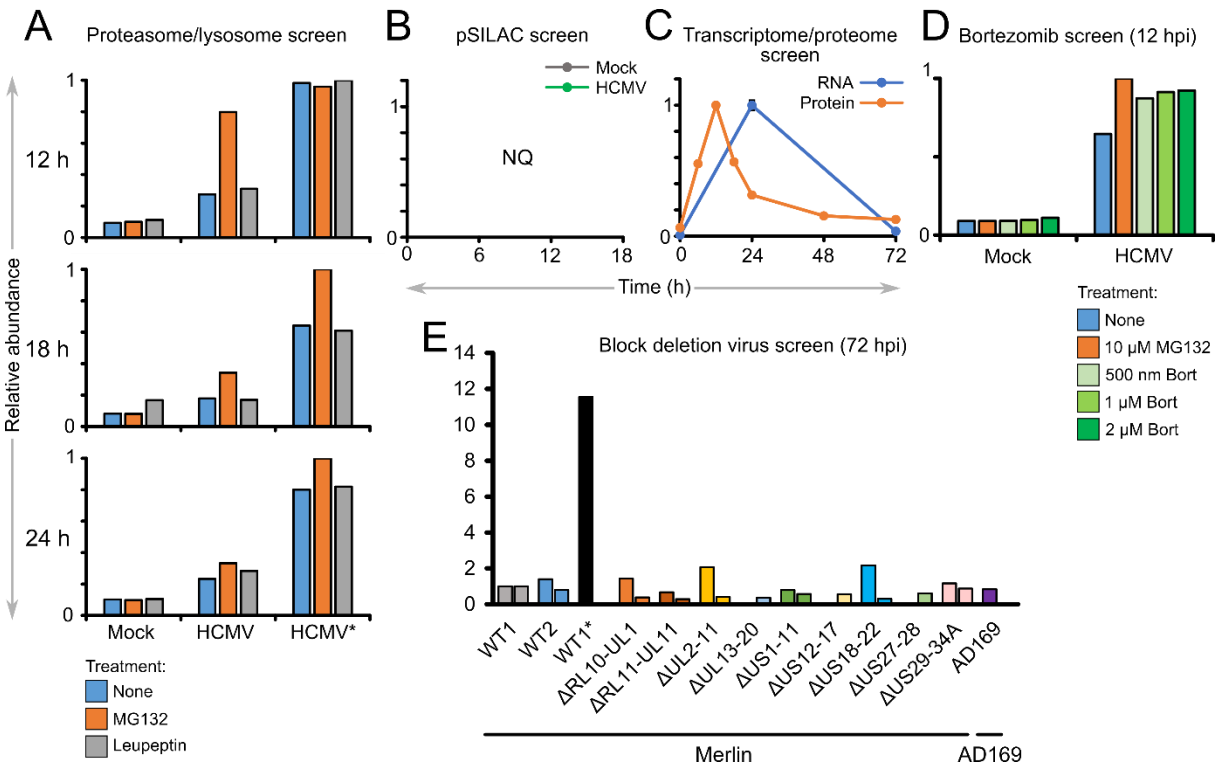

Figure 1.18: Evidence for the degradation of IFIT2 during HCMV infection.

As described in Figure 1.12.

1.6.7 LMAN2L

Lectin mannose-binding 2-like (LMAN2L) is a single-pass type I transmembrane glycoprotein resident in the ER. The function of LMAN2L remains elusive, but proposed roles include the regulation of glycoprotein trafficking through the ER, ER quality control, glycoprotein degradation, protein folding, and regulation of ER-Golgi intermediate compartment 53 kDa protein (ERGIC-53) [255–260].

LMAN2L was degraded in the proteasome/lysosome screen as judged by stringent criteria **(Figure 1.19A)**, with its downregulation at 12 h also rescued by bortezomib **(Figure 1.19D)**. Transcript levels were up at 24 hpi, suggesting that the mechanism of downregulation is post-translational **(Figure 1.19C)**. The gene block attributed to LMAN2L degradation was US1-11 **(Figure 1.19A)**. One of the genes in this region, pUS2, promotes the proteasomal degradation of a number of cell surface proteins, including the LMAN2L homolog LMAN2, although degradation of LMAN2 was not identified in our screens [188,261].

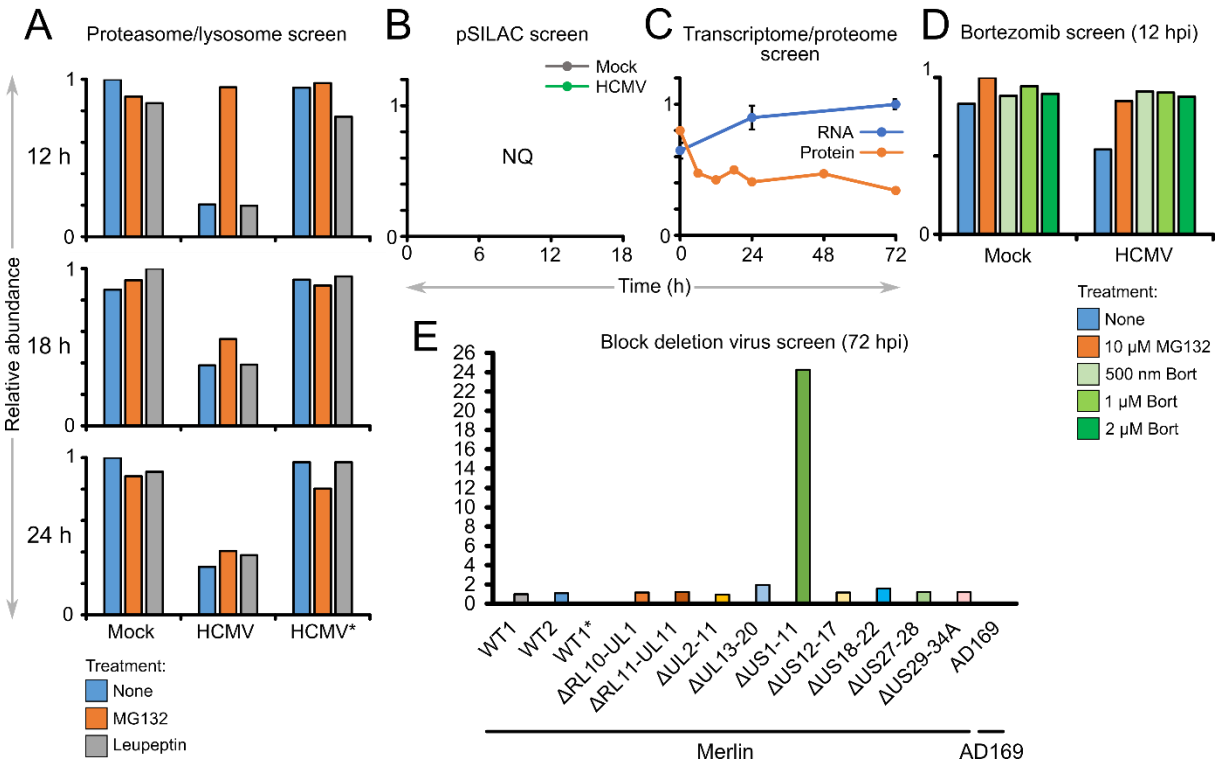

Figure 1.19: Evidence for the degradation of LMAN2L during HCMV infection.

As described in Figure 1.12.

1.7 Thesis overview

Chapter 3 describes how the seven candidate ARFs were screened for antiviral activity using restriction assays and plaque assays. Although many of the results obtained were inconsistent due to experimental variability imparted through short hairpin RNA (shRNA) transduction, there was no clear evidence of restriction by any of the proteins. However, ongoing analysis of the literature during this part of the project enabled formulation of some interesting hypotheses for the roles of MLKL and DMXL1 in infection, which were then selected for further follow-up (**Chapters 5** and **6**, respectively). Proteomics experiments aiming to determine the source of phenotypic variability among the shRNA cell lines identified global disruption of the cellular proteome. This effect was not observed in cell lines stably expressing exogenous protein or in small interfering RNA (siRNA)-transfected cells, therefore justifying the use of these techniques throughout the rest of the project. Furthermore, this chapter describes the development of a novel restriction assay system that enables control and test cell lines to be seeded and infected in the same well, reducing variability introduced through cell seeding. This system represents a positive methodological advancement that may enable identification of additional ARFs in the future.

Chapter 4 reports the results of a proteomic analysis that aimed to extend the MG132-based early degradation screen [62] to 48 hpi. Preliminary, unpublished data generated by our group and collaborators at Cardiff University suggested that MLKL was one of the proteins most significantly downregulated at 48 hpi. This experiment was repeated to build confidence in the observed effects, with data from the two biological replicates analysed in parallel. The finding that MLKL was significantly and consistently downregulated up until 48 h provided an indication of its important antiviral function.

Chapter 5 provides a functional and mechanistic analysis of MLKL downregulation. An IP of MLKL in the context of infection showed that MLKL interacts with HCMV protein pUL36. Using cell lines expressing UL36 and single-gene-deletion viruses lacking UL36, pUL36 was shown to be both necessary and sufficient for MLKL downregulation and the inhibition of necroptosis. The interaction between pUL36 and MLKL, and the ability of pUL36 to downregulate MLKL and suppress necroptosis, was dependent on a single cysteine residue at position 131 of pUL36. Although the exact mechanism of HCMV-mediated MLKL downregulation remains uncharacterised, proposals include proteasomal degradation, facilitated by interactions between pUL36 and cellular E3 ligases, or sequestration of MLKL in detergent-resistant membrane complexes. pUL36 is already well characterised as the viral inhibitor of apoptosis [209]. Results presented here therefore suggest that pUL36 is a multifunctional cell death inhibitor.

Finally, **Chapter 6** describes the results of a series of proteomic analyses of cells infected with single-gene-deletion viruses covering each of the genes in the US29-34A block, as well as cells constitutively expressing each of these genes. These experiments showed that uncharacterised HCMV protein pUS33A

was both necessary and sufficient for DMXL1 downregulation. These screens also facilitated an analysis of the other genes in this block, with indications that pUS31 is involved in the regulation of semaphorin-plexin signalling, and that pUS30 and pUS34A are involved in the regulation of innate immunity.

Each of the chapters have their own independent discussion sections, which summarise the findings, relevance and limitations of the results. Further experiments to develop on the work presented in this thesis are proposed in 'Future directions' boxes.

Chapter 2: Materials and Methods

2.1 Cells and cell culture

2.1.1 Cell lines

Human fetal foreskin fibroblast cells (HFFFs) immortalised with human telomerase (HFFF-TERTs), and HFFF-TERTs constitutively expressing the tetracycline (Tet) repressor were kindly provided by Dr. Peter Tomasec and Dr. Richard Stanton (Cardiff University). HFFF-TERTs are fully permissive to human cytomegalovirus (HCMV) infection and exhibit the same morphology and growth characteristics as non-immortalised HFFFs [262]. They have been tested at regular intervals since isolation to confirm that HLA and MHC class I polypeptide-related sequence A (MICA) genotypes, cell morphology and antibiotic resistance are unchanged. A number of experiments previously published by our group and cited in this thesis used primary, rather than immortalised, HFFFs. These are the gene block deletion virus screens described in **5.3.1**, **Figure 6.2** and **6.3** [62], the RNA-sequencing screen in **Figure 6.9** [62], and the whole cell lysate (WCL) and plasma membrane profiling (PMP) infection time courses described in **Figure 5.4** and **6.5.2** [86].

Mouse embryonic fibroblasts (MEFs) immortalised with simian vacuolating virus 40 large T antigen were a gift from Dr. Rachel Allison and Dr. Evan Reid (University of Cambridge) and are described in Allison *et al.* [263]. Human embryonic kidney cells (HEK293s) and HEK293s immortalised with large T antigen (HEK293T) were kindly provided by Professor Paul Lehner (University of Cambridge).

2.1.2 Growth of adherent cell lines

HFFFs, MEFs and HEK293s were grown in Dulbecco's Modified Eagle's Medium (DMEM) supplemented with 10% (v/v) fetal bovine serum (FBS), 100 U/ml penicillin and 0.1 mg/ml streptomycin (all from Sigma-Aldrich, hereinafter referred to as Sigma). For stable isotope labelling by amino acids in cell culture (SILAC) immunoprecipitations (IPs), HFFF-TERTs were grown for seven passages in SILAC DMEM (Thermo Fisher Scientific, hereinafter referred to as Thermo), which was supplemented with 10% dialysed FBS (Thermo), penicillin/streptomycin, 280 µg/ml L-proline (Sigma), and either medium (Arg 6, Lys 4) or heavy (Arg 10, Lys 8) amino acids (CK Isotopes) at 50 µg/ml. All cells were incubated at 37 °C in 5% (v/v) carbon dioxide in a static incubator.

2.1.3 Preparation of cells for long-term storage

Cells were pelleted at 400 × g for 5 min, resuspended in 1 ml freezing medium [FBS + 10% (v/v) dimethyl sulfoxide (DMSO, Sigma)] for every 3×10^6 to 5×10^6 cells, and transferred to cryovials in 1 ml

aliquots. Vials were cooled to -80 °C in a Nalgene Mr. Frosty (Sigma) for 24 h and then transferred to liquid nitrogen storage. To recover cells from storage, vials were thawed at 37 °C in a water bath for 1 min then transferred into a 75 cm^2 flask containing 14 ml of growth media.

2.2 Molecular biology

2.2.1 Generation of complementary DNA (cDNA)

RNA was extracted from cells using the RNeasy® Mini Kit (Qiagen) as per the manufacturer's instructions. 1 µg of RNA was treated with 1 µl TURBO deoxyribonuclease (DNase) (Thermo) and 5 µl 10× TURBO DNase buffer in a total volume of 50 µl. The mixture was incubated at 37 °C for 30 min. 5 µl of DNase inactivation reagent (Thermo) was added and incubated for 5 min at room temperature with occasional agitation. The samples were centrifuged for 1.5 min at 10,000 × g and then the RNA transferred to a fresh tube. 4 µl of RNA was mixed with 0.5 µg of $Oligo(dT)_{15}$ primer, heated at 70 °C for 5 min, and then chilled at 4 °C for 10 min. Next, 4 µl of GoScript™ 5× Reaction Buffer, 2 µl 25 mM magnesium chloride, 1 µl polymerase chain reaction (PCR) Nucleotide Mix [final concentration of 0.5 mM for each deoxynucleoside triphosphate (dNTP)], 0.5 µl of RNasin® Ribonuclease Inhibitor and 1 µl of GoScript™ Reverse Transcriptase (all Promega) were made up to a total volume of 15 µl per reaction in nuclease-free water (NFW, Thermo). 15 µl of the reverse transcription mix was added to the RNA primer mix, heated at 25 °C for 5 min and then 42 °C for 1 h. The reverse transcriptase was then inactivated in a heat block at 70 °C for 15 min.

2.2.2 Polymerase chain reaction (PCR)

PCR primers were designed to recognise the 5' and 3' ends of the gene or domain of interest and to contain *att*B sites for Gateway cloning **(2.3.1) (Appendix I)**. 1 µl template DNA (5-30 ng/µl) was mixed with 2.5 pmol of each primer, 1.25 µl 10× PfuUltra II reaction buffer (Agilent), 0.31 µl 10 mM dNTP mix (Thermo), 0.25 µl PfuUltra II Fusion HotStart DNA polymerase (Agilent) and diluted to 12.5 µl with NFW. The PCR programme began with an initial denaturation step at 94 °C for 4 min, proceeded with 30 cycles of 94 °C for 30 s, annealing temperature for 30 s, and 72 °C for 15 s per kilobase, and ended with a final extension at 72 °C for 5 min. The annealing temperature was the lower primer melting temperature of the two primers minus 5 °C. For cDNA templates, four reactions were set up per primer pair and run at a gradient of annealing temperatures. All reactions were carried out in a peqSTAR thermal cycler (VWR).

2.2.3 Agarose gel electrophoresis

DNA was run on 0.8-1.2% agarose (Sigma) gels containing 1× SYBR® Safe DNA gel stain (Life Technologies) in Tris-acetate-ethylenediaminetetraacetic acid (EDTA) (TAE) buffer. Samples were mixed with 5× GelPilot DNA Loading Dye (Qiagen). Electrophoresis was performed at 90 V for 45

min, before visualisation of the gel using an ultraviolet transilluminator. Bands of the correct size were extracted and purified with QIAquick Gel Extraction Kit (Qiagen) as per the manufacturer's instructions.

2.2.4 Annealing oligonucleotides

Complementary oligonucleotides encoding short hairpin RNA (shRNA) and CRISPR guides, which were designed to contain the desired restriction site sticky-ends, were synthesised by Sigma **(Appendix I)**. Oligonucleotides were phosphorylated by incubating with 10× T4 ligase buffer and T4 polynucleotide kinase [New England Biolabs, (NEB)] at 37 °C for 30 min. The oligonucleotides were annealed by heating at 95 °C for 10 min and cooling to room temperature.

2.2.5 Restriction digestion

Destination vectors were digested with restriction endonucleases [EcoRI-HF, BamHI-HF, ClaI, KpnI-HF (all NEB) or BpiI (Thermo)] (10 U per 1 µg DNA) in 10× CutSmart buffer (NEB) at 37 °C for 2 h. The vectors were then dephosphorylated by adding shrimp alkaline phosphatase (NEB) and incubating for a further 30 min at 37 °C. The vectors were then column purified with QIAquick Gel Extraction Kit (Qiagen), as described by the manufacturer's instructions for DNA clean up from enzymatic reactions.

2.2.6 DNA ligation

Vector and inserts were ligated at a ratio of 1:3 with T4 DNA ligase (NEB) in T4 ligase buffer to a final volume of 10 µl overnight at 4 °C.

2.2.7 Transformation of competent cells

5 µl of ligated DNA product or 1 µl of purified vector DNA was added to 20 µl of 5-alpha Competent *Escherichia coli* (*E. coli*) (NEB) and incubated on ice for 20 min. For amplification of pDONR and pHAGE-SFFV destination vectors encoding the ccdB toxin **(Appendix II)**, One Shot ccdB Survival 2 $T1^R$ Competent Cells (Thermo) were used. Cells were heat-shocked at 42 °C for 45 s and placed back on ice for 1 min. 200 µl of Luria-Bertani (LB) media was added and the cells then placed in a 37 °C shaking incubator for 1 h. The cells were then spread on LB/agar plates supplemented with the appropriate antibiotic (ampicillin, 100 µg/ml; spectinomycin, 50 µg/ml; kanamycin, 50 µg/ml) and incubated at 37 °C overnight. Single bacterial colonies were used to inoculate 5 ml of LB media containing the appropriate antibiotic (ampicillin, 500 µg/ml; spectinomycin, 50 µg/ml; kanamycin, 50 µg/ml). Cultures were shaken at 37 °C overnight. For long-term storage, 400 µl of bacterial culture was mixed thoroughly with 400 µl of 80% glycerol (Fisher Chemical) in sterile water, and stored at -80 °C.

2.2.8 Plasmid DNA isolation from bacteria

Plasmid DNA was purified from 2 ml of culture using the QIAprep Spin Miniprep Kit (Qiagen) according to the manufacturer's instructions and resuspended in elution buffer (10 mM Tris-HCl). Plasmids were stored at -20 °C.

2.2.9 DNA sequencing

Sanger sequencing of plasmid DNA and PCR products was performed by Genewiz [264].

2.2.10 Sequence analysis

DNA sequences were analysed using the pairwise sequence alignment tool EMBOSS Needle provided by EMBL-EBI [265], Lasergene (DNASTAR [266]) and SnapGene (GSL Biotech [267]).

2.3 Overexpression plasmids

2.3.1 Gateway cloning

The pHAGE-pSFFV lentiviral expression vector system used for overexpression of exogenous proteins utilises Gateway cloning technology (Thermo) [268]. 30 ng pDONR223 vector **(Appendix II)** was incubated with 0.5 µl *att*B-flanked PCR product and 0.4 µl Gateway BP Clonase II enzyme mix overnight at room temperature. After proteinase K (Thermo) treatment, the resulting entry clone was transformed into competent cells, the cells grown up in the presence of spectinomycin and the vector purified **(2.2.7-2.2.8)**. The entry clone was then used to donate the gene of interest to a destination vector (pHAGE-pSFFV, **Appendix II**): 30 ng pHAGE-pSFFV was combined with 30 ng of the entry clone and 0.4 µl Gateway LR Clonase II enzyme mix and incubated overnight at room temperature. The expression clone was proteinase K treated, transformed into competent cells in the presence of ampicillin and purified. Sequencing of regions inserted into pDONR223 and pHAGE-pSFFV vectors was achieved using primers described in **Appendix I**.

2.3.2 pHAGE-pSFFV overexpression plasmids

2.3.2.1 pHAGE-pSFFV-BSR

The original pHAGE-pSFFV expression vector encoded puromycin resistance (puroR) **(Appendix II)**. The puromycin resistance gene was replaced by an insert encoding the blasticidin resistance gene (BSR) and flanking regions that were removed by restriction enzyme digestion **(Appendix I)**. 400 ng of the insert and 2 µg of the pHAGE-pSFFV-puroR vector were digested with ClaI and KpnI-HF as described in **2.2.5**. The vector was dephosphorylated and purified by running on a 0.8% agarose gel and extracting with QIAquick Gel Extraction Kit (Qiagen). The insert was purified using the same kit as described by the manufacturer's instructions for DNA clean up from enzymatic reactions. The vector and insert were ligated as described in **2.2.6**.

2.3.2.2 mCherry and iRFP

pDONR223 entry clones encoding mCherry and near-infrared fluorescent protein (iRFP) were made by Dr. Benjamin Ravenhill (University of Cambridge). mCherry and iRFP were cloned into the pHAGE-pSFFV-BSR vector using a Gateway LR reaction **(2.3.1)**.

2.3.2.3 ARHGAP35, DHCR24, LMAN2L, IFIT2, FRMD6, MLKL and DAXX

ARHGAP35 entry clone (pDONR225) was obtained from Addgene (Plasmid #70296). This plasmid does not contain a stop codon at the end of the ARHGAP35 coding sequence, meaning ARHGAP35 is fused to FLAG and hemagglutinin (HA) tags when expressed from pHAGE-pSFFV. DHCR24 and LMAN2L entry clones (pDONR221) were obtained from Harvard Plasmid (HsCD0045422 and HsCD00295987, respectively).

MLKL, IFIT2 and FRMD6 were cloned by PCR from cDNA **(2.2.1-2.2.3)** using primers described in **Appendix I**, and recombined into pDONR223 and then pHAGE-pSFFV-puroR using Gateway cloning **(2.3.1)**. pHAGE-pSFFV-puroR-DAXX (death domain-associated protein) was kindly provided by Dr. Katie Nightingale (University of Cambridge).

2.3.2.4 Viral proteins

Plasmids expressing V5-tagged HCMV proteins were generated by Dr. Luís Nobre (University of Cambridge) [269]. The viral genes were cloned from a library of recombinant adenovirus vectors (UL24, UL36-38, UL133-150, and UL29-34A) or synthesised as a double-stranded DNA fragment (UL150A) (gBlocks®, Integrated DNA Technologies), before being cloned into the pHAGE-pSFFV-puroR vector using Gateway cloning **(2.3.1)**.

2.3.2.5 UL36 amino acid mutants

Five separate amino acid mutations were made in the sequence encoding HCMV strain Merlin UL36 by site-directed mutagenesis. Site-directed mutagenesis was performed in two rounds of PCR using primers described in **Appendix I**. In the first round, two pairs of primers were employed in two separate PCRs using a plasmid containing the wild type (WT) gene as the template. In the first reaction, a reverse primer encompassing the point mutation was combined with a forward primer that recognised the 5' end of the gene. In the second reaction, a forward PCR primer encompassing the point mutation was combined with a reverse primer recognising the 3' end of the gene. A second round of PCR joined the two PCR products using primers recognising the 5' and 3' ends of the gene. The resulting sequences were cloned into the pHAGE-pSFFV-puroR vector using Gateway cloning **(2.3.1)**.

2.3.2.6 MLKL-HA domains

C-terminal HA-tagged full-length MLKL and four C-terminal HA-tagged MLKL domains were cloned using primers described in **Appendix I** by PCR **(2.2.2-2.2.3)**. For the domains, the primers were

designed according to locations of the well-characterised four-helix bundle, brace region, and pseudokinase domain of MLKL [200,307].

All MLKL-HA sequences were cloned into the pHAGE-pSFFV-puroR vector using Gateway cloning **(2.3.1)**.

2.3.2.7 UL36-V5 domains

Six C-terminal V5-tagged UL36 constructs were made encoding different regions corresponding to the location of US22-like domains predicted by HHpred and regions that were predicted to be ordered by I-TASSER and trRosetta **(2.20)**. The sequences were cloned from a vector encoding full-length pUL36 (originally made by Dr. Luís Nobre) by PCR using primers outlined in **Appendix I**, into the pHAGE-pSFFV-puroR vector using Gateway cloning **(2.3.1)**. Full-length pUL36-V5 was also cloned into the pHAGE-pSFFV-BSR vector so it could be co-transduced into cells expressing the MLKL domain constructs from pHAGE-pSFFV-puroR.

2.3.2.8 US33A

An untagged version of the viral gene US33A, US33A with an N-terminal V5 tag separated by a serine-alanine linker (V5-SA-US33A), US33A with an N-terminal V5 tag separated by a glycine-glycine-glycine-serine linker (V5-GGGS-US33A) and US33A with a C-terminal V5 tag separated by a glycine-glycine-glycine-serine linker (US33A-GGGS-V5) were cloned from a pHAGE-pSFFV vector encoding US33A with a C-terminal V5 tag separated by an SA linker (originally made by Dr. Luís Nobre). Cloning was performed by PCR as described in **2.2.2** and **2.2.3** using primers listed in **Appendix I**. The PCR products were then recombined into pHAGE-pSFFV-puroR using Gateway cloning **(2.3.1)**.

2.4 shRNA plasmids

shRNA target sequences were taken from commercial shRNA products that had been validated for the gene of interest, or taken from the literature. Oligonucleotides were designed to contain the target sequences and BamHI and EcoRI overhangs **(Appendix I)** for cloning into the lentiviral pHR-SIREN vector (a gift from Professor Paul Lehner, **Appendix II**). Each pair of oligonucleotides **(Appendix I)** were phosphorylated, annealed and cloned into vector pHR-SIREN as described in **2.2.4**-**2.2.6**. The vector was transformed into bacteria in the presence of ampicillin **(2.2.7)**. Presence of the insert was confirmed by sequencing with primer U6P **(Appendix I)**. HLTF sh1 and sh2, FRMD6 sh1 and sh2, and control sh2 shRNA constructs were made by Dr. Kai-Min Lin (University of Cambridge). Speckled protein of 100 kDa (Sp100) sh1 and ctrl sh1 shRNA constructs were made by Dr. Luís Nobre. IFIT2 sh1 and sh2 and DHCR24 sh1 and sh2 constructs were made by Dr. Katie Nightingale. pLKO shDPS [triple knockdown plasmid targeting DAXX, promyelocytic leukemia (PML) and Sp100] and pLKO

shNEG (control) were kindly donated by Dr. Mandy Glass (University of the West of Scotland) and are described in Glass *et al.* 2013 [270].

2.5 CRISPR plasmids

CRISPR knockout cell lines were created following protocols described in Sanjana *et al.* and Shalem *et al.* [271,272]. Four guide RNA (gRNA) oligonucleotides targeting each gene were selected from the Sabatini library **(Appendix I)** [273]. Each pair of oligos were phosphorylated and annealed as described in **2.2.4.** 100 ng of pKLV-U6gRNA(BbsI)-PGKpuro2ABFP plasmid (Addgene Plasmid #50946), a gRNA expression vector from Kosuke Yusa [274], was mixed with 800 nmol of the oligonucleotide duplex, 10× FastDigest buffer (Thermo), 1 nmol dithiothreitol (DTT, Thermo, **Appendix III**), 10 nmol adenosine triphosphate (NEB), 0.5 µl BpiI (Thermo), 0.25 µl T4 ligase and diluted to 10 µl with Milli-Q water. The digestion-ligation reaction was incubated at 37 °C for 5 min followed by 23 °C for 5 min, 6 times, and then transformed into *E. coli* in the presence of ampicillin **(2.2.7)**. Presence of the insert was confirmed by sequencing with primer U6P **(Appendix I)**.

2.6 Stable cell line production

2.6.1 Lentivirus generation

24 h prior to transfection, 1.5×10^5 HEK293T cells/well were seeded into a 12-well plate. 500 ng lentiviral expression plasmid was combined with two helper plasmids [200 ng VSV-g and 400 ng pCMV.DR8.91, both kindly provided by Professor Paul Lehner], 3 µl TransIT-293 transfection reagent (Mirus) and diluted in 100 µl OptiMEM (Thermo). The mixture was incubated for half an hour at room temperature before adding dropwise to the HEK293Ts.

2.6.2 Transduction

The transfection reagent/DNA mix was incubated with the cells for 24 h, after which the media was changed. After a further 24 h, the supernatant was collected, diluted, and filtered through a 0.22 µm filter onto the desired cells that were seeded 24 h previous in a 12-well plate. The lentiviral supernatant was diluted to a concentration that would be expected to give around 30% transduction rate, and therefore the dilution factor had to be optimised for each vector. 48 h after transduction, cells were placed under antibiotic selection [puromycin (Acros organics) 1 µg/ml for 1 week, hygromycin (TOKU-E) 50 µg/ml for 1 week, blasticidin (TOKU-E) 10 µg/ml for 2 weeks].

2.6.3 Transduction for generation of CRISPR populations

For expression of CRISPR guides, pKLV vectors expressing a given gRNA were transduced into HFFF-TERTs stably expressing pSpCas9(BB)-2A-GFP (PX458) Cas9 plasmid (Addgene Plasmid #48138) from Dr. Feng Zhang (Massachusetts Institute of Technology, USA) [275], in the presence of 2 µM

raltegravir to prevent gRNA integration. Transduced cells were selected in puromycin for 2 days. Cells were kept in raltegravir-supplemented media for one week.

2.7 Single cell cloning

Cells from polyclonal CRISPR populations were seeded into a 96-well plate at a density of 0.5 cells/well in 50:50 fresh/conditioned media. Media was conditioned by incubating with subconfluent WT HFFF-TERTs for 3 days and then filtered through a 0.22 µm filter. After 3-4 weeks, single cell-derived clones were transferred to 24-well plates for expansion.

2.8 TOPO® cloning

Genomic DNA was isolated from monoclonal CRISPR cell lines using DNeasy Blood and Tissue kit (Qiagen). A PCR was performed with primers **(Appendix I)** that bound at least 100 bp upstream or downstream of the relevant CRISPR target sequence. 500 ng template DNA was mixed with 0.5 µM of each primer, 5 µl 10× PCR buffer (Qiagen), 1 µl 10 mM dNTP mix (Qiagen), 10 µl Q-solution (Qiagen) and 0.25 µl HotStarTaq DNA polymerase (Qiagen) in a total volume of 50 µl. The PCR programme began with an initial heat activation step of 95 °C for 15 min, proceeded with 35 cycles of 94 °C for 45 s, annealing temperature for 45 s, 72 °C for 1 min, and ended with a final extension at 72 °C for 10 min. 25 µl of the PCR reaction was run on a 1.2% agarose gel **(2.2.3)** to check for bands of the correct length. The rest of the PCR reaction was purified using QIAquick PCR Purification Kit (Qiagen). 1 µl of the PCR product was then used in a TOPO® cloning reaction with 1 µl of the pCR™4-TOPO® vector (Thermo) and 1 µl salt solution (Thermo), in a total volume of 6 µl, and incubated for 5 min at room temperature. Next, 2 µl of the reaction was transformed into *E. coli* in the presence of kanamycin **(2.2.7)**. Plasmid DNA from 10 colonies per cell line was purified and sent for sequencing, and the CRISPR modifications identified by aligning with the WT gene sequence **(2.2.8-2.2.10)**.

2.9 Small interfering RNA (siRNA) transfection

HFFF-TERTs were seeded into a 6-well plate and transfected with ON-TARGETplus SMARTPool siRNAs (Horizon) **(Appendix I)**. For 48 h siRNA treatments, cells were seeded at a density of 3×10^5 cells/well. For siRNA treatment of cells prior to infection, cells were seeded at a density of 1.3×10^5 or 2×10^5 cells/well **(Table 2.2)**. 24 h later, for each well, 5 µl lipofectamine RNAiMAX (Thermo) was mixed with 145 µl OptiMEM and left for 5 min at room temperature. 5 µl of siRNA (20 µM) was added to 145 µl OptiMEM and then added to the RNAiMAX mixture and left for 15 min at room temperature. The mixture was then added to the well containing 2 ml DMEM + 10% FBS. Cells were typically harvested 48 h after transfection unless otherwise stated.

2.10 Quantitative PCR (qPCR)

cDNA was generated as described in **2.2.1** and diluted 1:10 in NFW.

2.10.1 TaqMan™ qPCR

For each reaction, 10 µl of TaqMan™ Gene Expression Master Mix (Thermo) was mixed with 1 µl TaqMan™ Gene Expression Assay primers (dye FAM-MGB) for the given target gene or control [glyceraldehyde 3-phosphate dehydrogenase (GAPDH)] in a total volume of 18 µl. 18 µl reaction mix was transferred to each well of a MicroAmp® Optical 96-Well Reaction Plate (Life Technologies) or a 96-well Hard-Shell PCR plate (Bio-Rad). 2 µl of the diluted cDNA template was added to each well. For each sample and a no-template control, the expression of both the target gene and an endogenous control (GAPDH) was analysed in triplicate. The qPCR was performed using a 7500 Real Time PCR System (Applied Biosystems) or a Bio-Rad CFX96 Touch Real-Time PCR Detection System. The thermal cycling protocol was as follows: 50 °C for 2 min, 95 °C for 10 min, followed by 40 cycles of 95 °C for 15 s and 60 °C for 1 min, followed by the system's default protocol for generating a melt curve to check for non-specific binding.

2.10.2 SYBR Green qPCR

qPCR analysis of US33A expression in infected cells and transduced HFFF-TERTs was performed using the SYBR Green system. For each reaction, an 18 µl reaction mix consisting of 10 µl 2× Fast SYBR Green Master Mix, 1 µl of each primer (10 µM) **(Appendix I)** and 6 µl NFW was added to each well of a 96-well Hard-Shell PCR plate (Bio-Rad), along with 2 µl of diluted cDNA. For each sample and a no-template control, the expression of both the target gene and a control (GAPDH) was analysed in duplicate. The qPCR was performed using a Bio-Rad CFX96 Touch Real-Time PCR Detection System. The thermal cycling protocol was 95 °C for 2 min, followed by 40 cycles of 95 °C for 15s and 60 °C for 1 min, followed by the system's default protocol for generating a melt curve to check for non-specific binding.

2.10.3 Data analysis

The comparative cycle threshold (Ct) (ΔΔCt) method was used to calculate relative gene expression based on average Ct values from the technical replicates. Where biological replicates were performed, average relative expression across the biological replicates was calculated and standard error of the mean displayed in the error bars.

2.11 Viruses

2.11.1 Recombinant viruses

The genome sequence of HCMV strain Merlin is designated the reference HCMV sequence by the National Center for Biotechnology Information [67,276]. A recombinant version (RCMV1111) of this strain was derived by transfection of a sequenced bacterial artificial chromosome clone [67]. RCMV1111 contains point mutations in two genes (RL13 and UL128), which enhance replication in fibroblasts [67]. RCMV1502 is a RCMV1111 recombinant that has tet-operators 5' to UL128 and RL13 coding sequences (Merlin-RL13tetO-UL128tetO,) and is described in Stanton *et al.* (2010) [67]. These two viruses form the background of all other recombinant viruses used in this project, as detailed in **Table 2.1**. All viruses were made by Dr. Richard Stanton and colleagues (Cardiff University). Whole-genome consensus sequences of passage 1 of each recombinant virus were confirmed using the Illumina platform by Jenna Nichols and Professor Andrew Davison (University of Glasgow) [145]. The sequences of the deleted genes from the ΔUS29-34A single-gene-deletion viruses, which have not been described in published work, are listed in **Appendix IV**.

RCMV Number	*Description*	*Background*	*Reference*
1111	Merlin (Merlin*)		[67]
1502	Merlin-RL13tetO-UL128tetO (Merlin**)		[67]
1278	Merlin ΔUL16/ΔUL18, UL32-GFP	1111	[62,145]
2582	Merlin UL36-P2A-GFP	1111	[269]
2344	Merlin ΔRL13 UL36-P2A-GFP	1111	[62]
2270	Merlin UL36-P2A-GFP	1502	
2288	Merlin ΔUL36	2270	[214]
2289	Merlin ΔUL36 exon 2	2270	
1333	Merlin ΔRL10-UL1	1278	
2209	Merlin ΔRL11-UL11	1111	
1293	Merlin ΔUL2-UL11	1278	
1295	Merlin ΔUL22A-UL25	1278	
1528	Merlin ΔUS1-US11	1278	[62,145]
1297	Merlin ΔUS12-US17	1278	
1318	Merlin ΔUS18-US22	1278	
1299	Merlin ΔUS27-US28	1278	
1300	Merlin ΔUS29-US34A	1278	
3082	Merlin ΔUS29	2582	
3066	Merlin ΔUS30	2582	
3083	Merlin ΔUS31	2582	
3045	Merlin ΔUS32	2582	
3037	Merlin ΔUS33A	2582	
2936	Merlin ΔUS34	2582	
2935	Merlin ΔUS34A	2582	
N/A	AD169		[145]
288	AD169 GFP		[262]

Table 2.1: Recombinant viruses used in this project.

2.11.2 Virus infection

HFFF-TERTs were seeded to achieve 70-80% confluence at the point of infection **(Table 2.2)**. The required volume of viral stock to achieve the multiplicity of infection (MOI) described in **Table 2.2** was diluted in serum-free DMEM, mixed gently and applied to HFFF-TERTs. Mock infections were performed identically but with DMEM instead of viral stock. Time zero was considered the time at which cells first were exposed to virus. Cells were incubated with virus for 2 h at 37 °C on a rocking platform, and then the medium was replaced with DMEM + 10% FBS.

For some experiments, cells to be infected were grown in serum free media with 4 µg/ml dexamethasone (Sigma) for 24 h before the infection, to increase the efficiency of infection **(Table 2.2)** [225]. For experiments investigating protein degradation, growth media was replaced with that supplemented with 10 µM MG132, 12 h before harvesting the cells for analysis **(Table 2.2)**.

Experiment	***Flask/well/ dish size***	***Seeding density***	***Dexamethasone and/or MG132?***	***MOI***
Restriction assay ***(Chapter 3)***	24-well	1.35×10^5 cells/well	None	0.01-0.3
Plaque assay ***(Chapter 3)***	12-well	1.3×10^5 cells/well	None	0.006-0.02
48 h degradation screen repeat 2 ***(Figure 4.1)***	T25	8×10^5 cells/flask	Dexamethasone and MG132	10
Immunoblots for MLKL ***(Figure 5.2B and C)***	T25	1×10^6 cells/flask	Dexamethasone and MG132	5
SILAC IP ***(Figure 5.3A)***	10 cm^2 dish	3×10^6 cells/dish	Dexamethasone and MG132	3
Immunoblot for MLKL ***(Figure 5.5)***	12-well	1.1×10^5 cells/well	Dexamethasone	5
Necroptosis assays ***(Figure 5.9A and C)***	96-well	1.4×10^3 cells/well	None	5
Infection of FBXO3/UBAC1 siRNA cells ***(Figure 5.15B)***	6-well	2×10^5 cells/well (prior to siRNA treatment)	Dexamethasone	5
US29-34A single-gene-deletion virus screen ***(Figure 6.3)***	T25	5×10^5 cells/flask	Dexamethasone	7.5
RNF123/UBAC1 knockdown screen ***(Figure 6.9)***	6-well	1.3×10^5 cells/well (prior to siRNA treatment)	Dexamethasone	5

Table 2.2: Details of the virus infection experiments presented in this thesis.

2.11.3 Generation of virus stocks

Virus stocks were prepared by growing the virus in HFFF-TERTs or HFFFs expressing tetracycline (for tet-regulated viruses) as described in Stanton *et al.* (2007) [277]: 5-10 175 cm^2 flasks of cells at 70-80% confluence were infected with virus at an MOI of 0.01 **(2.11.2)**. The media was changed twice a week until approximately 70% of cells showed cytopathic effect. The supernatant was then harvested and stored at -80 ˚C and fresh media added onto the cells. The supernatant was harvested every two days until all the cells were dead. All harvests were thawed in a 37 ˚C water bath. Cell debris was pelleted by spinning at 1500 rpm for 5 min. The supernatants were then transferred into 250 ml high-speed centrifuge bottles. The virus was pelleted by spinning at 14,000 rpm for 2 h at 35 ˚C in an Avanti JXN-26 centrifuge (Beckman Coulter) with a JLA-16.250 rotor without the brake. The supernatant was then discarded and the pellets resuspended in 0.5 ml DMEM + 10% FBS for every flask infected. The pellets were broken up using a 19G 1.5" needle and syringe. The supernatant was then aliquoted into 100 µl aliquots and frozen at -80 ˚C.

2.11.4 Titration of virus stocks

1.35×10^5 HFFF-TERTs were seeded into a 24-well plate. 24 h later, the cells were infected with four-fold serial dilutions from 1:16 to 1:4096, in duplicate **(2.11.2)**.

After 24 h of infection, the infected cells were harvested and fixed. For viruses expressing green fluorescent protein (GFP), cells were fixed as described in **2.13**. For viruses with no endogenous GFP expression, cells were stained for HCMV protein IE1 **(2.12.1)**. Infected cells were counted by flow cytometry **(2.12.2)**, and the number of infected cells used to infer the concentration of infectious virus particles in each stock. The virus titre could not be calculated according to plaque-forming units (pfu) as the strain Merlin viruses used by our group do not produce clearly demarcated plaques that are easily quantifiable (see **3.7**).

For all virus infection experiments presented in this thesis, the MOI was defined as the number of virus particles capable of initiating productive infection of a single cell, determined by the presence of GFP (for viruses expressing a GFP-tagged protein) or IE1 expression, per cell. This method produced highly reproducible results, both for experiments that required a low MOI (restriction assays) and those that required near to 100% infection (proteomics experiments).

2.12 Flow cytometry

2.12.1 Intracellular staining for flow cytometry

Cells were washed in phosphate-buffered saline (PBS), trypsinised, resuspended in media and then spun down at 400 × g for 5 min. The supernatant was removed and the pellet resuspended in 200 µl of 4% paraformaldehyde and incubated for 20 min at 4 °C. 800 µl of PBS was added and the cells spun down

at 800 × g for 5 min. The supernatant was removed, the pellet resuspended in 200 µl of 100% ice cold methanol and incubated for 15 min at 4 °C. 800 µl of PBS/2% FBS was added and the cells spun down as before. The supernatant was removed, the cells resuspended in 25 µl PBS/2% FBS/10% (v/v) Human TruStain FcX™ (BioLegend) and then incubated for 10 min at 4 °C. Cells were then probed with the primary antibody (HCMV IE1, EMD Millipore, MAB810R, 1:1000) in PBS/2% FBS for 1 h at room temperature. 950 µl of PBS/2% FBS was added and the cells spun down as before. The cell pellet was resuspended in 50 µl of secondary antibody [anti-mouse Alexa Fluor® 488, Cell Signalling Technology (CST), 4408S, 1:1000] and incubated for 1 h at room temperature. 950 µl of PBS/2% FBS was added and the cells spun down as before. The cell pellet was then resuspended in 250 µl PBS and stored at 4 °C.

2.12.2 Flow cytometry and analysis

Infected cells were counted using a BD LSRFORTESSA flow cytometer (two-colour restriction assays) or a BD FACSCalibur flow cytometer (infection titrations) and analysed with FlowJo vX software [278].

2.13 Restriction assay

1.35×10^5 cells/well were plated into a 24-well plate. For two-colour restriction assays, iRFP HFFF-TERTs expressing the desired shRNA or overexpression construct, and mCherry HFFF-TERTs expressing the corresponding control construct were counted, diluted to 1.35×10^5 cells/ml, and mixed thoroughly at a 1:1 ratio before seeding. 24 h later, cells were infected with HCMV Merlin UL36-GFP (RCMV2344) in a total volume of 200 µl per well **(2.11.2)**. After a further 24 h, cells were trypsinised in 200 µl trypsin, 200 µl media added to inactivate the trypsin, and then a further 200 µl of 4% paraformaldehyde Fixation Buffer (BioLegend) added to fix the cells. After incubating at room temperature for 15 min, cells were spun down at 800 × g for 5 min and the cell pellet resuspended in 250 µl PBS. Infected cells were counted by flow cytometry **(2.12.2)**.

2.14 Plaque assay

2.14.1 Infection and fixation

1.3×10^5 cells/well were seeded into a 12-well plate. 24 h later, cells were infected with HCMV AD169-GFP (RCMV288) in a total volume of 400 µl **(2.11.2)**. The concentration used was 6×10^3 infectious particles per ml for assays on overexpression cell lines and 2×10^3 infectious particles per ml for assays on shRNA and CRISPR cell lines. The virus was removed and 3 ml of a 1:1 mix of 2× DMEM **(Appendix III)** and Avicel (FMC BioPolymer) was added onto the cells. After 2 weeks, the DMEM/Avicel was removed and the cells were washed thoroughly with PBS. For plaque analysis, cells

were fixed with 4% paraformaldehyde for 20 min and then stored in PBS. For flow cytometry analysis, cells were treated as described in **2.13 and 2.12.2**. All conditions were performed in biological triplicate.

2.14.2 Image capture and quantitation

Photographs of the plaques were taken on either an EVOS FL Imaging System with a 10× objective (small plaques) or an AxioObserver Inverted Microscope with a 5× objective (larger plaques). Using ImageJ, pictures of GFP-positive plaques were converted into monochromatic images according to a set GFP threshold and the total area of the plaque determined.

2.15 Immunoblotting

2.15.1 Sample preparation

To generate RIPA lysates, cells were lysed in radioimmunoprecipitation assay (RIPA) buffer (CST, **Appendix III**) containing cOmplete EDTA-free Protease Inhibitor Cocktail (Roche) for 15 min at 4 °C. To generate sodium dodecyl sulphate (SDS) lysates, cells were lysed in 2% SDS [20% SDS (Thermo) diluted in PBS] supplemented with protease inhibitors and 2.5 U/µl benzonase (Sigma) for 30 min at 37 °C. Supernatants were sonicated and insoluble cellular debris spun down at 14,000 × g for 10 min. A bicinchoninic acid (BCA) assay (Pierce) was used to measure protein concentration. 40 µg of protein (unless otherwise stated in the figure legend) was reduced by adding 6× Protein Loading Dye **(Appendix III)** and boiled for 5 min at 95 °C.

2.15.2 Protein separation, transfer and staining

Proteins were separated by SDS-polyacrylamide gel electrophoresis (PAGE) using Mini-PROTEAN TGX precast gels (Bio-Rad). Samples were loaded into wells and run in running buffer **(Appendix III)** at 100 V for around 1.5 h. Precision Plus Protein™ Standards ladder (Bio-Rad) was used to determine protein size. Proteins were transferred to polyvinylidene fluoride membranes (0.45 µm pore, Immobilon) using the Trans-Blot system (Bio-Rad) at 0.35 milliampere for 1 h 15 min in transfer buffer **(Appendix III)** containing 20% (v/v) methanol. For proteins over 250 kDa, 10% methanol was used. After blocking in 5% (w/v) milk (Marvel) in TBS-T [1× Tris-buffered saline (TBS) with 0.2% (v/v) TWEEN (NBS Biologicals)] for 1 hour, membranes were incubated with the primary antibody **(Table 2.3)** in 2% milk/TBS-T overnight at 4 °C. Membranes were then washed three times in TBS-T, incubated with the secondary antibodies **(Table 2.3)** in 2% milk/TBS-T for 1 hour at room temperature, and washed as before.

2.15.3 Quantitative analysis of immunoblots

Membranes were imaged using Odyssey CLx Imaging System (LI-COR) and images processed and quantified using Image Studio Lite V5.2 (LI-COR). Protein levels were quantified by determining the

signal of each band relative to the background and normalising against a control protein, GAPDH or calnexin (CANX).

Primary antibodies	***Manufacturer***	***Code***	***Dilution***
ARHGAP35	Abcam	ab85950	1:1000
CANX	LifeSpan BioSciences	B6881	1:1000
CUL1	Thermo	#71-8700	1:500
DAXX	Sigma	D7910	1:1000
DHCR24	CST	2033S	1:1000
DMXL1	Proteintech	24413-1-AP	1:300
FBXO3	Santa Cruz	sc-514625	1:300
FRMD6	CST	14688S	1:500
GAPDH	R&D Systems	MAB5718	1:10000
HA	CST	C29F4	1:1000
HLTF	Abcam	ab17984	1:1000
IE1/2 (HCMV)	Abcam	ab53495	1:1000
IFIT2	Proteintech	12604-1-AP	1:1000
LMAN2L	Novus Biologicals	NBP1-84152	1:100
MLKL	CST	14993S	1:1000
Sp100	GeneTex	GTX131570	1:2000
UBR5	Novus Biologicals	NB100-1591	1:2000
V5	Thermo	R960-25	1:2000
	CST	13202S	1:1000
Secondary antibodies	***Manufacturer***	***Code***	***Dilution***
IRDye 680RD goat anti-mouse	LI-COR	925-68070	1:10000
IRDye 680RD goat anti-rabbit	LI-COR	926-68071	1:10000
IRDye 800CW goat anti-mouse	LI-COR	926-32210	1:10000
IRDye 800CW goat anti-rabbit	LI-COR	925-32211	1:10000

Table 2.3: Antibodies for immunoblotting.

2.16 Immunoprecipitation

2.16.1 Cell preparation and lysis

For IPs in the absence of infection, 6×10^6 HFFF-TERTs were seeded into a 15 cm^2 dish and incubated for 24 h. For IPs in the presence of infection, 3×10^6 HFFF-TERTs were seeded into a 10 cm^2 dish, and 24 h later treated with 4 µg/ml dexamethasone. After another 24 h, the cells were infected with WT HCMV strain Merlin (RCMV1111) at an MOI of 3 for 24 h, with 10 µM MG132 added for the latter 12 h of infection. Additional details for individual experiments are provided in **Table 2.4**. Cells were washed twice with ice cold PBS and harvested in 1 ml mammalian cell lysis buffer (MCLB) **(Appendix III)**. The samples were tumbled on a rotator for 15 min at 4 °C and then centrifuged at 16,100 × g for 15 min at 4 °C. Immobilised mouse monoclonal anti-V5 or anti-HA agarose resin (Sigma) was washed

three times in MCLB (spinning at 2000 × g for 2 min each time) and diluted approximately two-fold in MCLB. Lysates were clarified by filtration through a 0.7 µm filter and incubated for 3 h with 30 µl of 50% agarose resin. Samples were transferred into Pierce™ Spin Columns (Thermo) and washed multiple times with MCLB and PBS (for proteomic analysis, seven washes with each; for immunoblot analysis, two washes with each).

Immunoprecipitation	***Details***	***Analysis***
Full-length MLKL-HA in infected cells ***(Figure 5.3A)***	10 µM MG132 added for the last 12 h of infection. MCLB with 300 mM sodium chloride (NaCl).	Mass spectrometry
Full-length UL36-V5 ***(Figure 5.3B)***	12 h MG132 treatment (10 µM). MCLB with 300 mM NaCl	Mass spectrometry
UL36-V5 amino acid mutants ***(Figure 5.11)***	12 h MG132 treatment (10 µM). MCLB with 300 mM NaCl.	Immunoblot
UL36-V5 domains ***(Figure 5.12C)***	Two IPs performed, one with 300 mM NaCl and one with 50 mM NaCl.	Immunoblot
MLKL-HA domains in UL36-V5-expressing cells ***(Figure 5.12D)***	MCLB with 50 mM NaCl.	Immunoblot

Table 2.4: Details of the immunoprecipitation experiments.

2.16.2 Sample preparation for proteomic analysis

Proteins bound to the resin were eluted twice with 200 µl of 250 µg/ml V5 (Alpha Diagnostic International) or HA (Sigma) peptide in PBS at 37 °C for 30 min with agitation. The medium- and heavy-labelled samples were then combined and frozen at -20 °C. Proteins were precipitated by adding trichloroacetic acid (TCA) to the frozen lysates to a total concentration of 20% (v/v) and incubating for 45 min at 4 °C. The precipitate was spun down at maximum speed for 30 min at 4 °C. The supernatant was removed and the pellet washed with 1 ml 10% TCA, before centrifuging for 20 min at 4 °C. The pellet was washed three times with cold acetone (Fisher Chemical) (spinning between each wash, as before) and then dried to completion in a centrifugal vacuum. The proteins were then digested in 20 µl digestion buffer **(Appendix III)** and incubated at 37 °C overnight with agitation. The digestion reaction was quenched with 50 µl 50% formic acid (FA, Thermo) and the peptides subjected to C18 solid-phase extraction using a StageTip assembly **(2.17.5)** and dried in a centrifugal vacuum. Samples were

resuspended in 10 µl 4% acetonitrile (AcN, Sigma)/5% FA in high-performance liquid chromatography (HPLC) grade water (VWR) and analysed by mass spectrometry (MS) as described below **(2.18.2)**.

2.16.3 Sample preparation for immunoblot analysis

Proteins bound to the resin were incubated with 40 µl 2.5 mg/ml V5 or 5 mg/ml HA peptide at 37 °C for 1 h with agitation then eluted. Proteins were reduced with 6× Protein Loading Dye **(Appendix III)** at 95 °C for 5 min prior to separation of half the sample by SDS-PAGE as described in **2.15**. For the input blot, 1.5-2% of the original lysates were removed prior to IP, and heated in 6× Loading Dye at 95 °C for 5 min prior to SDS-PAGE.

2.17 Whole cell lysate proteomics sample preparation

A range of proteomic experiments are presented in this thesis, some of which used lysates or data that were not generated by myself. For clarity, a summary of the proteomic experiments presented in this thesis are described in **Table 2.5**. For all experiments, operation of the mass spectrometer was conducted by Dr. Robin Antrobus (Cambridge Institute for Medical Research Proteomics Facility).

Experiment	***Reference***	***Experimental methods done by others***	***Experimental methods done by the author***	***Mass spectrometry runs used for data analysis***
shRNA cell line proteomics ***(Figure 3.25)***	Unpublished		Entire protocol	Single-shot
48 h degradation screen repeat 1 ***(Figure 4.1)***	[214]	Infection and cell lysis was performed by Dr. Peter Tomasec and sample preparation by Dr. Michael Weekes.	Data analysis	Single-shot and fractions
48 h degradation screen repeat 2 ***(Figure 4.1)***	[214]		Entire protocol	Fractions
US29-34A single-gene-deletion virus screen ***(Figure 6.3)***	Unpublished		Entire protocol	Fractions
US29-34A gene expression screen ***(Figure 6.4)***	Unpublished		Entire protocol	Fractions
US33A expression screen ***(Figure 6.6)***	Unpublished		Entire protocol	Fractions
ΔUS33A time course ***(Figure 6.7)***	Unpublished	Infection and sample preparation was performed by Dr. Katie Nightingale.	Data analysis	Fractions
RNF123/UBAC1 knockdown screen ***(Figure 6.9)***	Unpublished		Entire protocol	Fractions
DMXL1 siRNA knockdown screen ***(Figure 6.10)***	Unpublished		Entire protocol	Single-shot
Whole cell lysate gene block deletion virus screen ***(Figure 6.11)***	[62]	Infection and cell lysis was performed by Dr. Katie Nightingale.	Data analysis	Fractions
Plasma membrane gene block deletion virus screen* ***(Figure 6.12)***	Unpublished	Infection and cell lysis was performed by Dr. Ceri Fielding and the sample preparation by Dr. Katie Nightingale.	Data analysis	Single-shot and fractions

Table 2.5: Summary of the proteomics experiments presented in this thesis.

* Note that this experiment analysed a plasma membrane-enriched fraction rather than WCLs. The experimental method is described in [86,190].

2.17.1 Cell lysis

All reagents used for proteomic sample preparation were made up in HPLC grade water. Cells were washed twice with ice cold PBS and lysed in 6 M guanidine lysis buffer **(Appendix III) (Table 2.6)**. Cells were scraped in lysis buffer, removed to an Eppendorf tube, vortexed extensively and sonicated. Samples were kept on ice throughout. Cell debris was removed by centrifuging at 13,000 × g for 10 min twice. For samples harvested from T25 flasks in 250 µl of lysis buffer **(Table 2.6)**, the samples were split in two and half of the sample taken forward for protein digestion. Otherwise, the entire sample was used.

Experiment	*Flask/well size*	*Volume of lysis buffer*
shRNA cell line proteomics ***(Figure 3.25)*** *48 h degradation screen repeat 2* ***(Figure 4.1)*** *US29-34A single-gene-deletion virus screen* ***(Figure 6.3)*** *US29-34A gene expression screen* ***(Figure 6.4)*** *US33A expression screen* ***(Figure 6.6)***	T25	250 µl
RNF123/UBAC1 knockdown screen ***(Figure 6.9)*** *DMXL1 siRNA knockdown screen* ***(Figure 6.10)***	6-well	100 µl

Table 2.6: Details of the cell lysis protocols performed for proteomic analysis of whole cell lysates.

2.17.2 Protein digestion

DTT was added to a final concentration of 5 mM and the samples incubated at room temperature for 20 min. Cysteines were alkylated with 14 mM (final concentration) iodoacetamide (Sigma, **Appendix III**) and incubated for 20 min at room temperature in the dark. Excess iodoacetamide was quenched with DTT (the same volume originally added for disulphide bond reduction) for 15 min. Samples were diluted with 200 mM HEPES pH 8.5 to a final concentration of 1.5 M guanidine followed by digestion with LysC protease **(Appendix III)** for 3 h at room temperature at a 1:100 protease-to-protein ratio. Samples were further diluted with 200 mM HEPES pH 8.5 to a final concentration of 0.5 M guanidine. Trypsin (Promega, **Appendix III**) was then added to a concentration of 3.33 ng/µl followed by overnight incubation at 37 °C. The reaction was quenched with FA to a concentration of 2% (v/v) and centrifuged at 21,000 × g for 10 min to remove undigested protein.

2.17.3 C18 solid-phase extraction (Sep-Pak)

Peptides were subjected to C18 solid-phase extraction: 50 mg C18 columns (Sep-Pak, Waters) were attached to a vacuum manifold. The C18 material was activated with two washes with 1 ml of 100% AcN and one wash with 1 ml 70% AcN/1% FA. The column was then washed three times with 1 ml 1%

FA. The sample was loaded onto the column and allowed to run through slowly before washing three times with 1% FA. Peptides were eluted with two elutions of 350 µl 70% AcN/1% FA. The samples were vacuum-centrifuged for 2-3 h at room temperature to complete dryness, then resuspended thoroughly in 60-100 µl 200 mM HEPES pH 8.5 depending on the expected peptide yield. Peptide concentration was measured by microBCA (Thermo) according to the manufacturer's instructions.

2.17.4 Peptide labelling with tandem mass tags

Peptides were labelled with either 11plex tandem mass tag (TMT) or 16plex TMTpro reagents (Thermo) [279] **(Table 2.7)**. 25-50 µg of peptide from each sample was made up to a minimum equal volume in 200 mM HEPES pH 8.5. TMT reagents (0.8 mg) were dissolved in 45 µl anhydrous AcN (Acros Organics). AcN was added to each sample so that the final concentration after the addition of TMT would be 28-30% (v/v) AcN. 5 µl of TMT reagent was added to each sample and incubated at room temperature for 1 h.

11plex TMT label	*Reagent*	*16plex TMT label*	*Reagent*
1	TMT^{10}-126	1	TMTpro-126
2	TMT^{10}-127N	2	TMTpro-127N
3	TMT^{10}-127C	3	TMTpro-127C
4	TMT^{10}-128N	4	TMTpro-128N
5	TMT^{10}-128C	5	TMTpro-128C
6	TMT^{10}-129N	6	TMTpro-129N
7	TMT^{10}-129C	7	TMTpro-129C
8	TMT^{10}-130N	8	TMTpro-130N
9	TMT^{10}-130C	9	TMTpro-130C
10	TMT^{10}-131	10	TMTpro-131N
11	TMT11-131C	11	TMTpro-131C
		12	TMTpro-132N
		13	TMTpro-132C
		14	TMTpro-133N
		15	TMTpro-133C
		16	TMTpro-134N

Table 2.7: Details of the 11plex TMT and 16plex TMTpro reagents.

2.17.5 C18 solid-phase extraction (StageTip)

TMT-labelled samples were combined at a 1:1 ratio so that the final amount of protein was 10-12 µg. The TMT was then quenched with hydroxylamine (Thermo, **Appendix III**) to a final concentration of 0.5% (v/v). FA was added to a total concentration of 2% (v/v) and the sample diluted 1:10 in 1% FA to reduce the AcN concentration to less than 5%. The sample was subjected to C18 solid-phase extraction using a StageTip assembly containing six layers of C18 material. Reagents were run through the assembly by centrifuging at 1800 × g for 30 seconds. The StageTip was washed and activated with one wash of 50 µl 100% methanol, one wash of 50 µl 70% AcN/1% FA and a final wash of 50 µl 1% FA.

The sample was loaded, followed by one wash with 100 µl 1% FA, and eluted with 50 µl 70% AcN/1% FA. The samples were then vacuum-centrifuged to complete dryness and resuspended in 10 µl 4% AcN/5% FA.

2.17.6 Single-shot analysis

Unfractionated material was first analysed using a one or three hour 'single-shot' LC-MS3 run **(2.18.1)** to ensure the TMT labelling was successful (defined as more than 95% of peptides labelled) and that there were roughly equal amounts of peptide in each TMT channel. For some experiments, data from the single-shot experiment were analysed with data from the corresponding fractions to increase the overall number of peptides quantified **(Table 2.5)**.

2.17.7 Offline high pH reversed-phase chromatography (HpRP) fractionation

The remaining labelled peptide samples were quenched with hydroxylamine to a final concentration of 0.5% (v/v). Samples were combined, normalising according to the total amount of protein in each TMT channel as measured in the single-shot analysis. FA was added to a total concentration of 2% (v/v), the volume reduced by 50% using a centrifugal vacuum, and the sample diluted to 1 ml in 1% FA. Peptides were purified using a Sep-Pak clean-up **(2.17.3)**, dried down and resuspended in 38 µl ammonium formate (Sigma).

TMT-labelled peptides were subjected to HpRP using an Ultimate 3000 rapid separation liquid chromatography (RSLC) nano ultra-high-performance liquid chromatography (UHPLC) system (Thermo) equipped with a 2.1 mm internal diameter × 25 cm long, 1.7 µm particle Kinetix Evo C18 column (Phenomenex). The mobile phase was comprised of 3% AcN (A), 100% AcN (B) and 200 mM ammonium formate pH 10 (C). Isocratic conditions were 90% A/10% C, and C was maintained at 10% throughout the gradient elution. Separations were conducted at 45 °C. Samples were loaded at 200 µl/min for 5 min, and then the flow rate was increased to 400 µl/min over 5 min. The gradient elution consisted of 0-19% B over 10 min, 19-34% B over 14.25 min, 34-50% B over 8.75 min, followed by a 10 min wash with 90% B. Ultraviolet absorbance was monitored at 280 nm and 15 s fractions were collected into 96-well microplates. Fractions were recombined orthogonally in a checkerboard fashion, combining alternate wells from each column of the plate into a single fraction, so that each column generated two sets of fractions (A and B). Only wells that were collected during the elution phase, as identified from the ultraviolet trace, were included. This created two sets of 12 combined fractions, A and B, which were dried in a vacuum centrifuge and resuspended in 10 µl 4% AcN/5% FA prior to LC-MS3. 12 set 'A' fractions were used for MS analysis and 'B' fractions stored for if reanalysis was necessary.

2.18 Mass spectrometry

Operation of the mass spectrometer was conducted by Dr. Robin Antrobus.

2.18.1 LC-MS3 for whole cell lysate proteomics

MS data were generated using an Orbitrap Fusion Lumos (Thermo). An Ultimate 3000 RSLC UHPLC machine equipped with a 300 µm internal diameter × 5 mm Acclaim PepMap µ-Precolumn (Thermo) and a 75 µm internal dimeter × 50 cm 2.1 µm particle Acclaim PepMap RSLC analytical column were used. The loading solvent was 0.1% FA. The analytical solvent consisted of 0.1% FA (A) and 80% AcN + 0.1% FA (B). All separations were carried out at 40 °C. Samples were loaded at 5 µl/min for 5 min in loading solvent. The analytical gradient consisted of 3-7% B over 3 min, 7-37% B over 173 min, followed by a 4 min wash at 95% B and equilibration at 3% B for 15 min. Each analysis used a MultiNotch MS3-based TMT method [280,281]. The following settings were used: MS1: 380-1500 Th, 120,000 resolution, 2×10^5 automatic gain control (AGC) target, 50 ms maximum injection time. MS2: Quadrupole isolation at an isolation width of mass-to-charge ratio (m/z) 0.7, collision-induced dissociation fragmentation (normalised collision energy (NCE) 34) with ion trap scanning in turbo mode from m/z 120, 1.5×10^4 AGC target, 120 ms maximum injection time. MS3: In Synchronous Precursor Selection mode, the top 10 MS2 ions were selected for higher energy collision dissociation (HCD) fragmentation (NCE 45) and scanned in the Orbitrap at 60,000 resolution with an AGC target of 1×10^5 and a maximum accumulation time of 150 ms. Ions were not accumulated for all parallelisable time. The entire MS/MS/MS cycle had a target time of 3 s. Dynamic exclusion was set to ± 10 ppm for 70 s. MS2 fragmentation was trigged on precursors 5×10^3 counts and above.

2.18.2 LC-MS/MS for immunoprecipitations

SILAC IP MS data were acquired using an Orbitrap Fusion (Thermo). The same UHPLC set up was used as described in **2.18.1**. Peptides were separated using a 3 h gradient of 3-37% AcN in 0.125% FA at a flow rate of 250 nl/min. The following settings were used: MS1: 350-1500 Th, quadrupole isolation, 120,000 resolution, 2×10^5 AGC target, 50 ms maximum injection time, ions injected for all parallisable time. MS2: Quadrupole isolation at an isolation width of m/z 0.7, HCD fragmentation (NCE 34) with ion trap scanning out in rapid mode from m/z 120, 10000 AGC target, 250 ms maximum injection time, in centroid mode. Dynamic exclusion was set to +/- 10 ppm for 25 s. MS2 fragmentation was trigged on precursors 5×10^3 counts and above.

2.18.3 Mass spectrometry quantitation and data analysis

2.18.3.1 Protein assignment

Mass spectra were processed using a Sequest-based software pipeline for quantitative proteomics, MassPike, through a collaborative arrangement with Professor Steven Gygi (Harvard Medical School,

USA). MS spectra were converted to mzXML using an extractor built upon Thermo's RAW File Reader library (version 4.0.26). In this extractor, the standard mzXML format has been augmented with additional custom fields that are specific to ion trap and Orbitrap MS and essential for TMT quantitation. These additional fields include ion injection times for each scan, Fourier Transform-derived baseline and noise values calculated for every Orbitrap scan, isolation widths for each scan type, scan event numbers, and elapsed scan times.

A combined database was constructed from (a) the human UniProt database (26th January, 2017), (b) the HCMV strain Merlin UniProt database, (c) all additional non-canonical HCMV open reading frames (ORFs) described by Stern-Ginossar *et al.* (10), (d) a six-frame translation (6FT) of HCMV strain Merlin filtered to include all potential ORFs of ≥8 amino acids (delimited by stop-stop rather than requiring ATG-stop) and (e) common contaminants. The combined database was concatenated with a reverse database composed of all protein sequences in reverse. Searches were performed using a 20 ppm precursor ion tolerance. Fragment ion tolerance was set to 1.0 Th. TMT tags on lysine residues and peptide N-termini (229.162932 Da) and carbamidomethylation of cysteine residues (57.02146 Da) were set as static modifications, while oxidation of methionine residues (15.99492 Da) was set as a variable modification. For SILAC analysis, the following variable modifications were used: heavy lysine (8.01420 Da), heavy arginine (10.00827 Da), medium lysine (4.02511 Da), and medium arginine (6.02013 Da). SILAC-only searches were performed in the same manner, omitting the TMT static modification. To control the fraction of false protein identifications, a target-decoy strategy was employed [282]. Peptide spectral matches (PSMs) were filtered to an initial peptide-level false discovery rate of 2%. Reverse peptide hits were later removed to achieve a final protein-level false discovery rate of 1%. PSM filtering was performed using a linear discriminant analysis, as described previously [282]. This distinguishes correct from incorrect peptide identifications in a manner analogous to the widely used Percolator algorithm [283], though employing a distinct machine-learning algorithm that considers cross correlation and delta-correlation scores, missed cleavages, peptide length, charge state, and precursor mass accuracy. Protein assembly was guided by principles of parsimony to produce the smallest set of proteins necessary to account for all observed peptides [282]. Where all PSMs from a given HCMV protein could be explained by either a canonical gene or non-canonical ORF, the canonical gene was picked in preference. In a small number of cases, PSMs assigned to a non-canonical or 6FT-ORF were a mixture of peptides from the canonical protein and the ORF. This most commonly occurred where the ORF was a 5'-terminal extension of the canonical protein. In these cases, the peptides corresponding to the canonical protein were separated from those unique to the ORF, generating two separate entries.

2.18.3.2 Quantitation

Proteins were quantified by summing TMT reporter ion counts across all matching PSMs using MassPike, as described previously [281]. Briefly, a 0.003 Th window around the theoretical m/z of each

reporter ion was scanned for ions and the maximum intensity nearest to the theoretical m/z was used. The main determinant of quantitation quality is the number of TMT reporter ions detected in each MS3 spectrum, which is proportional to the signal-to-noise ratio (S:N) observed for each ion. Every individual peptide was required to contribute sufficient TMT reporter ions (minimum of ~1,250 per spectrum) so that each on its own could be expected to provide a representative picture of relative protein abundance [281]. An isolation specificity filter with a cut-off of 50% was used to minimise peptide co-isolation [281]. PSMs with a combined S:N of less than 25 per channel, or no MS3 spectra at all, were excluded from quantitation. Peptides for each parent protein were summed, in effect weighting the contributions of individual peptides to the total protein signal based on their individual TMT reporter ion yields. Protein quantitation values were exported for further analysis in Excel.

2.18.3.3 Data analysis

For protein quantitation, reverse and contaminant proteins were removed, then each reporter ion channel was summed across all quantified proteins and normalised assuming equal protein loading across all channels. As it was not possible to confidently assign peptides to separate HLA alleles, the values presented for the HLA molecules represent combined S:N values.

For the 48 h degradation screen described in **Chapter 4**, each signal was normalised to the summed signal observed for each protein across the three conditions (Mock + HCMV + HCMV+MG132). This effectively corrected for differences in the numbers of peptides observed per protein in different replicates.

Hierarchical clustering of protein fold changes was performed using Cluster 3.0 (Stanford University) and visualised using Java Treeview [284].

The Database for Annotation, Visualisation and Integrated Discovery (DAVID) was used for functional enrichment of Gene Ontology biological process terms and UniProt keywords [285,286]. A background of all proteins quantified in each experiment was employed with the default settings for functional annotation clustering. DAVID groups enriched terms with similar meanings into clusters. A representative term from each significantly enriched cluster (Benjamini-Hochberg-adjusted p-value <0.05) was selected.

Statistical analysis is described in **2.22.3**.

2.18.4 Data availability

The raw MS data for the 48 h degradation screen described in **Chapter 4** have been deposited to the ProteomeXchange Consortium via the PRIDE partner repository [287,288] with the dataset identifier PXD017279.

2.19 Cell death assays

Input cell numbers and length of stimulation were optimised to ensure that sufficient cells died to facilitate quantitation of statistically significant differences between cell populations, and resulted in absorbance values within the dynamic range of the plate reader.

For assays in the absence of infection, 96-well plates were seeded with HFFF-TERTs (18,000 cells/well) or immortalised MEFs (6000 cells/well) then incubated for 24 h. For test cells, the media was changed to DMEM supplemented with 5% FBS, 30 ng/ml tumour necrosis factor alpha (TNFα) (R&D systems), 5 μM BV-6 (Selleckchem), and/or 25 μM Z-VAD(OMe)-fluoromethyl ketone (BD Pharmingen) in the presence or absence of 0.5 μM necrosulfonamide (NSA, Merck) or 1.5 μM GSK'872 (Cayman Chemical) for 18 h. Each compound was solubilised in DMSO, and DMSO was added such that the final concentration of DMSO in each experimental condition was identical. For control cells, the medium was changed to DMEM supplemented with 5% FBS and the equivalent concentration of DMSO. All conditions were examined in triplicate. 45 min prior to harvest, half of the control cells were treated with 10 μl 10× Lysis Solution (Promega). The other half were used to measure background lactate dehydrogenase (LDH) release from live, untreated cells. Supernatants were harvested and the amount of LDH measured using the CytoTox 96 Non-Radioactive Cytotoxicity Assay (Promega).

For assays in the presence of infection, HFFF-TERTs (14,000 cells/well) were seeded into 96-well plates, incubated for 24 h, and infected with HCMV at an MOI of 5. 48 h after infection, the cells were treated as above to stimulate and measure cell death.

2.20 Bioinformatics

Selectome, a publicly-available database [289,290], was used to identify evidence of positive selection.

Alignment of pUL36 amino acid sequences with performed using Clustal Omega by EMBL-EBI [291,292].

Structural homology analysis and structure prediction was performed with HHpred 3.2.0 against databases PDB_mmCIF70_8_Apr and Pfam-A_v32.0 with the default parameters [293], Phyre2 using the default parameters [294], I-TASSER [295] and trRosetta [296]. Molecular graphics were generated with UCSF ChimeraX [297].

Information on host protein interactions was gained from BioPlex 3.0 [220].

Prediction of peptides generated by LysC and trypsin digestion that could be identified by MS employed ExPASy PeptideCutter (Swiss Institute of Bioinformatics).

2.21 Data presentation

2.21.1 Graphs

All graphs were generated in Microsoft Excel, except for the box and whisker plots, which were generated using R version 3.4.1 [298]. R uses the inclusive method for calculating box and whisker plot quartiles.

2.21.2 Figures

All figures were made using Inkscape 0.92, a free and open source vector graphics editor [299]. Interactome maps were generated using Cytoscape 3.7.2 [300]. Vector maps **(Appendix II)**, were generated with SnapGene [267].

2.22 Statistical analysis

Throughout this thesis, the standard p-value annotation is used (*p<0.05 **p<0.01 ***p<0.001 ****p<0.0001), unless stated otherwise in the figure legend.

2.22.1 Restriction assays

To measure the significance of differences in the percentage of GFP cells between infected iRFP- and mCherry-positive populations, a p-value was calculated using a two-tailed Student's t-test (n=3) in R version 3.4.1 [298]. A Shapiro-Wilk test was used to determine that the data were normally distributed and therefore valid for analysis by a t-test. Homogeneity of variance was confirmed with a Bartlett's test.

2.22.2 Plaque assays

All plaque assay statistical analysis was performed in R version 3.4.1 [298].

To calculate the probability that the number of plaques on the test cell line differed from that on the control cell line, p-values were calculated using Tukey's post-hoc test following a one-way analysis of variance (ANOVA) test (n=3).

The sizes of a random selection of plaques across the three biological replicates were calculated as described in **2.14.2**. To calculate the probability that the size of plaques on the test cell line differed from that on control cells, p-values were determined using a non-parametric Mann-Whitney U test, as the data did not fit the assumptions of normality required for a Student's t-test.

A two-tailed Student's t-test was used to calculate the probability that the number of GFP-positive cells differed between the conditions (n=3).

2.22.3 Mass spectrometry data

2.22.3.1 Significance B

The method of significance B was used to assess whether the fold change in a protein's abundance between two conditions was significantly different to 1 [301]. Values were calculated and corrected for multiple hypothesis testing using the method of Benjamini-Hochberg in Perseus version 1.5.2.20 [301].

2.22.3.2 Z-score

The Z-score (or standard score) is the number of standard deviations by which an observed is above or below the mean of the other values in the comparison.

$$Z: \frac{\chi - \mu}{\sigma}$$

Where χ: observed value, μ: mean (excluding the observed value) and σ: standard deviation (excluding the observed value).

2.22.3.3 Non-parametric ANOVA for the analysis of viral gene expression

A Kruskal-Wallis non-parametric ANOVA test was used to test differences between the expression profiles of viral genes in different Tp classes **(Figure 6.22)**, as a Shapiro-Wilk test showed that the data did not fit a normal distribution in every condition. A Dunn's post-hoc test was used to calculate p-values for each pairwise comparison. These analyses were performed in R version 3.4.1 [298].

2.22.4 SILAC immunoprecipitations

P-values for the significance of enrichment in IPs were estimated using the method of significance A and corrected for multiple hypothesis testing in Perseus version 1.5.2.20 [301].

2.22.5 Cell death assays

P-values were calculated using a Student's two-sample, two-tailed t-test (n=3) in R version 3.

Chapter 3: Do proteins degraded by human cytomegalovirus exhibit antiviral activity?

Some of the experiments presented in this chapter utilised reagents generated by other members of our group or collaborators. Dr. Katie Nightingale, Dr. Kai-Min Lin, Dr. Luís Nobre (all University of Cambridge) and Dr. Mandy Glass (University of the West of Scotland) provided shRNA vectors, as detailed in the Materials and Methods. Collaborators at Cardiff University (Dr. Richard Stanton and colleagues) provided the recombinant viruses used in this chapter and the rest of this thesis. A couple of experiments performed by Dr. Lior Soday and Dr. Benjamin Ravenhill (both University of Cambridge) are described to provide context to the work, as indicated in the text and figure legends. All other work is my own.

3.1 Introduction

As described in the Introduction to this thesis **(1.5)**, seven candidate antiviral restriction factors (ARFs) were selected for study, based on:

1. Evidence of protein degradation during infection, from the Nightingale, Lin *et al.* (2018) early degradation screens **(1.4.5)** [62];
2. Evidence of IFN-stimulation, based on unpublished data evaluating IFN-stimulated changes in the proteome and/or data from the interferome [200];
3. The presence of literature that indicated potential mechanisms of antiviral restriction, and/or;
4. Screens of proteins downregulated by other viruses, including vaccinia virus (VACV) and herpes simplex virus type 1 (HSV-1).

The candidate ARFs were MLKL, DMXL1, ARHGAP35, DHCR24, FRMD6, IFIT2 and LMAN2L.

In addition to being stimulated in response to IFN and/or infection and antagonised by the virus, the two other common features of ARFs are their ability to restrict virus infection and evidence of positive selection **(1.2.1)**. This part of the project aimed to determine whether the candidate ARFs do indeed exhibit these latter two characteristics.

3.2 Aims

1. **Determine whether any of the candidate proteins act as ARFs** by screening them for antiviral activity. This involved:
    a. Generating overexpression, short hairpin RNA (shRNA) knockdown and CRISPR/Cas9 knockout cell lines for each of the candidate proteins.
    b. Evaluating the effect of the proteins on virus immediate early gene expression and virus replication through restriction assays and plaque assays, respectively.
2. **Develop and validate a two-colour restriction assay system** that allows test and control cell lines to be seeded into the same well and differentiated, in order to avoid variability in cell population density and spread.
3. **Search the literature for evidence of positive selection** in the genetic sequences of the candidate ARFs.

3.3 Two-colour restriction assay development and validation

The primary system used by our group to probe the effects of putative ARFs on virus infection is a restriction assay **(Figure 3.1A)**, in which cells are infected with a green fluorescent protein (GFP)-expressing virus and the percentage of GFP-positive cells quantified after 24 h. The virus used is based on human cytomegalovirus (HCMV) strain Merlin, with the immediate-early (IE) gene UL36 fused to enhanced GFP via a self-cleaving P2A peptide, which releases GFP following synthesis (RCMV2344). UL36 was chosen as it is one of the most abundantly expressed viral proteins within the first 6 h of infection. Insertion of GFP did not affect the ability of pUL36 to inhibit Fas-mediated apoptosis [62]. Analysing differences in the frequency of GFP-positive cells 24 hours post-infection (hpi) enables identification of factors that influence the early stages of infection, prior to IE gene expression. Our group has previously shown that effects of restriction are highly dependent on the amount of virus, with the virus being able to overcome restriction at a high multiplicity of infection (MOI). Therefore, all restriction assays are performed at a low MOI to achieve 1-10% infection [62]. Preliminary attempts at restriction assays on control, DHCR24 and FRMD6 shRNA knockdown cell lines yielded variable results, even with knockdown of the known ARF Sp100 **(Figure 3.1B)**. The fact that biological repeats (where cells were seeded in parallel) produced highly consistent results indicated that differences in the infection rates of cell types observed between experiments might be due to differences in cell density.

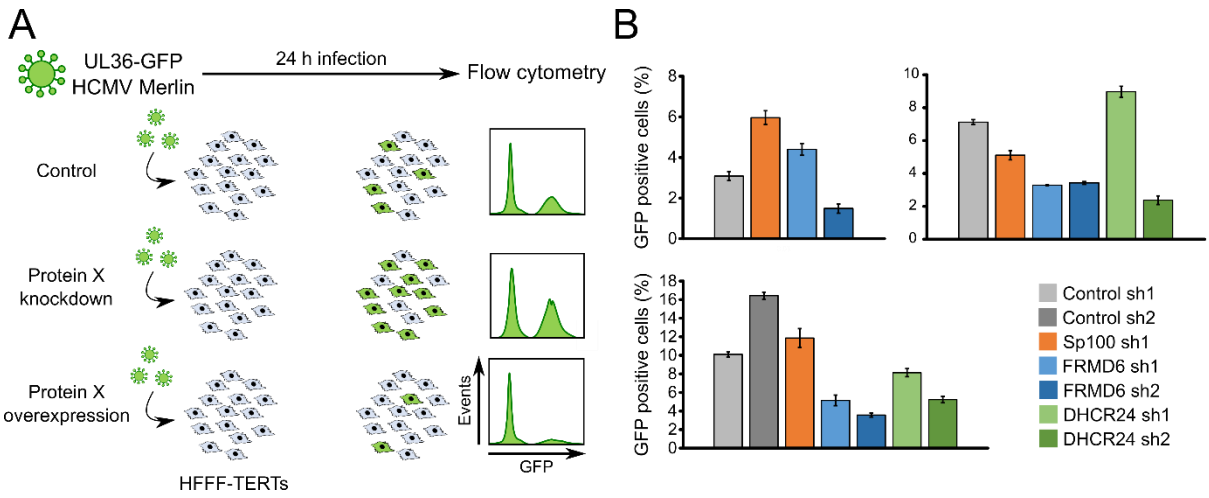

Figure 3.1: Preliminary restriction assay data revealed variable results between independent experiments. **(A)** Restriction assay schematic. shRNA knockdown or overexpressing cell lines were infected with UL36-GFP Merlin virus (RCMV2344) at a low MOI. 24h later, the percentage of GFP-positive cells was determined by flow cytometry. **(B)** Data from preliminary restriction assays on shRNA cell lines, showing the average of three biological repeats. Error bars represent standard error of the mean (SEM).

To limit this effect, a system was developed in which test and control cell lines can be mixed and seeded into the same well **(Figure 3.2A)**. The system made use of human fetal foreskin fibroblasts immortalised with telomerase (HFFF-TERTs), which were used throughout the experiments presented in this thesis. Primary HFFFs are limited to a total of around 25 passages and exhibit diminished rates of growth as passage number increases [62]. HFFF-TERTs were therefore chosen as the principal system for this project as they can be passaged without effects on growth and cell phenotype, particularly important when creating stably transduced cell lines which need to be passaged in selection media, and consequently produce less variable results. Our group previously performed a proteomic comparison of primary HFFFs and HFFF-TERTs infected with HCMV or mock-infected for 24 or 72 h [62]. This showed that HCMV infection has a highly similar effect on the proteome of these two cell types, with a significant correlation between HCMV/mock ratios of all human and viral proteins (R^2 of 0.81 at 24 h and 0.9 at 72 h) [62].

To generate the two-colour restriction assay system, HFFF-TERTs were transduced with vectors expressing mCherry and near-infrared fluorescent protein (iRFP). The transduced 'coloured' cells were selected with blasticidin for two weeks but failed to reach 100% of the population **(Figure 3.2B)**. The cells were sorted by fluorescence-activated cell sorting, but soon reverted to a mixed population that was stable at a frequency of 70-90% coloured cells. The reason for this is unclear, but it is likely that the uncoloured cells did not represent a wild type (WT) population. To ensure that the expression of mCherry and iRFP does not hinder HCMV infection, a mixed population of mCherry and iRFP cells

were infected with UL36-GFP HCMV at a range of MOIs **(Figure 3.2C)**. mCherry- and iRFP-positive cells were infected to the same extent, with slightly more variation found at lower MOIs, and at a similar frequency to the WT HFFF-TERTs. The 'uncoloured' (UC) cells were infected at a significantly lower frequency, in accordance with the hypothesis that this population does not represent WT HFFF-TERTs.

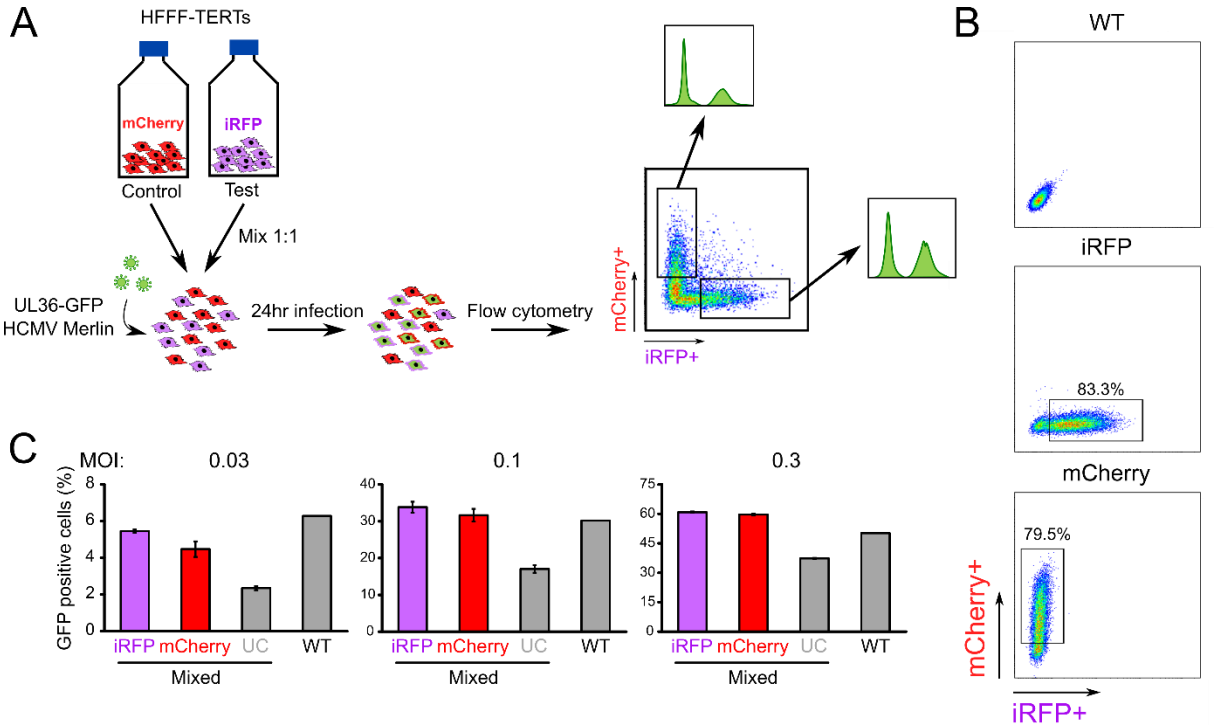

Figure 3.2: Two-colour restriction assay development.

(A) HFFF-TERTs expressing mCherry were transduced with a control shRNA or control overexpression plasmid. iRFP-expressing HFFF-TERTs were transduced with shRNA or overexpression plasmids targeting positive controls (Sp100 or DAXX) or the protein of interest. The two cell lines were mixed, seeded into the same well, and infected with UL36-GFP HCMV Merlin (RCMV2344). 24 hpi, GFP-expressing populations were analysed by flow cytometry. Cells were gated according to iRFP or mCherry levels and then the percentage of GFP-positive cells within each group was determined. **(B)** Percentage of iRFP- and mCherry-positive cells after 2 weeks in selection with blasticidin (10 µg/ml). **(C)** A mixed population of iRFP and mCherry HFFF-TERTs ('Mixed') and WT HFFF-TERTs (Control) were infected with UL36-GFP virus at an MOI of 0.03, 0.1 or 0.3. At 24 hpi, the percentage of GFP-positive cells within each population was determined by flow cytometry as shown in (A). Frequency of infection of uncoloured cells (UC) within the mixed coloured population was also determined. Average of three biological replicates is shown, except for the WT condition, which was analysed as a single experiment. Error bars represent SEM.

Next, the system was validated. The coloured cells were stably transduced with shRNA constructs targeting the known anti-HCMV restriction factors HLTF and Sp100, and a restriction assay performed **(Figure 3.3)**. Knockdown of HLTF and Sp100 was confirmed by immunoblot **(Figure 3.3A)**. The results presented in **Figure 3.3B**, which show that both HLTF and Sp100 inhibit IE gene expression, were representative of four independent experiments performed at different MOIs. Effects of restriction, although small, were highly consistent. Many restriction assays were carried out over the course of this project, and Sp100 consistently produced a restriction ratio between two and four **(Figure 3.3D)**.

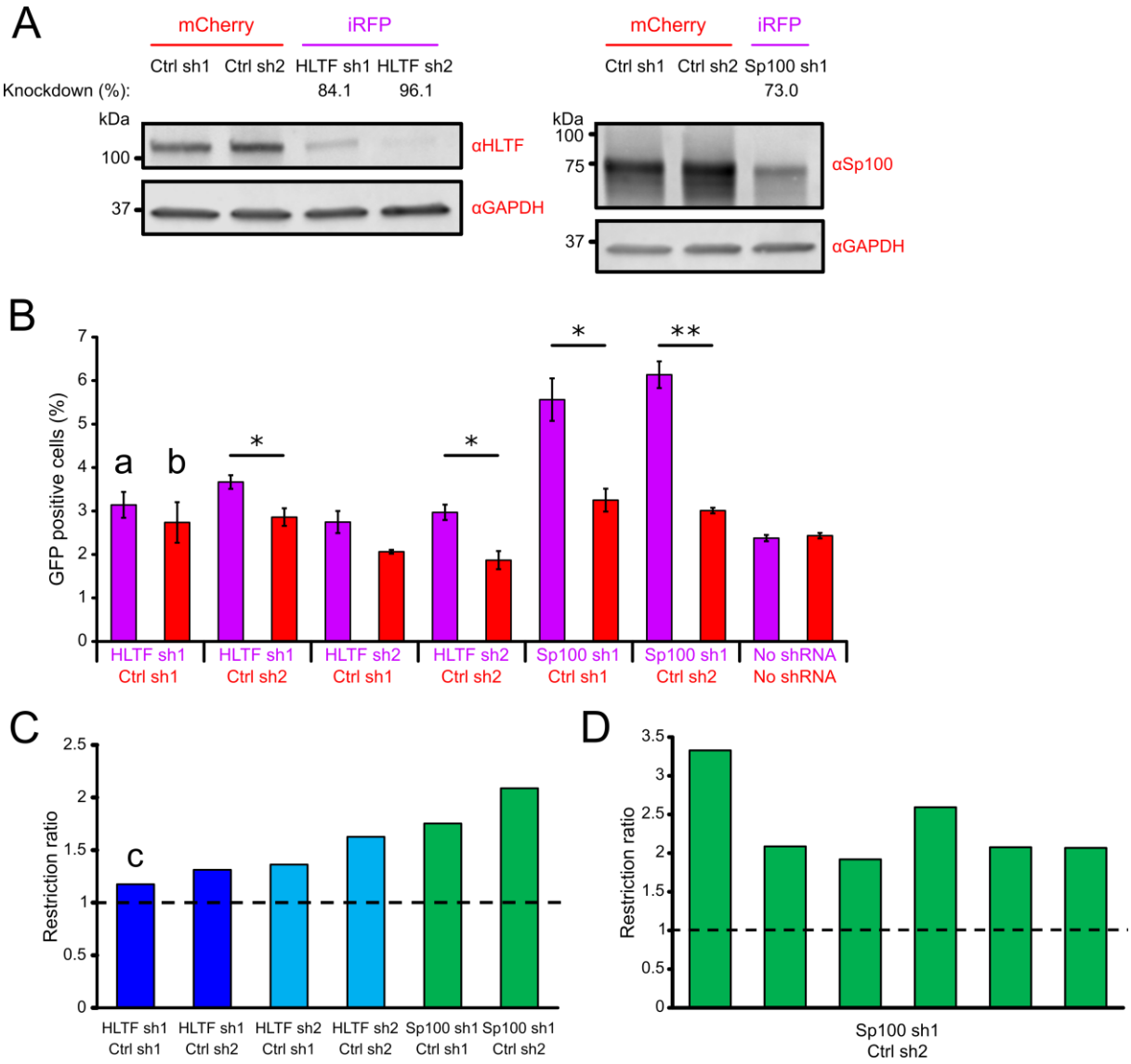

Figure 3.3: Two-colour restriction assay validation.

(A) HLTF and Sp100 shRNA knockdown in coloured cells. mCherry cells were transduced with control shRNA constructs and iRFP cells transduced with constructs targeting HLTF and Sp100. **(B)** HLTF and Sp100 restrict infection. mCherry-positive control cells were mixed with iRFP-positive HLTF or Sp100 knockdown cells. Cells were infected with UL36-GFP Merlin virus (RCMV2344) virus (MOI: 0.02). 24 h later, the percentage of GFP-positive cells within each coloured cell population was determined by flow cytometry. P values were calculated using a Student's t-test (n=3). *p<0.05 **p<0.001. Average of three biological replicates is shown, and error bars represent SEM. **(C)** Restriction ratios (c) were calculated by dividing the percentage of GFP-positive cells in the iRFP population (a) by the percentage of GFP-positive cells in the mCherry population (b). **(D)** Restriction ratio of Sp100 compared to control sh2 across multiple independent restriction assay experiments. Ctrl, control; sh, shRNA.

Restriction factors often act synergistically [270]. In an attempt to generate a system where knockdown of a single restriction factor produces a larger fold change in infection rates, cell lines used in the previous assay were transduced with a triple knockdown plasmid (shDPS) targeting DAXX, PML and Sp100 [270] **(Figure 3.4A)**. The HLTF restriction assay was then repeated in an shDPS background **(Figure 3.4B-C)**. Knockdown of DAXX, Sp100 and PML alone led to a 25-fold increase in the frequency of infection. However, knockdown of HLTF in the presence of shDPS had a negative effect, with fewer cells becoming infected than those with shDPS alone. Exactly why this would happen is unclear. Due to this result, the use of shDPS was not continued.

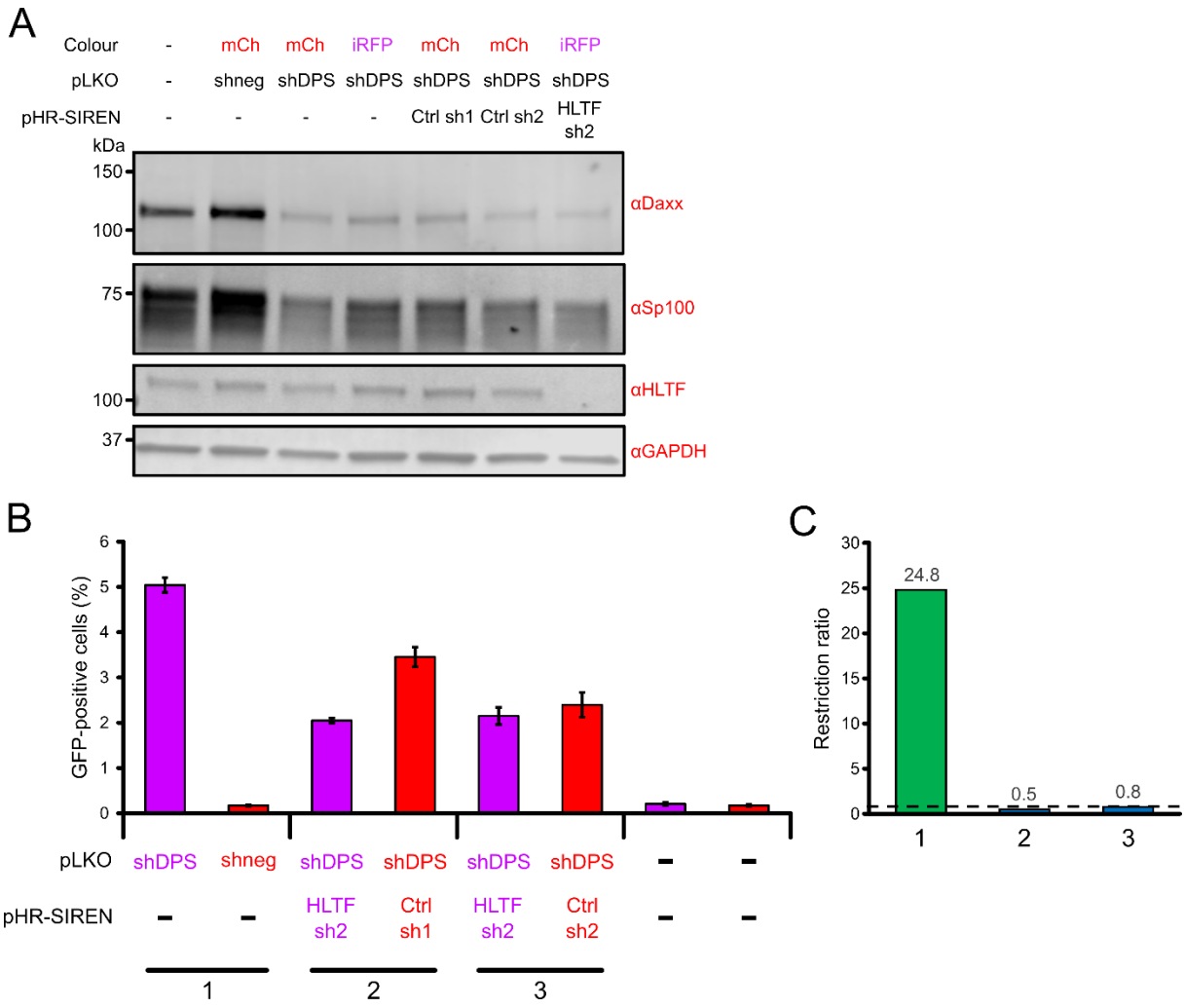

Figure 3.4: Two-colour restriction assay in an shDPS background.

(A) Two-colour system cell lines were transduced with a combination of pLKO plasmids encoding shRNAs against DAXX, PML and Sp100 (shDPS) or control (shneg), and pHR-SIREN plasmids encoding control or HLTF-targeting shRNA sequences. Knockdown of DAXX, Sp100 and HLTF was confirmed by immunoblot. There was no antibody available for PML. **(B)** mCherry and iRFP HFFF-TERTs transduced with different combinations of shRNA constructs were mixed and a restriction assay performed as described in Figure 3.3B (MOI: 0.01). **(C)** Restriction ratios for the data shown in (B).

3.4 shRNA knockdown of target proteins

shRNA constructs targeting each of the seven genes were transduced into non-coloured HFFF-TERTs for plaque assays, and iRFP-positive HFFF-TERTs for restriction assay analysis. Knockdown was confirmed by immunoblot **(Figure 3.5A)**. Despite attempting multiple immunoblot protocols for optimising the detection of large proteins, detection of DMXL1 (338 kDa) remained challenging. Transduction of cells with a vector encoding a DMXL1 shRNA resulted in the appearance of a prominent smaller band below 250 kDa. Although 5' shRNA cleavage products are thought to be degraded by the exosome, the accumulation and translation of 5' messenger RNA fragments has been previously reported [302]. Therefore, this smaller band detected by the αDMXL1 antibody might represent the translation of a 5' cleavage product. Given the poor signal observed from the DMXL1 antibody, quantitative reverse transcription polymerase chain reaction (RT-qPCR) was also used to confirm knockdown **(Figure 3.5B)**.

3.5 Overexpression of target proteins

The generation of lentiviral expression vectors for the overexpression of the candidate ARFs utilised the Gateway cloning system, as described in **2.3.1**. Where available, entry clones encoding the protein of interest were bought online from Harvard Plasmid Repository (ARHGAP35, DHCR24 and LMAN2L). For MLKL, FRMD6 and IFIT2, entry clones were generated by PCR cloning the genes from cDNA into an entry clone vector. Sequencing of the entry clones confirmed that cloning was successful, and revealed that two isoforms of FRMD6 had been cloned. DMXL1 could not be cloned by PCR due to its large size. Lentiviral expression vectors were transduced into non-coloured and coloured cells and overexpression validated by immunoblot **(Figure 3.6)**.

3.6 CRISPR knockout of target proteins

HFFF-TERTs stably expressing Cas9 were transduced with gRNA-expressing vectors in the presence of raltegravir to prevent integration **(Figure 3.7)**. Unexpectedly, expression of ARHGAP35 and IFIT2 gRNAs resulted in an increase in protein expression. Polyclonal DMXL1, FRMD6 and LMAN2L CRISPR populations with a knockdown of >38% were single-cell cloned. Knockout in monoclonal cell lines was confirmed by immunoblot **(Figure 3.8)**. As the knockout did not always appear complete by immunoblot, topoisomerase-based (TOPO) cloning was used to check for mutations and to rule-out the presence of subclones carrying different variants in the DHCR24 monoclonal CRISPR cell lines. After TOPO cloning and transformation into bacteria, DNA from 10 colonies per cell line was purified and sequenced. All sequences contained nonsynonymous mutations **(Table 3.1)**. The presence of only one or two mutations within each cell line and absence of any WT sequences indicated that the single cell cloning was successful.

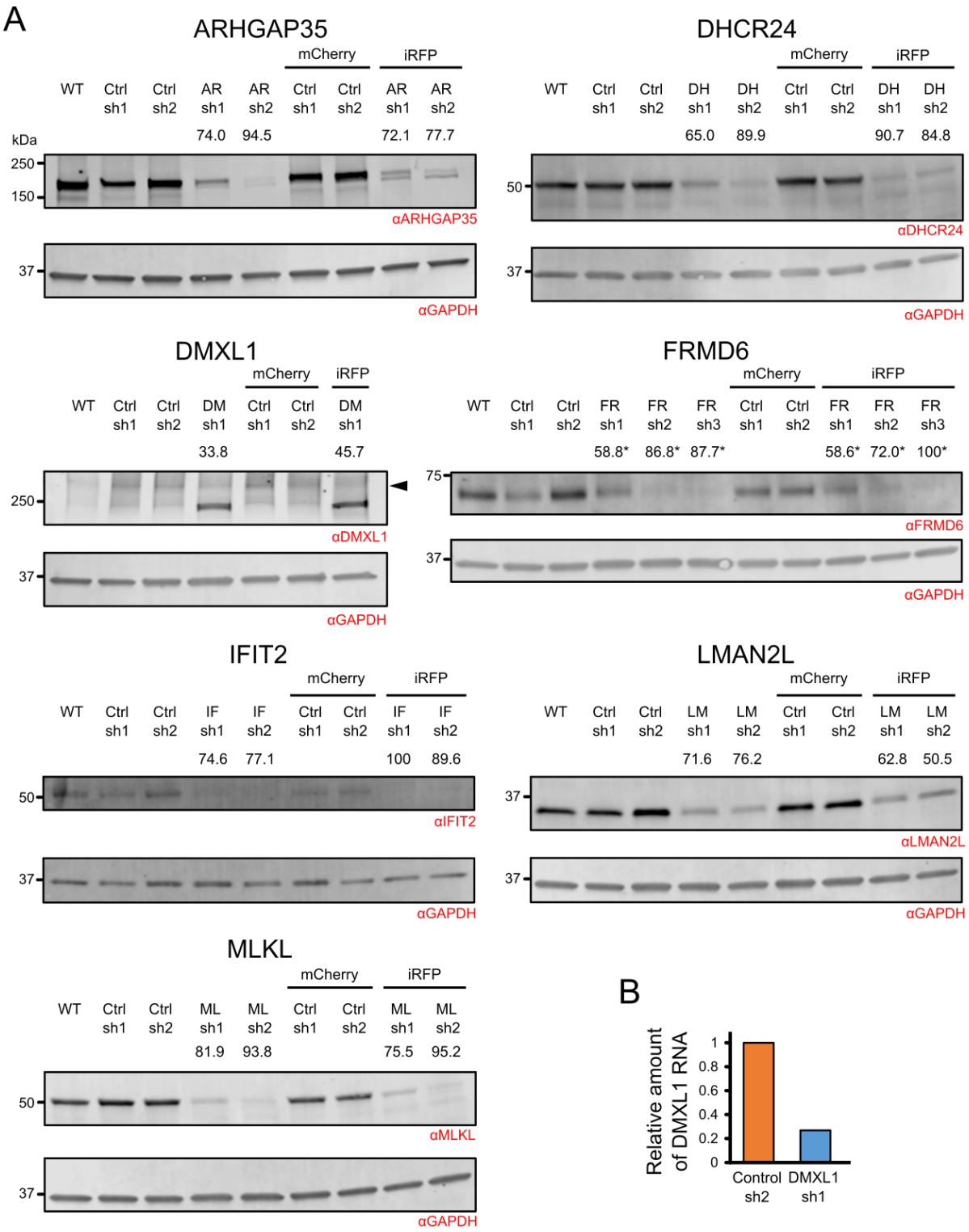

Figure 3.5: shRNA knockdown of target proteins in WT and coloured HFFF-TERTs.

(A) Immunoblot of lysates from cell lines transduced with pHR-SIREN plasmids encoding shRNAs against each of the genes of interest. The values noted represent percentage knockdown in comparison to average levels in control sh1 and sh2 cell lines. *Control sh1 cells appeared to express lower levels of FRMD6 in comparison to WT cells, and so levels of FRMD6 in the knockdown cell lines were compared to that of control sh2 only. Expected protein sizes: ARHGAP35, 190 kDa; DHCR24, 54 kDa; MLKL, 54 kDa; DMXL1, 338 kDa; LMAN2L, 32 kDa; IFIT2, 54 kDa; FRMD6, 78 kDa. (B) RT-qPCR validation of DMXL1 knockdown.

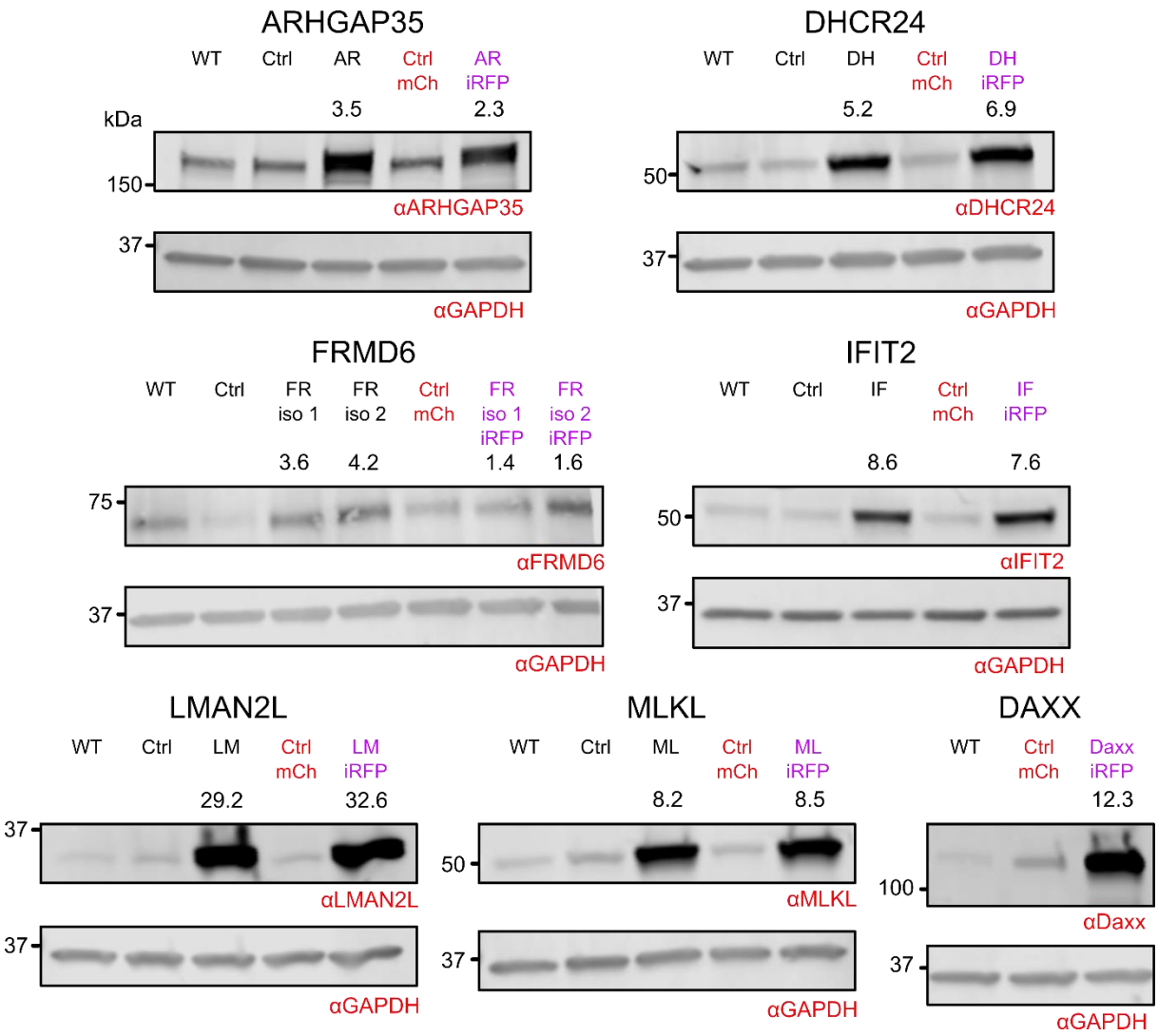

Figure 3.6: Overexpression of target proteins in WT and coloured HFFF-TERTs.

HFFF-TERTs were transduced with pHAGE-pSFFV overexpression plasmids encoding each of the genes of interest. The values quoted represent fold increase with respect to the corresponding non-coloured or coloured control.

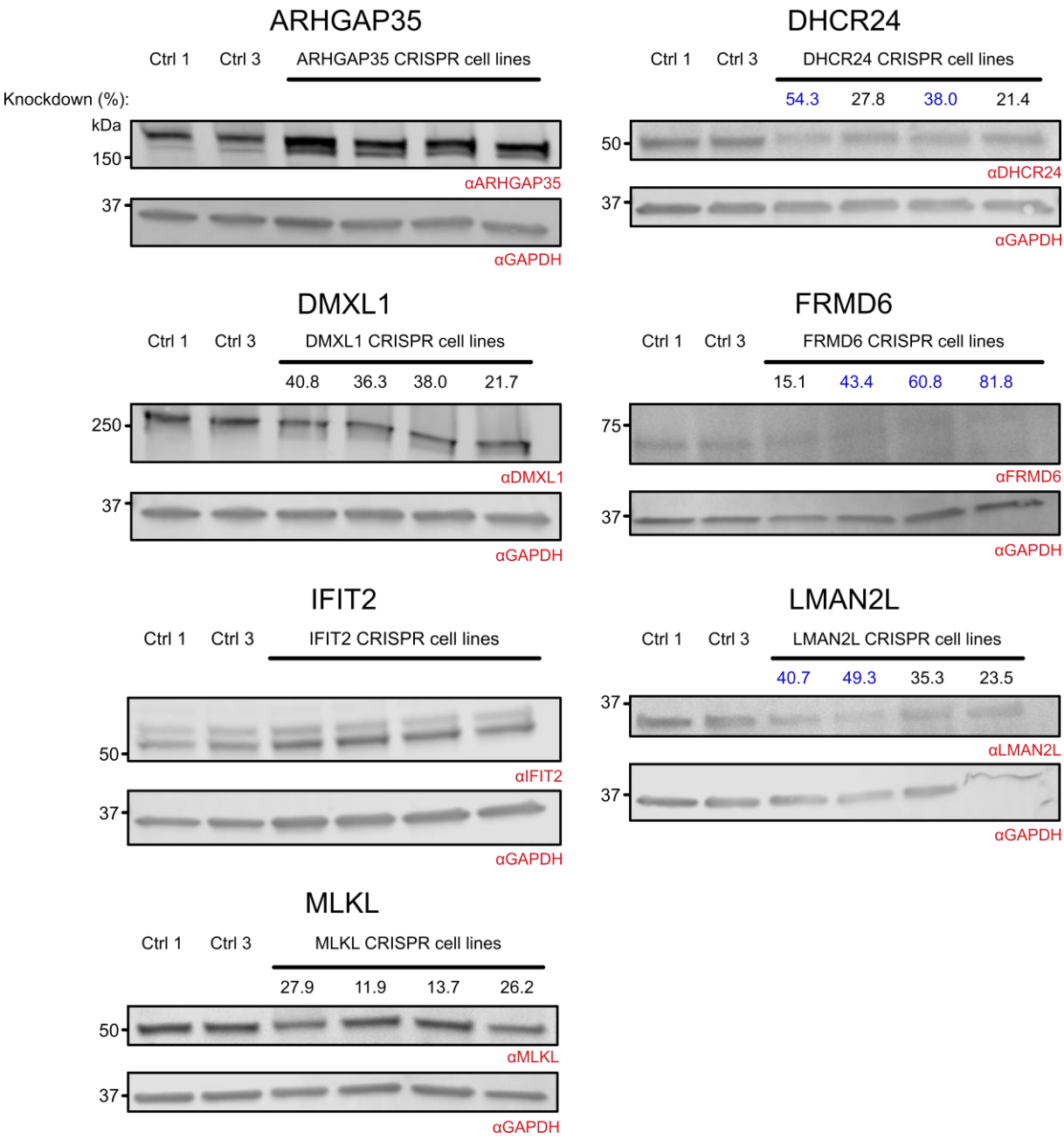

Figure 3.7: Polyclonal CRISPR populations.

Amount of target protein (relative to GAPDH loading control) in cells lines expressing one of four gRNAs against the seven proteins of interest was compared to the average relative protein levels in cells expressing control gRNAs (Ctrl 1 and Ctrl 3). Values quoted represent percentage decrease in protein abundance. Cell lines highlighted in blue were selected for single-cell cloning.

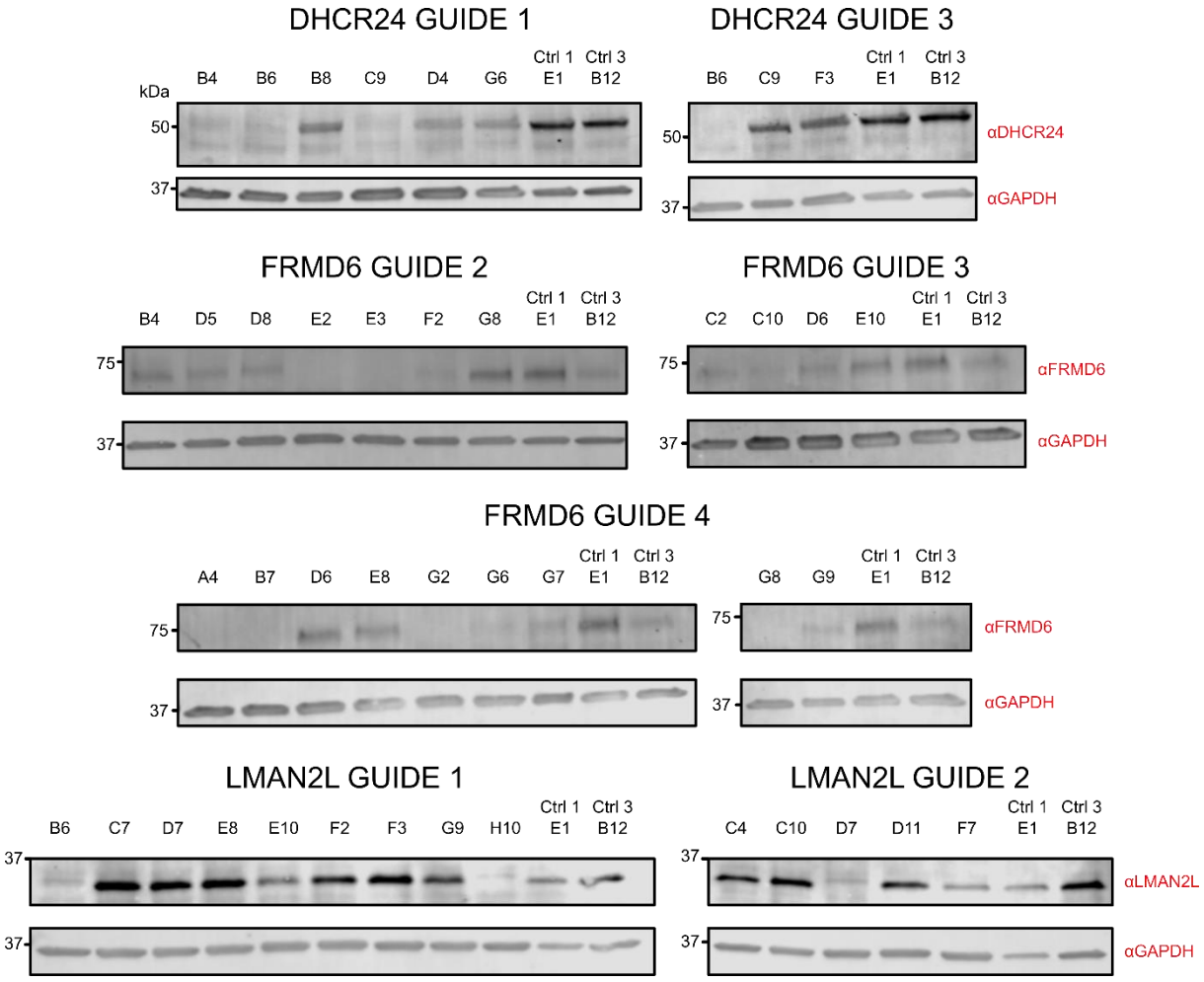

Figure 3.8: Monoclonal CRISPR populations.

Polyclonal populations with a knockdown of >38% were single-cell cloned by seeding cells into wells at a limiting dilution, grown up and lysed for immunoblot analysis.

Guide	*Single cell clone*	*TOPO clone*	*Mutation*
1	B6	1	5 bp deletion
		2	1 bp insertion
		3	1 bp insertion
		4	1 bp insertion
		5	5 bp deletion
		6	1 bp insertion
		7	5 bp deletion
		8	1 bp insertion
		9	5 bp deletion
		10	5 bp deletion
1	B4	1	1 bp insertion
		2	1 bp insertion
		3	1 bp insertion
		4	1 bp insertion
		5	1 bp insertion
		6	1 bp insertion
		7	1 bp insertion
		8	1 bp insertion
		9	1 bp insertion
		10	1 bp insertion
3	B6	1	2 bp deletion
		2	5 bp deletion
		3	5 bp deletion
		4	2 bp deletion
		5	5 bp deletion
		6	2 bp deletion
		7	5 bp deletion
		8	5 bp deletion
		9	2 bp deletion
		10	2 bp deletion

Table 3.1: TOPO clone sequencing results for DHCR24 monoclonal CRISPR cell lines.

3.7 Assays for determining the effect of target proteins on viral infection

Two-colour restriction assays were performed using the shRNA and overexpression cell lines for each target protein. For screening purposes, the shRNA cell line with the biggest knockdown was used initially. The original plan was to transduce the monoclonal CRISPR cell lines with iRFP so they could also be used in the same assay. However, a restriction assay on the non-coloured single-cell cloned control CRISPR cell lines showed that the permissibility of these cells to infection varied significantly (experiment performed by Dr. Lior Soday) **(Figure 3.9)**.

As UL36 is an HCMV IE gene, restriction of UL36-GFP levels will only identify ARFs that act early in the lifecycle, prior to viral gene expression. To assess whether the proteins of interest affect virus replication at any other point in the replication cycle, plaque assays were also performed, which examine virus replication over multiple infectious cycles. For the plaque assay, non-coloured HFFF-TERTs expressing shRNA, overexpression or CRISPR constructs were infected with HCMV AD169-GFP

(RCMV288). Two weeks later, the resulting plaques were counted, photographed, and the size of the plaques measured using ImageJ. For the shRNA plaque assays, cells were also trypsinised and subjected to flow cytometry analysis.

RCMV288, based on strain AD169, encodes a copy of enhanced GFP under the control of the HCMV β-2.7 early promoter. As described in **1.1.6**, strain AD169 acquired a number of mutations during passage in cell culture, meaning it is unlikely to adequately represent clinical HCMV. Although research should make use of a strain that represents the clinical virus as closely as possible, low-passage strains such as Merlin are highly cell associated, making them difficult to use in functional assays [66]. This is indeed the situation our group has observed previously when performing plaque assays: viruses based on strain Merlin do not produce clearly demarcated plaques that are easily quantifiable, hence the choice of AD169 for these assays.

Results for the two proteins that are investigated further in this thesis, MLKL and DMXL1, are described in detail. Results for the remaining proteins, ARHGAP35, DHCR24, FRMD6, IFIT2 and LMAN2L, are outlined briefly.

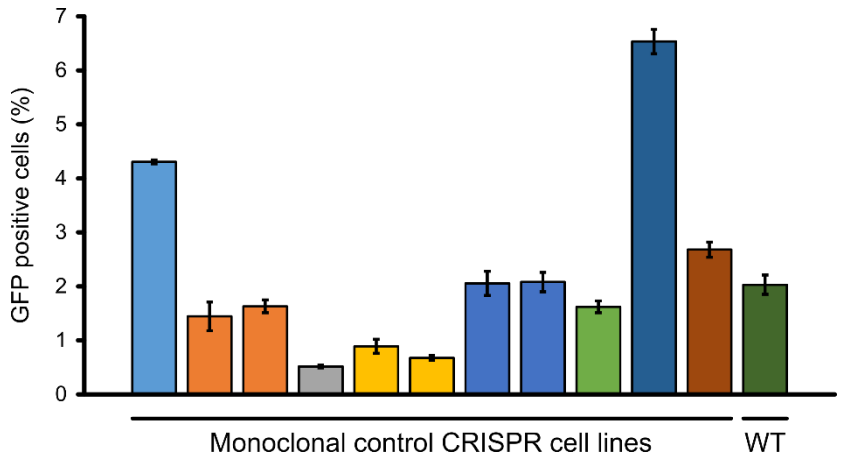

Figure 3.9: Restriction assay on non-coloured monoclonal control CRISPR cell lines.
HFFF-TERTs expressing Cas9 were transduced with gRNAs that contain no known target (control guide 1 or control guide 3) in the presence of raltegravir. The cells were single-cell cloned to obtain a monoclonal population. Populations grown up from different single cells (represented by different colour bars) were infected with UL36-GFP Merlin virus (RCMV2344) (MOI: 0.05), harvested after 24 h and analysed by flow cytometry. Bars of the same colour represent populations of cells that were grown up independently from the same single cell clone. This experiment was performed by Dr. Lior Soday.

3.8 MLKL

While overexpression of the known HCMV ARF DAXX resulted in a 17-fold restriction of IE gene (UL36-GFP) expression, overexpression of MLKL had no effect **(Figure 3.10A)**. In the shRNA restriction assay, knockdown of MLKL resulted in a significant increase in virus infection **(Figure 3.10B)**. The assay was repeated with both MLKL knockdown cell lines. Infection rates in the MLKL sh1 cell line relative to the control were greater than for the MLKL sh2 cell line **(Figure 3.10C)**, despite exhibiting a weaker knockdown **(Figure 3.5).**

In the plaque assay using AD169-GFP, cells overexpressing DAXX were much less permissive to initial infection, as reflected by the smaller number of plaques **(Figure 3.11A)**. Unexpectedly, the size of the plaques was unaffected, suggesting that secondary infection of adjacent cells was less restricted **(Figure 3.11B)**. Infection of MLKL-overexpressing cells was also inhibited **(Figure 3.11A)**. This is particularly interesting as the AD169-GFP virus has been shown not to downregulate MLKL **(Figure 1.12E)**, therefore augmenting the effect of overexpressing MLKL. As with DAXX, the reason why plaque size was unaffected is unclear **(Figure 3.11B)**. Surprisingly, knockdown of MLKL resulted in a decrease in plaque number, size and overall GFP-positive cell number in comparison to the control, the opposite effect to what would be expected for a protein that restricts infection **(Figure 3.11C-F)**. However, a significant caveat for this experiment was that Sp100 knockdown did not increase the plaque-forming ability of HCMV strain AD169 as has been previously reported [117].

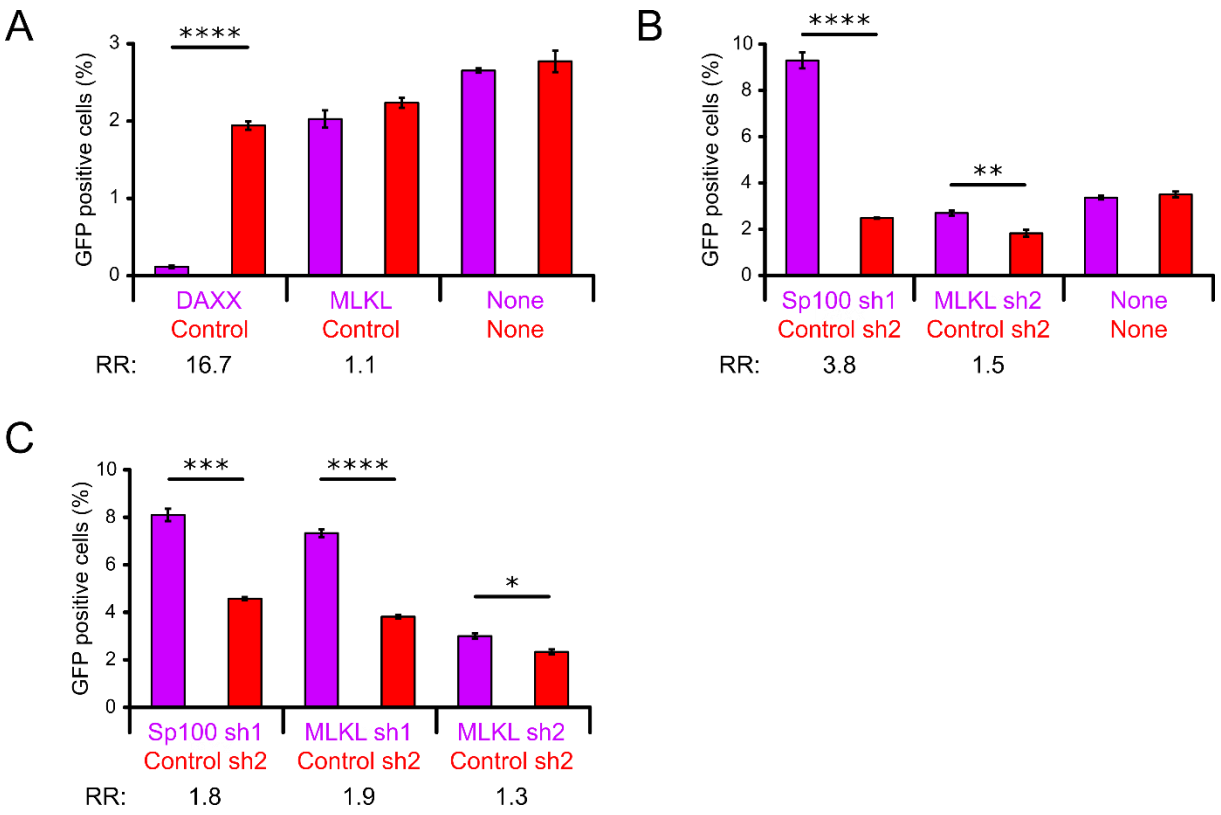

Figure 3.10: MLKL restriction assays.

(A) Overexpression restriction assay. mCherry cells were transduced with a control vector and mixed with iRFP cells overexpressing the protein of interest or the known ARF, DAXX. Cells were infected with UL36-GFP Merlin virus (RCMV2344) (MOI: 0.1) and the percentage of GFP-positive cells within each coloured cell population was determined after 24 h by flow cytometry. iRFP- and mCherry-positive cells that had not been further transduced were included to show that expression of iRFP or mCherry did not differentially affect early virus replication. A restriction ratio (RR) was calculated by dividing the percentage of GFP-positive cells in the mCherry population by the percentage of GFP-positive cells in the iRFP population. **(B)** shRNA restriction assay. mCherry cells transduced with the control sh2 construct were mixed with iRFP cells expressing an shRNA construct against the protein of interest or the known ARF, Sp100. Cells were infected with UL36-GFP Merlin (MOI: 0.05) and percentage of GFP-positive cells within each coloured cell population determined after 24 h by flow cytometry. A restriction ratio was calculated by dividing the percentage of GFP-positive cells in the iRFP population by the percentage of GFP-positive cells in the mCherry population. **(C)** A repeat of (B) with the addition of the MLKL sh1 cell line. Average of three biological replicates is shown, error bars represent SEM. P-values were calculated with a Student's t-test (n=3). Standard p-value notation is used. These results are representative of two independent experiments.

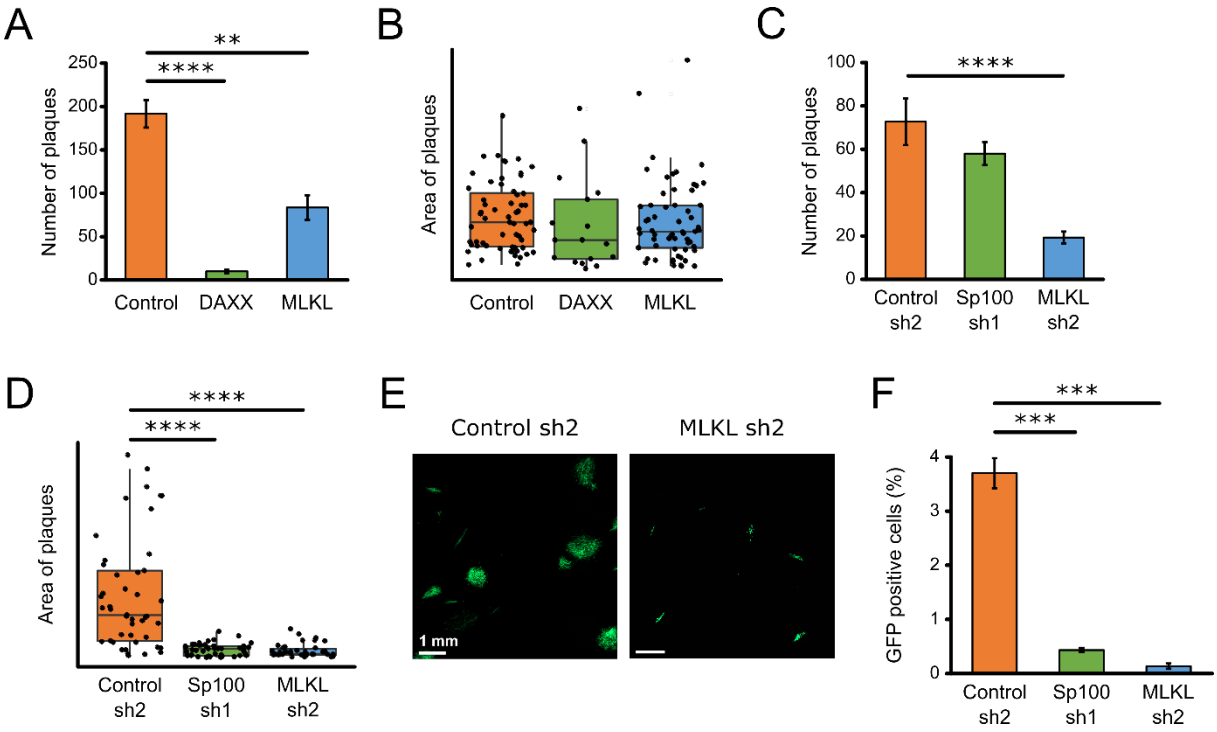

Figure 3.11: MLKL plaque assays.

Non-coloured HFFF-TERTs expressing control, overexpression or shRNA vectors were infected with AD169-GFP (RCMV288) virus and covered with a 1:1 mix of Avicel and 2× Dulbecco's Modified Eagle's Medium (DMEM) to prevent transmission via the media. After 14 days, cells were washed and fixed. **(A-B)** Overexpression plaque assay. **(A)** Number of plaques (group of greater than five infected cells). P-values were calculated with a Tukey' HSD post-hoc test following an ANOVA test (n=3). Standard p-value notation is used. **(B)** Area of plaques. A random selection of plaques were photographed under a 10× objective. The area of the GFP-positive plaques was determined using ImageJ. The centre line represents the median, the box shows the interquartile range and the bar shows the 95% confidence interval of the median. Points represent individual plaques. P-values were calculated with a non-parametric Mann-Whitney U test. **(C-F)** shRNA plaque assay. **(C)** Number of plaques. **(D)** Area of plaques. **(E)** Plaques were photographed using an AxioObserver Inverted Microscope with a 5× objective. **(F)** Number of GFP-positive cells. Cells were trypsinised, fixed and the percentage of GFP-positive cells measured by flow cytometry. P-values were calculated with a Student's t-test (n=3).

3.9 DMXL1

In contrast to the effect of knocking down a restriction factor such as Sp100, knockdown of DMXL1 resulted in a consistent three-fold decrease in virus infection **(Figure 3.12)**, suggesting that DMXL1 might be required for infection, rather than acting as an ARF.

In agreement with the restriction assay, knockdown of DMXL1 with the same shRNA construct resulted in a significant decrease in the number and size of the plaques and the overall number of GFP cells **(Figure 3.12A-D)**. This result was reproducible when using the same cell line and seen from as early as 7 days post-infection **(Figure 3.12E-F)**. As before, Sp100 knockdown unexpectedly led to a decrease in plaque number and plaque size.

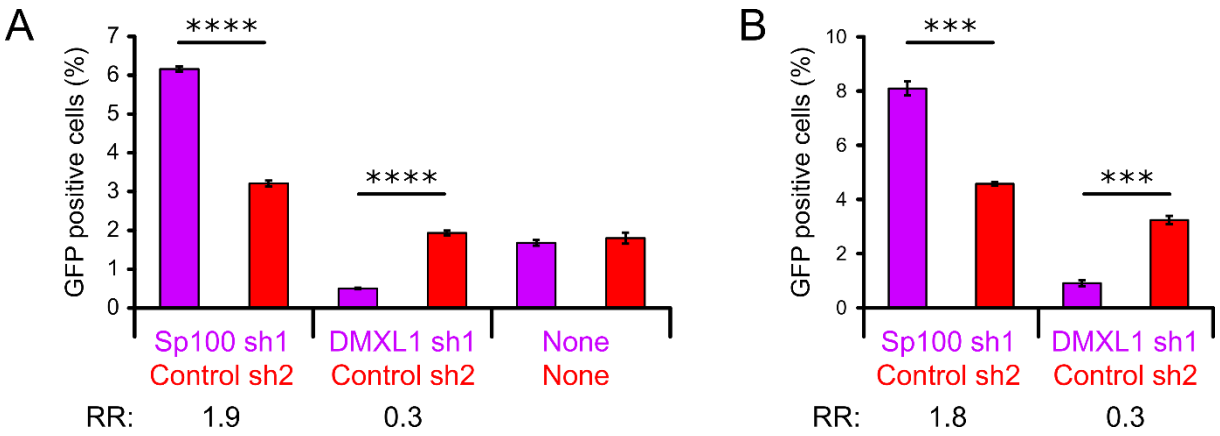

Figure 3.12: DMXL1 restriction assays.

(A) shRNA restriction assay. See Figure 3.10B. **(B)** Repeat assay.

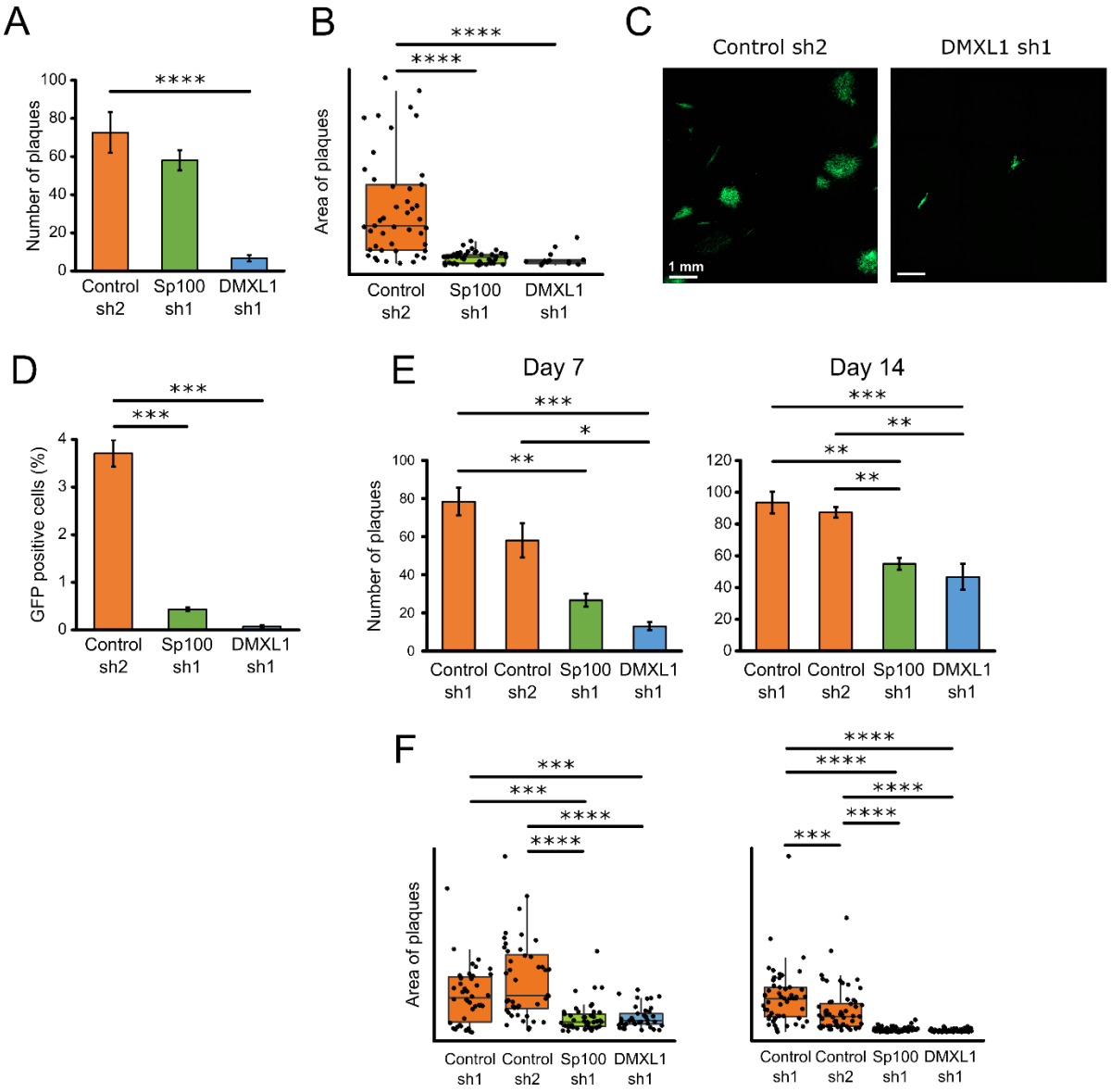

Figure 3.13: DMXL1 plaque assays.

(A-D) shRNA plaque assays. See Figure 3.11C-F. **(E-F)** Repeat of plaque assay with additional quantification of plaques at 7 as well as 14 days.

3.10 ARHGAP35, DHCR24, FRMD6, IFIT2 and LMAN2L

In the two-colour restriction assays, overexpression of ARHGAP35, DHCR24, FRMD6, IFIT2 or LMAN2L did not result in any restriction **(Figure 3.14A, Figure 3.16A, Figure 3.18A, Figure 3.20A and Figure 3.22A)**. shRNA knockdown produced highly variable results. Knockdown of ARHGAP35 (sh2), LMAN2L (sh1) and FRMD6 (sh3) led to a decrease in the percentage of GFP-expressing cells **(Figure 3.14B, Figure 3.18B and Figure 3.22B)**, while knockdown of DHCR24 (sh1) and IFIT2 (sh1 and sh2) resulted in significant increases **(Figure 3.16B and Figure 3.20B)**.

The shRNA restriction assay was repeated for the genes that showed a restriction ratio of >1 (DHCR24 and IFIT2), this time with both shRNA cell lines, using a different UL36-GFP virus stock. The DHCR24 sh1 cell line showed a similar permissibility to infection as in the first assay **(Figure 3.16C)**. However, the DHCR24 sh2 cell line did not behave in the same manner as the DHCR24 sh1 cell line, instead being infected at a lower frequency compared to the control cells **(Figure 3.16C)**. Both IFIT2 knockdown cell lines failed to reproduce the increase in infection seen in the first assay **(Figure 3.20C)**. The contrasting results (particularly with respect to IFIT2) could have been due to the use of different virus stocks, which may contain different amounts of secreted factors such as IFNs. The assay was therefore repeated once more using a third viral stock, which gave results that were highly consistent with those from the second assay (**Figure 3.16B and Figure 3.20B**, third repeat not shown).

In the plaque assays, overexpression of all of the proteins resulted in a non-significant decrease in plaque number, with no effect on plaque size **(Figure 3.15A-B, Figure 3.17A-B, Figure 3.19A-B, Figure 3.21A-B and Figure 3.23A-B)**. In the shRNA plaque assays, only knocking-down IFIT2 (sh2) produced a significant increase in the number of plaques, which were also larger in size than the plaques on the control cell line (**Figure 3.21C-E)**. Knockdown of ARHGAP35 (sh2), FRMD6 (sh3) and LMAN2L (sh2) resulted in a decrease in plaque number and plaque size in comparison to the control **(Figure 3.15C-E, Figure 3.19C-E and Figure 3.23C-E)**. Although the numbers of plaques on control and DHCR24 sh2 cell lines were not significantly different, the plaques produced on DHCR24 knockdown cells were much larger, indicating that DHCR24 may inhibit cell-to-cell spread **(Figure 3.17C-E)**. The plaques on the DHCR24 and IFIT2 knockdown cell lines often extended past the field of view using a 10× objective, leading to an underestimation of true plaque size. More photographs were taken using a 5× objective and analysed separately **(Figure 3.17D and Figure 3.21D).** Infection of DHCR24 and IFIT2 shRNA cell lines also resulted in a larger number of GFP-positive cells overall **(Figure 3.17F and Figure 3.21F)**. As described in **3.8**, a significant caveat for this experiment was that the positive control (Sp100 knockdown) did not produce the expected results, with plaques being significantly smaller than those formed on control cells and no increase in plaque number as previously documented [117].

The shRNA plaque assay was repeated using both control cell lines and both shRNA cell lines available for DHCR24 and IFIT2 **(Figure 3.17G-H and Figure 3.21G-H)**. Plaques were analysed at both 7 and 15 days post-infection. At both 7 and 15 days, the effect of IFIT2 sh2 knockdown on plaque number seen in the first assay was reproduced but was not seen with the IFIT2 sh1 cells **(Figure 3.21G)**. Infection of DHCR24 sh2 cells again produced larger plaques than that of the control cell lines after 2 weeks of infection, but this effect was not seen at the earlier time point **(Figure 3.17H)** Furthermore, the size of plaques on DHCR24 sh1 cells was not significantly different to those on control cells. Again, the Sp100 knockdown control did not behave as expected.

A selection of monoclonal CRISPR cell lines that showed total or almost complete knockout of DHCR24, FRMD6, or LMAN2L by immunoblot were also used in a plaque assay. Consistent with the variation in infection rates of control CRISPR cell lines by restriction assay **(Figure 3.9)**, there was significant variation in the number and size of plaques between the cell lines, including between the controls **(Figure 3.17I-J, Figure 3.19G-H and Figure 3.23G-H)**.

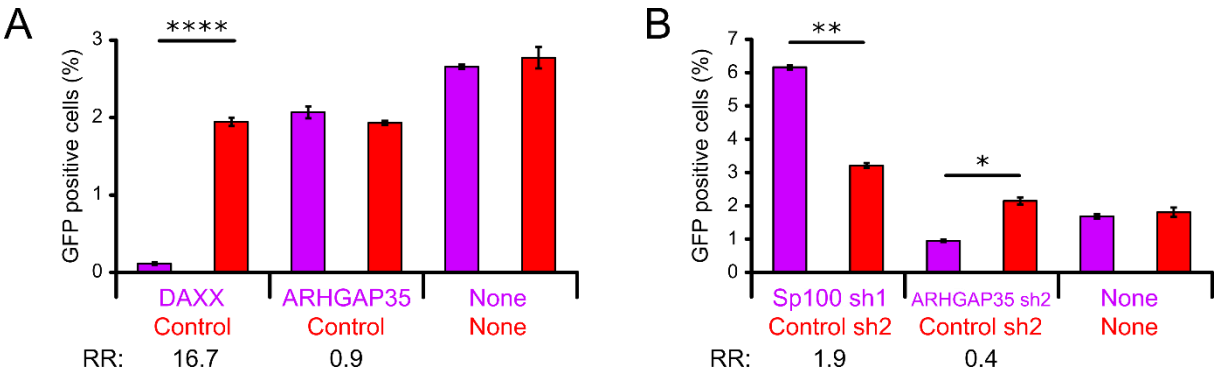

Figure 3.14: ARHGAP35 restriction assays.

(A) Overexpression restriction assay, as described in Figure 3.10A**. (B)** shRNA restriction assay, as described in Figure 3.10B**.**

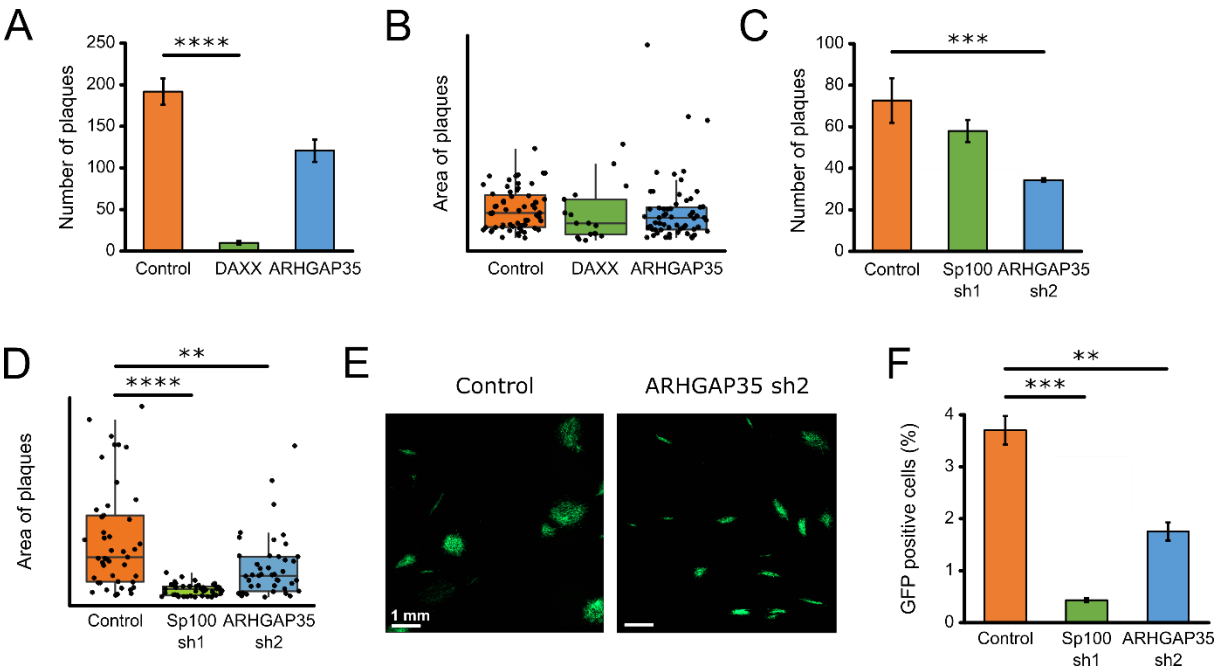

Figure 3.15: ARHGAP35 plaque assays.

(A-B) Overexpression plaque assay, as described in Figure 3.11A-B**. (C-F)** shRNA plaque assay, as described in Figure 3.11C-F**.**

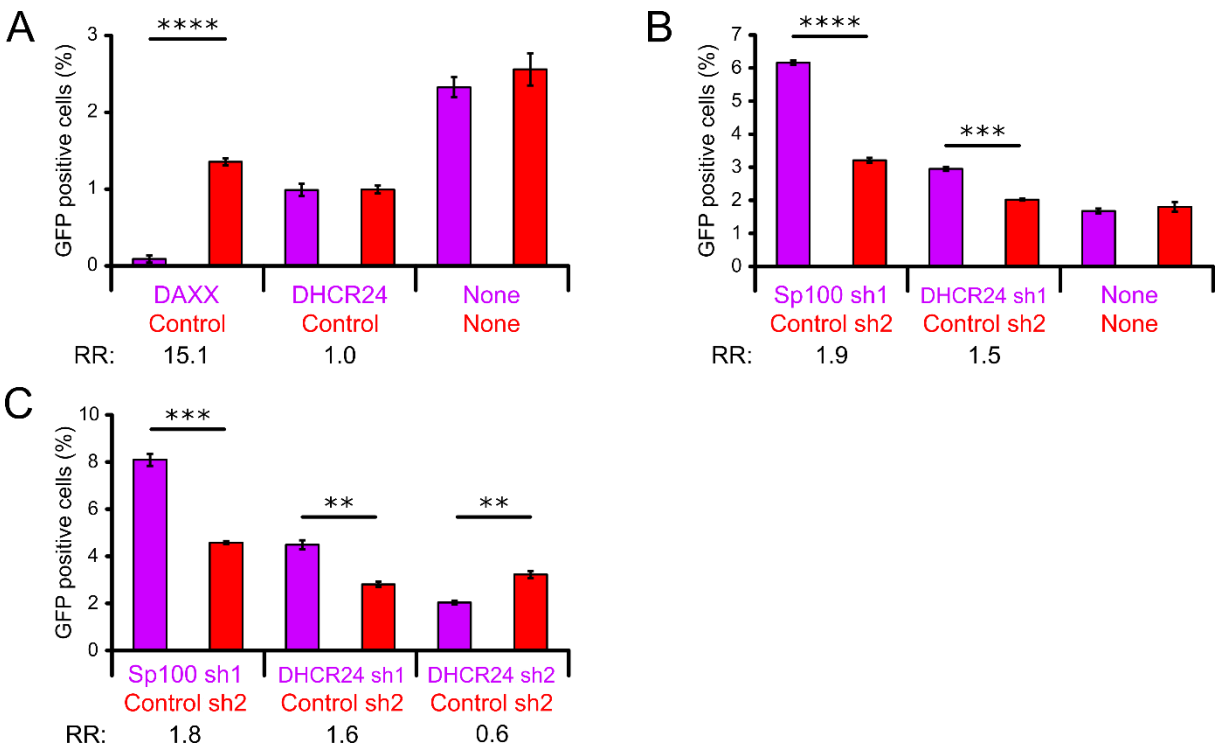

Figure 3.16: DHCR24 restriction assays.

(A) Overexpression restriction assay, as in Figure 3.10A. **(B)** shRNA restriction assay, as in Figure 3.10B. **(C)** Repeat of (B) with additional DHCR24 shRNA cell line.

(Following page)

Figure 3.17: DHCR24 plaque assays.

(A-B) Overexpression plaque assay, as described in Figure 3.11A-B. **(C-F)** shRNA plaque assay, as described in Figure 3.11C-F. As the plaques were very large and extended past the field of view using a 10× objective, more photographs were taken using an AxioObserver Inverted Microscope with a 5× objective and analysed separately. **(G-H)** Repeat of plaque assay with additional quantification of plaques at 7 as well as 14 days, and using an additional DHCR24 shRNA cell line. **(I-J)** Plaque assay on monoclonal DHCR24 CRISPR cell lines and controls.

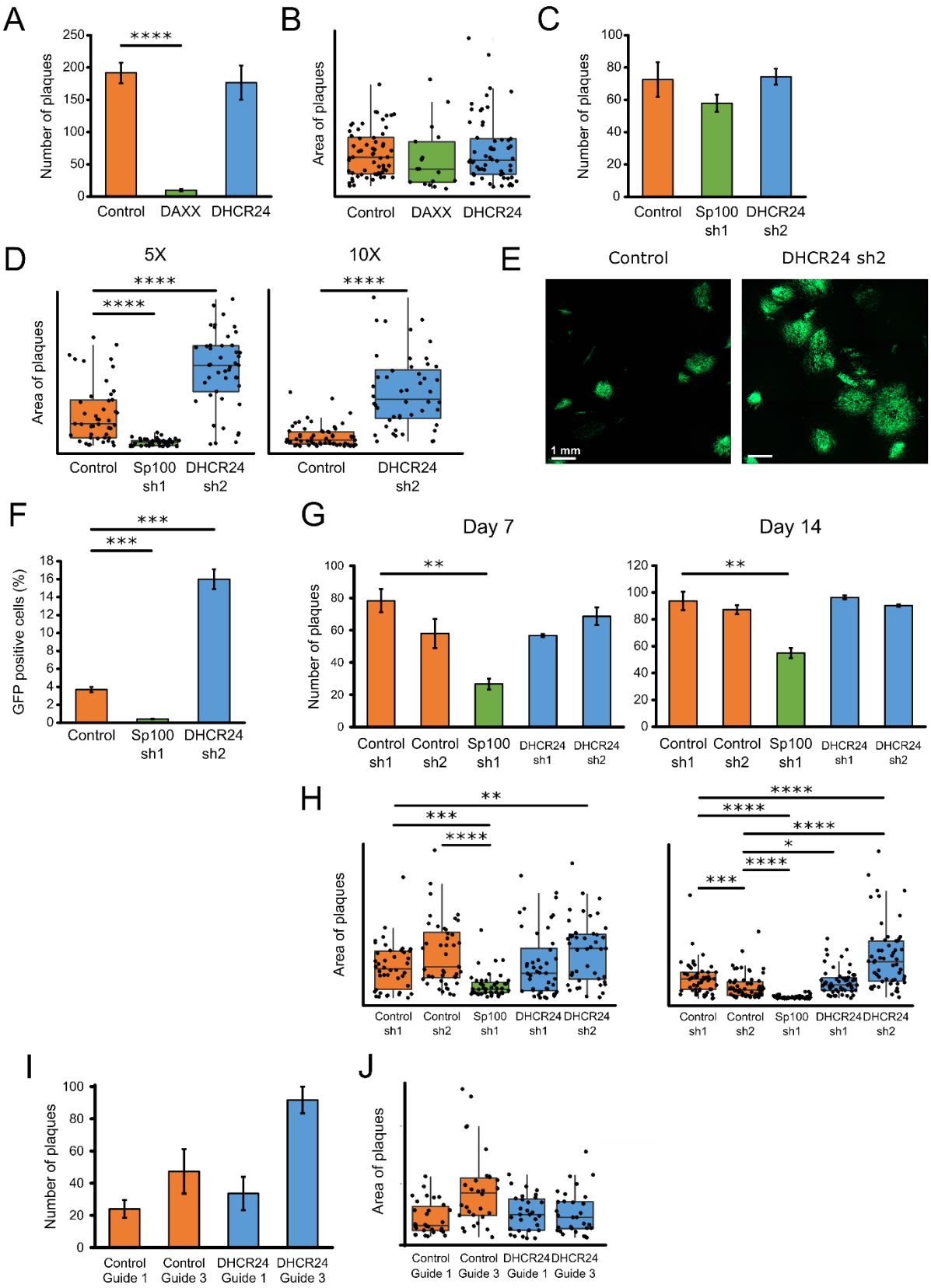
A
Number of plaques
****
Control
DAXX
DHCR24
B
Area of plaques
Control
DAXX
DHCR24
C
Number of plaques
Control
Sp100 sh1
DHCR24 sh2
D
5X
10X
Area of plaques
Control
Sp100 sh1
DHCR24 sh2
DHCR24 sh2
E
Control
DHCR24 sh2
1 mm
F
GFP positive cells (%)
***
Control
Sp100 sh1
DHCR24 sh2
G
Day 7
Day 14
Number of plaques
**
Control sh1
Control sh2
Sp100 sh1
DHCR24 sh1
DHCR24 sh2
H
Area of plaques
**
***
****
*
I
Number of plaques
Control Guide 1
Control Guide 3
DHCR24 Guide 1
DHCR24 Guide 3
J
Area of plaques

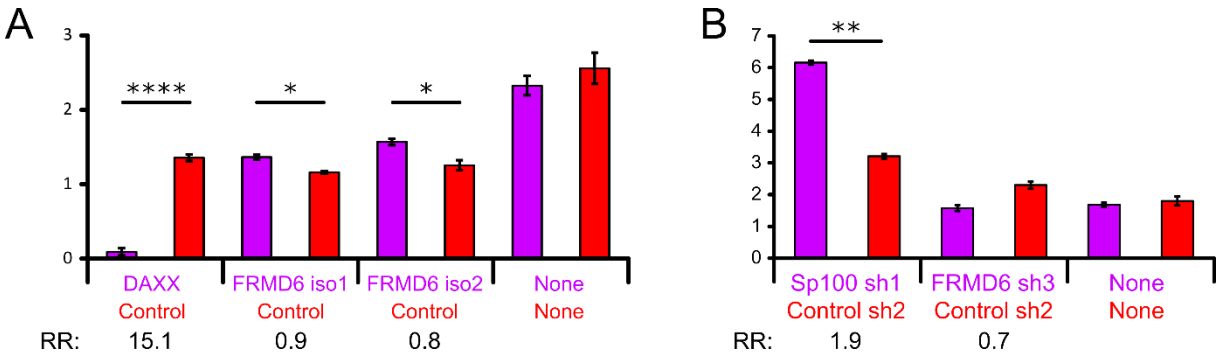

Figure 3.18: FRMD6 restriction assays.

(A) Overexpression restriction assay, as in Figure 3.10A. iso, isoform. **(B)** shRNA restriction assay, as in Figure 3.10B.

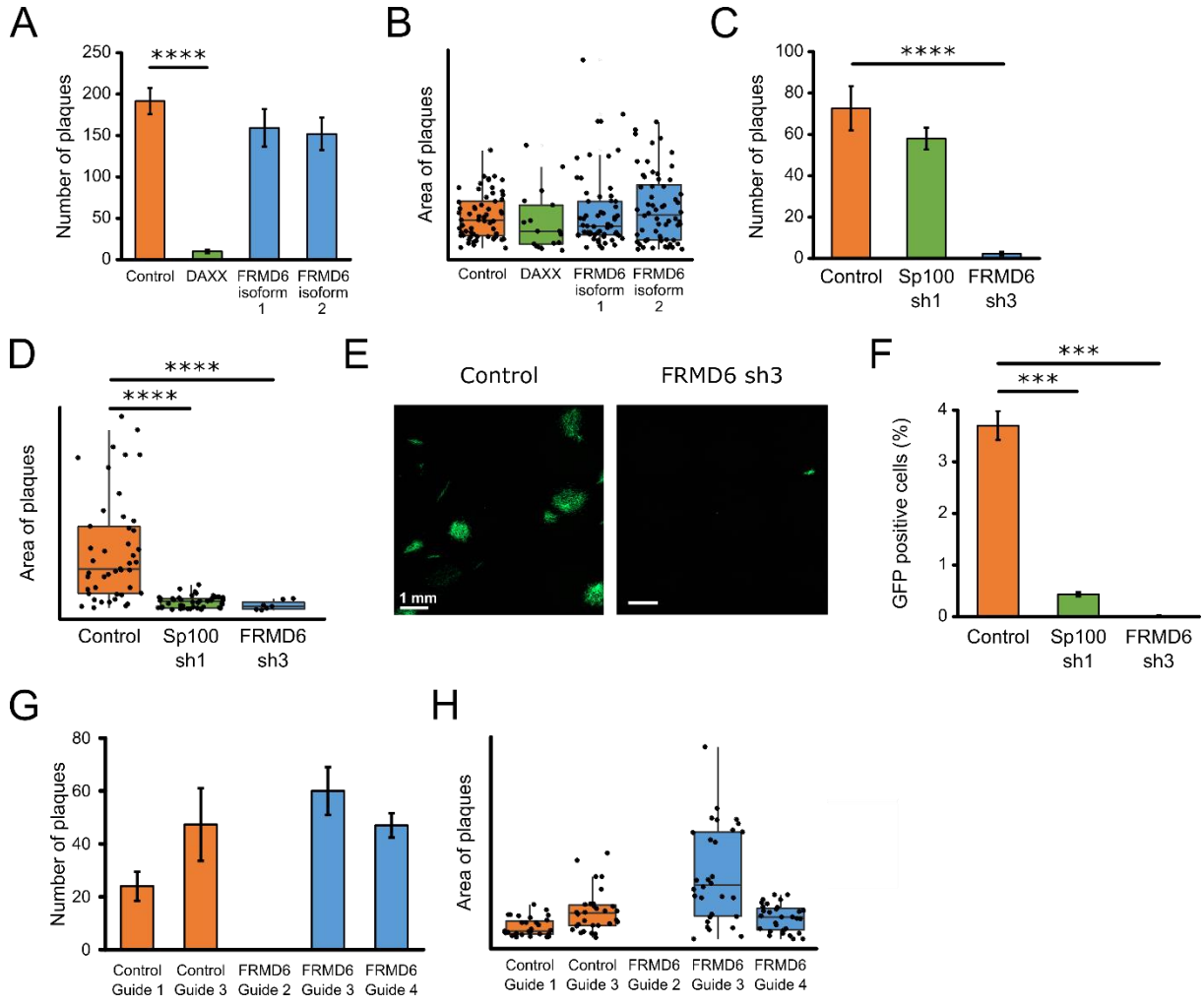

Figure 3.19: FRMD6 plaque assays.

(A-B) Overexpression plaque assay, as described in Figure 3.11A-B. **(C-F)** shRNA plaque assay, as described in Figure 3.11C-F. **(G-H)** Plaque assay on monoclonal FRMD6 CRISPR cell lines and controls. There were no plaques on the FRMD6 Guide 2 CRISPR cells.

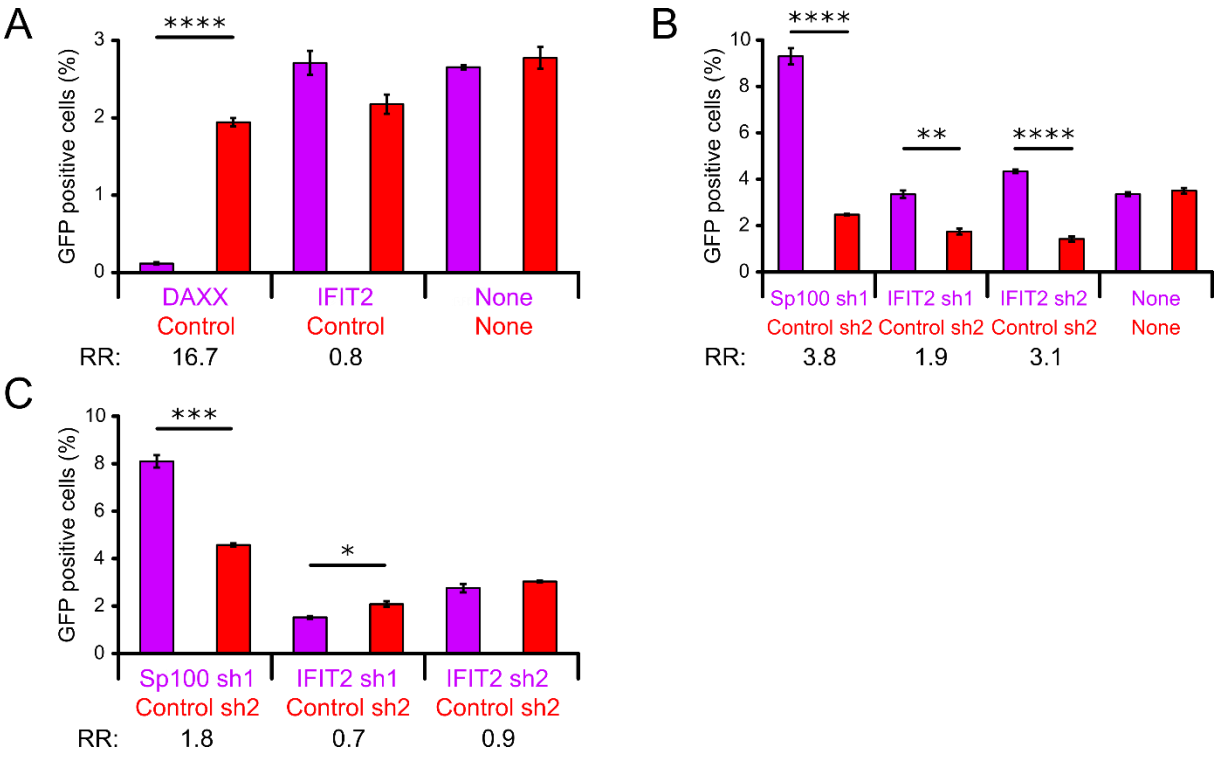

Figure 3.20: IFIT2 restriction assays.

(A) Overexpression restriction assay, as in Figure 3.10A. **(B)** shRNA restriction assay, as in Figure 3.10B. **(C)** Repeat of (B).

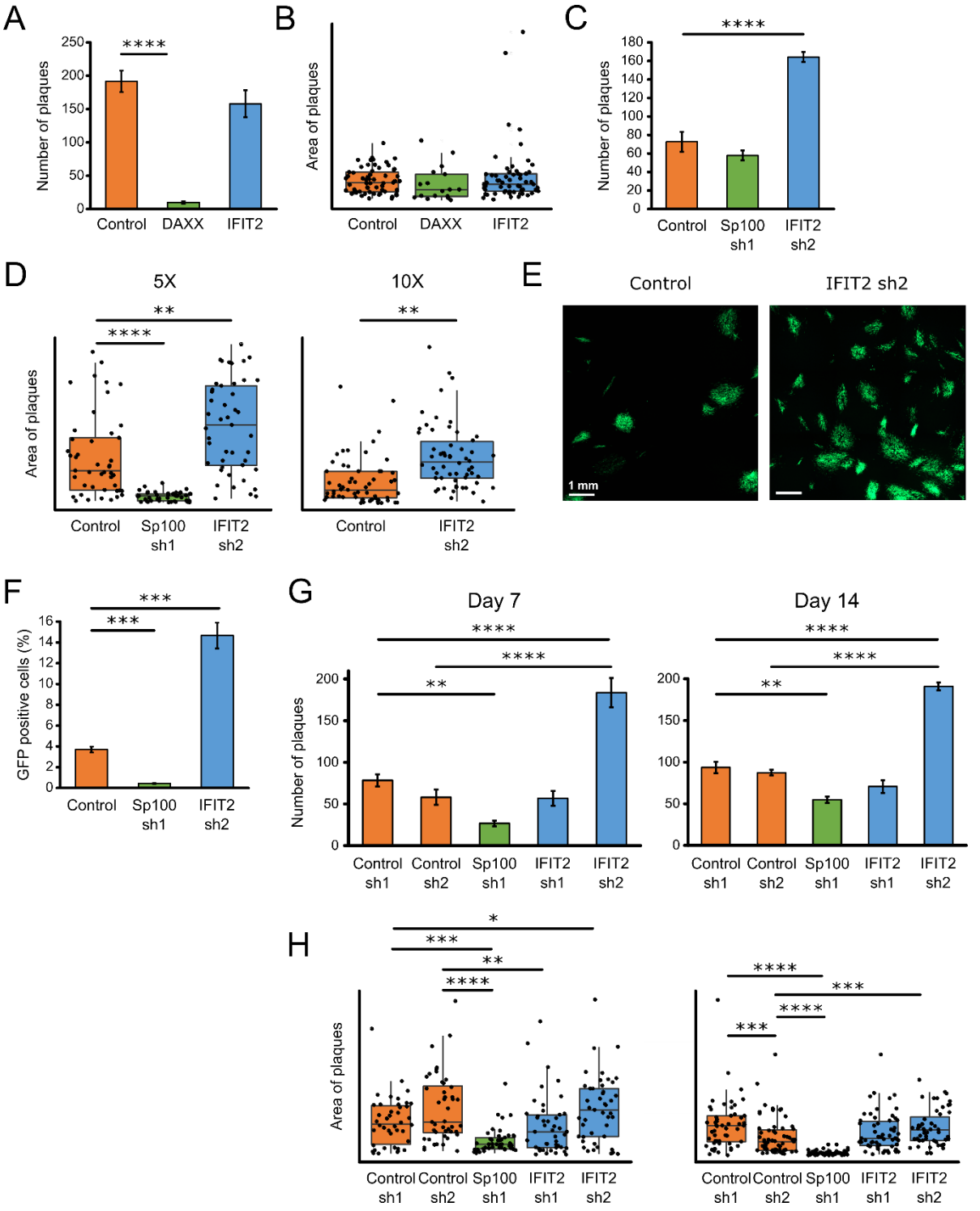

Figure 3.21: IFIT2 plaque assays.

(A-B) Overexpression plaque assay, as described in Figure 3.11A-B. **(C-F)** shRNA plaque assay, as described in Figure 3.11C-F. As the plaques extended past the field of view using a 10× objective, more photographs were taken with a 5× objective and analysed separately. **(G-H)** Repeat of plaque assay with additional quantification of plaques at 7 as well as 14 days.

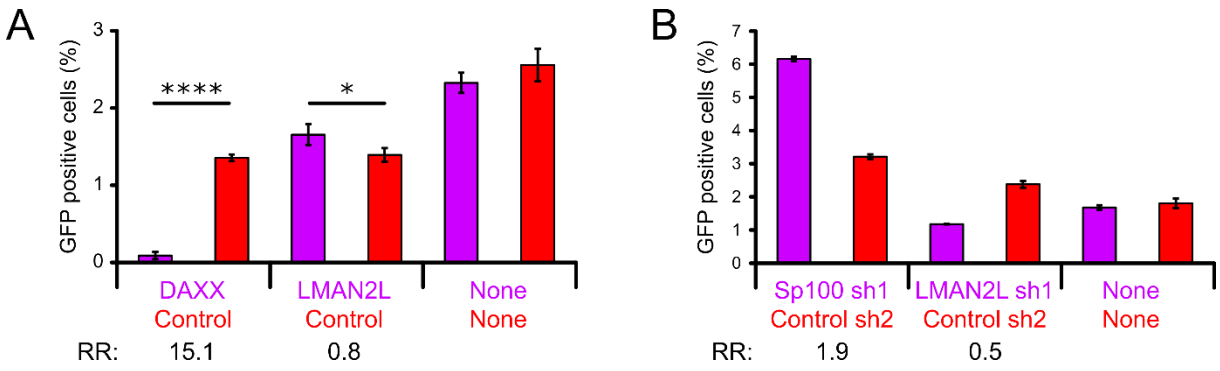

Figure 3.22: LMAN2L restriction assays.

(A) Overexpression restriction assay, as in Figure 3.10A. **(B)** shRNA restriction assay, as in Figure 3.10B.

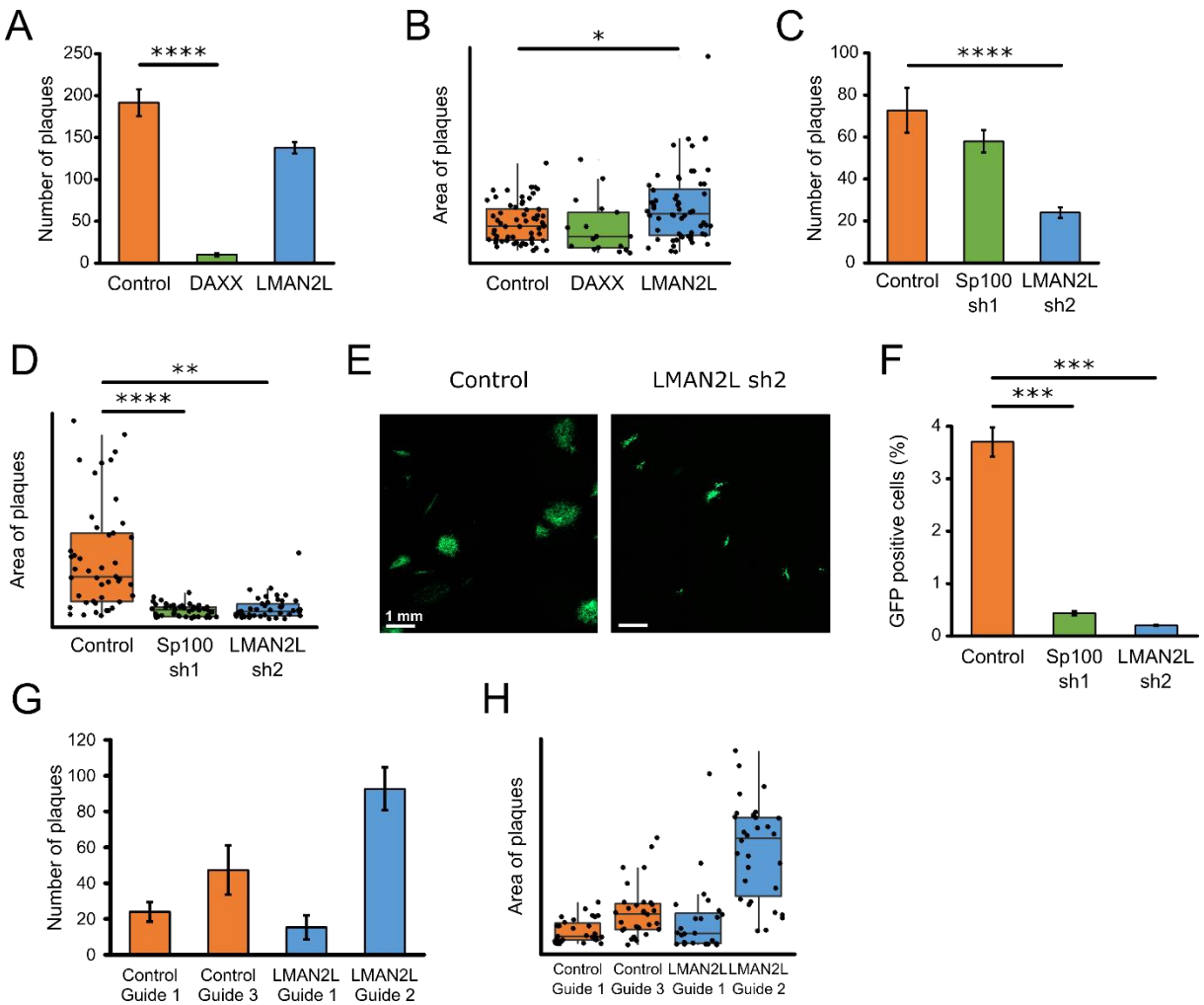

Figure 3.23: LMAN2L plaque assays.

(A-B) Overexpression plaque assay, as described in Figure 3.11A-B. **(C-F)** shRNA plaque assay, as described in Figure 3.11C-F. **(G-H)** Plaque assay on monoclonal LMAN2L CRISPR cell lines and controls.

3.11 shRNA knockdown has variable effects on the plaque assay read-out

Due to the unexpected result seen with the Sp100 shRNA knockdown cells, as well as differences seen between cell lines expressing shRNAs targeting different sequences of the same protein, the DMXL1 plaque assay was repeated using cells expressing different DMXL1 shRNA constructs **(Figure 3.24A)**. Included in this experiment were the original control sh2 and DMXL1 sh1 cell lines used in the first experiment **(Figure 3.13),** and cell lines re-transduced with the control sh2 and DMXL1 sh1 constructs, as well as a range of other control and DMXL1 shRNA constructs targeting different sequences. Knockdown in these cell lines was validated using RT-qPCR, due to problems detecting DMXL1 by immunoblot as discussed previously **(Figure 3.24B)**.

Cell lines re-transduced with DMXL1 sh1, or expressing other shRNA constructs targeting different sequences, did not show the same phenotype as the original cell line. There was no consistent effect on plaque number **(Figure 3.24A)**, despite showing significant DMXL1 knockdown by RT-qPCR **(Figure 3.24B)**.

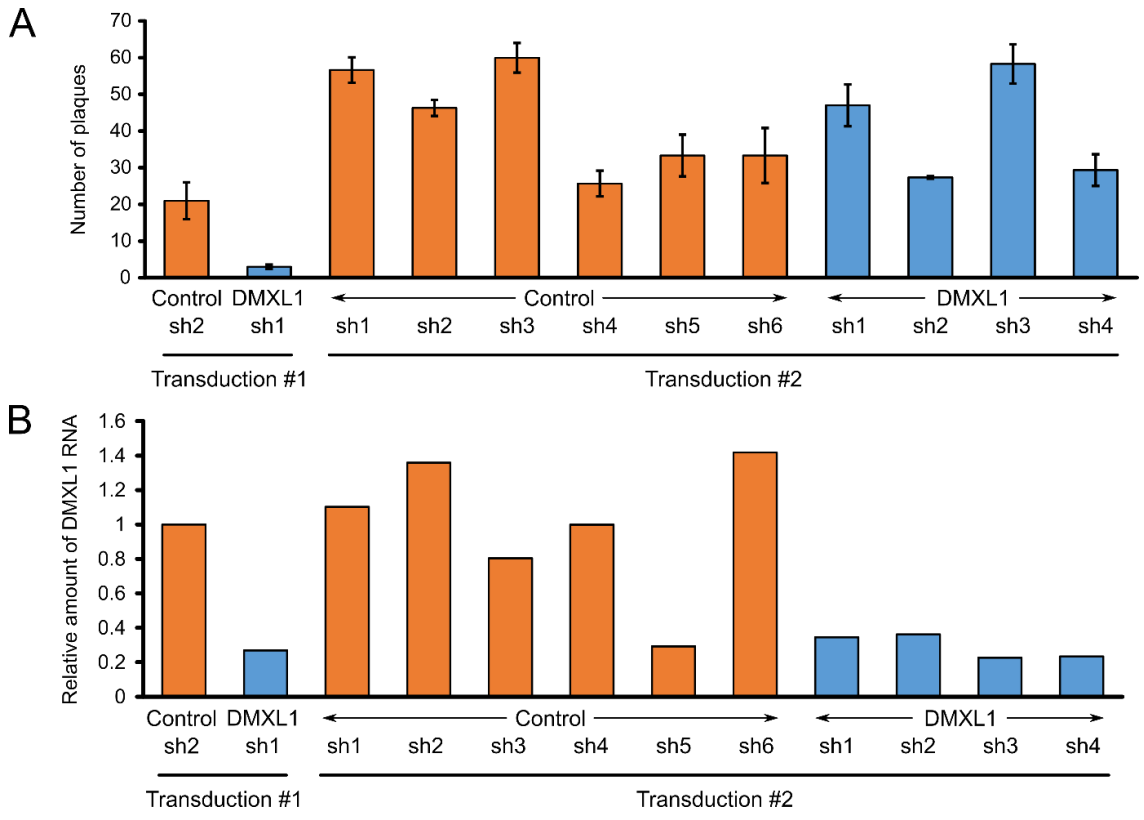

Figure 3.24: DMXL1 plaque assay repeat: shRNA transduction leads to variable results.

(A) Number of plaques from a plaque assay on control and DMXL1 shRNA cell lines, as described in Figure 3.11C. Included in this assay were the original cell lines used in Figure 3.13, as well as cell lines re-transduced with the control sh2 and DMXL1 sh1 constructs, and additional control and target shRNA constructs. **(B)** RT-qPCR validation of DMXL1 knockdown.

3.12 shRNA knockdown has variable effects on the cell proteome

One hypothesis for why shRNA transduction led to such variable restriction and plaque assay results was that the concentration of lentivirus being used was too high, leading to multiple simultaneous infection and integration events that could have a large effect on the cellular proteome. Even at dilutions of lentivirus as high as 1:512, knockdown of Sp100 could still be observed **(Figure 3.25A)**, indicating that neat lentivirus, which had been previously used for shRNA transduction, may have been resulting in an overly high infection rate. To investigate the effect on the cellular proteome, mass spectrometry (MS) analysis of whole cell lysates from HFFF-TERTs transduced with different concentrations of lentivirus (from neat to 1:244) was performed for two different shRNAs - Sp100 and IFIT2. Hierarchical cluster analysis of the fold changes in protein abundance compared to untransduced cells showed that samples did not cluster according to the dilution factor, indicating that alterations in the proteome did not correlate with the lentivirus concentration **(Figure 3.25B)**.

Levels of proteins encoded by IFN-stimulated genes (ISGs), which are likely to have an impact on the plaque assay read-out, varied significantly from that in untransduced cells and were somewhat variable between cell lines transduced with different concentrations of lentivirus **(Figure 3.25C)**. This may help to explain the differences in phenotype we see for cell lines transduced with the same shRNA at different times **(Figure 3.24A)**. A number of proteins, including those encoded by ISGs, appeared to be commonly up- or down-regulated by both Sp100 and IFIT2 shRNAs, indicating that shRNA lentiviral transduction in general might have a number of reproducible effects on the cell, irrespective of the target sequence.

To evaluate whether cell lines transduced with different shRNAs against the same target protein exhibit variability at the proteome level, the control and DMXL1 shRNA cell lines used in the plaque assay in **Figure 3.24A** were analysed by quantitative MS **(Figure 3.25D-E)**. The control and DMXL1 shRNA cell lines did not cluster together, nor did the cell lines that were transduced in parallel under the same conditions, indicating that shRNA lentiviral transduction has highly variable off-target effects on the cellular proteome. Again, there was considerable upregulation of some ISGs in comparison to untransduced cells in both the control and DMXL1 shRNA cell lines.

This proteomic variability seen upon transduction of shRNAs was not seen with transduction of pHAGE-pSFFV overexpression vectors, exemplified by a proteomic experiment of cell lines expressing the HCMV protein pUS33A that was performed for a later section of this thesis **(Figure 3.26)**. The control cell line clustered separately from the US33A-expressing cell lines, and little variability across the cellular proteomes was observed (in comparison to **Figure 3.25B and D**, where the same scale and contrast were used).

As well as explaining the lack of reproducibility in the plaque assays, these observations also bring into question the validity of the two-colour shRNA restriction assay results, despite seeing the expected

results with the positive controls. siRNA transfection was shown to have fewer off-target effects on the cell proteome **(Figure 6.10)** and was therefore used as an alternative from this point onwards.

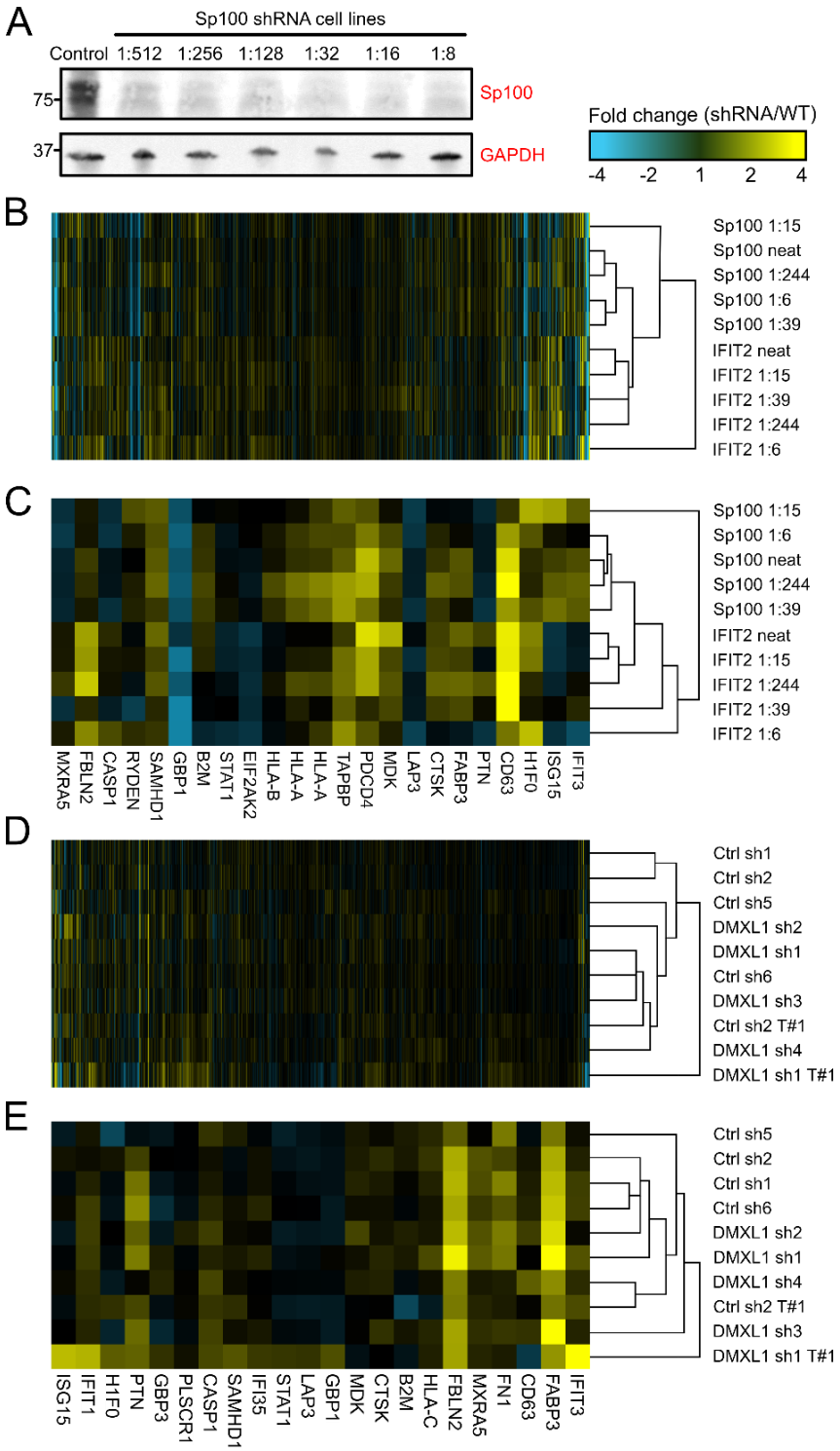

(Previous page)

Figure 3.25: shRNA lentiviral transduction results in off-target effects on the cellular proteome.

(A) Immunoblot validation of Sp100 knockdown in cells transduced with various concentrations of lentivirus containing an Sp100 shRNA construct. This blot was performed by Dr. Benjamin Ravenhill. **(B-C)** Sp100 and IFIT2 (sh1) shRNA cell lines, generated by transduction with varying concentrations of lentivirus, were analysed by quantitative MS alongside WT cells. **(B)** Hierarchical cluster analysis of fold changes in protein abundance, compared to WT cells, for all proteins quantified. **(C)** Hierarchical cluster analysis of IFN-stimulated genes (defined as those upregulated more than two-fold by IFN, from unpublished data collected by Dr. Katie Nightingale and Dr. Michael Weekes). **(D-E)** The control and DMXL1 shRNA cell lines used in the plaque assay analysis from Figure 3.24 were also analysed by MS. T#1, transduction number 1. **(D)** Hierarchical cluster analysis of fold changes in protein abundance, compared to WT cells, for all proteins quantified. **(E)** Hierarchical cluster analysis of IFN-stimulated genes.

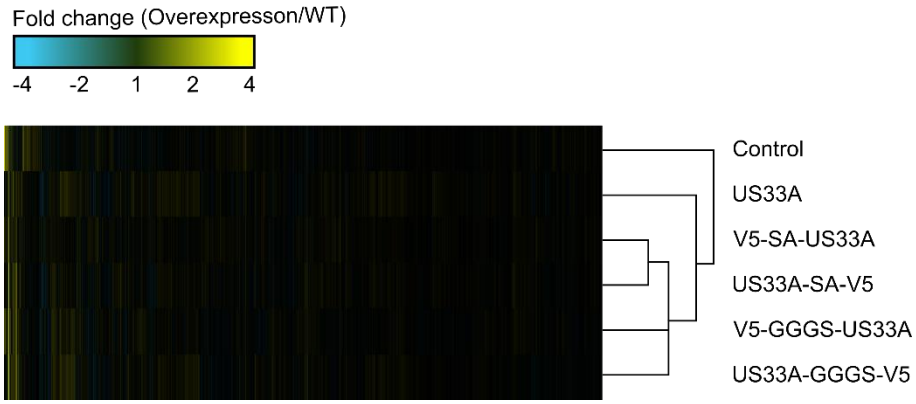

Figure 3.26: Transduction with lentiviral overexpression vectors does not result in the same variability as shRNA transduction.

Six cell lines constitutively expressing a control vector, HCMV protein pUS33A, or pUS33A tagged with V5 at the N- or C-terminus with different linker sequences were generated by lentiviral transduction for Chapter 6 of this thesis. The cell lines were analysed by MS along with WT untransduced cells. Hierarchical cluster analysis was performed on the fold changes in protein abundance, compared to WT cells, for all proteins quantified. The same contrast was used as in Figure 3.25 to enable comparison.

3.13 Analysis of positive selection

As positive selection is a common feature of ARFs **(1.2.1)** [104], the presence of positive selection in the genetic sequences of the candidate ARFs was investigated using Selectome, a publicly-available database [289,290]. Selectome reports results of branch-site likelihood tests on particular branches of the phylogenetic tree [303]. DHCR24, MLKL, DMXL1, and LMAN2L were all positively selected during evolution of the Euteleostomi (or 'bony vertebrates'), while IFIT2 was positively selected during

primate evolution **(Table 3.2)**. Analysis of individual speciation events showed that MLKL was positively selected during evolution of the Homininae taxon (or 'African apes', including humans) **(Figure 3.27)**.

Gene	*Taxon*	*Positively selected?*
ARHGAP35	Glires	No
	Primates	No
DHCR24	Euteleostomi	YES
	Primates	No
MLKL	Euteleostomi	YES
DMXL1	Euteleostomi	YES
	Primates	No
LMAN2L	Euteleostomi	YES
	Primates	No
FRMD6	Euteleostomi	No
	Primates	No
IFIT2	Primates	YES

Table 3.2: Analysis of positive selection of each of the seven candidate ARFs.
Data from Selectome v6.

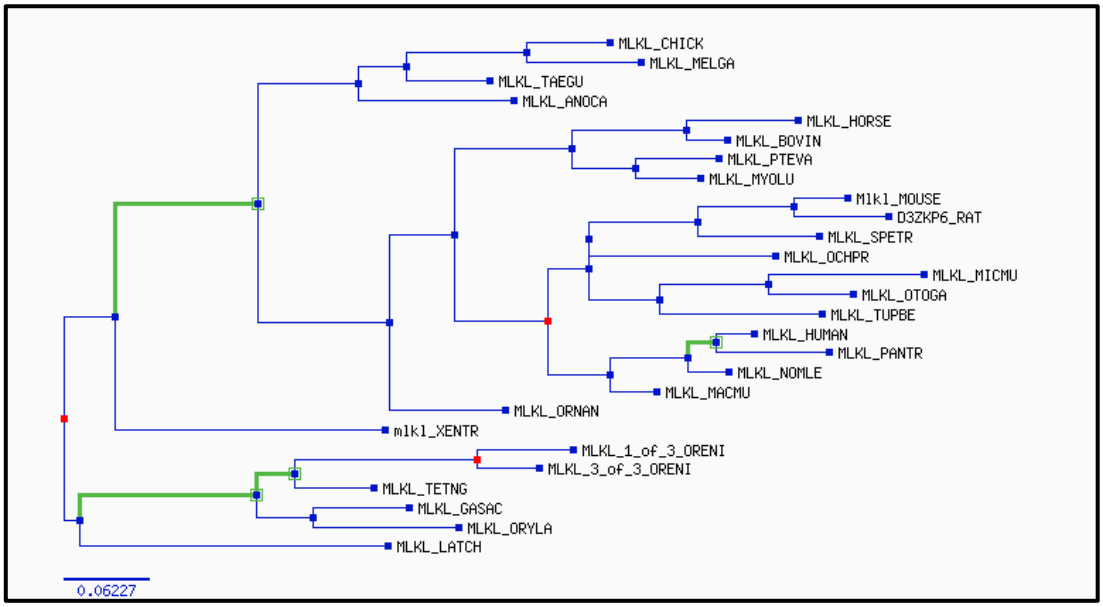

Figure 3.27: MLKL phylogenetic tree.
Blue nodes represent speciation events, red represent duplication events, and green branches represent branches under positive selection.

3.14 Discussion

The purpose of this part of the project was to screen candidate ARFs for antiviral activity using restriction assays and plaque assays. Some evidence of restriction was seen for MLKL, DHCR24 and IFIT2 **(Table 3.3)**. All three genes show signatures of positive selection, indicating that they may represent good candidate ARFs **(Table 3.2)**. However, the value of these screens was weakened by problems with reproducibility, particularly between shRNA cell lines targeting the same protein.

In the two-colour restriction assays, overexpression of six of the target proteins (excluding DMXL1, which could not be overexpressed due to its size), did not result in any restriction of early viral gene expression. shRNA knockdown produced highly variable results that could not be explained by differences in knockdown efficiency. The relative level of infection varied between cell lines expressing shRNAs targeting different sequences of the same protein (DHCR24) and repeats of the experiment with the same cell lines (IFIT2).

Despite these limitations, the two-colour system represents a valuable development in the use of restriction assays for evaluating virus replication. Except for the variation seen with the IFIT2 cell lines, the results showed high levels of consistency between biological repeats and independent experiments. This technique is therefore superior to the restriction assays performed in WT cells, which show extreme variability between experiments, likely due to the effect of cell population density. One additional source of variation that was considered was differing amounts of secreted factors in our viral stocks. However, our group has since shown that when cells are treated with the supernatants of our viral stocks, the expression of ISGs shows a similar pattern to that of mock-infected cells (incubated with DMEM alone), indicating that our viral stocks contain very little IFN and other secreted factors [62].

		Evidence of restriction?	
	Cell line	***Restriction assay*** *(UL36-GFP Merlin, coloured cells)*	***Plaque assay*** *(AD169-GFP, non-coloured cells)*
Overexpression	DHCR24 overexpression	No	No
	IFIT2 overexpression	No	No
	MLKL overexpression	No	Yes
Knockdown	DHCR24 sh1	Yes	No
	DHCR24 sh2	No	Yes (increase in plaque size)
	IFIT2 sh1	Assay #1: Yes Assay #2: No	No
	IFIT2 sh2		Yes (increase in plaque number)
	MLKL sh1	Yes	NT
	MLKL sh2	Some	No

Table 3.3: Summary of restriction assay and plaque assay results.

Only proteins that showed any evidence of restriction in any of the assays are included. NT, not tested.

In the plaque assays, only overexpression of DAXX and MLKL significantly reduced the numbers of plaques, indicating that MLKL may restrict productive HCMV infection. The lack of effect of protein overexpression of other proteins in both the restriction and plaque assays might be because the virus is able to counteract this overexpression via degradation of the target proteins. This is particularly likely where only a modest level of overexpression is achieved. Restriction and plaque assays could make use of deletion viruses lacking the viral genes responsible for degradation of individual proteins of interest in order to restore endogenous protein levels **(Future directions 3)**.

Overexpression of none of the proteins, including DAXX, resulted in any difference in the plaque size. Given the role of DAXX in suppressing viral IE gene transcription and replication [112], overexpression of DAXX would be expected to result in fewer and smaller plaques, although this has never been reported in the literature. The explanation for why a reduction in plaque size was not observed is unclear.

Although an increase in plaque number was seen in IFIT2 sh2 knockdown cells, and an increase in plaque size was seen upon expression of DHCR24 sh2, these results were not reproduced when using cell lines expressing different shRNAs for the same proteins **(Future directions 3)**. Furthermore, knockdown of Sp100 did not produce the expected results, bringing into question the validity of the shRNA knockdown approach. Indeed, it was then shown that cell lines transduced with the same shRNA vectors at different times produced different plaque assay outcomes **(Figure 3.24)** and exhibited variation in the cellular proteome in a manner that was not dependent on lentivirus concentration **(Figure 3.25)**. While knockdown of Sp100 was sufficient to override the phenotypic off-target effects of shRNA transduction and enable evaluation of its effect on IE gene expression **(Figure 3.3)**, this effect was lost over multiple rounds of virus replication (as seen in the plaque assay) **(Figure 3.11)**. Individual shRNA cell lines produced reproducible outcomes across independent experiments, indicating that the off-target effects on the proteome and cell phenotypes were stable.

Another difficulty encountered was the finding that single-cell cloned CRISPR cell lines behave very differently, irrespective of the gRNA target **(Figure 3.9, Figure 3.17I-J, Figure 3.19G-H and Figure 3.23G-H)**. Potential explanations include the differential expression of Cas9 or the integration of Cas9-encoding sequences causing different off-target effects in different clones. To overcome this problem, our group now utilises nucleofection of single guide RNA (sgRNA):Cas9 ribonucleoprotein complexes, with preliminary experiments resulting in significant knockdown in polyclonal populations **(Future directions 3)**.

A. Two-colour restriction assays and plaque assays on siRNA and CRISPR/Cas9 nucleofected cells.

Since these original assays were performed, our group has now developed protocols for siRNA transfection and sgRNA:Cas9 nucleofection. These systems could be applied to the two-colour restriction assay and plaque assay, facilitating a more reliable evaluation of the candidate ARFs.

B. Viral replication assays utilising deletion viruses.

This of course will only be possible for those candidate proteins that have known viral antagonists. Identification of the viral proteins targeting MLKL and DMXL1 are described in Chapter 5 and 6, respectively.

Future directions 3: Further experiments for the elucidation of candidate ARFs.

Later in this thesis, evidence is presented for a role of pUL36 in the degradation of MLKL. It was also found that tagging UL36 with GFP inhibited this function of UL36, despite it being tagged with a self-cleaving linker. Although it is not clear whether MLKL levels influence IE gene expression, there is a possibility that this inhibition of MLKL degradation and other unidentified functions of pUL36 may affect the restriction assay results. Consequently, another GFP-tagged recombinant HCMV could be used for restriction assays in the future.

Despite these limitations, three proteins, MLKL, DMXL1 and LMAN2L, were selected for further investigation. The gene blocks responsible for downregulation of these proteins had already been identified **(Figure 1.12E, Figure 1.13E and Figure 1.19E)**, facilitating study of the mechanism of protein degradation. Furthermore, a review of the literature highlighted potential infection-specific functions of these proteins, giving an indication of the functional assays that could be utilised to determine their effect on virus replication. MLKL and DMXL1 form the focus of this thesis, while the mechanism and function of LMAN2L degradation is being studied by another PhD student in our group, Leah Hunter.

3.14.1 MLKL

Whereas overexpression of MLKL did not have an effect on early viral replication **(Figure 3.10A)**, it did have a significant effect on plaque number **(Figure 3.11A)**. Overexpression of human MLKL alone cannot induce necroptotic cell death, but may make the cells more susceptible to the effects of virus-induced TNFα-dependent necroptosis [208]. This may explain why overexpression of MLKL only had an effect over multiple rounds of replication. The absence of an effect on early gene expression indicated that MLKL does not likely have any additional role in restricting early virus infection beyond its role in necroptosis. Although MLKL would not be considered an ARF, as it does not directly restrict virus infection, cell death is considered a mechanism of cell-intrinsic immunity.

In **Chapter 4**, analysis of protein degradation by HCMV at 48 h, later than the time points investigated in the early degradation screen, indicated that MLKL was one of the most significantly degraded proteins throughout infection. **Chapter 5** then goes on to investigate the mechanism and function of MLKL downregulation by HCMV.

3.14.2 DMXL1

Rather than acting as an antiviral factor, preliminary results indicated that DMXL1 facilitates infection. Results using the original DMXL1 shRNA cell line **(Figure 3.12 and Figure 3.13)**, showing that knockdown of DMXL1 inhibits infection, are in line with the finding that knockdown of vacuolar-type H^+-adenosine triphosphatase (V-ATPase) component ATP6V0C disrupts HCMV viral assembly compartment formation and suppresses viral replication [221,222]. However, the reliability of these results was brought into question by the finding that shRNA transduction has highly variable effects on the restriction assay and plaque assay read-outs. Nonetheless, given that there is already some evidence for the role of the V-ATPase in virus infection, it was decided that the mechanism of DMXL1 degradation should be investigated further **(Chapter 6)**. Importantly, although the evidence provided here does not provide reliable evidence for a role of DMXL1 in either restricting or facilitating virus infection, it also does not rule out a potential role for DMXL1. Indeed, given the importance of the V-ATPase for so many cellular processes, it is unlikely that downregulation of DMXL1 would not have any effect on virus replication. The work conducted for this chapter provides a foundation for more reliable experimental analysis of DMXL1 function in the future.

Chapter 4: Degradation of host proteins by human cytomegalovirus at 48 hours post-infection

The experiment presented in this chapter was published in PNAS in July 2020 [214]. *Some of the following figures have been reproduced or adapted from those in the manuscript, which were originally made by myself. PNAS authors do not need to obtain permission to use their original figures in their future works. Parts of the experiment were performed by Dr. Peter Tomasec and Dr. Michael Weekes, as indicated in the text. Collaborators at Cardiff University (Dr. Richard Stanton and colleagues) provided the recombinant viruses.*

4.1 Introduction

Our group previously published an extensive proteomic analysis of host protein stability during early human cytomegalovirus (HCMV) infection, revealing that 35 host proteins are degraded with high significance in the first 24 hours of infection [62] **(1.4.5)**. A preliminary unpublished experiment performed by Dr. Peter Tomasec and Dr. Michael Weekes, which analysed protein degradation at the later time point of 48 hours post-infection (hpi), identified MLKL as one of the host proteins most significantly downregulated at this time point. To improve the analysis, I performed a biological replicate of this experiment, analysing the new data in parallel with that from the first replicate.

4.2 Aims

1. **Extend the analysis of proteins degraded during HCMV infection to 48 hpi**, by performing a quantitative mass spectrometry (MS) analysis of cells infected with HCMV for 48 h in the presence or absence of proteasomal inhibitor MG132.
2. **Identify proteins that are significantly degraded both early in infection and at 48 hpi**, under the assumption that significant and consistent virus-mediated degradation through infection is an indication of important antiviral function.
3. **Identify proteins that are degraded specifically at 48 hpi**, and therefore may exhibit antiviral properties during the late stages of infection.

4.3 MLKL is significantly downregulated at 48 hours post-infection

Human fetal foreskin fibroblasts immortalised with telomerase (HFFF-TERTs) were infected with HCMV clinical strain Merlin at a multiplicity of infection (MOI) of 10, or mock-infected, for 48 h. For all virus infection experiments presented in this thesis, the MOI was defined as the number of virus particles capable of initiating productive infection of a single cell, determined by the presence of GFP (for viruses expressing a GFP-tagged protein) or IE1 expression, per cell **(2.11.4)**. The proteasomal inhibitor MG132 or an equivalent volume of dimethyl sulfoxide (DMSO) was added at the 36 h time point, for the final 12 h of infection **(Figure 4.1A)**. It should be noted that MG132 also inhibits lysosomal cathepsins and calpains [198]. Although the majority of proteins rescued by MG132 treatment at 12 hpi are also rescued by the specific proteasomal inhibitor bortezomib [199], MG132 alone cannot be used to define the exact mechanism of degradation. Therefore, MG132 was used to generate a global picture of protein degradation late in the HCMV replication cycle, rather than to identify proteins specifically degraded by the proteasome. The infected cells were lysed in 6 M guanidine, generating whole cell lysates (WCLs) that were then processed for tandem mass tag (TMT)-based liquid chromatography tandem mass spectrometry (LC-MS3) analysis.

Protein quantitation was achieved using the MassPike software **(2.18.2)**, with the raw MS data processed in parallel with that from the first biological replicate of the experiment that had been performed previously by Dr. Peter Tomasec and Dr. Michael Weekes. Signal-to-noise values (a measure of protein abundance) were normalised to the sum signal-to-noise across the three conditions within each replicate (Mock, HCMV, HCMV+MG132). This corrected for differences in the numbers of peptides quantified in the different replicates. The data from the two replicates were compared by plotting HCMV/Mock and HCMV+MG132/HCMV ratios for each replicate. The two datasets showed good correspondence for biological data, with an R^2 value of 0.43 for HCMV/Mock and 0.49 for HCMV+MG132/HCMV **(Figure 4.1B)**.

8,476 human and 186 HCMV proteins were quantified in at least one of the replicates. The values from the two replicates were averaged, and two ratios and associated significance values were calculated for each protein: (i) HCMV/mock infection, to observe downregulation, and (ii) HCMV+MG132/HCMV infection, to observe rescue **(Figure 4.2A)**. Fifty-two proteins were degraded with a fold downregulation and rescue of greater than two and $p<0.05$ for both ratios (data in **Appendix V**). Only one protein, MLKL, was downregulated and rescued with a significance of $<1\times10^{-7}$ **(Figure 4.2A)**, although unfortunately it was only quantified in one of the replicates.

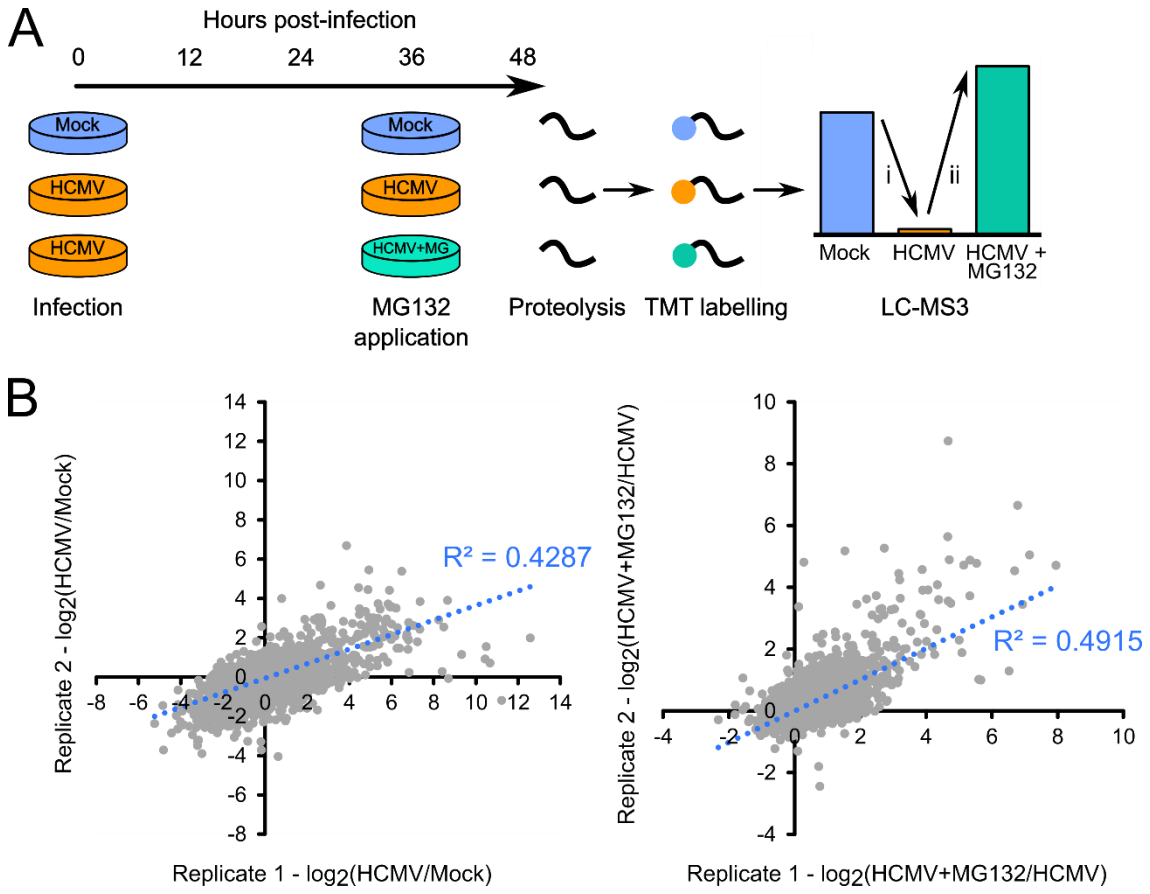

Figure 4.1: Data from replicates of a 48 h degradation screen showed good correspondence.

(A) Schematic of the experimental method, conducted in biological duplicate. Data from the two replicates were analysed simultaneously to ensure that identical peptides from each experiment were assigned to the same protein. **(B)** Signal-to-noise values were normalised to the sum signal-to-noise across the three conditions within each replicate (Mock, HCMV, HCMV+MG132). Two ratios were generated, HCMV/Mock (i in A) and HCMV+MG132/HCMV (ii in A), which were compared between replicates using a scatter plot. Only proteins quantified in both replicates are shown.

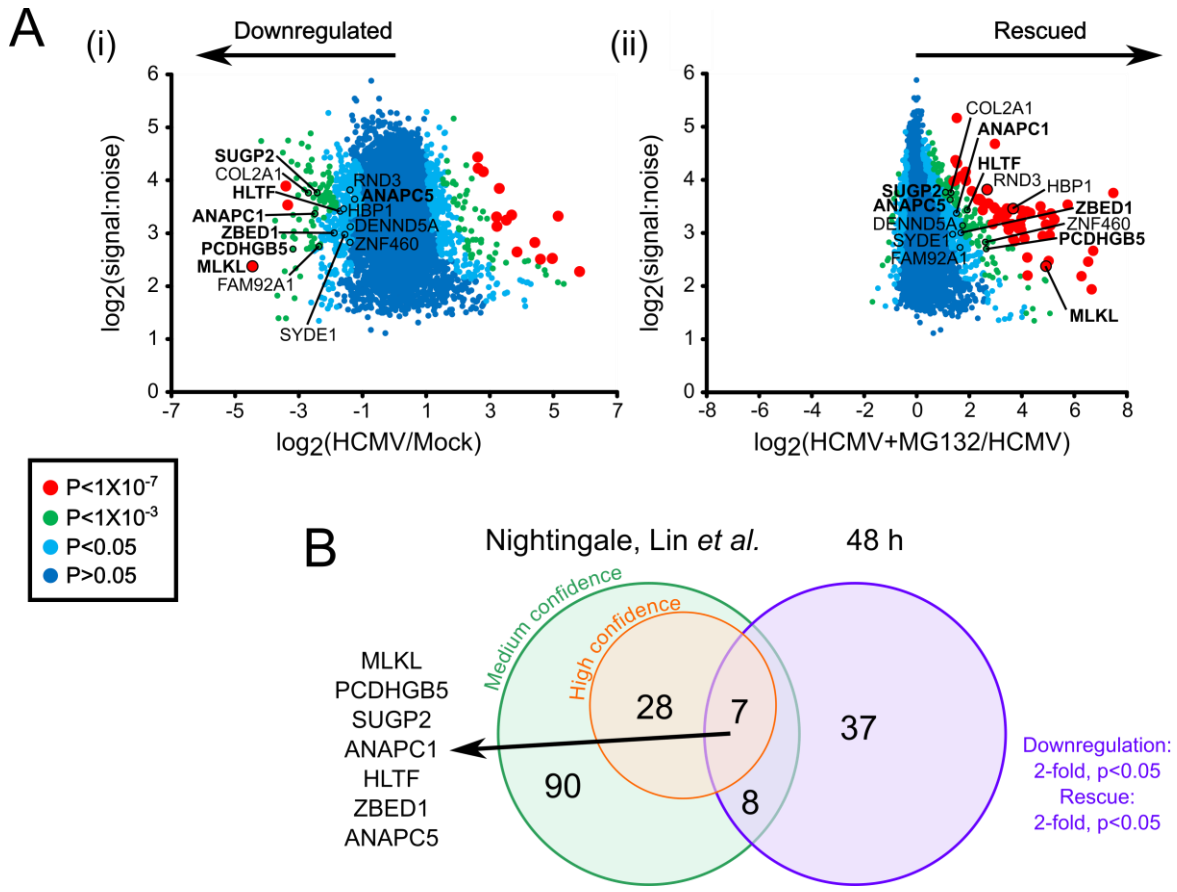

Figure 4.2: MLKL is significantly downregulated at 48 hpi and rescued by application of MG132.

(A) Scatterplots showing fold change against signal intensity for all of the human proteins quantified in one or both replicates. P-values were calculated using the significance B method and corrected for multiple hypothesis testing. Proteins labelled in bold were also degraded at early time points in the Nightingale, Lin *et al.* (2018) study [62] (see B). The other proteins labelled are examples of the 37 proteins degraded at 48 hpi but not in the Nightingale, Lin *et al.* (2018) study (Figure 4.3). **(B)** Overlap between the 133 proteins scored as degraded in the Nightingale, Lin *et al.* (2018) study and those degraded at 48 hpi. The seven proteins listed showed signatures of highly significant degradation at both early time points (Nightingale, Lin *et al.*) and at 48 hpi. The data for the 52 proteins degraded at 48 hpi with a fold downregulation and rescue of greater than two and $p<0.05$ for both ratios are displayed in Appendix V.

The data were compared to that from the Nightingale, Lin *et al.* (2018) [62] study, which examined protein degradation between 6 and 24 hpi **(Figure 4.2B)**. Seven proteins showed evidence of degradation in both the early degradation study and the 48 h data presented here, indicating that their degradation is sustained throughout infection **(Figure 4.2)**. Data for four of these proteins are shown in **Figure 4.3A**. As inferred from the comparative scatter plots in **Figure 4.1B**, the range bars also show that the data was highly reproducible **(Figure 4.3A)**, increasing confidence in the single replicate data for MLKL. In addition to MLKL, the other six proteins degraded at early and late time points were the known HCMV targets HLTF and anaphase promoting complex subunits 1 and 5 (ANAPC1/5) [62,304], protocadherin gamma subfamily B5 (PCDHGB5), SURP and G-patch domain-containing 2 (SUGP2) and zinc finger BED-type-containing 1 (ZBED1) **(Figure 4.2 and Figure 4.3A)**. Several protocadherins, including PCDHGB5, have been previously found to be downregulated during HCMV infection, and identified as potential natural killer (NK) cell or T cell receptors [86]. SUGP2 is an uncharacterised putative RNA-binding protein thought to be involved in RNA processing and quality control [305]. In the early degradation screen, SUGP2 was only significantly rescued by MG132 at the later time points tested (18 – 24 h), suggesting that its degradation begins slightly later in infection than some of the other early targets. ZBED1 is a transcription factor that regulates the expression of a number of genes involved in cell proliferation and localises to PML nuclear bodies (PML-NBs) [306,307]. It has been shown to perform a multifaceted role in adenovirus replication, contributing to the activation of viral gene expression and functioning as a restriction factor [307].

One of the novel aspects of these results is the identification of proteins degraded solely at late time points. Thirty-seven proteins degraded at 48 hpi were not classified as degraded between 6 and 24 hpi by Nightingale, Lin and colleagues [62] **(Figure 4.2B and Figure 4.3B and C)**. These included proteins not degraded at early time points **(Figure 4.3B)**, proteins that were insufficiently degraded to pass filtering criteria at early time points **(Figure 4.3C)**, and proteins not quantified in the Nightingale, Lin *et al.* (2018) study. Degradation of a protein specifically at late time points may indicate that it exhibits antiviral activity late in the replication cycle (e.g. inhibiting virus assembly) and/or that it is targeted by a viral protein exhibiting a Tp3-5 temporal profile. Proteins degraded exclusively at 48 hpi included zinc finger protein 460 (ZNF460), implicated in the regulation of JAK2/STAT3 signalling [308]; synapse defective Rho GTPase homolog 1 (SYDE1), involved in placental development and trophoblast migration [309], transcriptional repressor HMG-box transcription factor 1 (HBP1) [310]; and guanine nucleotide exchange factor DENN domain-containing 5A (DENND5A) [311] **(Figure 4.3B)**.

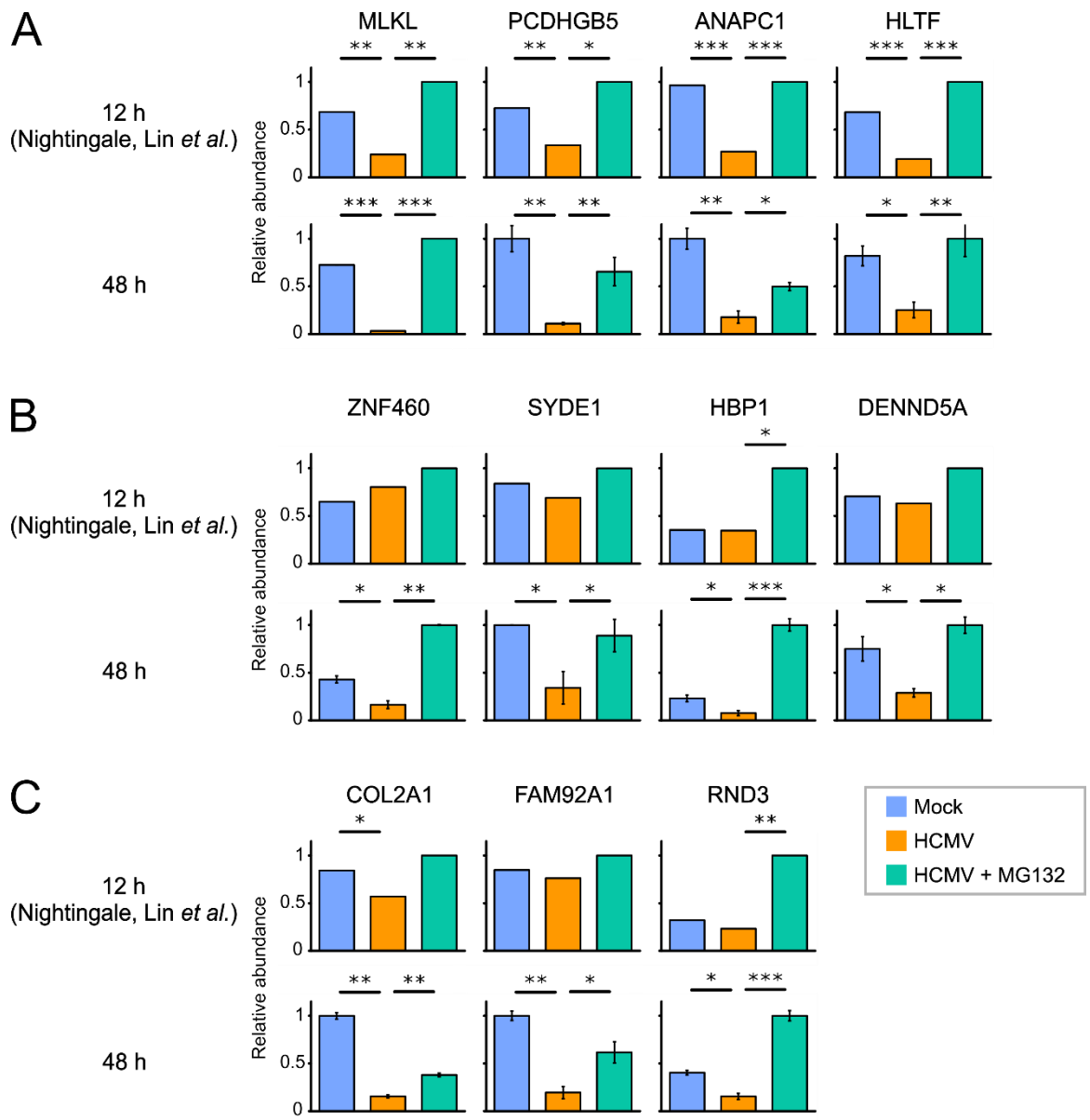

Figure 4.3: Host proteins degraded by HCMV at 48 hpi.

The data from the 48 h experiment are shown alongside the original data from the single-replicate 12 h degradation screen published in Nightingale, Lin *et al.* (2018) [62], as an indicator of degradation at an early time point. **(A)** Four examples of the seven proteins degraded with high confidence early and late during infection. MLKL was quantified in one replicate of the 48 h screen. **(B)** Four proteins degraded at 48 h but not at early time points. **(C)** Three proteins that were degraded at 48 h, and showed some evidence of degradation early time points but did not pass filtering criteria in the Nightingale, Lin *et al.* (2018) study. All graphs show protein abundance relative to that in the sample with the highest abundance. Error bars show the range between the replicates. P-values were calculated using the significance B method and corrected for multiple hypothesis testing. *p<0.05, **p<0.001, ***$p<1\times10^{-7}$.

4.4 Degradation of the seven candidate restriction factors at 48 hours post-infection

Next, the degradation profiles of the seven candidate ARFs were examined. Although DMXL1, ARHGAP35, FRMD6 and LMAN2L remained suppressed at 48 hpi, the level of these proteins was not significantly rescued with MG132, despite observing MG132-dependent rescue of MLKL and HLTF **(Figure 4.4)**. This might be explained by a lack of active degradation occurring at later time points, with the protein levels remaining low due to slow turnover. The abundance of IFIT2 also did not change significantly upon MG132 treatment at 48 hpi **(Figure 4.4)**. Indeed, previous results showed that IFIT2 is downregulated rapidly between 12 and 24 hpi, after which its abundance stabilises **(Figure 1.18)**. DHCR24 was not significantly downregulated in HCMV-infected cells at 48 hpi **(Figure 4.4)**.

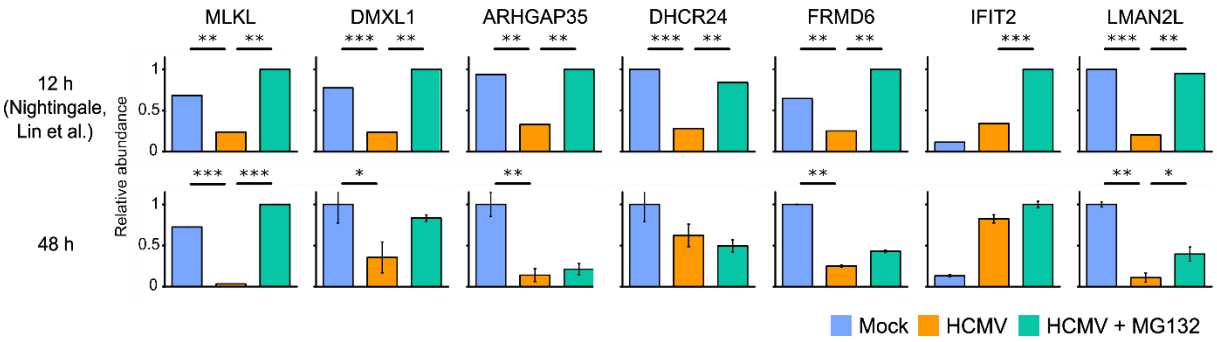

Figure 4.4: DMXL1, ARHGAP35, FRMD6 and LMAN2L are downregulated at 48 hpi.
As described in Figure 4.3.

4.5 Discussion

This short chapter provides an analysis of host protein degradation at 48 h of infection with HCMV strain Merlin, approximately 50-66% of the way through the lytic replication cycle. A searchable database displaying all the data from this experiment can be found in Fletcher-Etherington *et al.* (2020) Database S1 [214].

MLKL was one of the host proteins most significantly downregulated at 48 hpi and rescued by application of MG132 (with $p<1\times10^{-7}$ for both downregulation and rescue) **(Figure 4.2A)**. This significant and ongoing degradation through infection suggests that MLKL plays a prominent antiviral role throughout the replication cycle. **Chapter 5** discusses the function and mechanism of HCMV-mediated MLKL downregulation.

Other proteins that were on the high confidence shortlist of proteins degraded early in infection and significantly degraded at 48 hpi include PCDHGB5, SUGP2 and ZBED1 **(Figure 4.2B)**. The function of these proteins in the context of HCMV infection has not been defined, and therefore these proteins represent good opportunities for further study **(Future directions 4)**. Proteins exclusively degraded at 48 hpi, including ZNF460, SYDE1, HBP1 and DENND5A, may have interesting antiviral roles restricted to specific stages of the virus lifecycle. Experiments that could be used to characterise antiviral activity are described in **Future directions 4**.

In addition to identifying proteins that are consistently degraded throughout infection, and proteins specifically degraded late in infection, these data may be particularly useful for identifying which viral protein(s) targets each host factor. Our group has previously defined the kinetics of expression of the majority of canonical HCMV proteins [62,86], which can now be compared to the kinetics of host protein degradation from 6 to 48 hpi. Identifying viral proteins whose temporal profiles correlate directly or inversely with host proteins of interest can identify the viral proteins responsible for observed changes in protein abundance. This principle was previously used to help identify vaccinia virus protein C6 as the viral protein responsible for downregulation of histone deacetylase 5 (HDAC5) [196].

A. Characterisation of degraded proteins using viral replication assays on overexpression and knockdown cell lines to identify antiviral activity.

As described in Chapter 3, knockdown could be achieved by siRNA transfection or CRISPR using sgRNA:Cas9 nucleofection and viral replication measured using restriction and plaque assays. For the proteins degraded specifically at later time points, a recombinant HCMV expressing mCherry-P2A-UL36 and GFP-UL32 could be used in restriction assays to study both early and late gene expression concomitantly [312].

B. Identification of the viral proteins responsible for host protein degradation.

This will be most straightforward for host proteins that have been shown to be targeted by a gene in one of the gene block deletion viruses **(1.4.6)**. For example, PCDHGB5, appears to be targeted by one or more genes in the US1-11 region [62].

C. Analysis of the infection-specific functions of proteins degraded at 48 hpi.

As an example, for PCDHGB5, this might include NK cell degranulation and T cell activation assays to determine whether PCDHGB5 is a novel immunomodulator. For SUGP2, identification of the RNAs bound by SUGP2 during infection (e.g. by RNA-protein cross-linking and immunoprecipitation), or proteomic analysis of infected cells lacking SUGP2, may give an indication of its effect on host or viral protein expression during infection.

Future directions 4: Do the host proteins degraded at 48 hpi have antiviral activity?

Chapter 5: Human cytomegalovirus protein pUL36 is a multifunctional cell death pathway inhibitor

The majority of the work presented in this chapter was published in PNAS in July 2020 [214]. *Many of the following figures have been reproduced or adapted from those in the manuscript, which were originally made by myself. PNAS authors do not need to obtain permission to use their original figures in their future works. Experiments performed by Dr. Katie Nightingale and Dr. Luís Nobre (both University of Cambridge) are described to provide context and further insights, as indicated in the text. Collaborators at Cardiff University (Dr. Richard Stanton and colleagues) provided the recombinant viruses. All other work is my own.*

5.1 Introduction

5.1.1 MLKL and the necroptotic pathway

Necroptosis can be activated by various stimuli, including TNFα, Fas, TNF-related apoptosis-inducing ligand (TRAIL), IFN, and pathogen-associated molecular patterns (PAMPs) such as viral nucleic acids and lipopolysaccharides [201] **(Figure 5.1) (1.6.1)**. These pathways of necroptosis activation converge with the assembly of a large filamentous structure termed the necrosome [205]. The formation of this structure is driven by interactions between proteins containing a RIP homotypic interaction motif (RHIM) domain [313]. Although the exact composition of the necrosome is dependent on the particular mechanism of activation and the cellular context, the universal components are RIP1, RIP3 and MLKL. Interactions between the RHIM domains of RIP1 and RIP3 facilitate their oligomerisation, which subsequently drives the autophosphorylation of RIP3. From here, RIP3 interacts with and phosphorylates the effector of necroptosis, MLKL.

The structure of MLKL comprises an N-terminal four-helix bundle (4HB) and a C-terminal pseudokinase domain (PsKD) separated by a two-helix brace region [314]. Upon autophosphorylation of RIP3, RIP3 recruits MLKL to the necrosome via its PsKD. Despite topologically resembling a kinase domain, the PsKD is missing key residues required for catalytic activity, and therefore acts solely to mediate protein-protein interactions [314]. In its unphosphorylated form, the PsKD forms an intramolecular interaction with the 4HB domain in order to maintain MLKL in its dormant autoinhibitory state [315,316]. RIP3-dependent phosphorylation of the PsKD activation loop triggers a

conformational change that releases MLKL from its inactive conformation, enables it to oligomerise into its active form, and exposes the 4HB domain. MLKL oligomerisation or the release of MLKL from the necrosome drives the translocation of MLKL to the plasma membrane (PM) [208,317]. The key role of oligomerisation is inferred from studies that show that while exogenous expression of the 4HB domain is insufficient to promote necroptotic death, forced dimerisation of 4HB domains or full-length MLKL induces necroptosis [318,319]. The 4HB domain binds membrane lipids and both the 4HB and full-length MLKL are able to permeabilise membranes *in vitro*, indicating that MLKL induces necroptosis via direct action on the PM [206,315,316,319,320]. Interestingly, a recent study showed that following activation of the necrosome and preceding cell death, RIP1, RIP3 and MLKL translocate to the nucleus, although this relocalisation was not required for cell death [321].

Crucially, necroptotic signalling only ensues in the absence of caspase-8 activity, which would otherwise cleave RIP1 and RIP3 and suppress MLKL activation [203,204,322,323]. Chemical or viral inhibition of caspase-8, for example upon expression of murine cytomegalovirus (MCMV) protein pM36, shifts the pathway of cell death towards necroptosis [324,325]. In order to study necroptosis *in vitro*, necroptosis is typically stimulated using a combination of TNFα, BV-6, and the pan-caspase inhibitor Z-VAD(OMe)-fluoromethyl ketone (Z-VAD-fmk). BV-6 is an antagonist of inhibitor of apoptosis (IAP) family proteins, which negatively regulate components of the apoptotic and necroptotic machinery, including RIP1 [326,327].

The description above gives a relatively simplistic overview of the necroptotic pathway. In reality, many positive and negative regulators of the necrosome dictate the specific conditions under which necroptosis is activated, and prevent unchecked cell death. Factors that have been implicated in the regulation of necroptosis include the chaperone heat shock protein 90 kDa (HSP90) [328], Tyro3, Axl, and Mer (TAM) kinases [329] and inositol phosphates [330]. Furthermore, three independent studies have identified a mechanism of regulation based on the exocytosis of phospho-MLKL to form MLKL-containing exosomes or ‘necroptotic bodies’ [331–333].

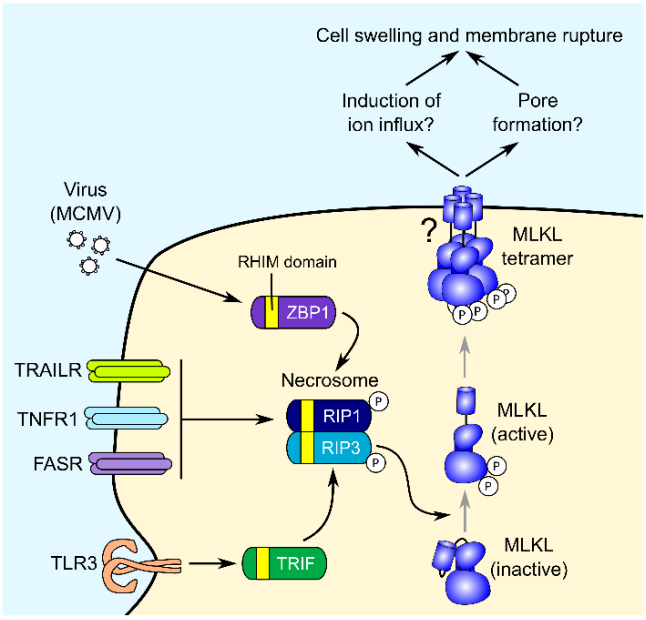

Figure 5.1: Simplified schematic of the necroptotic signalling pathway.
Necroptosis can be activated by death receptor stimulation, the cytoplasmic sensing of MCMV DNA by ZBP1, or the detection of PAMPs by TLR3/4. These three pathways converge with the assembly of a RIP1:RIP3 oligomeric complex termed the necrosome. This results in RIP3-dependent phosphorylation and activation of MLKL, which then interacts with the PM to cause cell swelling and loss of PM integrity. The exact steps that occur after MLKL phosphorylation, the nature of the interaction between MLKL and the PM, and the mechanism of membrane rupture, remain uncharacterised [201].

5.1.2 Functions of MLKL beyond cell death

The necroptotic pathway and MLKL itself have been implicated in a range of processes beyond cell death, which may contribute to the antiviral environment established in response to death receptor signalling [334].

Although primarily considered to have a pro-survival function by eliminating damaged proteins and organelles and suppressing necroptosis [335,336], autophagy can also promote cell death under certain circumstances [337]. Conversely, a number of studies have found that activation of necroptosis results in the accumulation of the autophagic marker, lipidated microtubule-associated protein light chain 3B (LC3B), and have concluded that autophagy is stimulated by necroptotic signalling [338,339]. However, it was recently shown that this accumulation of lipidated LC3B occurs due to MLKL-dependent inhibition of autophagic flux, not because autophagy is activated [340].

Necroptotic signalling culminates in cell lysis and the release of proinflammatory intracellular contents that propagate the inflammatory response characteristic of necroptosis. In addition, RIP3-MLKL signalling activates the NLR family pyrin domain-containing 3 (NLRP3) inflammasome and

subsequently triggers the processing of IL-1β by caspase-1, which may be a supplementary and important determinant of necroptosis-derived inflammatory signals [341,342].

MLKL has also been shown to enhance the degradation of cellular receptors and their ligands [including TNF and epidermal growth factor (EGF)] via its ability modulate endosomal transport [321], and has recently been found to regulate gene expression [343].

5.1.3 Activation of cell death by HCMV

Several mechanisms may act together to activate cell death in response to human cytomegalovirus (HCMV) infection in a manner dependent on cell type [336]. MCMV infection is recognised by TLR3, while MCMV and HCMV infection have been shown to stimulate ZBP1 [210,344,345]. TLR3 and ZBP1 can both activate necroptosis via the necrosome [210,346]. PKR, which recognises HCMV and restricts viral replication in the absence of IRS1 and TRS1 [347], has also been implicated in Fas associated via death domain (FADD)-dependent caspase-8 activation and cell death [348]. In addition to direct recognition of viral PAMPs, viral replication stimulates stress response pathways including the unfolded protein response and DNA damage response, both of which can result in intrinsic apoptosis [349]. Finally, the release of proinflammatory cytokines from infected cells and immune cells, including TNFα and IFN, drives extrinsic apoptotic and necroptotic pathways via the canonical death receptor pathway of activation.

5.1.4 Inhibition of apoptosis by HCMV

As a result of host-virus coevolution, herpesviruses and other large DNA viruses have evolved a variety of mechanisms to evade apoptosis and escape viral clearance. HCMV encodes multiple proteins that carry out this function. pUL36, or viral inhibitor of caspase-8 activation (vICA), inhibits Fas-induced extrinsic apoptosis via direct interaction with procaspase-8, preventing cleavage into its active form [209]. The product of UL37 exon 1 (pUL37x1), binds and sequesters BCL2-associated X (BAX) at the mitochondrial membrane, thus preventing execution of intrinsic apoptosis via mitochondrial outer membrane permeabilisation [350]. pUL38 protects against apoptosis by antagonising the endoplasmic reticulum stress response [351,352]. Finally, the immediate-early (IE) proteins IE1 and IE2 have also been implicated in the restriction of apoptotic cell death [353], likely through their ability to control global viral and host gene expression.

pUL36 was first characterised in 1999, when it was shown to be present throughout infection and to exhibit varied abundance, localisation and stability in cells infected with different strains of HCMV [354]. The structural determinants of the anti-apoptotic function of pUL36 are yet to be fully determined. However, comparisons of pUL36 encoded by different strains of HCMV and homologs of pUL36 encoded by different betaherpesviruses have given some indication of the important residues and regions. A single amino acid substitution, Cys^{131} to Arg^{131}, was sufficient to abrogate the ability of pUL36 to bind procaspase-8 and inhibit apoptosis [209]. This substitution is frequently observed in lab-

adapted HCMV strains, including AD169, occurring within a few passages of the virus in cell culture. pUL36 is a member of the US22 family of DNA virus proteins and is conserved across the betaherpesvirus family [355]. Both rhesus cytomegalovirus homolog pRh36 and MCMV homolog pM36 are sufficient for protection from extrinsic apoptosis, despite exhibiting significant sequence diversity (pM36 only shows 19% sequence similarity to pUL36) [355].

Although pUL36 is dispensable for viral replication in cultured fibroblasts [209,354], HCMV requires pUL36 function to replicate in macrophages and differentiating monocytes [356], cells that are responsible for viral dissemination *in vivo* [357,358]. Cell death induced by infection with a pUL36-deficient virus at early stages of monocyte differentiation was dependent on caspases and inhibited by Z-VAD-fmk. Interestingly, at late stages of differentiation, the mechanism of virus-induced death was caspase-independent, likely due to the differential regulation of cell death machinery through macrophage differentiation. pUL36 remained necessary for cell survival under these conditions, indicating that pUL36 suppresses both caspase-dependent and caspase-independent cell death programmes in monocyte-derived macrophages [356].

5.1.5 Necroptosis as a cell-intrinsic antiviral defence mechanism against HCMV

As mentioned previously, the suppression of caspase-8 activity by viral, cellular or chemical inhibitors releases the inhibitory effect of caspase-8 on the necroptotic pathway. Therefore, necroptosis acts an important second line of cell death defence against viruses that encode caspase-8 inhibitors, killing off infected cells and preventing viral replication and spread to neighbouring cells.

In addition, the fact that the necroptosis pathway is involved in cross talk with a range of cellular processes implies that the stimulation of necroptosis in infected cells may induce a cascade of antiviral processes. In particular, the activation of the inflammasome and release of IL-1β, backed up by the release of immunostimulatory cellular debris during cell lysis, will help drive a systemic inflammatory response that recruits immune cells to the site of infection and drives viral clearance.

As explained in **1.3.2**, the link between HCMV infection and autophagy is complex, with the outcome of autophagy stimulation or inhibition likely dependent on the time point of infection, the cellular context and the specific stage of the pathway that is impacted. Nonetheless, the inextricable link between necroptosis and autophagy undoubtedly has important implications on the tug of war between cell-intrinsic immunity and the viral antagonists of HCMV.

5.1.6 Inhibition of necroptosis by HCMV

MCMV, herpes simplex virus (HSV)-1 and HSV-2 inhibit necroptotic signalling through the activity of viral RHIM domain-containing proteins that compete with host RHIM domain adaptor proteins for binding to RIP3 within the necrosome [210–212]. In the herpes simplex viruses, this function is carried out by the large subunit of the ribonucleotide reductase (R1), also known as infected cell protein 6

(ICP6) (HSV-1) or ICP10 (HSV-2) [211]. R1 also inhibits caspase-8-dependent apoptosis using a mechanism analogous to HCMV pUL36, making it a multifunctional cell death suppressor [359]. In MCMV, necroptosis inhibition is dependent on the M45-encoded viral inhibitor of RIP activation (vIRA). The HCMV pM45 ortholog pUL45 does not contain a RHIM domain or inhibit necroptosis [360], and so a number of studies have aimed to establish whether and how HCMV evades necroptotic cell death. However, investigating the contest between HCMV and necroptotic signalling is complicated by that fact that human fibroblasts, the predominant cell type used for studying HCMV replication in cell culture, typically express insufficient levels of RIP3 and MLKL for the execution of necroptosis [213]. Using RIP3-transduced human fetal foreskin fibroblasts (HFFFs) that were sensitive to TNFα-stimulated necroptosis, Omoto *et al.* showed that HCMV suppresses necroptosis at a stage following phosphorylation of MLKL [213]. HCMV protein IE1 was necessary but not sufficient for this observation, indicating that necroptosis inhibition was dependent on the optimal expression of an IE1-regulated early gene [213]. Although HCMV pUL36 was shown to inhibit caspase-independent cell death in differentiating monocytes [356] **(5.1.4)**, deletion of UL36 did not have an impact on the ability of HCMV strain Towne to protect cells from necroptosis in this experimental system [213].

Several other mechanisms for HCMV-mediated necroptosis inhibition have been proposed. Dovey and colleagues recently showed that inositol phosphate (IP) kinases are essential for necroptosis, with binding of higher-order IPs promoting an active conformation of MLKL [330]. As HCMV is known to modulate IP levels [361], this provides a potential mechanism for HCMV-mediated repression of necroptosis following MLKL phosphorylation. In primary monocytes, HCMV-driven induction of autophagy early in infection was found to protect infected cells from necroptotic cell death [336]. Specifically, while HCMV induced the early steps of the necroptotic pathway, the induction of autophagy inhibited MLKL phosphorylation [336].

5.2 Aims

Previous work has shown that MLKL is downregulated from as early as 6 hours post-infection (hpi); an effect that is reversed by addition of the proteasomal inhibitors MG132 or bortezomib **(1.6.1)** [62,199]. The mechanism of downregulation is post-translational, implied by the significant upregulation of MLKL transcripts at 24 hpi, which may be induced by IFN **(1.6.1)** [62]. MLKL downregulation is dependent on *de novo* expression of a viral gene that is not expressed by HCMV strain AD169 **(1.6.1)** [62].

In **Chapter 4**, I showed that MLKL is one of seven proteins that were in the high confidence shortlist of proteins degraded early in infection [62] and significantly downregulated and rescued by MG132 at the later time point of 48 hpi **(4.3)**. Overexpression of MLKL resulted in significant decrease in the number of plaques formed by HCMV strain AD169 **(3.8)**, which may reflect the role of MLKL in the

necroptotic clearance of virus-infected cells. Unlike overexpression of the known antiviral restriction factor DAXX, overexpression of MLKL had no effect on IE gene expression **(3.8)**, implying that MLKL does not have any additional antiviral roles early in the replication cycle.

The work presented in this chapter aimed to:

1. **Identify the viral protein (or proteins) responsible for MLKL downregulation.**
2. **Elucidate the mechanism of MLKL downregulation**, for example by characterising interactions between the viral protein and MLKL and identifying E3 ligases that may direct the degradation of MLKL.
3. **Establish and validate an assay for studying the effect of viral proteins and virus infection on apoptotic and necroptotic cell death.**
4. **Demonstrate whether the protein responsible for MLKL downregulation is necessary and sufficient for inhibition of necroptosis.**

5.3 MLKL is downregulated by HCMV protein pUL36

5.3.1 Lab-adapted HCMV strain AD169 is unable to degrade MLKL

A previous screen, performed by Dr. Katie Nightingale, employed a panel of recombinant viruses with various gene block deletions to identify the viral proteins responsible for the degradation of cellular proteins [62] **(1.4.6)**. The viruses included eight recombinant viruses based on HCMV clinical strain Merlin, each with a different block of non-essential genes removed, and the highly passaged laboratory-adapted strain AD169. MLKL was downregulated by the strain Merlin viruses but not by strain AD169 **(Figure 5.2A)**. This finding was confirmed by immunoblot of infected cell lysates solubilised in radioimmunoprecipitation assay (RIPA) buffer **(Figure 5.2B)**. Downregulation of MLKL was also observed when cells were solubilised in 2% sodium dodecyl sulphate (SDS), indicating that MLKL is degraded rather than being translocated to RIPA-insoluble membrane complexes **(Figure 5.2C)**. MLKL was partly rescued by the addition of MG132, suggesting that at least some of the downregulation was due to proteasomal degradation **(Figure 5.2B)**.

AD169 contains a deletion in the U_L/*b'* region, frameshifts in genes RL5A, RL13 and UL131A, and five substitutions in gene UL36 **(1.1.6)**. One of the UL36 mutations, a non-synonymous cysteine to arginine substitution, inactivates the ability of pUL36 to bind procaspase-8 and inhibit apoptosis [209,362].

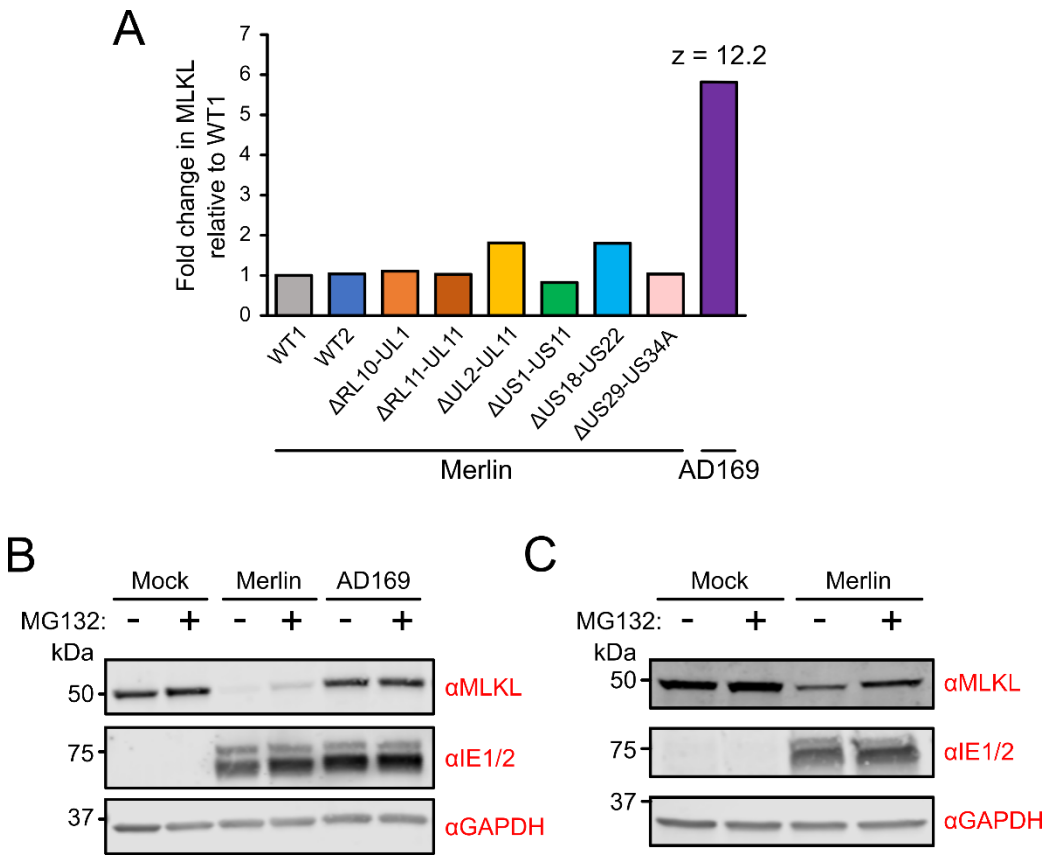

Figure 5.2: MLKL is degraded by HCMV strain Merlin but not strain AD169.

(A) Relative abundance of MLKL in HFFFs infected with strain Merlin [wild type 1(WT1)], WT1 that lacked UL16 and UL18 (WT2), one of six block-deletion viruses derived from WT1 or WT2, or strain AD169 [multiplicity of infection (MOI): 10, 72 h infection]. A Z-score of greater than five was considered significant. This figure was generated from data published in Nightingale, Lin *et al.* (2018) [62] under a Creative Commons CC-BY license, relating to a screen performed by Dr. Katie Nightingale. **(B)** Immunoblot confirming that MLKL is downregulated by strain Merlin but not by strain AD169 (MOI: 5, 48 h infection, cells lysed in RIPA buffer). 10 µM MG132 or an equivalent volume of DMSO was added for the final 12 h of infection. **(C)** Immunoblot confirming that MLKL is downregulated by HCMV strain Merlin, with cells solubilised in 2% SDS instead of RIPA (MOI: 5, 48 h infection).

5.3.2 MLKL interacts with HCMV protein pUL36

To identify viral proteins that interact with MLKL, a stable isotope labelling by amino acids in cell culture (SILAC) immunoprecipitation (IP) of C-terminal hemagglutinin (HA)-tagged MLKL was performed in HCMV strain Merlin-infected HFFFs expressing telomerase (HFFF-TERTs) in the presence of MG132 **(Figure 5.3A)**. HCMV protein pUL36 was one of the most significant interactors of MLKL. This interaction was confirmed by a reciprocal IP of C-terminal V5-tagged pUL36 from a constitutively expressing cell line **(Figure 5.3B)**. Proteins that were enriched in both pulldowns with a

fold change of greater than 1.5 are listed in **Table 5.1**. To determine whether pUL36 interacts with inactive unphosphorylated MLKL or active phosphorylated MLKL, the pUL36-V5 SILAC IP data were searched using a variable phospho-modification. All identified MLKL peptides were unphosphorylated and encompassed all known sites of activating phospho-modifications **(Figure 5.3C)**. This suggests that pUL36 interacts with unphosphorylated MLKL but does not exclude an additional interaction with phosphorylated MLKL.

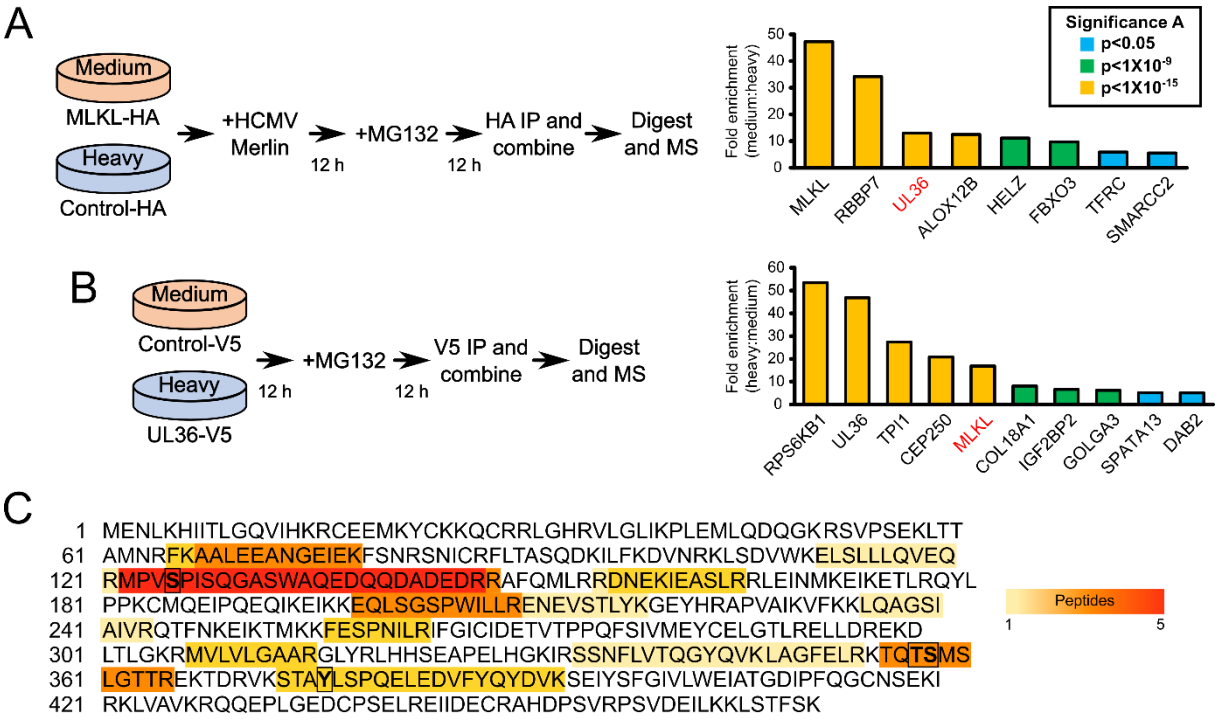

Figure 5.3: MLKL interacts with HCMV strain Merlin protein pUL36.

(A) SILAC-IP of C-terminal HA-tagged MLKL or control in the presence of strain Merlin infection (MOI: 3, 24 h). 10 µM MG132 was added for the final 12 h. Proteins enriched >five-fold are shown. P-values were calculated using the method of significance A and corrected for multiple hypothesis testing. **(B)** SILAC-IP of C-terminal V5-tagged pUL36 or control in the presence of 10 µM MG132 for 12 h. Proteins that were enriched >five-fold are shown, and p-values were estimated as in (A). **(C)** Amino acid sequence of MLKL, with the peptides identified in the pUL36-V5 IP highlighted in different colours according to the frequency of identification. The residues highlighted with boxes are known sites of phosphorylation [320,329,363,364]. No phospho-MLKL peptides were identified.

Gene Symbol	*Species*	*Description*	*HA IP MLKL/Control*	*V5 IP UL36/Control*
MLKL	HUMAN	Mixed lineage kinase domain-like protein	47.27	16.83
UL36	HCMV	Viral inhibitor of caspase-8-induced apoptosis (VICA)	13.02	46.82
FBXO3	HUMAN	F-box only protein 3	9.71	2.52
IGF2BP2	HUMAN	Insulin-like growth factor 2 mRNA-binding protein 2	2.53	6.58
FAM98A	HUMAN	Protein FAM98A	2.38	1.83
CEP170	HUMAN	Centrosomal protein of 170 kDa	2.25	1.57
RPL14	HUMAN	60S ribosomal protein L14	2.13	2.63
XPO1	HUMAN	Exportin-1	2.01	1.61
POFUT2	HUMAN	GDP-fucose protein O-fucosyltransferase 2	1.96	1.65
MPRIP	HUMAN	Isoform 2 of Myosin phosphatase Rho-interacting protein	1.83	1.62
LARP7	HUMAN	Isoform 3 of La-related protein 7	1.77	1.55
FASN	HUMAN	Fatty acid synthase	1.76	3.21
MDC1	HUMAN	Mediator of DNA damage checkpoint protein 1	1.66	2.29
GDI2	HUMAN	Rab GDP dissociation inhibitor beta	1.63	3.79
RBM4	HUMAN	RNA-binding protein 4	1.55	1.61
CCDC80	HUMAN	Isoform 2 of Coiled-coil domain-containing protein 80	1.53	1.88
HUWE1	HUMAN	E3 ubiquitin-protein ligase HUWE1	1.51	1.61

Table 5.1: Proteins that were enriched in both pUL36-V5 and MLKL-HA IPs more than 1.5-fold. Highlighted proteins were also identified as pUL36 interactors in the HCMV interactome [269]. The full dataset from these IPs can be found in Fletcher-Etherington *et al.* (2020) Dataset S2 [214].

5.3.3 HCMV pUL36 is necessary and sufficient to downregulate MLKL

Next, a series of HFFF-TERT cell lines stably expressing either strain Merlin UL36 or each of the genes in the U_L/*b'* region (which are missing in strain AD169) were screened to determine whether any of these viral proteins are sufficient to downregulate MLKL. Expression of UL36 was sufficient to reduce the level of MLKL four-fold in HFFF-TERTs **(Figure 5.4A-D)** and two-fold in human embryonic kidney (HEK293) cells **(Figure 5.4D)**. Downregulation of MLKL by pUL36 was partially rescued by the addition of MG132 **(Figure 5.4D)**. MLKL expression was not modulated more than two-fold by any other proteins in the U_L/*b'* region. Despite substantial variation in the level of expression of some of the viral proteins, this did not correlate with relative MLKL abundance **(Figure 5.4C)**. pUL36 can be detected from 6 hpi, and is expressed with Tp2 (temporal protein profile 2) kinetics, matching the kinetics of MLKL downregulation [86] **(Figure 5.4E)**. Infection with strain AD169 or two independent strain Merlin UL36 deletion mutants rescued MLKL, confirming that pUL36 is necessary as well as sufficient for MLKL downregulation **(Figure 5.5)**.

As described in **Chapter 3**, a recombinant virus based on HCMV strain Merlin that expresses pUL36 tagged with green fluorescent protein (GFP) via a self-cleaving peptide (P2A) at the C-terminus was generated to enable a read-out of IE gene expression. Insertion of P2A-GFP did not affect the ability of

pUL36 to inhibit Fas-mediated apoptosis [62], but did inhibit the downregulation of MLKL **(Figure 5.5)**. This is surprising, given that only a small linker peptide will remain after translation, and because tagging pUL36 with a V5 tag at the C-terminus did not affect its function **(Figure 5.4A-D)**. The reason for this finding is unclear, but it indicates that the C-terminus may have an important role in MLKL downregulation.

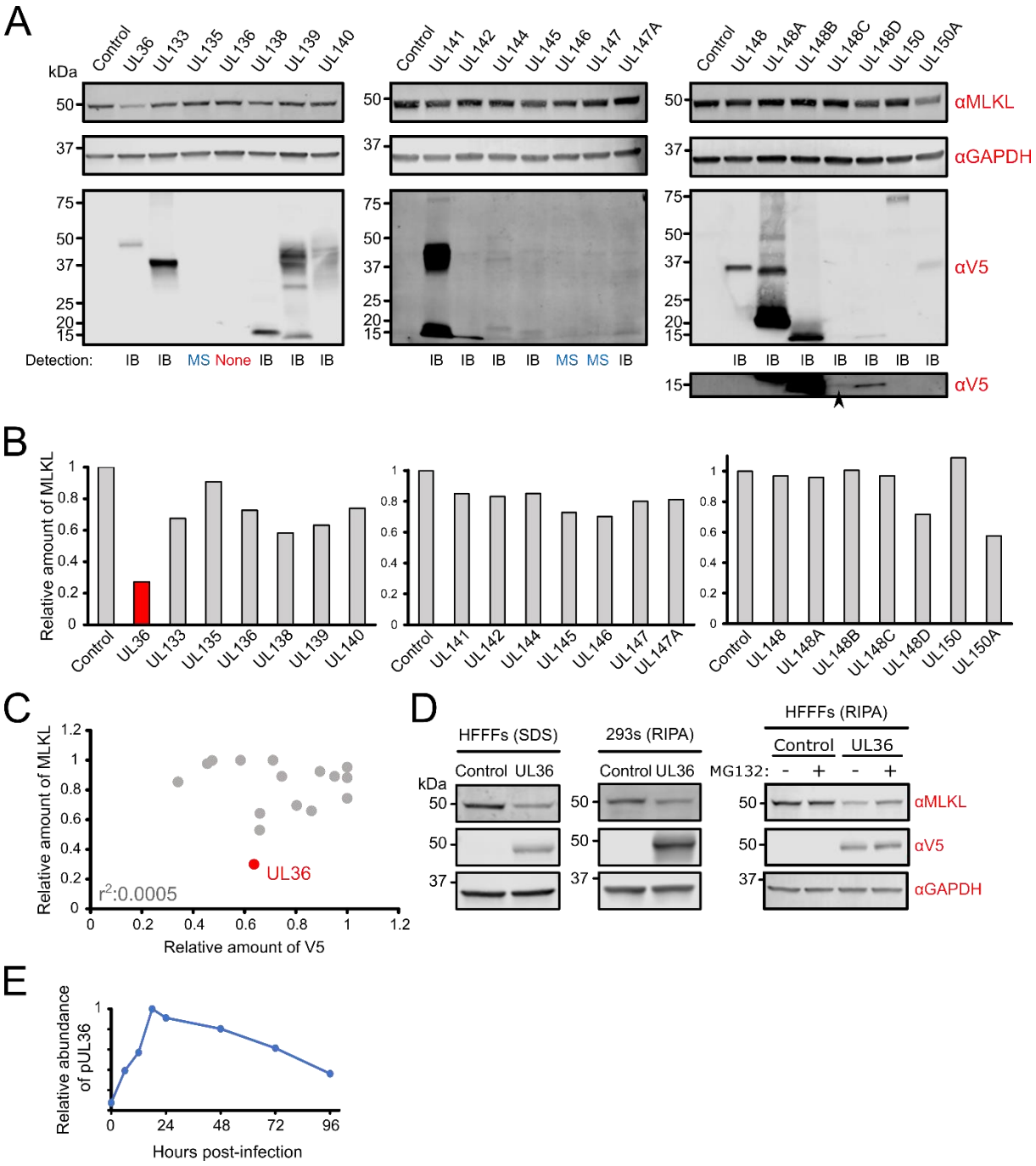

(Previous page)

Figure 5.4: pUL36 is sufficient for the downregulation of MLKL.

(A) A series of HFFF-TERT cell lines stably expressing genes in the U_L/b' region were lysed in RIPA buffer and analysed by immunoblot. Expression of 17/21 V5-tagged viral proteins was confirmed by anti-V5 immunoblot. Expression of pUL135, pUL146 and pUL147 was confirmed by mass spectrometry [269]. pUL136 was not detected by either method, and so further confirmation that pUL136 does not affect MLKL levels is required. A faint band corresponding to pUL148C could be detected upon over-exposure of the blot (bottom right panel). **(B)** Densitometry analysis of MLKL expression normalised by GAPDH expression in each cell line. **(C)** For every cell line in which V5 was detectable by immunoblotting, the relative abundances of MLKL (adjusted to GAPDH) and the V5-tagged viral protein (adjusted to GAPDH) were calculated. To prevent confounding effects from systematic expression level differences between each of the three blots, values derived from each blot were normalised to the maximum level of MLKL and V5 expression prior to comparison. No correlation between MLKL and V5 expression was observed. **(D)** HFFF-TERTs and HEK293s stably expressing UL36 were lysed in either RIPA buffer or 2% SDS, as indicated. For MG132 treatment, cells were grown in media containing 10 µM MG132 for 12 h before harvesting. **(E)** Temporal profile of strain Merlin pUL36 in HFFF whole cell lysates harvested at different times over the whole course of infection. Figure was generated from data published in Weekes *et al.* (2014) [86].

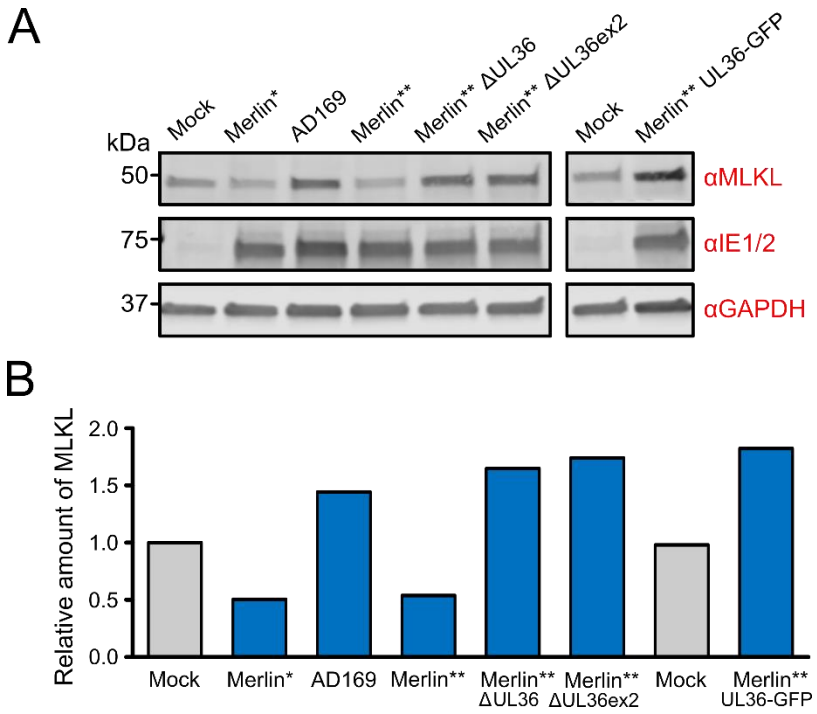

Figure 5.5: pUL36 is necessary for the downregulation of MLKL by HCMV strain Merlin.

Cells were infected with WT strain Merlin (Merlin*, RCMV1111), a version of Merlin in which UL128 and RL13 are under tetracycline regulation (Merlin**, RCMV1502), two UL36 deletion viruses derived from Merlin** (RCMV2288 and 2289), a UL36-P2A-GFP virus (RCMV2270), or strain AD169 (MOI: 5, 24 h infection). ΔUL36ex2 (RCMV2289) has a deletion in exon 2. **(A)** Immunoblot. **(B)** Densitometry analysis of the relative amount of MLKL normalised to GAPDH.

5.4 pUL36 inhibits TNF-stimulated necroptosis in the absence of caspase-8 activity

5.4.1 HFFF-TERTs are susceptible to canonical necroptosis

HCMV pUL36, otherwise known as the viral inhibitor of caspase-8 activation (vICA), inhibits apoptosis by binding the prodomain of procaspase-8 and impeding its proteolytic activation [209]. Inhibition of caspase-8 during death receptor stimulation triggers a bifurcation towards necroptotic signalling [324,325,365], and so pUL36 would be predicted to promote necroptosis. Although this has been reported for the MCMV pUL36 homolog pM36 [324], the same effect has not been observed for pUL36, potentially due to the use of HFFF cell lines that are not susceptible to necroptosis [209,213]. Due to its role in MLKL downregulation, an experiment was designed to determine whether Merlin pUL36 additionally inhibits necroptosis. Necroptosis can be stimulated in cell culture with a combination of TNFα (T), BV-6 (B), and the pan-caspase inhibitor Z-VAD-fmk (Z) **(Figure 5.6A)** [326,366]. To confirm that the stimulated death pathway was canonical MLKL- and RIP3-dependent necroptosis, two inhibitors were employed. GSK'872 binds to and inhibits the RIP3 kinase domain [367,368], whereas necrosulfonamide (NSA) inhibits downstream effector functions of MLKL via a covalent reaction with the Cys^{86} residue of human but not murine MLKL [207,369] **(Figure 5.6B)**.

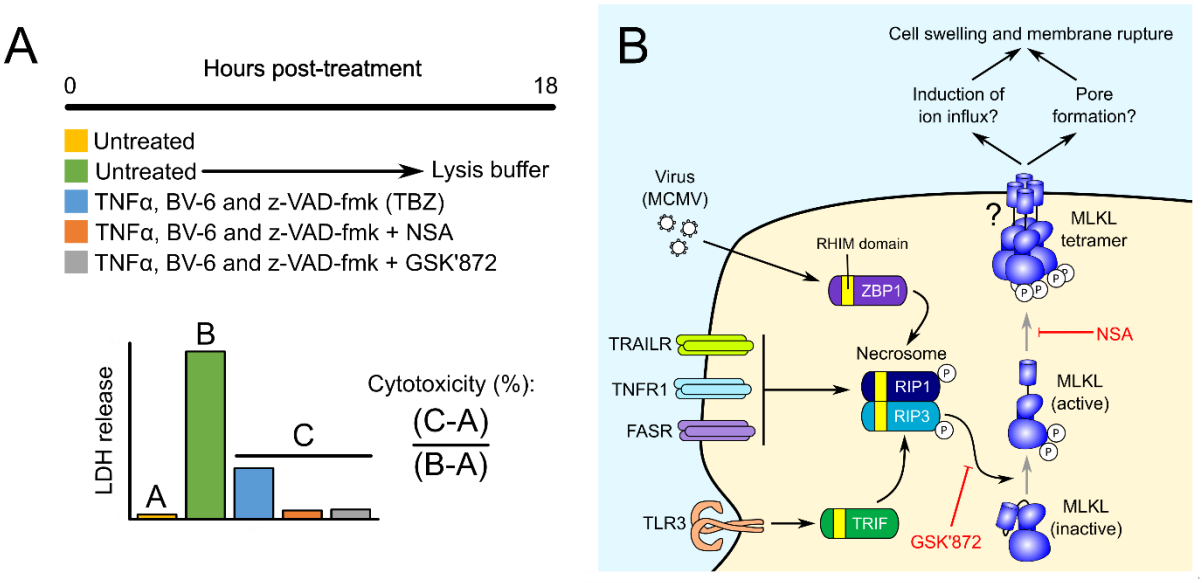

Figure 5.6: Necroptosis can be stimulated with a combination of TNFα, BV-6 and Z-VAD-fmk.
(A) Schematic of the necroptosis assay, which was performed in biological triplicate conducted in parallel and repeated in two or three completely independent experiments. 18 h after treatment with the relevant compounds, cytotoxicity was quantified by measuring LDH release. Cytotoxicity was calculated as a percentage of 100% lysis (from untreated cells lysed with lysis buffer) after subtraction of background LDH release from live cells. To stimulate apoptosis, cells were treated with TNFα and BV-6 in the absence of Z-VAD-fmk. **(B)** The necroptosis pathway and mechanisms of action of small molecule necroptosis inhibitors.

Previous studies have reported that HFFFs are not susceptible to necroptosis due to limiting levels of RIP3 [213]. However, both RIP3 and RIP1 were detectable in HFFF-TERTs by proteomics **(Figure 5.7A)**. T+B+Z (TBZ) induced cell death in HFFF-TERTs and immortalised mouse embryonic fibroblasts (MEFs), which are highly susceptible to necroptosis [370] and therefore used as a positive control **(Figure 5.7B)**. TBZ-stimulated cytotoxicity in HFFF-TERTs was inhibited by NSA and GSK'872, indicating that the cell line expresses sufficient RIP3 to execute canonical necroptosis. NSA did not suppress cell death in the MEFs as it is unable to bind and inhibit murine MLKL [207]. To dissect the conditions of this assay, the effects of T, B and Z alone or in combination were investigated **(Figure 5.7C-D)**. In addition to apoptosis stimulated by TB and necroptosis stimulated by TBZ, HFFF-TERTs also underwent cell death in response to B alone, which has been described in other cell types [371] **(Figure 5.7C)**. The cell death induced by B was MLKL- and RIP3-independent **(Figure 5.7D)** but required caspase-8 activity as it was inhibited by the addition of Z **(Figure 5.7C)**. Therefore, B alone was not responsible for the necroptotic cell death observed upon application of TBZ. In MEFs, cell death was also induced in the TZ condition, an observation that has been reported for other mouse fibroblast cell lines [372] **(Figure 5.7C)**. Collectively, these results confirm that only in the presence of TBZ was the death of HFFF-TERTs dependent on MLKL and RIP3. Furthermore, application of NSA and GSK'872 in the absence of T, B or Z indicated that the inhibitors themselves did not affect cell viability **(Figure 5.7D)**.

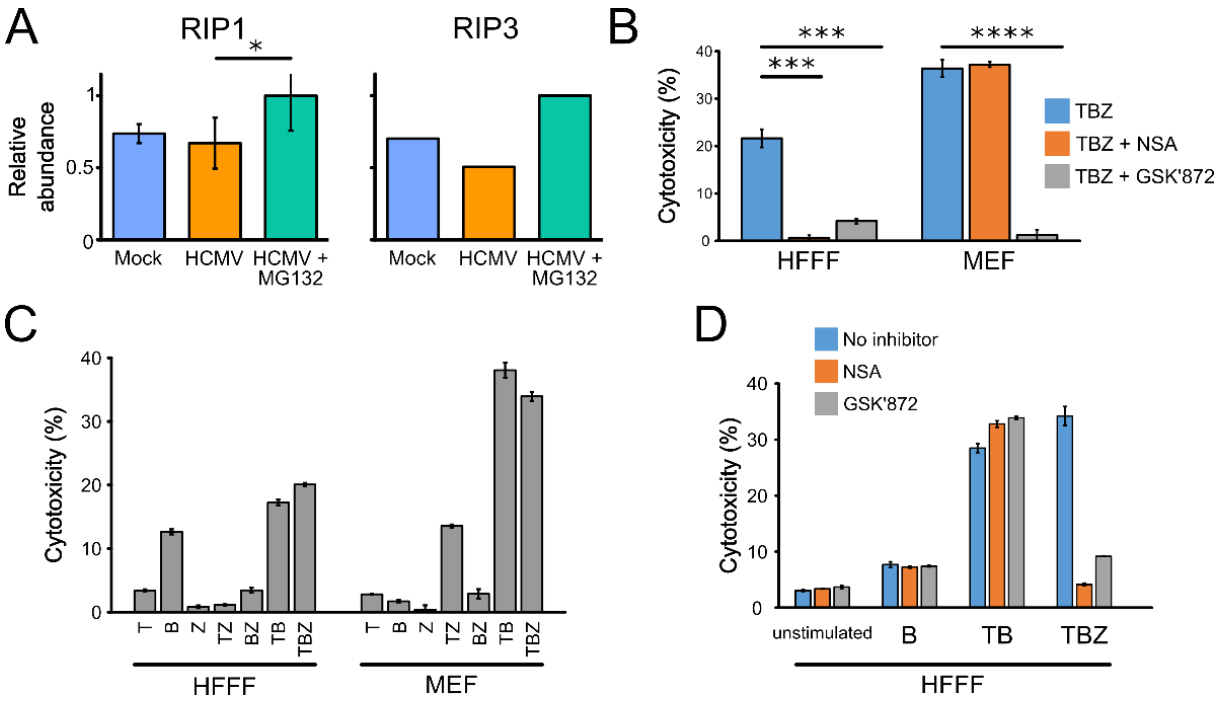

Figure 5.7: HFFF-TERTs are susceptible to canonical necroptosis.

(A) Expression of RIP1 and RIP3 in HFFF-TERTs quantified by proteomics (experimental setup as in Figure 4.1). RIP3 was only detected in the first of two biological replicates. *p<0.05. **(B)** HFFF-TERTs or MEFs were treated with TBZ in the presence or absence of two inhibitors of necroptosis, NSA and GSK'872. Cell death was measured according to LDH release 18 h post-treatment. P-values were estimated using a two-tailed t-test (n=3). ***p<0.001, ****p<0.0001. Data are representative of three independent experiments. **(C)** HFFF-TERTs or MEFs were treated with T, B or Z alone or in combination and cell death observed as before. Data are representative of three independent experiments. **(D)** HFFF-TERTs were treated with B, TB or TBZ for 18 h in the presence or absence of NSA or GSK'872. All experiments were performed in biological triplicate in parallel, with error bars showing standard error of the mean (SEM).

5.4.2 HCMV pUL36 inhibits TNFα-induced necroptosis

Previous work by Omoto and colleagues showed that deletion of UL36 does not impact the ability of HCMV strain Towne (which encodes UL36 with a cysteine at position 131) to protect against necroptosis in fibroblasts stably transduced with RIP3 [213]. In contrast, results presented here showed that stable expression of strain Merlin pUL36 in HFFF-TERTs was sufficient to inhibit TBZ-induced necroptosis **(Figure 5.8A)**. Expression of pUL37x1 or pUL38, the other two viral inhibitors of apoptosis [373,374], increased the amount of cell death observed upon stimulation **(Figure 5.8A)**. Although this cell death was MLKL-dependent, it was incompletely inhibited by GSK'872, suggesting that a RIP3-independent mechanism might be acting in addition.

Untransduced, control and UL36-expressing cell lines were treated with TB or TBZ to assess the impact of pUL36 on apoptosis and necroptosis, respectively **(Figure 5.8B)**. Other inhibitors of caspase-8, such as Z-VAD-fmk (Z) and MCMV protein pM36, do not inhibit death receptor-stimulated cell death but rather shift the pathway towards necroptosis [324,325,365,375]. In contrast, pUL36 was able to inhibit cell death stimulated by TB, with the residual cell death being partly RIP3- and MLKL-dependent. These results suggest that, in the presence of TB, pUL36 partly converts apoptotic cell death to necroptosis, and inhibits both apoptosis and necroptosis. In the presence of TBZ, apoptosis is potently inhibited by the addition of Z, and pUL36 inhibits purely necroptotic cell death.

Lastly, HFFF-TERTs were infected with HCMV strain Merlin or AD169 for 48 h prior to TBZ stimulation. Whereas strain AD169 sensitised cells to TBZ-stimulated cell death, strain Merlin was able to protect against this sensitisation and had a slight protective effect on MLKL-dependent necroptosis **(Figure 5.9A-B)**. Interestingly, cell death induced by TBZ after infection with HCMV was not inhibited by GSK'872, indicating that cell death was occurring independently of RIP3. A repeat of this experiment with UL36 single-gene-deletion viruses showed that a functional pUL36 is necessary to prevent this sensitisation **(Figure 5.9C)**. As well as being unable to degrade MLKL **(Figure 5.5)**, the UL36-P2A-GFP virus was also unable to protect cells from undergoing necroptosis.

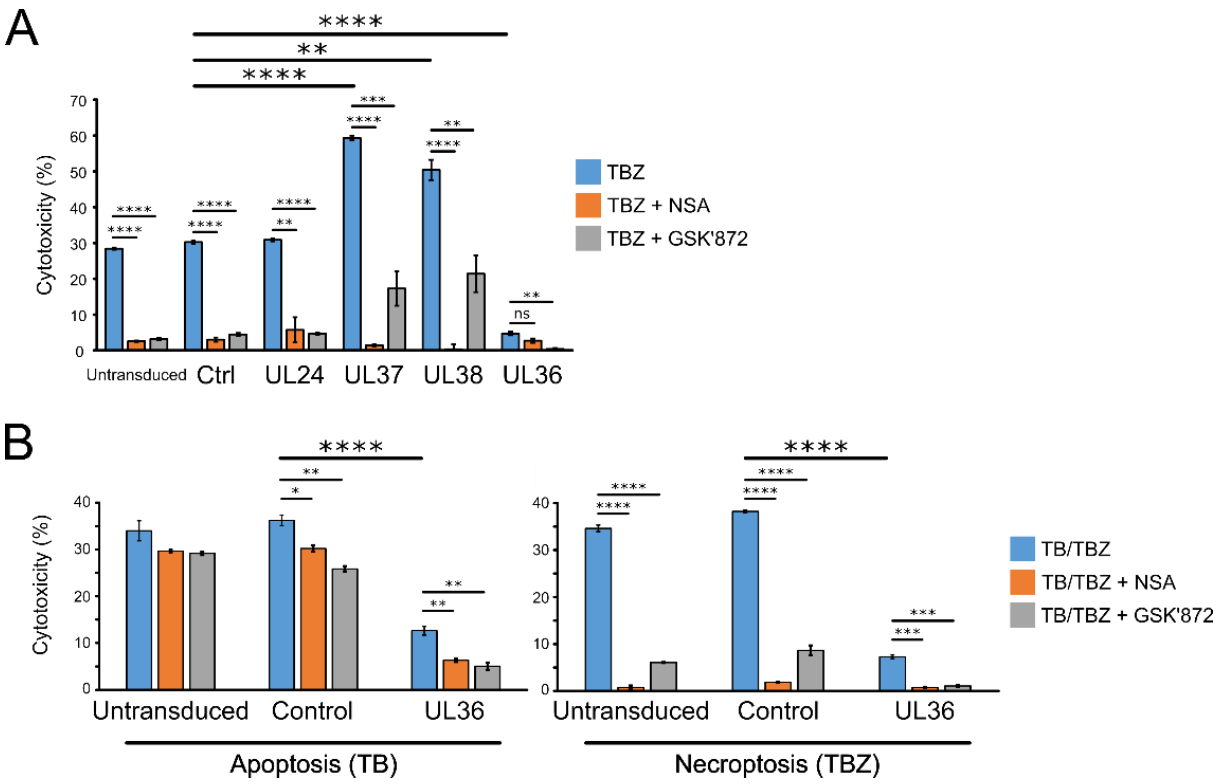

Figure 5.8: pUL36 inhibits both apoptosis and necroptosis.

(A) HFFF-TERTs were transduced with expression vectors encoding a short randomised DNA sequence (Ctrl) or HCMV proteins pUL24, pUL37, pUL38 or pUL36. pUL24 was included as a control HCMV tegument protein that is a similar size to pUL36 but lacks any known role in cell death. Cell death was stimulated and measured as described above (Figure 5.6A). Data are representative of two independent experiments. **(B)** Untransduced, control or UL36-expressing HFFF-TERTs were treated for 18 h with either TB or TBZ to stimulate apoptosis or necroptosis, respectively, in the presence or absence of NSA or GSK'872. Data are representative of two independent experiments. All experiments were performed in biological triplicate in parallel, with error bars showing SEM. P-values were estimated using a two-tailed t-test (n=3). *p<0.05, **p<0.01, ***p<0.001, ****p<0.0001.

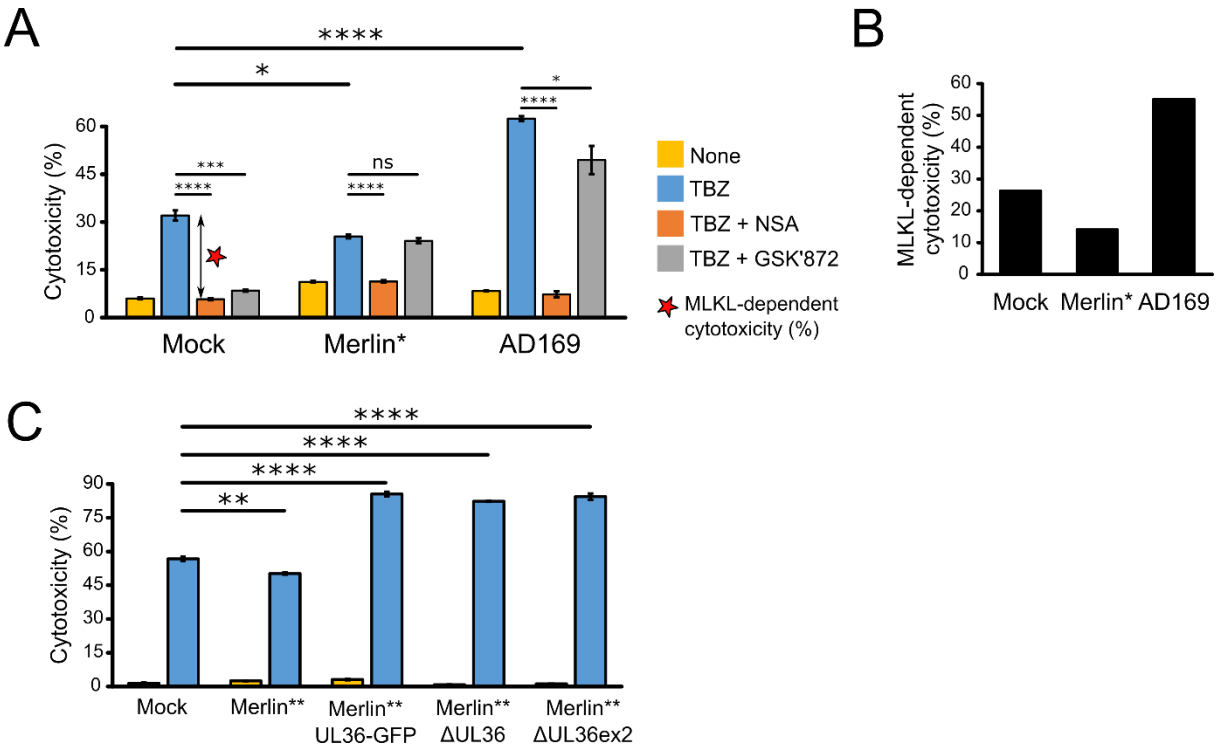

Figure 5.9: pUL36 prevents infected cells becoming sensitised to necroptosis.

(A) HFFF-TERTs were infected with HCMV strain Merlin* (RCMV1111) or AD169 (MOI: 5, 48 h infection), or mock-infected. Infected cells were subsequently stimulated with TBZ ± inhibitors for 18 h. The baseline cytotoxicity observed in untreated cells was not subtracted from the other values and is shown as a separate yellow bar, so that the effect of infection on cell death in the absence of stimulation could be analysed. Data are representative of two independent experiments. **(B)** MLKL-dependent cytotoxicity was calculated from the difference between the percentage cytotoxicity (TBZ alone) versus (TBZ+NSA), shown by the double-headed arrow in (A). **(C)** HFFF-TERTs were infected with WT strain Merlin with UL128 and RL13 under tetracycline regulation (Merlin**, RCMV1502), a UL36-P2A-GFP virus (RCMV2270), or one of two UL36 deletion viruses derived from Merlin** (RCMV2288 and 2289) (MOI: 5). 48 h later, necroptosis was stimulated with TBZ for 18 h. Inhibitors were not used in this experiment. ΔUL36ex2 has a deletion in exon 2. All experiments were performed in biological triplicate in parallel, with error bars showing SEM. P-values were estimated using a two-tailed t-test (n=3). *p<0.05, **p<0.01, ***p<0.001, ****p<0.0001.

5.5 Elucidating the mechanism of pUL36 degradation

5.5.1 MLKL-pUL36 interaction is dependent on pUL36 Merlin residue Cys^{131}

The pUL36 proteins encoded by strain Merlin and strain AD169 differ by five amino acids **(Figure 5.10)**, including a Cys^{131} (Merlin) to Arg^{131} (AD169) substitution. This substitution abrogates the ability of pUL36 to suppress apoptosis, as pUL36(Arg^{131}) cannot bind procaspase-8 [209]. Five pUL36 mutants based on strain Merlin corresponding to the five amino acid substitutions were constructed in order to determine which were important for the downregulation of MLKL. Only the C131R substitution prevented pUL36 from binding and downregulating MLKL **(Figure 5.11A-B)**. The same pUL36 mutant was also unable to protect cells from necroptosis, suggesting that this single residue plays a key role in inhibition of both apoptosis and necroptosis by pUL36 **(Figure 5.11C)**. However, structural prediction of the pUL36 N-terminus using I-TASSER [295] and trRosetta [296] indicated that Cys^{131} is likely embedded within the structure (results not shown). It is therefore likely that this residue is essential for the tertiary structure of the protein, rather than acting at an interaction interface.

```
 AD169  MDDLRDTLMAYGCIAIRAGDFNGLNDFLEQECGTRLHVAWPERCFIQLRSRSALGPFVGK  60
Merlin  MDDLRDTLMAYGCIAIRAGDFNGLNDFLEQECGTRLHVAWPERCFIQLRSRSALGPFVGK  60
        ************************************************************

 AD169  MGTVCSQGAYVCCQEYLHPFGFVEGPGFMRYQLIVLIGQRGGIYCYDDLRDCVYELAPTM  120
Merlin  MGTVCSQGAYVCCQEYLHPFGFVEGPGFMRYQLIVLIGQRGGIYCYDDLRDCIYELAPTM  120
        ************************************************:*******

 AD169  KDFLRNGFRHRDHFHTMRDYQRPMVQYDDYWNAVMLYRGDVESLSAEVTKRGYASYTIDD  180
Merlin  KDFLRHGFRHCDHFHTMRDYQRPMVQYDDYWNAVMLYRGDVESLSAEVTKRGYASYSIDD  180
        *****:**** ************************************************:***

 AD169  PFDECPDTHFAFWTHNTEVMKFKETSFSVVRAGGSIQTMELMIRTVPRITCYHQLLGALG  240
Merlin  PFDECPDTHFAFWTHNTEVMKFKETSFSVVRAGGSIQTMELMIRTVPRITCYHQLLGALG  240
        ************************************************************

 AD169  HEVPERKEFLVRQYVLVDTFGVVYGYDPAMDAVYRLAEDVVMFTCVMGKKGHRNHRFSGR  300
Merlin  HEVPERKEFLVRQYVLVDTFGVVYGYDPAMDAVYRLAEDVVMFTCVMGKKGHRNHRFSGR  300
        ************************************************************

 AD169  REAIVRLEKTPTCQHPKKTPDPMIMFDEDDDDELSLPRNVMTHEEAESRLYDAITENLMH  360
Merlin  REAIVRLEKTPTCQHPKKTPDPMIMFDEDDDDELSLPRNVMTHEEAESRLYDAITENLMH  360
        ************************************************************

 AD169  CVKLVTTDSPLATHLWPQELQALCDSPALSLCTDDVEGVRQKLRARTGSLHHFELSYRFH  420
Merlin  CVKLVTTDSPLATHLWPQELQALCDSPALSLCTDDVEGVRQKLRARTGSLHHFELSYRFH  420
        ************************************************************

 AD169  DEDPETYMGFLWDIPSCDRCVRRRRFKVCDVGRRHIIPGAANGMPPLTPPHVYMNN      476
Merlin  DEDPETYMGFLWDIPSCDRCVRRRRFKVCDVGRRHIIPGAANGMPPLTPPHAYMNN
        ************************************************.****
```

Figure 5.10: Strain Merlin and strain AD169 pUL36 differ by five amino acids.

Amino acid sequence alignment of pUL36 from HCMV strains Merlin and AD169 using Clustal Omega by EMBL-EBI [291]. The five amino acid sequence differences are highlighted. '*' indicates positions that have an identical, fully conserved residue. ':' indicates a substitution with a residue with strongly similar properties. '.' indicates a substitution with a residue with weakly similar properties.

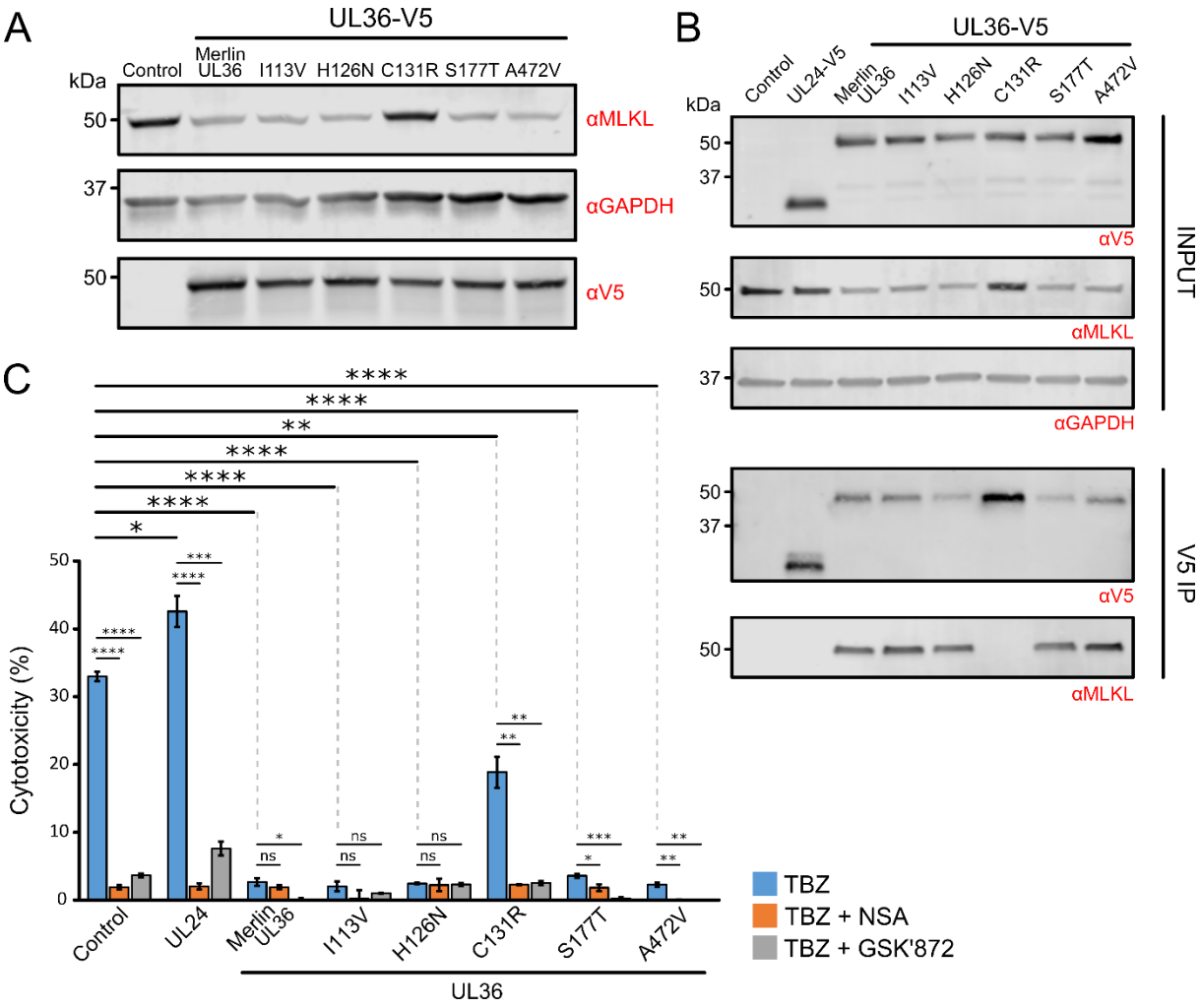

Figure 5.11: Substitution of Merlin pUL36 Cys^{131} abrogates inhibition of necroptosis.

(A) HFFF-TERTs were stably transduced with vectors encoding a control sequence or pUL36-V5 variants with point mutations corresponding to the five amino acid substitutions between strain Merlin and strain AD169. Abundance of MLKL was measured by immunoblot. **(B)** The cell lines used in (A), plus an additional control (pUL24-V5), were used in a V5 co-IP. Input and pulldown samples were analysed by immunoblot. **(C)** Percentage cytotoxicity of cell lines described in (A) that were treated with TBZ ± NSA or GSK'872 for 18 h. Error bars: SEM. P-values were estimated using a two-tailed t-test (n=3). *p<0.05, **p < 0.01, ***p < 0.001, ****p< 0.0001. Data are representative of two independent experiments.

In order to aid structural analysis, attempts were made to identify regions of pUL36 and MLKL that interact with one another. For pUL36, six V5-tagged constructs were made corresponding to the location of US22-like domains predicted by HHpred [293] and regions that were predicted to be ordered by I-TASSER and trRosetta **(Figure 5.12A)**. For MLKL, four HA-tagged constructs were designed according to locations of the well-characterised four-helix bundle (4HB), brace region, and pseudokinase domain (PsKD), taking into account the exact regions that have previously been successfully expressed [208,315] **(Figure 5.12B)**. The pUL36-V5 constructs were expressed in WT HFFF-TERTs and the MLKL-HA constructs expressed in HFFF-TERTs that were also stably expressing pUL36-V5 from a vector encoding a different selection marker. All pUL36-V5 domains were successfully expressed, except for the 320-476 C-terminal construct of 157 amino acids (**Figure 5.12C**, input). MLKL was only downregulated in cells expressing full-length pUL36-V5 (**Figure 5.12C**, input). An IP of the V5-tagged constructs was first performed under strict salt conditions [300 mM sodium chloride (NaCl)]. MLKL only co-precipitated with the full-length pUL36-V5 protein **(Figure 5.12C, V5-IP)**. Unusually, no V5 signal was detected in the pulldown samples, even after repeating the electrophoresis and transfer and probing with a different V5 antibody. As the high salt concentration may have inhibited weak ionic interactions, the IP was repeated under sensitive salt conditions (50 mM NaCl). Again, no interactions between any of the pUL36 domains and MLKL were identified **(Figure 5.12C, V5-IP)**. This time, V5 signals were detected in the immunoprecipitates, confirming that the pulldown had been successful.

The reciprocal IP was then performed, pulling down HA-tagged MLKL domains from pUL36-V5-expressing cells. Immunoblot analysis of the input samples showed that HA was detected in all of the MLKL-expressing cell lines **(Figure 5.12D, input)**. Full length MLKL, the 4HB and the 4HB+Brace constructs were all detected with bands of the expected sizes. However, expression of the PsKD with and without the brace led to detection of a band around 25 kDa, smaller than the expected sizes of 32 and 37 kDa, respectively **(Figure 5.12B and D)**. Addition of the brace region did result in a second larger and weaker band, but this was still smaller than the expected size. If the construct is being cleaved, this must be occurring at the N-terminal end as the HA tag is positioned at the C-terminus. However, if this were the case, addition of the brace region wouldn't be expected to generate a larger band.

The HA-IP successfully precipitated all of the MLKL-HA domains **(Figure 5.12D, HA-IP)**. Multiple bands were detected in the precipitates of the samples expressing the MLKL 4HB with the brace region (4HB+Br) indicating that this domain might be oligomerising into higher order structures, in accordance with the literature [201], despite the electrophoresis being performed under reducing conditions. Evidence of co-precipitation of pUL36-V5 was detected in the sample expressing full-length MLKL. Again, multiple bands were detected, roughly corresponding to the size of one, two or three molecules of pUL36, indicating that pUL36 may form strong hetero-oligomers with MLKL, even under reducing conditions.

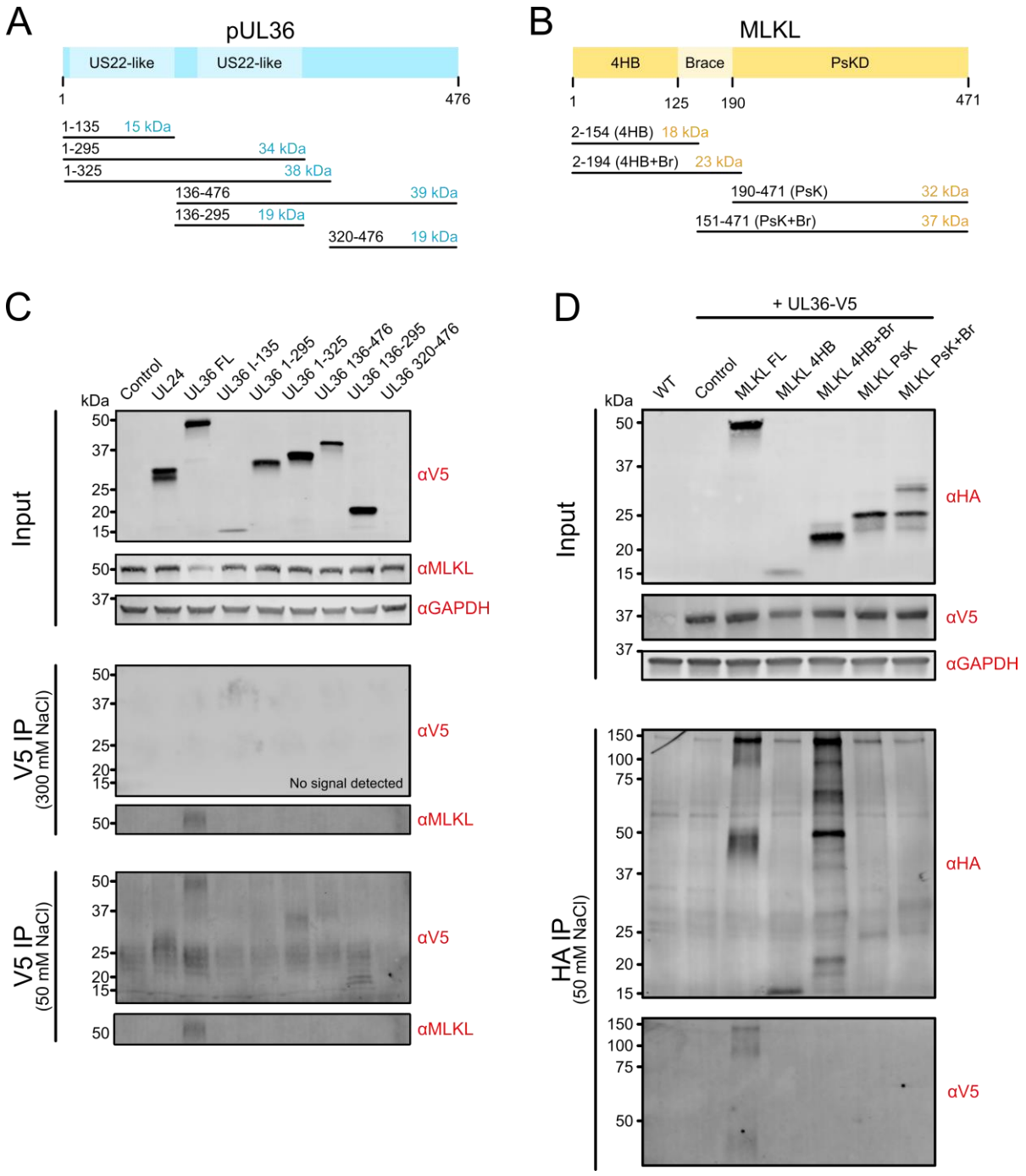

Figure 5.12: pUL36 and MLKL domain immunoprecipitations.

(A) The six pUL36 regions that were expressed in WT HFFF-TERTs. V5 was added to the C-terminus of each construct, which adds 1.4 kDa to the molecular weight of each domain. **(B)** The four MLKL domains that were expressed in HFFF-TERTs along with pUL36-V5. HA was added to the C-terminus of each protein, which adds 1.1 kDa to each domain. **(C)** HFFF-TERTs expressing a randomised control sequence, UL24-V5 (control virus protein), full-length UL36-V5 or V5-tagged UL36 domains were used in a V5 IP. Input and pulldown samples were analysed by immunoblot. **(D)** HFFF-TERTs expressing UL36-V5 and either a control sequence, full-length MLKL or one of four MLKL domain constructs were used in an HA IP. Input and pulldown samples were analysed by immunoblot. 4HB, four-helix bundle; Br, brace region; FL, full-length; IP, immunoprecipitation; PsKD, pseudokinase domain.

5.5.2 pUL36 interacts with E3 ligase components and accessory proteins

To generate the HCMV interactome, Dr. Luís Nobre performed an IP of 169 exogenously expressed V5-tagged HCMV strain Merlin proteins from infected cells, and analysed the precipitates by mass spectrometry. The interactome revealed that pUL36 interacts with a number of E3 ligase components and accessory proteins, which may explain how pUL36 targets MLKL for degradation **(Figure 5.13A)** [269]. Cullin 1 (CUL1) is a member of the cullin family of proteins, which tether substrate-binding proteins to the RING finger components in Cullin-RING E3 ligase complexes [376]. In particular, CUL1 is a component of the [S-phase kinase-associated protein 1 (Skp1)]-CUL1-F-box (SCF) E3 ligase complex, where the F-box protein is the variable substrate recognition subunit and Skp1 acts as an adaptor to mediate binding of the F-box to CUL1 **(Figure 5.13B)**. F-box proteins, of which there are approximately 70 in mammals, determine the substrate specificity of the SCF complex. F-box protein FBXO3, one of the other interactors of pUL36, has been implicated in pro-inflammatory signalling, the regulation of Wnt and RhoA pathways, and in transcriptional regulation [377–379]. The activity of FBXO3 is subverted by Rift Valley fever virus (RVFV) non-structural protein S (NSs) to degrade general transcription and DNA repair factor IIH (TFIIH) subunit p62, resulting in suppression of type I IFN transcription [380]. It can be hypothesised that HCMV pUL36 acts as an adaptor to drive the direct ubiquitination of MLKL through an interaction with FBXO3 and CUL1, similarly to RVFV NSs. This is supported by fact that FBXO3 was enriched in pulldowns of both pUL36 and MLKL in the presence of infection (2.5- and 9.7-fold, respectively) **(Figure 5.3 and Table 5.1)**.

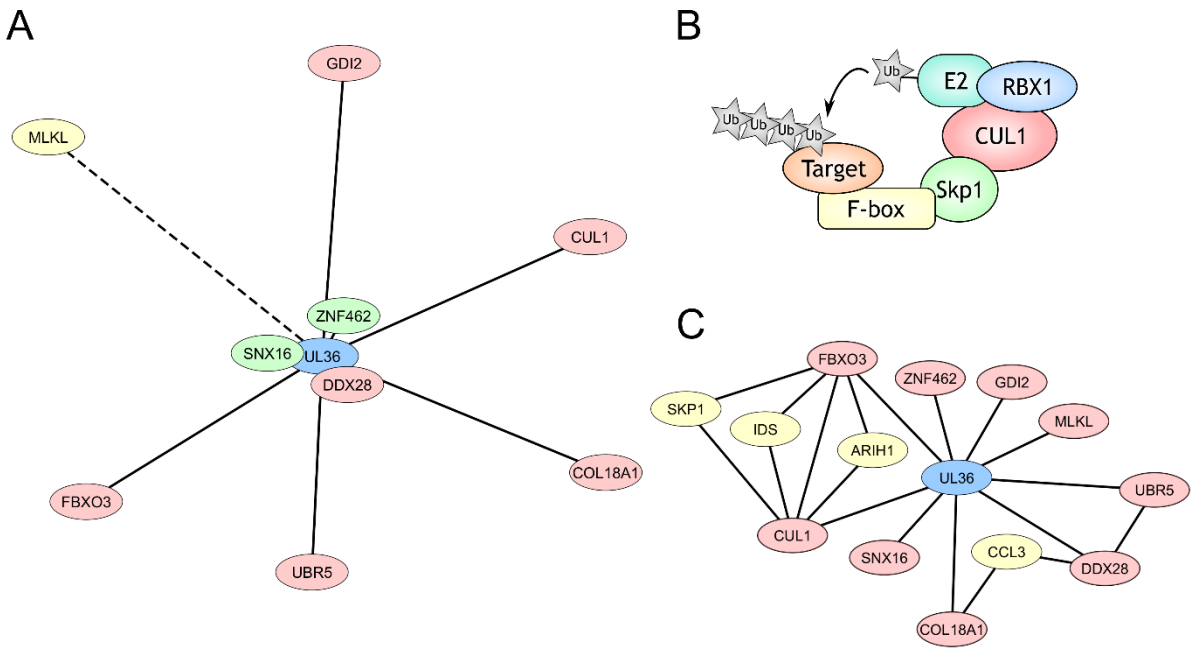

Figure 5.13: pUL36 interactome.

(A) pUL36 interactome generated by Dr. Luís Nobre [269]. The lengths of the lines connecting the viral bait protein pUL36 to each of the human interactors are inversely proportional to the normalised WD (NWD) score for the interaction. The NWD score reflects how frequently the protein was detected and whether it was detected reproducibly [269]. It was calculated as described in (Behrends *et al.* 2010 [381]) using the fraction of runs in which a protein was observed, the observed number of peptide spectral matches (PSMs), the average and standard deviation of PSMs observed for that protein across all IPs, and the number of replicates (1 or 2) containing the protein of interest. Two methods of filtering were used. Hits determined through CompPass filtering [382] are shown in green. Hits determined through CompPass Plus [383] are shown in yellow (note that CompPass Plus filtering does not produce an NWD score, represented with a dotted line). Hits found through both methods of filtering are shown in pink. **(B)** The SCF complex. The core components of the SCF E3 ligases are the scaffold protein CUL1, a RING-finger protein [e.g. RING-box 1 (RBX1)] and the adaptor protein Skp1. The variable component, the F-box protein, determines substrate specificity. The RING-finger protein binds the ubiquitin-conjugated E2 enzyme, facilitating transfer of the ubiquitin to the target. **(C)** Direct and indirect secondary interactions between the pUL36 interactors (pink), identified using BioPlex 3.0 [220]. Edges are not weighted.

Next, HHpred and Phyre2 [294] were used to identify pUL36 homologs and make predictions about its structure. This confirmed that pUL36 belongs to the US22-like family of DNA virus proteins, which typically contain two copies of a conserved domain that is also found within diverse bacterial and eukaryotic proteins belonging to the SUKH superfamily [384,385] **(Figure 5.14A)**. The SUKH domain possesses a versatile scaffold with a core fold comprising four conserved helices and six β-strands, which appears to have evolved to facilitate a large range of protein-protein interactions. Based on phylogenetic analyses, the SUKH superfamily can be divided into five major groups. SUKH-1, the likely ancestral group, includes both bacterial and eukaryotic homologs, one of which is human FBXO3. The US22-like proteins, which make up the SUKH-5 group, are most abundant in the herpesviruses, but are also found in certain adenoviruses, iridoviruses and poxviruses. Using Phyre2, 94 residues from the N-terminus of pUL36, from Phe^{21} to Arg^{129}, were modelled with 87.7% confidence based on Protein Data Bank (PDB) structure 3D5P, a crystal structure of a SUKH-1 family protein from *Bacteroides fragilis* **(Figure 5.14B-C)**. 3D5P, and the structures of many other SUKH proteins, are homodimers. These dimers are likely to form through crystal packing contacts and are unlikely to exist in the physiological state, but do illustrate the ability of the conserved cleft of the SUKH fold to accommodate other proteins [385]. Furthermore, a number of interactions can be seen between the HCMV US22-like proteins (including UL29 with UL38 and US26, and US23 with US24), which may be facilitated by their homologous US22-like domains [269]. This finding supports the hypothesis that pUL36 forms a direct interaction with FBXO3, which is even more closely related to 3D5P (the central domain of FBXO3 can be modelled using 3D5P as a template with a confidence of 98.6%) **(Figure 5.14C)**.

Another protein that co-precipitated with pUL36-V5 **(Figure 5.13A)**, ubiquitin protein ligase E3 component N-recognin 5 (UBR5), is a nuclear E3 ligase with known roles in the modulation of the DNA damage response and transcription [386]. To assess whether CUL1, FBXO3 or UBR5 were involved in the pUL36-dependent degradation of MLKL, small interfering RNA (siRNA) pools targeting each of these genes were transfected into HFFF-TERTs expressing UL36 or a control vector. Knockdown of the three proteins did not rescue MLKL levels in UL36-expressing cells, implying that none of these E3 ligase components are necessary for the downregulation of MLKL **(Figure 5.15A)**. The rescue of MLKL levels in cell lines constitutively expressing UL36 upon knockdown of the E3 ligases might depend on the rate of turnover of MLKL. Therefore, the same experiment was performed in the context of HCMV infection, with siRNA knockdown of FBXO3 and CUL1 being performed 72 h prior to infection **(Figure 5.15B)**. Once again, knockdown of FBXO3 and CUL1 had no impact on the downregulation of MLKL.

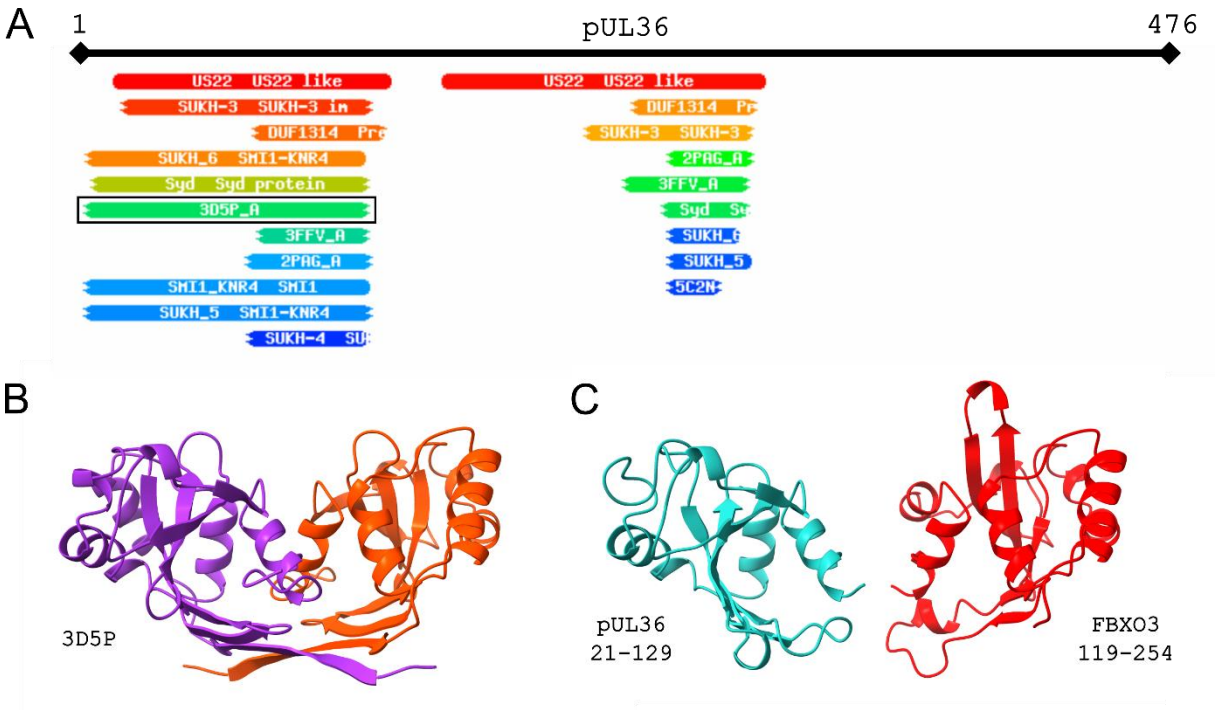

Figure 5.14: pUL36 and FBXO3 contain a conserved domain belonging to the SUKH superfamily.
(A) pUL36 protein remote homology detection against PDB_mmCIF70_8_Apr and Pfam-A_v32.0 databases using HHpred. **(B)** PDB structure 3D5P. **(C)** Predicted structures of pUL36 (amino acids 21-129) and FBXO3 (amino acids 199-254) using Phyre with PDB 3D5P as the template.

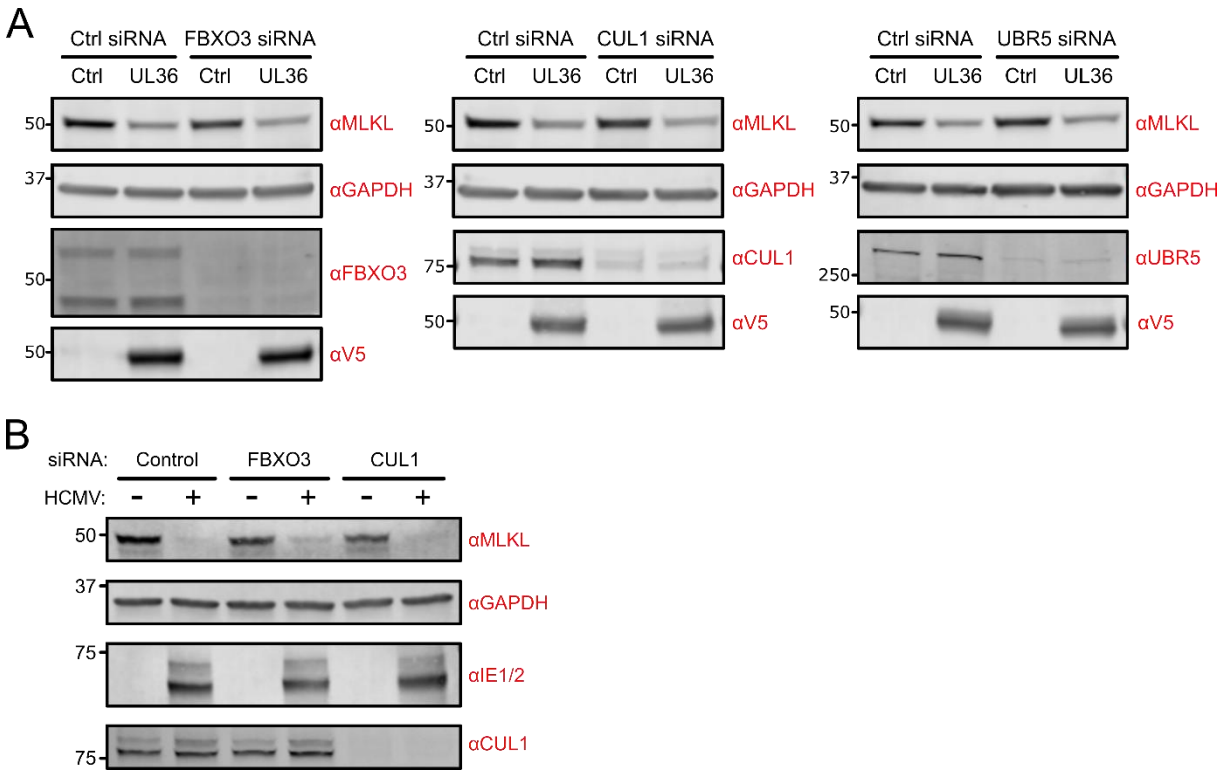

Figure 5.15: MLKL downregulation is not dependent on FBXO3, CUL1 or UBR5.
(A) HFFF-TERTs expressing control or UL36-V5-expressing vectors were transfected with a pool of siRNAs targeting FBXO3, CUL1, UBR5 or control sequences for 48 h before harvesting cells in RIPA and analysing the cell lysates by immunoblot. **(B)** HFFF-TERTs were transfected with a pool of siRNAs targeting control, FBXO3 or CUL1 sequences for 48 h, and then incubated in serum-free media supplemented with dexamethasone for 24 h. The cells were then infected with HCMV strain Merlin (RCMV1111) (MOI: 5) for 48 h before harvesting in RIPA and analysing cell lysates by immunoblot. FBXO3 knockdown was not confirmed in this experiment.

Another two factors of interest were HECT, UBA and WWE domain-containing E3 ubiquitin protein ligase 1 (HUWE1) and RB binding protein 7 (RBBP7). HUWE1 is a HECT E3 ubiquitin ligase that has been implicated in apoptosis and DNA damage repair [387], and was enriched more than 1.5-fold in immunoprecipitations of both UL36-V5 and MLKL-HA **(Table 5.1)**. RBBP7, which targets HUWE1 for degradation [387], was the most strongly enriched protein in the MLKL-HA immunoprecipitation **(Figure 5.3)**. Knockdown of HUWE1 and RBBP7 by siRNA transfection was confirmed by quantitative polymerase chain reaction (qPCR) **(Figure 5.16A-B)**. HUWE1 and RBBP7 knockdown did not rescue the level of MLKL in UL36-expressing HFFF-TERTs, but interestingly did lead to a decrease in the amount of MLKL protein in the absence of pUL36, indicating that interactions between HUWE1 and RBBP7 may have a functional role in MLKL stabilisation **(Figure 5.16C)**.

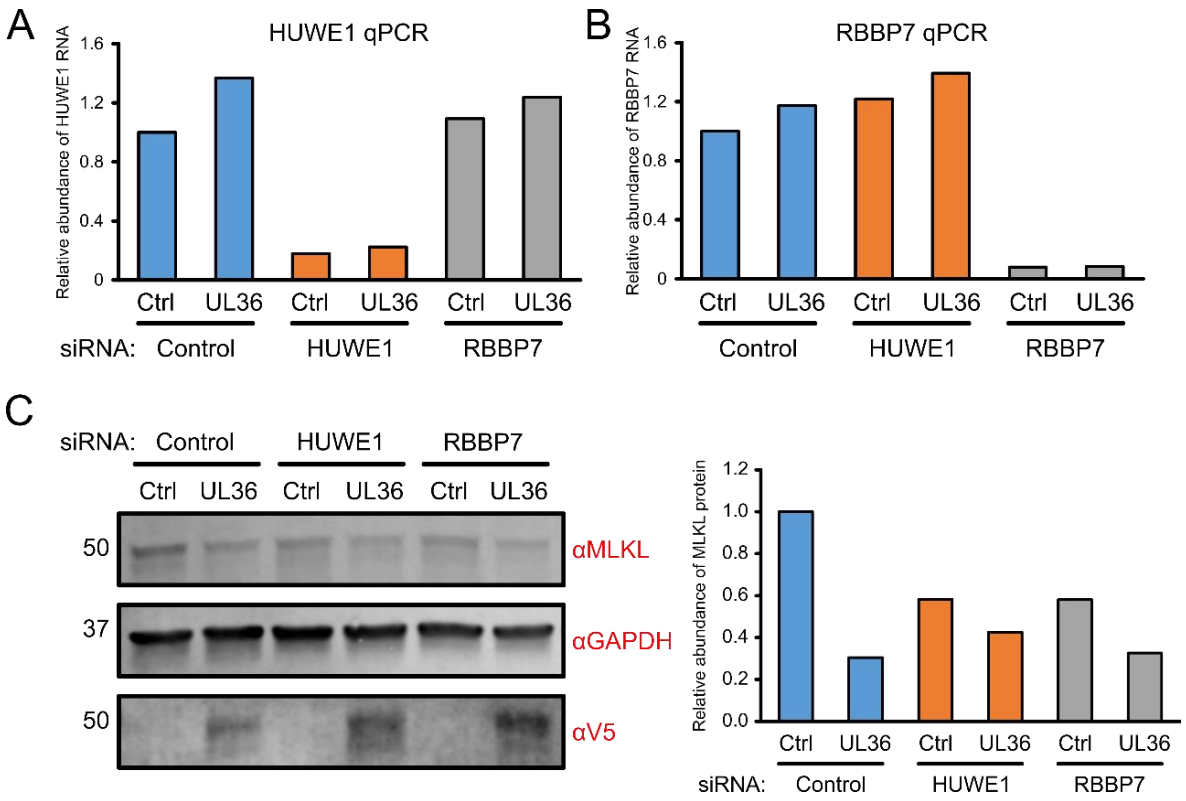

Figure 5.16: HUWE1 and RBBP7 are not responsible for pUL36-mediated MLKL downregulation.
HFFF-TERTs transduced with control or UL36-V5-expressing vectors were transfected with siRNA pools targeting HUWE1, RBBP7 or control sequences and left for 48 h before harvesting half of the cells for reverse transcription (RT)-qPCR analysis and the other half for immunoblot analysis. **(A)** RT-qPCR of HUWE1. **(B)** RT-qPCR of RBBP7. **(C)** Immunoblot (left) and densitometry analysis of MLKL abundance relative to GAPDH loading control (right).

5.6 Discussion

5.6.1 pUL36 is necessary and sufficient for MLKL downregulation and necroptosis inhibition

The suppression of caspase-8 activity by viral, cellular or chemical inhibitors releases the inhibitory effect of caspase-8 on the necroptotic pathway **(5.1.1)**. Indeed, a number of viral inhibitors of caspase-8 have been shown to sensitise cells to necroptotic cell death instead of completely inhibiting cell death upon stimulation of apoptosis [324,388]. It was previously thought that HCMV pUL36 would have a similar effect, requiring HCMV to encode a separate mechanism of necroptosis inhibition in order to evade cell death completely. However, this effect has never been observed, which may be because the cell lines previously used to study the effect of pUL36 lacked key components of the necroptosis machinery. However, in HFFFs that are susceptible to TNFα-stimulated, MLKL- and RIP3-dependent

necroptosis, pUL36 can completely inhibit cell death induced by TNFα instead of simply shifting the pathway towards necroptosis **(Figure 5.8)**. Therefore, pUL36 alone can inhibit both apoptosis and necroptosis.

These observations can be explained by results showing that in the presence of either UL36 expression or infection with HCMV strain Merlin, the level of MLKL protein is downregulated **(Figure 5.2 and Figure 5.4)**. The downregulation of MLKL can be rescued by the addition of MG132 or bortezomib, although the level of rescue can vary **(Figure 5.2 and Figure 5.4)**. When observing the abundance of MLKL by proteomics, addition of either MG132 or bortezomib resulted in a significant increase in MLKL **(Figure 1.12)**. However, the rescue appeared less significant when analysing MLKL abundance by immunoblot **(Figure 5.2 and Figure 5.4)**. The downregulation of MLKL was typically more significant in cells infected with HCMV strain Merlin **(Figure 4.3 and Figure 5.2 and Figure 5.15)** than in cells expressing pUL36 alone **(Figure 5.4)**. This may be due to different expression levels of pUL36, or could mean that other viral factors or cellular proteins acting specifically in the context of infection work in concert with pUL36 to drive maximal MLKL downregulation.

The action of pUL36 is important to protect infected cells from necroptotic cell death. Infection with HCMV strain AD169 or strain Merlin viruses that lack a functional pUL36 protein sensitised cells to necroptosis **(Figure 5.9)**. This may be explained by the observed increase in MLKL protein upon infection with viruses lacking pUL36 **(Figure 5.4)**, which is likely to be due to IFN-mediated upregulation of MLKL [200] **(1.6.1)**. Strain Merlin protein pUL36 was able to counteract the effect of necroptosis sensitisation, rather than abrogating necroptosis entirely **(Figure 5.9)**. Interestingly, the pUL36-P2A-GFP recombinant virus (RCMV2270) did not downregulate MLKL nor protect infected cells from necroptosis **(Figure 5.4 and Figure 5.9)**. However, a different recombinant virus also expressing pUL36-P2A-GFP (RCMV2344) has previously been shown to restrict Fas-mediated apoptosis to the same extent as WT strain Merlin [62]. This suggests that the ability of strain Merlin to counteract sensitisation to necroptosis is dependent on the ability of pUL36 to downregulate MLKL, and not due to its effect on caspase-8.

Previous studies investigating the modulation of necroptosis by HCMV have utilised HFFF-TERTs stably transduced with RIP3 in order to confer susceptibility to necroptosis, which can otherwise be lost during cell propagation. Using these cells, Omoto and colleagues found that all tested HCMV strains, including AD169, were able to inhibit TNFα-stimulated necroptosis, although strain Merlin inhibited necroptosis more potently than AD169 [213]. Furthermore, comparison of WT strain Towne (encoding pUL36 with a cysteine at position 131) with a Towne ΔUL36 mutant found that pUL36 was necessary for inhibition of apoptosis but had no effect on necroptosis [213]. In addition to mediating cell death, RIP3 has been implicated in NF-kB and inflammasome activation and can induce apoptosis when overexpressed [368,389]. It is possible that overexpression of RIP3 has off-target effects, which may explain the discrepancy between the previously published work [213] and the work presented in this

thesis. The HFFF-TERT cell line used by our group is susceptible to RIP3 and MLKL-dependent canonical necroptosis **(Figure 5.7)** and therefore may be an invaluable resource for future studies of viral evasion of necroptosis.

While the Omoto *et al*. study [213] suggested that HCMV targets necroptosis downstream of MLKL phosphorylation, all MLKL peptides in our pUL36-V5 SILAC IP were unphosphorylated **(Figure 5.3)**, suggesting that pUL36 may affect the monomeric MLKL pool. However, this does not exclude the potential for additional HCMV-mediated direct or indirect mechanisms of necroptosis inhibition. Certainly, there are now a number of studies observing HCMV-mediated regulation of necroptotic pathways that suggest that HCMV uses multiple mechanisms of necroptosis inhibition. While pUL36 has been shown to inhibit caspase-independent as well as caspase-dependent modes of cell death in differentiating monocytes [356], pUL36 is not expressed in infected undifferentiated primary monocytes [336]. Instead, the induction of autophagy in these cells upon infection is thought to inhibit the activation of MLKL [336]. It appears that the mechanism of necroptotic inhibition utilised by HCMV may be dependent on the cell type, particularly whether or not the cell type supports lytic or latent infection.

Outstanding questions regarding the mechanism and function of MLKL downregulation in HCMV infection include:

a) Is the interaction between pUL36 and MLKL necessary for MLKL downregulation?

b) Is the downregulation of MLKL necessary for the effect of pUL36 on necroptosis?

These questions are difficult to answer given the apparent multifaceted role of pUL36. In order to establish whether the effects of pUL36 are dependent on its interaction with either caspase-8 or MLKL, it will be necessary to define the structural determinants of these interactions, as discussed below **(5.6.3)**. The pUL36-P2A-GFP recombinant virus, which can inhibit apoptosis but not downregulate MLKL, may be a useful tool for distinguishing between the differential outcomes of MLKL and caspase-8 binding by pUL36.

5.6.2 Other reflections from the cell death assays

In addition to revealing the ability of pUL36 to inhibit both apoptosis and necroptosis, the cell death assays described here led to some other findings that have not been previously reported in the literature. Namely, that infection of HFFF-TERTs with HCMV prior to TBZ stimulation resulted in induction of a form of cell death that was not completely inhibited by GSK'872, which is suggestive of an RIP3-independent but MLKL-dependent mechanism **(Figure 5.9)**. A similar but less significant effect was observed in cells expressing the HCMV inhibitors of apoptosis pUL37 and pUL38 **(Figure 3D)**. RIP3-independent necroptosis in fibroblasts has been reported previously by others [370] but remains poorly characterised, and would be an interesting topic for further investigation. Another intriguing finding was that expression of pUL37 or pUL38 alone can sensitise cells to necroptotic cell death. Although the

reasons for this are far from clear, this effect may indicate the presence of feedback loops between intrinsic and extrinsic forms of cell death.

5.6.3 Structural determinants of pUL36 function

Mutation of Cys^{131} in strain Merlin pUL36 to an arginine residue was sufficient to inhibit the interaction between pUL36 and MLKL and prevent the downregulation of MLKL and the inhibition of necroptosis **(Figure 5.11)**. The same amino acid substitution has previously been shown to disrupt the interaction between pUL36 and procaspase-8 [209]. Cys^{131} sits within the first US22-like domain of pUL36 **(Figure 5.12)** and is conserved within the primate cytomegaloviruses [355]. The MCMV ortholog pM36 lacks the region that includes Cys^{131} but can still effectively inhibit apoptosis [355], implying that the Arg^{131} residue present in the AD169 form of pUL36 has an inhibitory effect, as opposed to Cys^{131} being required for this function. In accordance with this hypothesis, structural prediction of pUL36 suggests that Cys^{131} will be buried within the structure of the protein, rather than forming an interaction interface. It is possible that the substitution disrupts a disulphide bond that is key to the tertiary structure of the protein, or that the positively charged Arg residue promotes a structural change that renders pUL36 non-functional.

Attempts were made to identify the regions of MLKL and pUL36 responsible for the interaction between the two proteins. None of the domains expressed were sufficient for the interaction **(Figure 5.12)**. An alternative approach could be to compare the sequence of pUL36 with that of MCMV pM36, which inhibits apoptosis but not necroptosis, and sequentially mutate the sequences of pUL36 that are different in pM36 **(Future directions 5.1)**. Identification of specific structural determinants required for MLKL downregulation will not only enable mechanistic characterisation, but will also enable the effects of pUL36 on cell death to be attributed to either MLKL or procaspase-8 binding.

A. Identification of regions or residues that are specifically required for the interaction between pUL36 and MLKL.

This could be achieved by sequentially mutating regions of pUL36 that differ significantly in MCMV pM36.

B. Characterisation of interactions between pUL36, procaspase-8 and MLKL *in vitro.*

Purification of pUL36, procaspase-8 and MLKL will enable *in vitro* characterisation of the interactions between these proteins, for example by *in vitro* co-immunoprecipitation, tandem affinity purification, affinity chromatography, isothermal titration calorimetry, surface plasmon resonance, microscale thermophoresis and/or analytical ultracentrifugation.

Future directions 5.1: What are the structural determinants of the pUL36-MLKL interaction?

5.6.4 The mechanism of MLKL downregulation

5.6.4.1 Are cellular E3 ligases involved?

Across two mass spectrometry IPs (IP-MS), pUL36-V5 was found to interact with several E3 ligase components, including FBXO3, CUL1, UBR5, HUWE1 and RBBP7 **(Figure 5.3 and Figure 5.13)**. Many viruses implement strategies to subvert cellular E3 ligase machinery to target host proteins for proteasomal degradation [62,127,269,390]. It was hypothesised that pUL36 could be using the same mechanism to downregulate MLKL. However, knockdown of each of these proteins did not affect the ability of pUL36 to downregulate MLKL. Although the amount of knockdown achieved with siRNA transfection appeared significant by immunoblot or qPCR, residual protein expression may be sufficient to mediate MLKL downregulation. These experiments could be repeated using a CRISPR/Cas9 system to achieve full knockout. Other experiments to identify cellular proteins (E3 ligases or otherwise) that are involved in the downregulation of MLKL are described in **Future directions 5.2**.

The discovery that FBXO3 co-precipitated with both pUL36-V5 and MLKL-HA in the context of infection was particularly interesting given that it shows structural homology to pUL36 **(Figure 5.14)**. Proteins belonging to the SUKH superfamily are known to homo- and heterodimerise, which may help explain how FBXO3 and pUL36 interact. It would be interesting to investigate whether or not FBXO3 interacts with MLKL under homeostatic cellular conditions in the absence of infection. If it does, an alternative model could be that pUL36 mimics FBXO3 to interact with MLKL.

A. Verification of E3 ligase involvement by CRISPR/Cas9 knockout of E3 ligase interactors.

CRISPR/Cas9 knockout could be achieved via nucleofection of sgRNA:Cas9 complexes as described in 3.14.

B. Identification of host proteins that bind pUL36 and/or MLKL in the context of infection using proximity labelling.

Interactions with E3 ligases or other host proteins may occur via transient interactions that are not detectable by IPs. Coupling proximity labelling (e.g. BioID) with IP-MS may allow identification of transient interactions [391].

C. Identification of E3 ligase components necessary for MLKL downregulation using an unbiased forward genetic screen (FGS).

An sgRNA library targeting 1119 genes of the ubiquitin-proteasome system (UPS) has previously been used to identify UPS components involved in the degradation of cellular proteins [392]. This library could be used to perform a FGS for proteins involved in the downregulation of MLKL in HFFF-TERTs stably expressing pUL36 and a GFP-tagged version of MLKL. CRISPR knockout of proteins involved in MLKL downregulation will result in an increase in MLKL-GFP, allowing cells expressing that particular sgRNA to be isolated using fluorescence-activated cell sorting.

Future directions 5.2: Are cellular E3 ligases involved in the downregulation of MLKL?

5.6.4.2 Degradation or translocation to detergent-resistant membranes?

The induction of necroptosis is thought to drive the translocation of necrosome components to detergent-resistant membranes (DRMs) [206,393,394]. It has been suggested that pUL36, through its ability to inhibit caspase-8, is simply causing the translocation of MLKL to insoluble membrane complexes that arise in cells undergoing necroptosis. Furthermore, proteasome inhibitors have been shown to decrease the recruitment of necrosome machinery (including MLKL) to DRMs [393], which may explain the observed 'rescue' we see upon treatment with MG132 and bortezomib. In accordance with this theory, the 'abundance' of RIP1 and RIP3 also appeared to be upregulated in infected cells treated with MG132 **(Figure 5.7A)**.

DRMs are known to be insoluble in TritonX-100 and RIPA, but can be solubilised by boiling in SDS. MLKL abundance was therefore also analysed in infected cells lysed in 6 M guanidine and 2% SDS **(Figure 4.2 and Figure 5.4)** to show that MLKL downregulation is observed upon solubilisation with different detergents. A limitation to our work is that we have been unable to show that these conditions do in fact facilitate the solubilisation of active MLKL-complexes under conditions where necroptosis is stimulated, partly because we have been unable to find a suitable phospho-MLKL antibody. If this work is continued in the future, it should be established whether the methods used to solubilise MLKL in these experiments do indeed solubilise other proteins known to reside in detergent-resistant membrane vesicles as a positive control **(Future directions 5.3)**.

However, there are a few discrepancies between this hypothesis and the observed results. Firstly, experiments showing the recruitment of the necrosome to DRMs have found that MLKL, RIP1 and RIP3 show a similar distribution across a series of cellular fractions in the presence or absence of necroptotic stimulation [393]. One might therefore expect RIP1 and RIP3 to show the same profile of protein solubilisation in cells infected with HCMV as MLKL. However, RIP1 and RIP3 are minimally downregulated, if at all **(Figure 5.7A)**. Secondly, pUL36 appears to form a specific interaction with MLKL that can be abrogated by mutation of a single residue. In contrast, an interaction with procaspase-8 was never detected in the experimental conditions used here by either IP-MS or immunoblot IP (results not shown). Finally, if pUL36-mediated inhibition of caspase-8 is driving activation of the necrosome and translocation of MLKL into DRMs, why and how does pUL36 inhibit necroptosis? Interestingly, HSV-1 protein ICP6, which similarly functions as a suppressor of both caspase-8 activation and RIP3-dependent necroptosis, utilises the opposite mechanism – inhibiting the translocation of the necrosome to DRMs [394].

Certainly, given the known effects of proteasomal inhibitors on the necroptotic pathway, it is feasible that the mechanism of MLKL downregulation is not proteasomal degradation as previously hypothesised, and may instead involve the translocation of MLKL to DRMs prior to an alternative mode

of pUL36-mediated inhibition **(Figure 5.17)**. Experiments required to dissect the effect of pUL36 on the association of MLKL with DRMs are described in **Future directions 5.3**.

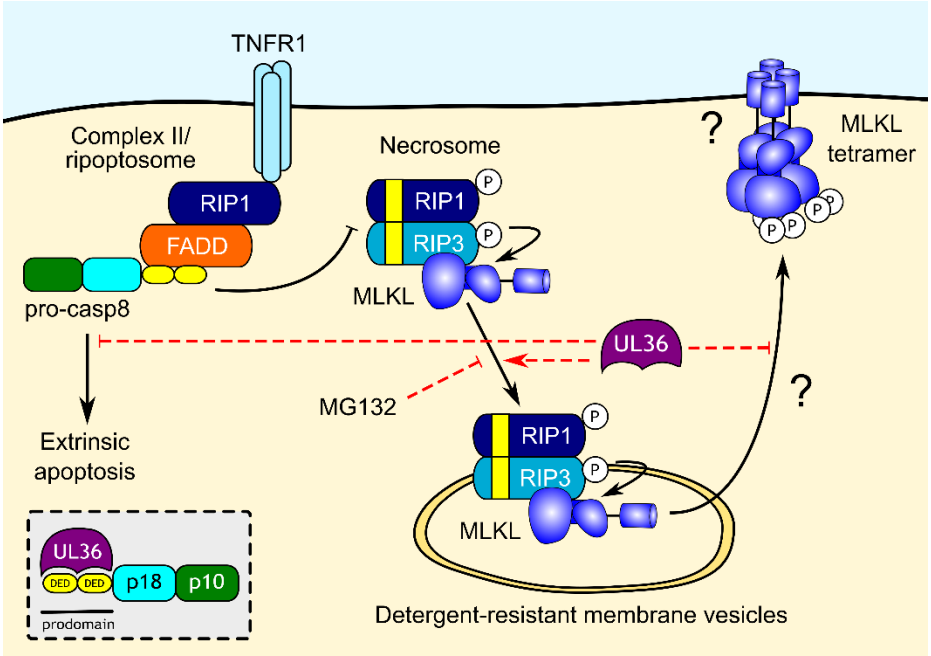

Figure 5.17: An alternative hypothesis of pUL36 function.

A. Solubilisation of infected and UL36-expressing HFFF-TERTs in DRM lysis buffer and immunoblot for MLKL.

Proteins known to reside in DRMs (e.g. calveolin-1) should be used as a positive control for DRM solubilisation.

B. Immunoblot for MLKL using RIPA, 6 M guanidine and 2% SDS lysis in TBZ-stimulated HFFF-TERTs.

To show whether or not MLKL can be solubilised under these conditions.

C. Analysis of RIP1 and RIP3 abundance under conditions of HCMV infection and UL36 expression by immunoblot.

This would establish whether the effect is specific to MLKL or is a more general effect on the necrosome. If pUL36 drives the necrosome into DRMs, RIP1 and RIP3 would be expected show the same pattern of solubilisation as MLKL under the various conditions tested.

D. DRM fractionation followed by immunoblot of MLKL under conditions of HCMV infection and pUL36 expression.

As described in Ali *et al.* (2019) [394].

Future directions 5.3: Does pUL36 direct MLKL to detergent resistant membranes?

5.6.4.3 A role for autophagy?

As eluded to in the introduction to this chapter, there is a wealth of literature concerning cross talk between cell death and autophagy [336,337]. For example, autophagy has been shown to be critical for the turnover of RHIM domain-containing proteins such as RIP1, RIP3, ZBP1 and TRIF [395]. In HCMV infection of primary monocytes, induction of autophagy plays a role in sequestering MLKL from RIP3 independently of pUL36 expression [336]. Furthermore, autophagy and the UPS are functionally coupled, with proteasomal inhibitors activating autophagic pathways [396]. It is therefore conceivable that the application of MG132 and bortezomib may have an impact on the abundance of necroptotic machinery. Although MG132 and bortezomib have been used successfully to identify host proteins degraded during virus infection [62,199], the ability of proteasomal inhibitors to impact fundamental cellular processes such as necroptosis [393] and autophagy [396] must be considered when using them for this purpose in the future. All in all, it is feasible that autophagy plays a role in pUL36-mediated cell death evasion, which could be investigated further.

5.6.5 Concluding remarks

Despite the questions that remain regarding the mechanism of MLKL downregulation and necroptosis inhibition by pUL36, the finding that pUL36 is necessary and sufficient for suppression of both apoptotic and necroptotic cell death represents a significant advance in our understanding of cell death evasion by HCMV. Indeed, this work has been met with considerable interest from researchers around the world. In particular, I am thankful to Professor Edward Mocarski (Emory University, USA) and Dr. Jason Upton (Auburn University, USA) for useful discussions and pointers.

The therapeutics currently in use for treating HCMV are all associated with significant toxicity and drug resistance. However, the potential for small molecule compounds to disrupt interactions between antiviral proteins and their cellular antagonists provides an opportunity for development of novel therapeutics. In particular, further characterisation of the molecular mechanisms underlying HCMV-mediated suppression of cell death could provide new pharmaceutical targets to release this inhibition of cell death and selectively eliminate infected cells.

Chapter 6: Investigating the degradation of DMXL1 and the function of genes in the US29-34A block

In this chapter, mass spectrometry data from samples prepared by Dr. Katie Nightingale (University of Cambridge) and Dr. Ceri Fielding (Cardiff University) were reanalysed, in parallel with data from samples generated by myself, to develop novel insights. Acknowledgements are given in the text and figure legends. Data from previously published papers were used to generate Figure 6.2 and Figure 6.8, as cited in the figure legends. Collaborators at Cardiff University (Dr. Richard Stanton and colleagues) provided the recombinant viruses and the cell lines expressing single genes from the US29-34A block were generated by Dr. Luís Nobre.

6.1 Introduction

In the Introduction of this thesis, DMXL1 was described as one of the host proteins degraded by human cytomegalovirus (HCMV) with the highest confidence **(1.6.2)**. In **Chapter 3**, preliminary results using a DMXL1 short hairpin RNA (shRNA) cell line in a two-colour restriction assay and plaque assay showed that DMXL1 knockdown decreased immediate-early (IE) gene expression, plaque size and plaque number, indicating that DMXL1 could be acting as a dependency factor rather than an antiviral restriction factor (ARF) **(Figure 3.12 and Figure 3.13)**. This result was particularly fascinating given that DMXL1 has been proposed as a regulator of the vacuolar-type H^+-adenosine triphosphatase (V-ATPase), a component of which, ATP6V0C, has also been shown to augment infection [221]. However, the validity of the shRNA restriction assay and plaque assay results were brought into question after it was shown that shRNA transduction has highly variable effects on the plaque assay read-out **(Figure 3.24)** and cellular proteome **(Figure 3.25)**. Despite this, given that the gene block responsible for DMXL1 downregulation has already been identified by work performed by Dr. Katie Nightingale [62], and because the existing literature hints at potential proviral and antiviral roles for the V-ATPase and DMXL1, further mechanistic analysis of HCMV-mediated DMXL1 degradation was performed and is presented in this chapter.

6.1.1 The vacuolar-type H^+-ATPase

The endomembrane organelles of eukaryotic cells are involved in a wide range of cellular processes including endocytosis, protein degradation and recycling, transport and sorting of proteins and lipids,

and signal transduction. Many of these functions rely on an intrinsic property of these organelles: their luminal acidic pH. Intracellular vesicle acidification is achieved through action of the V-ATPase [397], a highly conserved multisubunit enzyme that uses the energy of ATP hydrolysis to transport protons across membranes [398]. It consists of the catalytic cytoplasmic V_1 sector and the transmembrane V_0 sector, which is responsible for proton translocation.

Studies aiming to uncover the cellular function of the V-ATPase have historically made use of the V-ATPase inhibitor bafilomycin. Bafilomycin inhibits autophagosome-lysosome fusion [399], leading to the hypothesis that the V-ATPase is necessary for this process. However, it has been shown more recently that bafilomycin has off-target effects, with its effect on autophagosome-lysosome fusion occurring independently of its effect on the V-ATPase [400]. V-ATPase activity has also been implicated more broadly in vesicle trafficking [401], endosomal pH sensing [402], membrane fission and fusion [403], regulation of signalling [404,405], and protection of cells from stress-induced cell death [406], with the caveat that some of these studies also utilised bafilomycin. Knockdown of individual V-ATPase components including ATP6V0C have highlighted the role of the V-ATPase in lysosomal acidification and autophagic cargo degradation independently of autophagosome-lysosome fusion [400,406]. Of relevance to viral infection, the V-ATPase has been associated with mechanistic target of rapamycin (mTOR), Wnt, transforming growth factor beta and Notch signalling [407], TLR signalling [408] and MHC class II presentation [409].

Regulation of V-ATPase activity occurs at multiple levels: the subcellular localisation, subunit transcription and translation, incorporation of different tissue- and cell type-specific subunit isoforms, assembly and disassembly, recycling of vesicles from and to the plasma membrane (PM), and the uncoupling of ATP hydrolysis from proton pumping [219,397,410].

6.1.2 The DMXL family

DMXL1 and its homolog, DmX-like protein 2 (DMXL2), are large (~340 kDa) proteins consisting of a number of WD40 repeats folding to form β-propellers. Both DMXL1 and DMXL2 are thought to interact with WD repeat-containing protein 7 (WDR7) to form the complex Rabconnectin-3 [218,219,411]. Rabconnectin-3 was initially implicated in the release of synaptic vesicles, as it was shown to interact with both RAB3 guanine nucleotide exchange factor (GEF) and RAB3 GTPase activating protein (GAP). RAB3 GEF and GAP are regulators of the RAB3 family of small guanosine triphosphate (GTP)-binding proteins, which regulate Ca^{2+}-dependent exocytosis in neurons [411,412].

More recently, a number of papers have connected Rabconnectin-3 to the regulation of the V-ATPase. For example, a study in Drosophila showed that loss of function mutations in the Rabconnectin-3 subunits resulted in defective endosomal acidification and trafficking [413]. Merkulova *et al.* [219] found that DMXL1, DMXL2 and WDR7 form highly specific interactions with the V-ATPase in mouse kidney lysates, which has been corroborated by human interactome data from BioPlex 3.0 [220] **(Figure**

6.1). They also discovered that although knockdown of DMXL1 did not have an impact on intravesicular acidification under baseline conditions, re-acidification of intracellular vesicles after bafilomycin treatment was suppressed in DMXL1 and WDR7 knockdown cells, indicating cellular functions that require significant and sustained upregulation of V-ATPase activity may be dependent on DMXL1 and WDR7 [219]. On the other hand, DMXL2 silencing only had a modest effect, highlighting that the role of DMXL1 and DMXL2 may be cell-type specific.

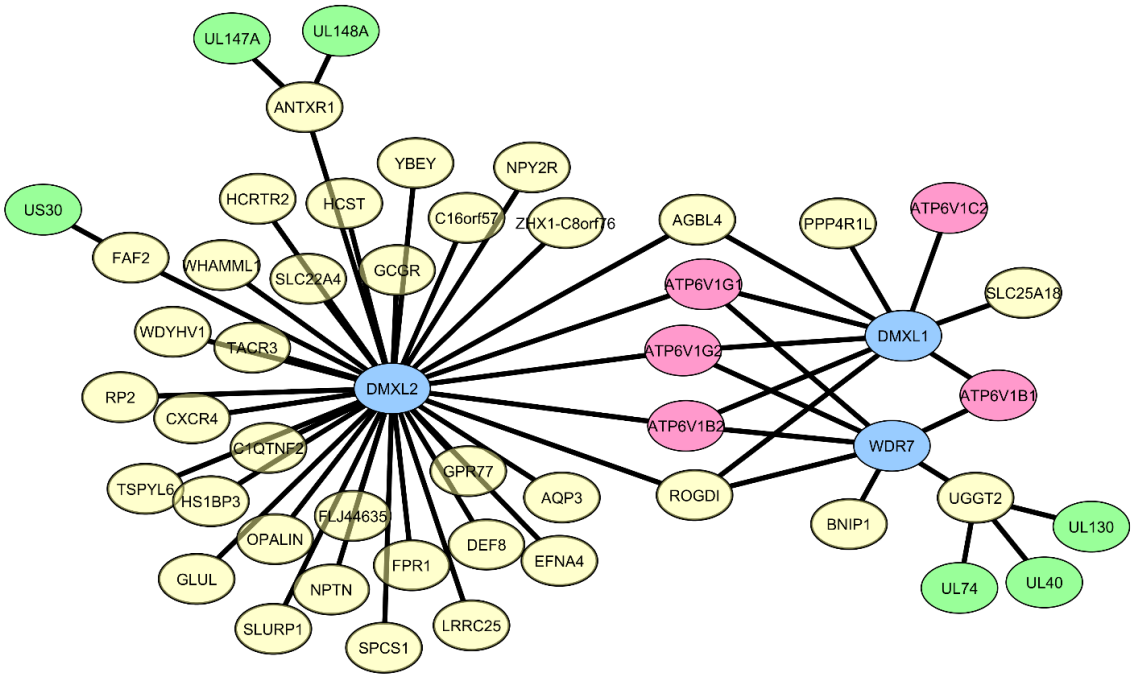

Figure 6.1: Interactors of DMXL1, DMXL2 and WDR7 and links to the HCMV interactome.
Human bait proteins that interact with DMXL1, DMXL2 and WDR7 (from BioPlex 3.0 [220]) are shown in yellow, with V-ATPase components shown in pink. DMXL1, DMXL2 and WDR7 have not yet been used as bait proteins in the BioPlex screens. For DMXL1 and DMXL2, this is likely due to their large sizes (~340 kDa). The HCMV interactome [269] was used to annotate each human protein with high-confidence interacting viral factors (shown in green).

How does Rabconnectin-3 regulate V-ATPase activity? Due to the proposed role of the complex in Ca^{2+}-dependent exocytosis, it was hypothesised that Rabconnectin-3 controls V-ATPase activity by regulating its transport to the PM [219]. The DMXL proteins are partially homologous to regulator of V-ATPase in vacuolar membrane protein 1 (RAV1), a component of the yeast regulator of H^+-ATPase of vacuolar and endosomal membranes (RAVE) complex which is involved in the reassembly of dissociated V_1 and V_0 sectors [414]. In addition to a potential role in the control of V-ATPase trafficking, DMXL1 and DMXL2 may play analogous roles to RAV1 in the assembly of V-ATPase subunits through their WD40 protein-protein interaction domains. Indeed, DMXL2 has been shown to promote

associations between the V_0 and V_1 sectors of the V-ATPase to form an active V_0/V_1 holoenzyme following Notch signalling [405].

6.1.3 The relationship between DMXL1, endosomal acidification and virus infection

Many viruses exploit the endocytic pathway to enter cells. One strategy of viral entry requires V-ATPase-mediated acidification of endosomes to allow fusion of enveloped viruses, such as influenza, vesicular stomatitis virus and coronaviruses, with endosomal membranes following endocytosis. A recent genome-wide CRISPR screen found that WDR7 was necessary for influenza virus infection, and that knockout of WDR7 led to defects in V-ATPase assembly [415]. HCMV uses this same strategy to enter endothelial and epithelial cells, but not fibroblasts **(1.1.8.1)**. In contrast, human immunodeficiency virus (HIV) uses a V-ATPase-dependent but acidification-independent strategy: HIV protein Nef interacts with the H-subunit of the V-ATPase which promotes CD4 (the HIV entry receptor) internalisation at the PM [416].

HCMV is already known to target the endosomal acidification complex by encoding a microRNA (miR-US25-1) that targets the enzymatic component ATP6V0C [221]. Intriguingly, knockdown of ATP6V0C, and inhibition of the V-ATPase, inhibits replication of HCMV [222], a phenomenon that cannot be attributed to the role of endosomal acidification in viral entry as HCMV entry into fibroblasts occurs at the PM in a pH-independent manner [79]. Instead, the defect in viral replication upon V-ATPase inhibition is thought to be due to the role of the V-ATPase in HCMV viral assembly compartment (VAC) formation [221,222]. ATP6V0C knockdown results in the mislocalisation of secretory and endocytic markers that are normally associated with the VAC during infection, without significantly impacting viral DNA replication or gene expression, suggesting that the V-ATPase is required for later stages of the replication cycle [222]. In contrast, knockdown of DMXL1 inhibits early stages of HIV-1 replication [417,418], although this effect has not been linked to the function of the V-ATPase.

But why would HCMV inhibit its own replication through targeting of the V-ATPase complex? It has been hypothesised that blocking endosomal acidification inhibits other antiviral cellular processes that are important *in vivo*, such as the latter stages of autophagy, the processing of antigens for MHC class II presentation and pattern recognition receptor signalling. Therefore, HCMV may downregulate DMXL1 and ATP6V0C in order to inhibit vacuolar acidification and evade cell-intrinsic, innate and/or adaptive immune responses, at the expense of inhibiting VAC formation (or another stage of virus replication) [222]. HCMV has been linked to the disruption of many cellular processes that are also likely to be affected by the deregulation of V-ATPase activity (e.g. Notch signalling), indicating that inhibition of vesicle acidification may have a multifactorial effect on many antiviral cell processes *in vivo*. Alternatively, it could be hypothesised that HCMV limits viral replication through targeting the V-ATPase in order to prevent cellular damage and host death or to limit viral replication during latency.

6.1.4 DMXL1 is downregulated by a viral protein in the US29-34A block

The HCMV gene block deletion screen, which has been described previously in this thesis **(1.4.6** and **5.3.1)**, identified the US29-34A gene block as necessary for DMXL1 downregulation **(Figure 6.2A)** [62]. Cells infected with irradiated HCMV had a greater amount of DMXL1 in comparison to cells infected with wild type (WT) virus **(Figure 6.2A)**. This indicates that *de novo* virus gene expression is required for DMXL1 downregulation or to prevent induction of DMXL1 levels upon infection. This experiment enabled identification of the viral gene blocks responsible for downregulation of multiple human proteins **(Figure 6.2B)**. Of those, US1-11, US18-22 and the U_L/*b'* region missing from HCMV strain AD169 all contain well-characterised viral proteins known for their ability to downregulate antiviral host proteins [62,145,188,419]. In contrast, the US29-34A gene block contains seven poorly characterised proteins - US29, US30, US31, US32, US33A, US34 and US34A **(Table 6.1)**.

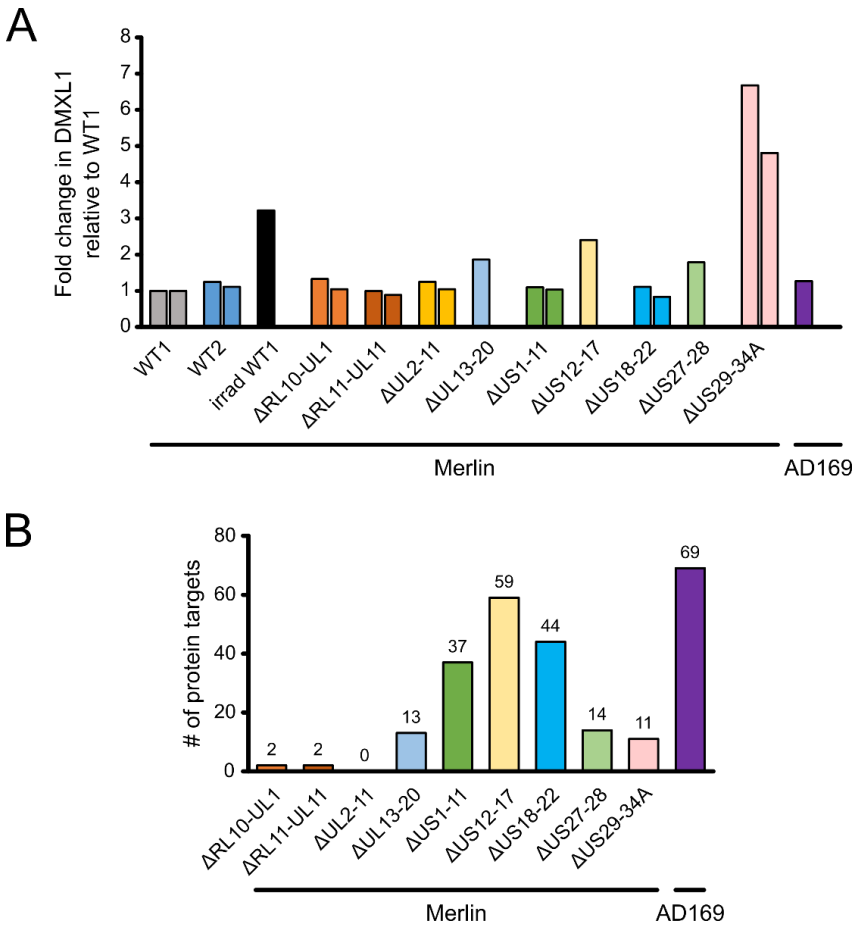

Figure 6.2: The US29-34A gene block is necessary for DMXL1 downregulation.

Both figures were made for this thesis using data published in Nightingale, Lin *et al.* (2018) [62]. HFFFs were infected with WT strain Merlin (WT1), WT1 that lacked UL16 and UL18 (WT2), one of nine block deletion viruses derived from WT1 or WT2, irradiated WT1 or strain AD169 [multiplicity of infection (MOI): 10, 72 h infection]. Whole cell lysates (WCLs) were analysed by quantitative mass spectrometry. **(A)** Relative abundance of DMXL1. irrad, irradiated. **(B)** Numbers of human proteins targeted by each block, with a fold change relative to the relevant WT control greater than 1.5 and a Z-score greater than 5.

Gene	***Growth*** [64]	***Kinetics*** [64]	***Tp class*** [86]	***Quantified in proteomics presented in this chapter?***	***Size (kDa)***	***Function***
US29	D	E/L	Uncharacterised	Yes	51	Enhances replication in epithelial cells [65]. Putative transmembrane protein [53].
US30	EG/D	E	Tp4	Yes	39	Inhibits replication in fibroblasts [65]. Putative transmembrane protein [53].
US31	D	N/A	Uncharacterised	No	19	May activate NF-κB2 and stimulate M1 macrophage differentiation [420].
US32	D	L	Uncharacterised	No	22	Might be expressed during latency [421]. Localises to PML nuclear bodies [422].
US33A	N/A	E*	Uncharacterised	No	7	Localises to mitochondria [63].
US34	D	E	Uncharacterised	Yes	18	Might be expressed during latency [421]. Putative secreted protein [53].
US34A	D	N/A	Uncharacterised	No	8	Putative transmembrane protein [53].

Table 6.1: Known characteristics of proteins encoded by the US29-34A block.

Information on growth and kinetic characteristics is adapted from Van Damme *et al*. [64]. Assignment of temporal protein profile (Tp) classes is explained in Weekes *et al.* 2014 [86]. D, dispensable; E, early; EG, enhances growth; L, late; N/A, no information available. *Designation of early gene expression for US33A is inferred from ribosomal footprinting data from Stern-Ginossar *et al*. [63] and our own qPCR data (Figure 6.8).

6.2 Aims

1. **Identify the HCMV gene (or genes) necessary for DMXL1 downregulation** by performing a proteomic analysis of cells infected with a panel of viruses each lacking one of the genes in the US29-34A region.
2. Determine whether the gene(s) necessary for DMXL1 downregulation are also **sufficient** for this effect, by performing a proteomic analysis of human fetal foreskin fibroblasts immortalised with telomerase (HFFF-TERTs) constitutively expressing each of the genes in the US29-34A block.
3. Use the HCMV interactome to **identify potential E3 ligases** utilised by the gene(s) responsible for DMXL1 degradation.
4. **Validate the role of these E3 ligases** in DMXL1 degradation through small interfering RNA (siRNA) knockdown and observation of the effect on DMXL1 abundance in infection.
5. Use these proteomic analyses to **make inferences about the function of each of the genes in the US29-34A gene block**, which are currently poorly characterised, by observing their effects on the cellular and viral proteomes.
6. **Identify the HCMV gene(s) responsible for the downregulation of other previously identified targets of the US29-34A block**, such as a number of members of the plexin family of transmembrane receptors.

This chapter is separated into two parts (**6.3** and **6.4**). The first concentrates on the mechanism of DMXL1 downregulation, and the second describes additional information, unrelated to DMXL1, that can be garnered from the proteomic analyses presented in the first section. The discussion is structured in the same way.

6.3 The mechanism of DMXL1 downregulation

6.3.1 pUS33A is necessary for DMXL1 downregulation

To identify which proteins encoded within the US29-34A block are necessary for downregulation of DMXL1, a single-gene-deletion virus screen was performed. HFFF-TERTs were infected with a control virus based on strain Merlin (RCMV2582) or one of seven single-gene-deletion viruses covering the US29-34A block, and WCLs prepared after 60 h of infection. The experiment was repeated so that each condition was analysed in biological duplicate, with both sets of samples analysed together in the same 16-plex mass spectrometry (MS) experiment **(Figure 6.3A)**. The data from this experiment were analysed and quantified using MassPike **(2.18.2)** together with the rest of the proteomics data presented in this chapter to enable comparative analyses. 7687 human and 158 HCMV proteins were quantified. For each protein in each deletion virus-infected sample, the signal-to-noise values (measures of protein abundance) from the two biological replicates were summed and divided by the summed signal-to-noise for the control sample to give a fold change (FC) [e.g. (ΔUS29(1)+ΔUS29(2))/(Control(1)+Control(2))] **(Figure 6.3B)**. A Z-score (or standard score) for each protein in each sample was calculated from the summed signal-to-noise values **(Figure 6.3B)**. The Z-score is the number of standard deviations by which an observed value (e.g. protein abundance in ΔUS29-infected cells) is above or below the mean of protein abundance across all other samples in the experiment **(2.22.3.2)**. For well-quantified proteins, the Z-score therefore represents a measure of how unique rescue of a protein is to a sample infected with a particular deletion virus. Proteins that are poorly quantified will exhibit highly variable signal-to-noise values across the samples and will therefore have a low Z-score. FCs and Z-scores were plotted for proteins with a FC>1 and Z-score>0, to identify proteins that increase in abundance upon deletion of a viral gene. Hits were categorised into one of three groups: those with a FC relative to the control of greater than 1.5, those with a Z-score greater than 3, or those with both FC>1.5 and Z>3. FCs and Z-scores for human proteins with FC>1.5 and Z>3 relating to deletion of any viral gene are listed in **Appendix V**. Proteins with FC>1.5 and Z>3 were then subjected to Database for Annotation, Visualization and Integrated Discovery (DAVID) functional enrichment analysis of Gene Ontology (GO) biological process terms and UniProt keywords against a background of all human proteins quantified (**Figure 6.3B** green boxes) [285,286]. DMXL1 was significantly rescued in cells infected with ΔUS33A HCMV, with a FC of 3.7 and Z-score of 25 **(Figure 6.3B, Appendix V)**. Interestingly, WDR7, the WD-repeat protein that interacts with DMXL1/2 to form rabconnectin-3, was also slightly rescued in cells infected with ΔUS33A **(Figure 6.3B)**.

As well as identifying the HCMV protein that is necessary for the downregulation of DMXL1, this screen also provides an indication of the function of other proteins encoded by the US29-34A block. Although an in depth analysis of the proteomic changes observed upon deletion of each of the genes is beyond the scope of this project, some of the most interesting findings are noted in 6.4.

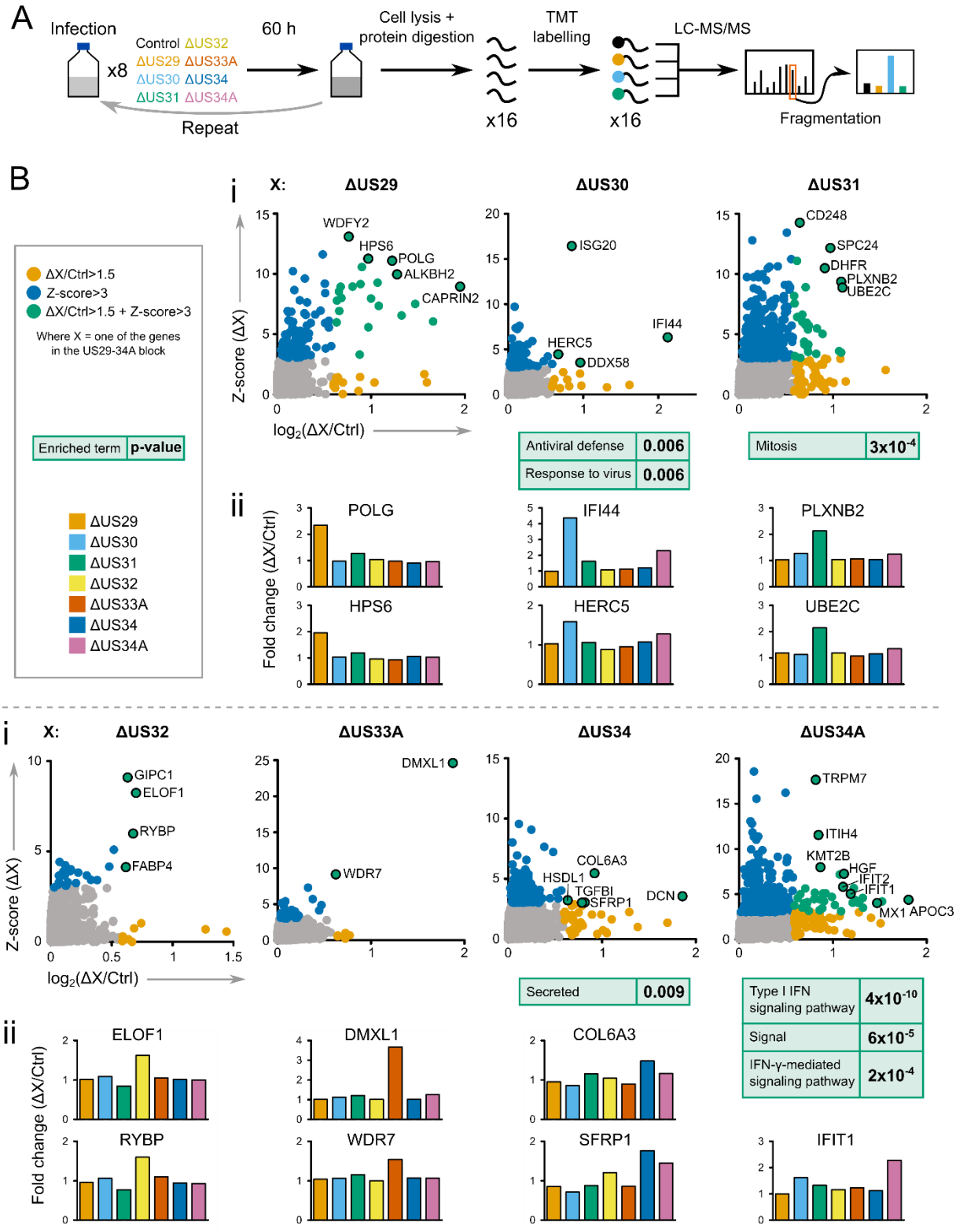
A
Infection
x8
Control ΔUS32
ΔUS29 ΔUS33A
ΔUS30 ΔUS34
ΔUS31 ΔUS34A
Repeat
60 h
Cell lysis + protein digestion
x16
TMT labelling
x16
LC-MS/MS
Fragmentation
B
ΔX/Ctrl>1.5
Z-score>3
ΔX/Ctrl>1.5 + Z-score>3
Where X = one of the genes in the US29-34A block
Enriched term
p-value
ΔUS29
ΔUS30
ΔUS31
ΔUS32
ΔUS33A
ΔUS34
ΔUS34A
i
X:
ΔUS29
ΔUS30
ΔUS31
Z-score (ΔX)
log2(ΔX/Ctrl)
WDFY2
HPS6
POLG
ALKBH2
CAPRIN2
ISG20
IFI44
HERC5
DDX58
CD248
SPC24
DHFR
PLXNB2
UBE2C
Antiviral defense
0.006
Response to virus
0.006
Mitosis
3x10-4
ii
Fold change (ΔX/Ctrl)
POLG
IFI44
PLXNB2
HPS6
HERC5
UBE2C
i
X:
ΔUS32
ΔUS33A
ΔUS34
ΔUS34A
GIPC1
ELOF1
RYBP
FABP4
DMXL1
WDR7
COL6A3
HSDL1
TGFBI
SFRP1
DCN
TRPM7
ITIH4
KMT2B
HGF
IFIT2
IFIT1
MX1
APOC3
Secreted
0.009
Type I IFN signaling pathway
4x10-10
Signal
6x10-5
IFN-γ-mediated signaling pathway
2x10-4
ii
ELOF1
DMXL1
COL6A3
RYBP
WDR7
SFRP1
IFIT1

(Previous page)

Figure 6.3: US33A is necessary for DMXL1 downregulation.

(A) HFFF-TERTs were treated with dexamethasone in serum-free media. 24 h later, cells were infected with a control (ctrl) virus (RCMV2582) or one of seven single-gene-deletion viruses (ΔUS29, ΔUS30, ΔUS31, ΔUS32, ΔUS33A, ΔUS34 or ΔUS34A) (MOI: 7.5, 60 h infection). RCMV2582 is based on strain Merlin, is the parental recombinant virus of all single-gene-deletion viruses used in the screen, and encodes UL36 tagged with green fluorescent protein (GFP) via a self-cleaving P2A peptide. The experiment was repeated so that each sample was analysed in biological duplicate, with both sets of samples analysed together in the same 16-plex MS experiment. All infections within a replicate were performed at the same time, except for ΔUS31, the second replicate of which had to be substituted for a third independent replicate due to significant cell death. Flow cytometry analysis of infected cells showed that the percentage infection was >94%. **(B i)** For each protein in each sample, the signal-to-noise values from the two biological replicates were summed and divided by the summed signal-to-noise for the control sample to give a FC [e.g. (ΔUS29(1)+ΔUS29(2))/(Control(1)+Control(2))]. A Z-score for each sample for each protein was calculated from the summed signal-to-noise values as described in 6.3. Z-scores and FCs for human proteins with a Z>0 and FC>1 are presented in a scatter plot. Proteins with Z>3 and FC>1.5 were subjected to DAVID enrichment of GO biological process and UniProt keyword terms against a background of all human proteins quantified using the default settings for functional annotation clustering. DAVID groups enriched terms with similar meanings into clusters. A representative term from each significantly enriched cluster is presented, alongside the Benjamini-Hochberg-adjusted p-value for that term. A list of human proteins targeted by each viral protein in the screen (FC>1.5, Z>3) can be found in Appendix V. **(B ii)** FCs (ΔX/Ctrl) for each deletion virus. Examples of proteins that were significantly rescued by deletion of a particular viral gene are shown.

6.3.2 pUS33A-V5 is insufficient for DMXL1 downregulation

To assess whether pUS33A is sufficient for DMXL1 downregulation, and to analyse individual effects of the US29-34A genes on the host cell proteome, WCLs of eight HFFF-TERT cell lines each expressing one of the genes in the US29-34A gene block (tagged with V5) or an empty control vector were analysed by MS. The expression of the viral genes in these cell lines was previously confirmed by MS or immunoblotting for the V5 tag (by Dr. Luís Nobre) [269]. 7862 human proteins were quantified, with 54 proteins being downregulated more than 1.5-fold with Z<-3 by any of the viral genes **(Figure 6.4, Appendix V)**. Note that Z-scores of downregulated proteins will be <0 as the observed protein abundance of downregulated proteins will be less than the mean protein abundance of the other samples. No viral protein was sufficient to downregulate DMXL1 **(Figure 6.5)**, and there were no proteins that were both rescued and downregulated with a FC>1.5 and Z>3 in the single-gene-deletion virus screen **(6.3.1)** and gene expression screens, respectively.

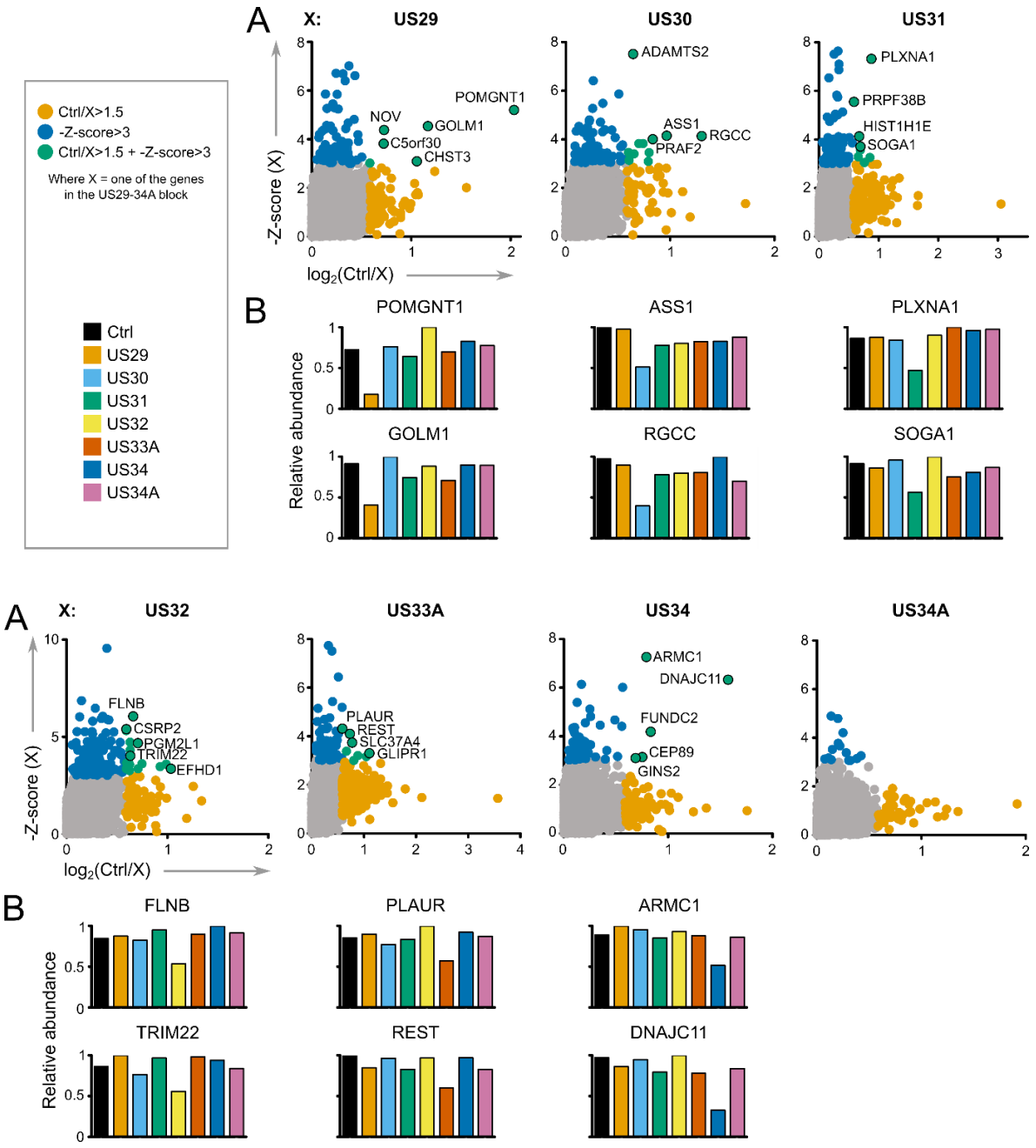

Figure 6.4: Effect of stable expression of proteins encoded by the US29-34A block on the host cell proteome. **(A)** For every protein, a FC was calculated by dividing protein abundance in HFFF-TERTs expressing an empty control (ctrl) vector by protein abundance in HFFF-TERTs expressing a gene in the US29-34A block (X). Z-scores were calculated as described in 6.3. The observed protein abundance of downregulated proteins is less than the mean protein abundance across the other samples. Therefore, the lower the Z-score, the more unique the downregulation effect to expression of that viral protein. –Z-score and $\log_2$(FC) is plotted for human proteins with Z<0 and FC>1. The cell lines used for this experiment were generated by Dr. Luís Nobre for the HCMV interactome study, and therefore each viral protein is tagged with a C-terminal V5 tag. Viral protein expression was confirmed by proteomics or immunoblot [269]. **(B)** Protein abundance relative to the highest protein abundance in any sample. Examples of proteins that were significantly downregulated by expression of each viral gene are shown.

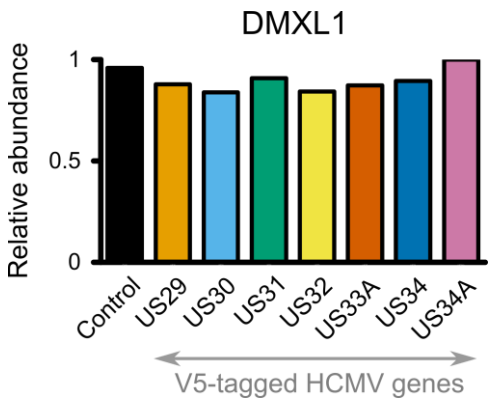

Figure 6.5: Expression of pUS33A-V5 is insufficient for DMXL1 downregulation.
DMXL1 protein abundance in HFFF-TERTs expressing V5-tagged viral genes in the US29-34A block or a control vector, relative to the maximum protein abundance observed across the samples.

6.3.3 Untagged pUS33A is sufficient for DMXL1 downregulation

Due to the lack of correspondence between the results of the gene expression screen **(6.3.2)** and the single-gene-deletion virus screen **(6.3.1)**, it was hypothesised that the V5 tag could be hindering the function of some or all of the genes in the block. This is particularly likely for small proteins, such as pUS33A, where addition of a tag could be causing steric hindrance. An untagged version of US33A was cloned, alongside four V5-tagged versions of the protein with the tag placed at different ends of the coding sequence and with different linking sequences. Vectors expressing the different constructs were transduced into HFFF-TERTs to make stably expressing cell lines, and US33A expression was confirmed by quantitative reverse transcription polymerase chain reaction (RT-qPCR) **(Figure 6.6A)**. WCLs were then prepared for proteomic analysis. Protein abundance in the cell line expressing untagged US33A relative to the control showed little correspondence to that in the US33A-V5-expressing cells in the gene expression screen **(6.3.2) (Figure 6.6B)**, indicating that the tag was indeed prohibiting the structure or function of the protein. DMXL1 was significantly and specifically downregulated in the cell line expressing untagged US33A, but not in any of the cell lines expressing the N-terminally and C-terminally tagged versions **(Figure 6.6C and D)**. Two other proteins, Golgi glycoprotein 1 (GLG1) and kinesin family member 1A (KIF1A), had a FC(Ctrl/US33A)>1.5 and Z<-3 **(Figure 6.6C and D)**, but were not significantly rescued in cells infected with ΔUS33A **(6.3.1)** or ΔUS29-34A [62]. DMXL1 was the only human protein downregulated by expression of any gene in the US29-34A block (FC>1.5, Z<-3) and rescued by the corresponding deletion virus (FC>1.5, Z>3) **(Figure 6.6E)**, although more correspondence might be seen when expressing untagged versions of the other viral proteins.

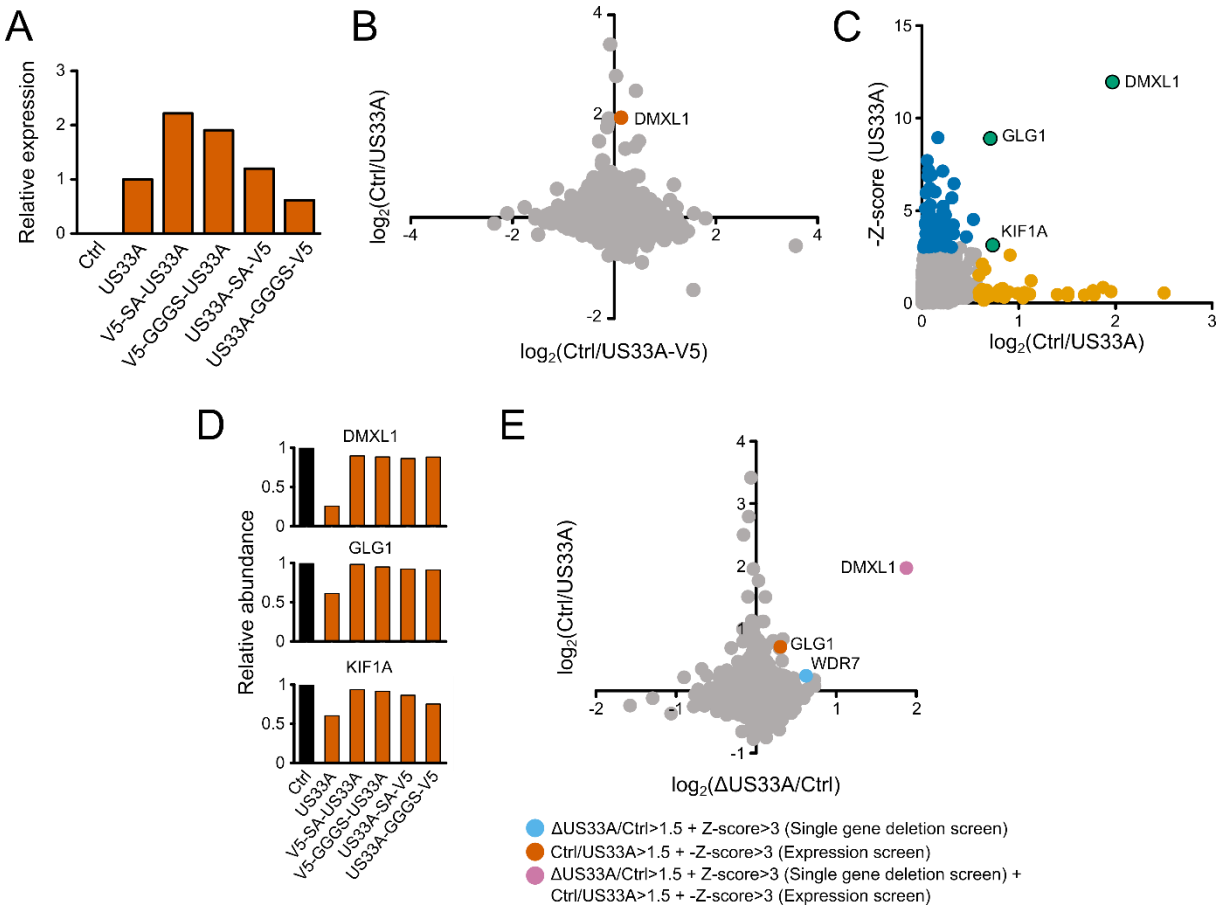

Figure 6.6: Untagged pUS33A is sufficient for DMXL1 downregulation.

Six cell lines constitutively expressing untagged US33A, US33A with an N-terminal V5 tag separated by a serine-alanine linker (V5-SA-US33A), US33A with an N-terminal V5 tag separated by a glycine-glycine-glycine-serine linker (V5-GGGS-US33A), US33A with a C-terminal V5 tag separated by a SA linker (US33A-SA-V5), or US33A with a C-terminal V5 tag separated by a GGGS linker (US33A-GGGS-V5), were generated by transduction. **(A)** RT-qPCR analysis of US33A expression in each cell line. **(B)** Comparison of protein abundance in US33A- and US33A-V5-expressing cells relative to control. Data for US33A-V5 is from the gene expression screen described in 6.3.2. **(C)** –Z-score against FC. Z-scores were generated as described in 6.3 with the observed value being protein abundance in cell lines expressing US33A and the mean and standard deviation relating to protein abundance across the other samples in the experiment. **(D)** Relative abundance of DMXL1, GLG1 and KIF1A across the samples. **(E)** Comparison of protein abundance in US33A-expressing cells and ΔUS33A-infected cells relative to the relevant controls.

6.3.4 pUS33A counteracts the upregulation of DMXL1 induced by infection

To better understand the kinetics of pUS33A-mediated DMXL1 downregulation through infection, an infection time course was performed. HFFF-TERTs were mock-infected or infected with ΔUS33A or a

control virus (RCM2582), and WCLs harvested at 0, 24, 48 and 72 hours post-infection (hpi) for proteomic analysis **(Figure 6.7A)**. The infection time course and proteomics sample preparation was performed by Dr. Katie Nightingale and the data analysis by myself. 7851 human and 143 HCMV proteins were quantified. Changes in protein abundance seen upon infection with the control virus showed good correspondence with previously published time courses. For example, HLTF was strongly downregulated by the 24 h time point, as seen previously **(Figure 6.7B)** [62,86].

Only DMXL1 was significantly upregulated in cells infected with ΔUS33A in comparison to cells infected with the control virus at every time point **(Figure 6.7C)**. As observed previously [62,214], DMXL1 was downregulated by HCMV Merlin at 24 and 48 hpi. This analysis shows that the amount of DMXL1 in infected cells remains below that in mock-infected cells up until the 72 h time point, albeit with its abundance increasing slightly from 48 h **(Figure 6.7D)**. Of particular interest is the finding that the level of DMXL1 rises through infection in the absence of pUS33A. The amount of DMXL1 protein appears to be stimulated by infection, which can be one of the defining characteristics of an ARF **(1.2.1)**. pUS33A is able to counteract that stimulation, bringing DMXL1 levels below that prior to infection.

Also interesting is the observed downregulation of IFIT1, IFIT2, IFIT3, MX dynamin-like GTPase 1 (MX1) and tryptophanyl-tRNA synthetase 1 (WARS) when US33A is deleted, which is especially significant at early time points of infection **(Figure 6.7E)**. IFIT1, IFIT2, IFIT3 and MX1 are known to function as ARFs [245,423], with IFIT1 previously shown to have antiviral activity against HCMV [123] **(Table 1.2)**. A recent study presented evidence that WARS is also antiviral, functioning as an antiviral cytokine that induces the secretion of proinflammatory cytokines and type I IFNs [424]. The results presented here, in which the IFITs, MX1 and WARS all show a remarkably similar time course profile, suggesting that these proteins may share a similar mechanism of induction in response to HCMV infection. Although it appears that pUS33A is able to augment this induction, with deletion of US33A resulting in a lower abundance of these proteins, it might be that the level of these proteins is very sensitive to the abundance of factors (e.g. IFN) in different viral preparations. Indeed, the same effect was not observed in the single-gene-deletion virus screen. Whether this is a true effect of pUS33A should be investigated.

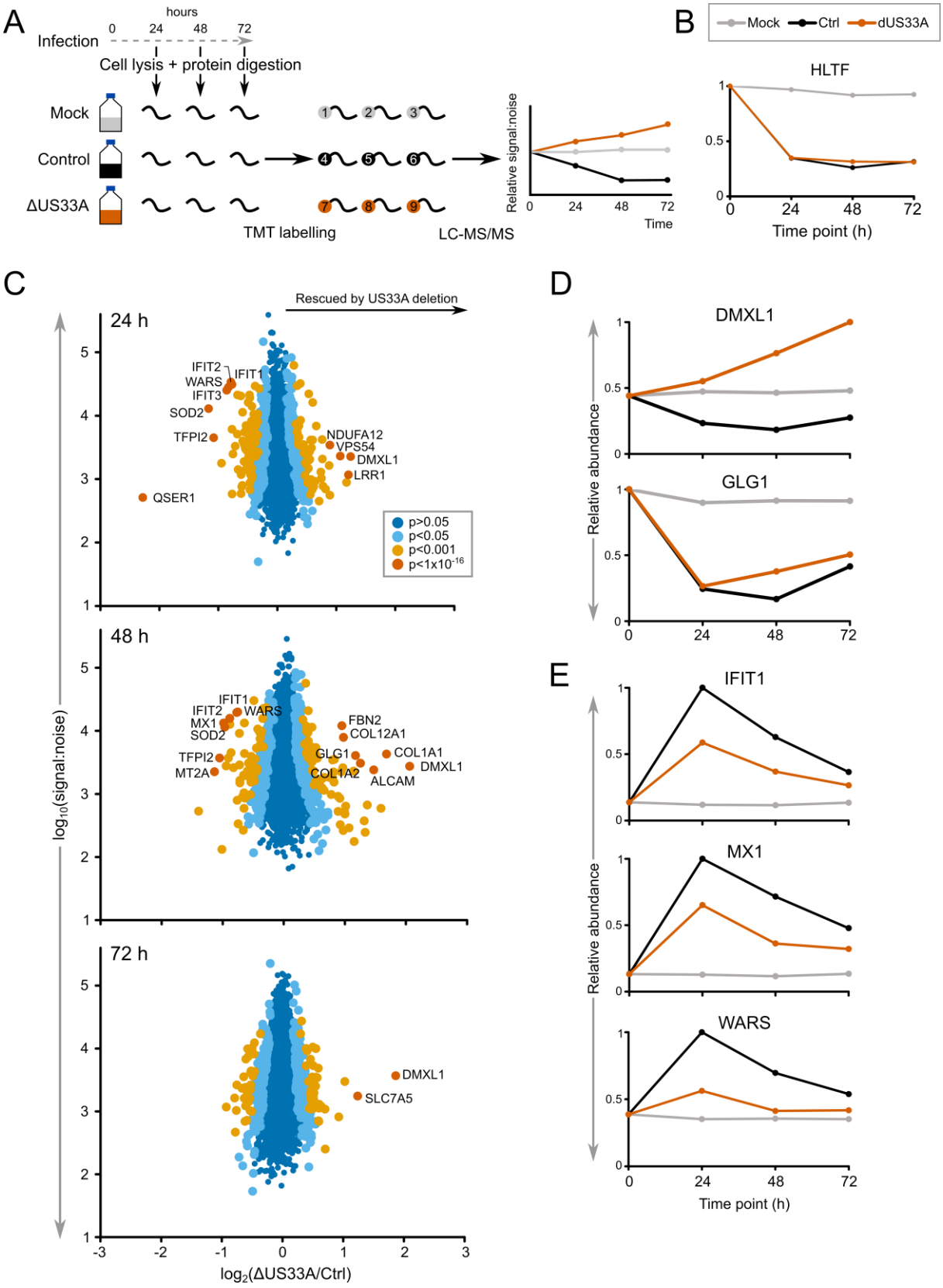
A
hours
0
24
48
72
Infection
Cell lysis + protein digestion
Mock
Control
ΔUS33A
TMT labelling
LC-MS/MS
Relative signal:noise
Time
B
Mock
Ctrl
dUS33A
HLTF
Time point (h)
C
Rescued by US33A deletion
24 h
48 h
72 h
IFIT2
WARS
IFIT1
IFIT3
SOD2
TFPI2
QSER1
NDUFA12
VPS54
DMXL1
LRR1
MX1
MT2A
FBN2
COL12A1
GLG1
COL1A1
COL1A2
ALCAM
SLC7A5
p>0.05
p<0.05
p<0.001
p<1x10-16
log10(signal:noise)
log2(ΔUS33A/Ctrl)
D
DMXL1
GLG1
Relative abundance
E
IFIT1
MX1
WARS
Relative abundance
Time point (h)

(Previous page)

Figure 6.7: pUS33A counteracts the upregulation of DMXL1 during infection.

(A) Schematic of the experiment. HFFF-TERTs were treated with dexamethasone in serum-free media for 24 h before infection. Cells were mock-infected or infected with ΔUS33A HCMV or the relevant control virus (RCMV2582) (MOI: 5) in triplicate. The cells were then harvested at 24, 48 and 72 hpi, before TMT labelling the samples from each condition and analysing by MS. The infection and sample preparation was performed by Dr. Katie Nightingale and the MS data analysis by myself. **(B)** Relative abundance of HLTF over the time course. **(C)** Dot plots of the 6569 human proteins that were quantified in the experiment with two or more peptides. P-values were estimated using the significance B method and corrected for multiple hypothesis testing [301]. **(D)** Relative abundance of two proteins that are rescued by US33A deletion, DMXL1 and GLG1, over the time course. **(E)** Relative abundance of three proteins that are downregulated as a result of US33A deletion, IFIT1, MX1 and WARS, over the time course.

6.3.5 pUS33A: an uncharacterised viral protein

The presence of HCMV protein pUS33A was first predicted by transcript analysis by Gatherer *et al.* in 2011 [58]. pUS33A has been shown to exhibit mitochondrial localisation in Henrietta Lacks (HeLa) cells transiently expressing US33A-GFP and to interact with members of the mitochondrial inner membrane transport machinery [63]. pUS33A is a short protein of 57 amino acids, however despite exhibiting a sequence conducive with the production of peptides that could be detected by MS under conditions of LysC and trypsin digestion **(Figure 6.8A)**, neither our nor other groups have been able to detect pUS33A by MS. An analysis of ribosome footprint density by Stern-Ginossar *et al.* predicts that pUS33A will exhibit a Tp1-like temporal protein profile [63], in agreement with the kinetics of DMXL1 downregulation **(Figure 6.8B)**. RT-qPCR analysis of RNA purified from HFFF-TERTs infected with WT HCMV strain Merlin (RCMV1111, the parental recombinant virus of all other viruses used in this study) for 24 and 72 h confirmed expression of pUS33A **(Figure 6.8C)**. Data from our group's HCMV interactome indicate that pUS33A interacts with four proteins that typically show nuclear localisation – scaffold attachment factor B like transcription modulator (SLTM), bromodomain adjacent to zinc finger domain 1B (BAZ1B), suppressor of zeste 12 polycomb repressive complex 2 subunit (SUZ12) and interleukin enhancer binding factor 3 (ILF3) [63,269] **(Figure 6.8D, Table 6.2)**. As in the Stern-Ginossar study, pUS33A was also found to interact significantly with ubiquitin-associated domain-containing 1 (UBAC1) and RING finger protein 123 (RNF123) **(Figure 6.8D, Table 6.2)**, which are the non-catalytic and catalytic subunits of the E3 ligase Kip1 ubiquitination-promoting complex (KPC), respectively [425]. Both subunits exhibit a diffuse cytoplasmic localisation, and have been implicated in the degradation of $p27^{Kip1}$ [425], NF-κB [426] and BAX [427]. RNF123 also has additional roles independent of its function as an E3 ligase, acting as a negative regulator of RIG-I and interferon-induced with helicase C domain 1 (IFIH1), inhibiting IFN-β production induced by RNA viruses and enhancing RNA virus replication [428]. None of the inner mitochondrial membrane transport proteins

that were identified as pUS33A interactors by Stern-Ginossar *et al.* were shown to interact with pUS33A. Furthermore, DMXL1 was not identified as a pUS33A interactor, which might be expected as tagged pUS33A does not downregulate DMXL1. Finally, structural homology and structure prediction analyses with HHPred and I-TASSER did not predict any significant homology to any proteins in the Protein Data Bank.

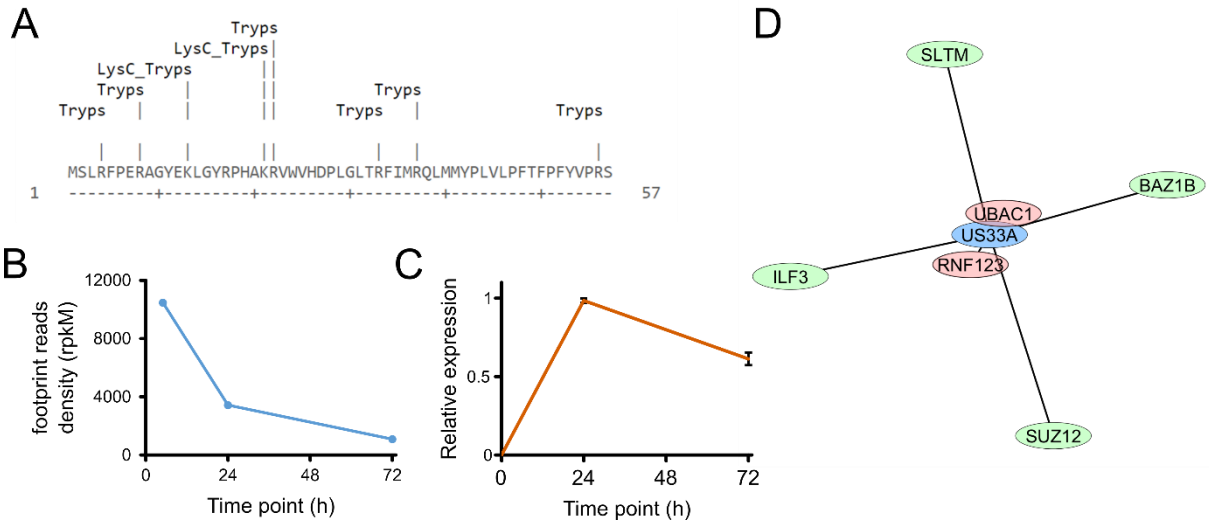

Figure 6.8: pUS33A is expressed early in infection and interacts with the E3 ligase complex KPC.
(A) Sites of LysC and trypsin digestion were determined with ExPASy PeptideCutter. Peptides of 8-13 amino acids can be detected by MS. **(B)** Graphical representation of ribosome footprint reads density data for US33A from Stern-Ginossar *et al.* 2012 [63]. **(C)** HFFFs were infected with WT HCMV strain Merlin (MOI: 10) and harvested for RT-qPCR analysis at three time points of infection in biological triplicate [62]. Relative expression of US33A in each of the biological replicates were combined to give an average and SEM (displayed in the error bars). The infections were performed by Dr. Michael Weekes, and the RNA extraction, reverse transcription and qPCR by myself. **(D)** pUS33A interactome generated by Dr. Luís Nobre [269]. The length of the lines connecting the viral bait protein pUS33A to each of the human interactors are inversely proportional to the NWD score for the interaction, which reflects how frequently the protein was detected and whether it was detected reproducibly [269] (Figure 5.13) (Table 6.2). Two methods of filtering were used. Hits determined through CompPass filtering [382] are shown in green. Hits determined through both CompPass and CompPass Plus methods of filtering, making them high-confidence interactors, are shown in pink.

Prey protein gene symbol	***NWD score***
UBAC1	75.72
RNF123	51.07
BAZ1B	2.65
SLTM	2.58
ILF3	1.62
SUZ12	1.25

Table 6.2: pUS33A interactors.

6.3.6 Is the E3 ligase complex KPC responsible for degradation of DMXL1?

As pUS33A interacts with RNF123 and UBAC1, the two subunits of E3 ligase complex KPC, it was hypothesised that pUS33A recruits KPC to DMXL1 to promote its ubiquitination and proteasomal degradation. HFFF-TERTs were transfected with siRNAs against RNF123 and/or UBAC1 before infection with WT HCMV strain Merlin. At 48 hpi, WCLs were prepared for proteomic and RT-qPCR analysis. The experiment was repeated, and all samples analysed in the same 16-plex MS run.

RT-qPCR showed that an average knockdown of 68% was achieved for RNF123 and 90% for UBAC1 **(Figure 6.9A)**. In the first biological replicate, treatment of cells with siRNA against RNF123 resulted in a 1.9-fold increase in UBAC1 RNA abundance, but this was not observed in the second replicate. RNF123 transcript levels were stimulated by UBAC1 siRNA treatment in both replicates. At the protein level, RNF123 levels were reduced by 67% and UBAC1 levels by 72% **(Figure 6.9B)**. Interestingly, siRNA knockdown of UBAC1 also resulted in a 56% reduction in RNF123. This result has been observed previously with shRNA knockdown of UBAC1 in mouse embryonic fibroblasts, and was attributed to the stabilisation of RNF123 by UBAC1 [429].

RNF123 was upregulated in response to HCMV infection in all siRNA conditions **(Figure 6.9B)**. At the RNA level, RNF123 was substantially upregulated at the 72 h time point **(Figure 6.9C)**, meaning that transcriptional activation may be responsible for this induction of RNF123 protein levels. The upregulation of RNF123 upon infection was also observed in the ΔUS33A virus time course experiment **(Figure 6.9D)**. Interestingly, deletion of US33A appeared to suppress this stimulation, illustrating that US33A may be required for the upregulation of RNF123 protein levels in infection. A similar but less significant trend was seen for UBAC1 **(Figure 6.9D)**.

Despite being upregulated, the canonical function of RNF123 was not observed in HCMV-infected cells: levels of cyclin-dependent kinase inhibitor 1B (CDKN1B or $p27^{Kip1}$), the first identified target of KPC [425,429], were rescued in cells with reduced RNF123 in the absence of infection, but not in HCMV-infected cells **(Figure 6.9B)**. The level of CDKN1B remained low during infection, indicating that either another protein is able to substitute for RNF123 specifically in the context of infection, or perhaps that HCMV-mediated modulation of the cell cycle has a side effect of suppressing CDKN1B levels. Previous results showed that levels of CDKN1B were rescued by addition of MG132 in mock or HCMV-infected cells, indicative of degradation occurring in infection [62]. CDKN1B levels did not change upon infection with any of the gene block deletion viruses, indicating that no viral gene covered by these block deletions is responsible for the suppression of CDKN1B during infection. It has previously been shown that RNF123 is sufficient for CDKN1B ubiquitination [425], which is confirmed by our results that show that knockdown of UBAC1 does not rescue CDKN1B levels **(Figure 6.9B)**. Neither of the other known targets of KPC - NF-κB [426] or BAX [427] - were rescued by either RNF123 or UBAC1 knockdown.

Unfortunately, DMXL1 was not significantly downregulated by HCMV infection in control siRNA-treated cells **(Figure 6.9B)**. DMXL1 downregulation at 48 h has been somewhat variable, varying from 86% downregulation in the first 48 h screen **(Figure 4.4)**, 61% in the ΔUS33A deletion virus time course **(Figure 6.7)**, to only 30% in the second 48 h screen **(Figure 4.4)**. It is likely that the level of downregulation observed is dependent on a range of factors such as percentage of cells infected, cell density and time point of infection. Although knockdown of either or both RNF123 and UBAC1 appears to attenuate the downregulation of DMXL1 by HCMV **(Figure 6.9E)**, this experiment requires further optimisation to ensure that the effect of RNF123 and UBAC1 are studied under conditions of maximal and active DMXL1 downregulation.

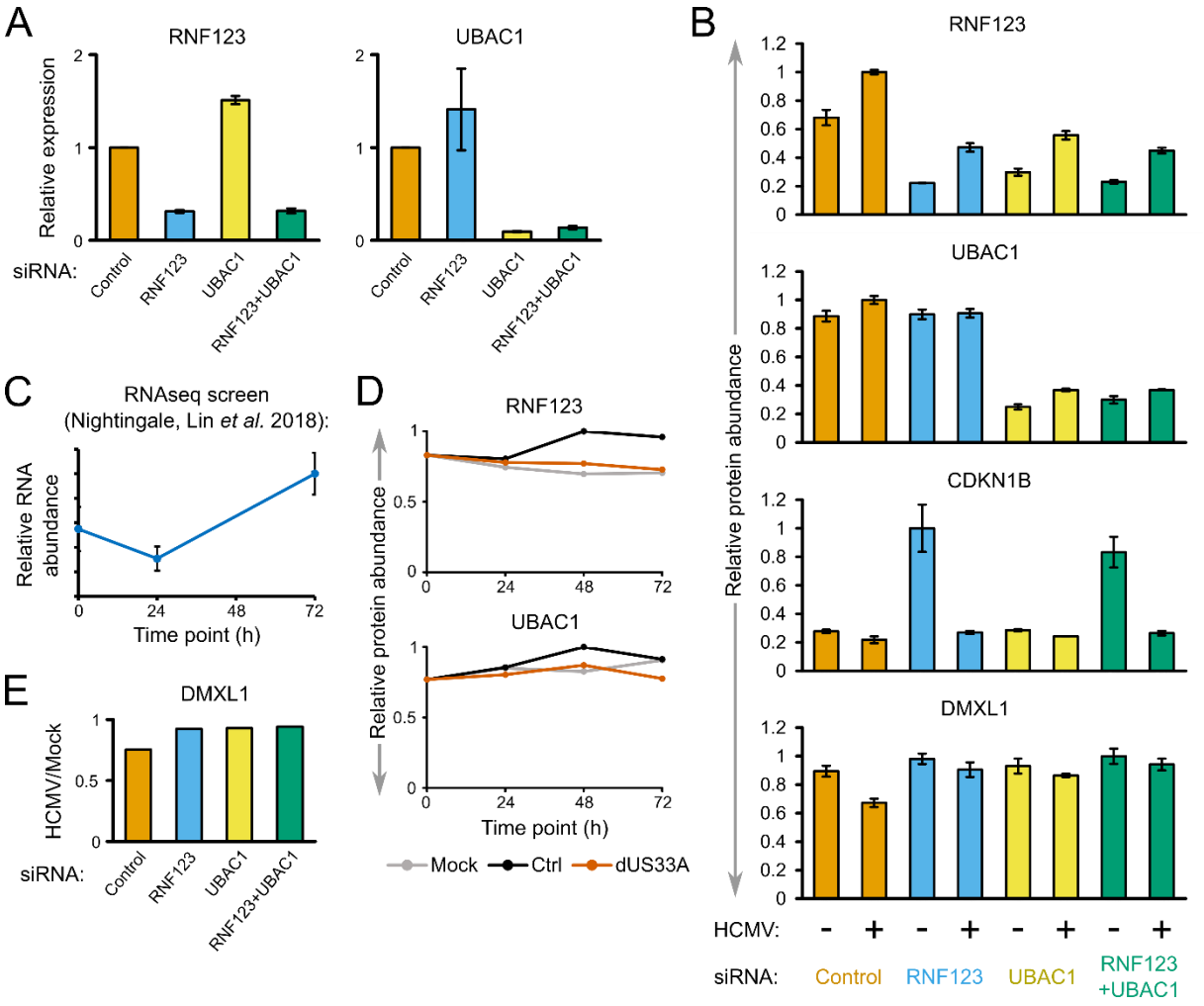

Figure 6.9: Is the E3 ligase complex KPC responsible for degradation of DMXL1?

(A-B) HFFF-TERTs were transfected with siRNAs targeting RNF123 and/or UBAC1. The cells were treated 48 h later with dexamethasone in serum-free media and then left for 24 h before infecting with WT HCMV strain Merlin (RCMV1111) (MOI: 5). After 48 h of infection, cells were harvested for proteomic analysis of WCLs and RT-qPCR analysis. The experiment was performed twice. As the first replicate resulted in only a 68% knockdown of RNF123, for the second replicate, a second round of RNA transfection was performed just prior to the 48 h infection. This had no impact on the level of knockdown. **(A)** Relative expression of RNF123 (left) and UBAC1 (right) as quantified by RT-qPCR. An average of the relative expression of US33A in the biological duplicates was calculated and SEM displayed in the error bars. **(B)** Quantitation of RNF123, UBAC1, CDKN1B and DMXL1 from the proteomic analysis of mock- or HCMV-infected HFFF-TERTs treated with control, RNF123, UBAC1 or RNF123 and UBAC1 siRNAs. Protein abundance from the biological duplicates was averaged and normalised to the maximum protein abundance observed across the samples. Error bars show SEM of the biological duplicates. **(C)** Relative abundance of RNF123 RNA through a time course of infection as reported in Nightingale, Lin *et al.* (2018) [62] (MOI: 10). **(D)** Relative abundance of RNF123 and UBAC1 protein over a time course of infection with control-, ΔUS33A- or mock-infected cells, from the experiment shown in Figure 6.7. **(E)** Effect of HCMV-infection on DMXL1 protein abundance in cells treated with control, RNF123, UBAC1 or RNF123 and UBAC1 siRNAs.

6.3.7 DMXL1 knockdown does not cause a profound effect on the cellular proteome

To gain insights into the potential role of DMXL1 in infection, a proteomic analysis of DMXL1 knockdown cells was performed. HFFF-TERTs were transfected with DMXL1 or control pooled siRNAs on three independent occasions, and the six samples analysed by a 'single-shot' MS run, without prior fractionation of peptides by high pH reversed-phase liquid chromatography **(1.4.1)**. DMXL1 is not typically quantified in unfractionated samples, and so the knockdown of DMXL1 could not be verified. However, an independent experiment using qPCR to validate DMXL1 knockdown showed DMXL1 transcript levels are reduced by 76% 48 h after transfection with DMXL1 siRNAs using the same protocol (results not shown). For every protein quantified, a FC was calculated for each biological replicate (siDMXL1/Ctrl) and then the FCs averaged. In comparison to the effects seen when cells were transduced with shRNA constructs **(Figure 3.25)**, there were generally very few changes in the cellular proteomes upon DMXL1 knockdown **(Figure 6.10A and B)**. Samples from cells treated with control and DMXL1 siRNA at the same time generally clustered together **(Figure 6.10A)**, indicating that variation introduced through cell culture conditions or cell lysis had a larger effect on the proteome than DMXL1 knockdown. FCs were compared to those observed when cells were infected with ΔUS33A HCMV vs WT HCMV **(Figure 6.10C)**. It was thought that this could enable identification of proteins that were both downregulated in DMXL1 knockdown cells and upregulated in ΔUS33A-infected cells (where DMXL1 is upregulated), or vice versa. No proteins with these criteria were identified **(Figure 6.10C)**. Given that the data from the single-shot experiment did not yield any interesting findings, it was decided that the samples would not be analysed further by fractionation and additional rounds of MS.

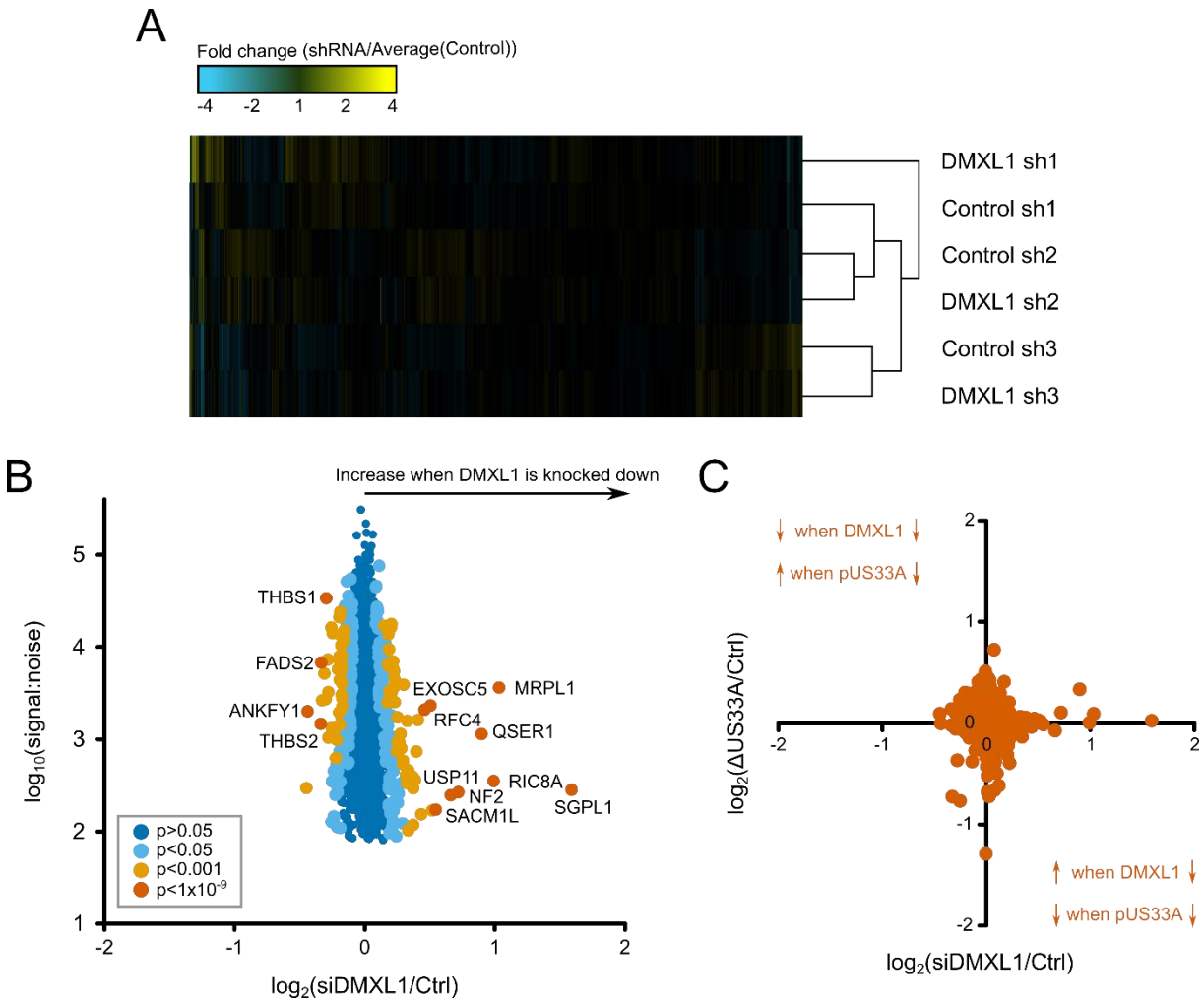

Figure 6.10: DMXL1 knockdown does not cause a profound effect on the cellular proteome.

HFFF-TERTs were transfected with pools of control or DMXL1 siRNAs and left for 48 h. Three independent experiments were performed, and then WCLs analysed by proteomics in a 6-plex MS single-shot experiment. **(A)** Hierarchical cluster analysis of protein abundance relative to the average protein abundance across the three control siRNA samples. Compared to shRNA knockdown (Figure 3.25), few changes were observed across the proteome. **(B)** A FC was calculated for each protein quantified for each biological replicate (siDMXL1/Ctrl) and then the FCs averaged. Scatter plot showing the proteins most significantly up or downregulated upon knockdown of DMXL1 is shown. P-values were calculated using the method of significance B with multiple hypothesis correction. All 3474 human proteins that were quantified are shown. **(C)** Comparison of FCs between DMXL1 siRNA-treated vs control cells, and ΔUS33A-infected cells vs WT HCMV-infected cells (from the single-gene-deletion virus screen, 60 h infection).

6.4 The function of proteins encoded by the US29-34A gene block

6.4.1 Gene block deletion screen reveals that the US29-34A block plays a role in the regulation of innate immunity and plexin signalling

As well as providing evidence for the role of US33A in the downregulation of DMXL1, the US29-34A single-gene-deletion virus screen **(6.3.1)** and the US29-34A gene expression screen **(6.3.2)** also allow inferences to be made about the function of other genes in the US29-34A block.

To identify cellular targets of proteins encoded by the US29-34A block, data from the original WCL gene block deletion screen [62] **(Figure 6.2)** were reanalysed and re-quantified together with the rest of the proteomics data presented in this chapter to enable comparative analyses. For every protein quantified in at least one of the two multiplexed proteomics experiments that made up the screen, a Z-score and fold change (FC) relative to the corresponding control virus (WT2) were calculated from the signal-to-noise values (as described in **6.3**). As before, hits were characterised using three criteria: a FC relative to WT2 of greater than 1.5 (59 proteins), a Z-score of greater than 3 (38 proteins), or both (18 proteins) **(Figure 6.11A, Appendix V)**. These groups of proteins were then subjected to DAVID functional enrichment analysis **(Figure 6.11B)**. The group of proteins that had a high FC, but for which rescue was not necessarily unique to the US29-34A block, was enriched in proteins involved in innate immunity (p: 0.01), such as OAS-like protein (OASL) and ISG15. This suggests that, similarly to a number of other gene blocks, the US29-34A block contains members that are involved in the regulation of innate immunity. As well as including DMXL1, the group of 18 proteins with a high FC and Z-score was enriched in proteins belonging to the semaphorin-plexin signalling pathway (p: 0.01), such as plexin (PLXN)A2, PLXNA1 and PLXNB2.

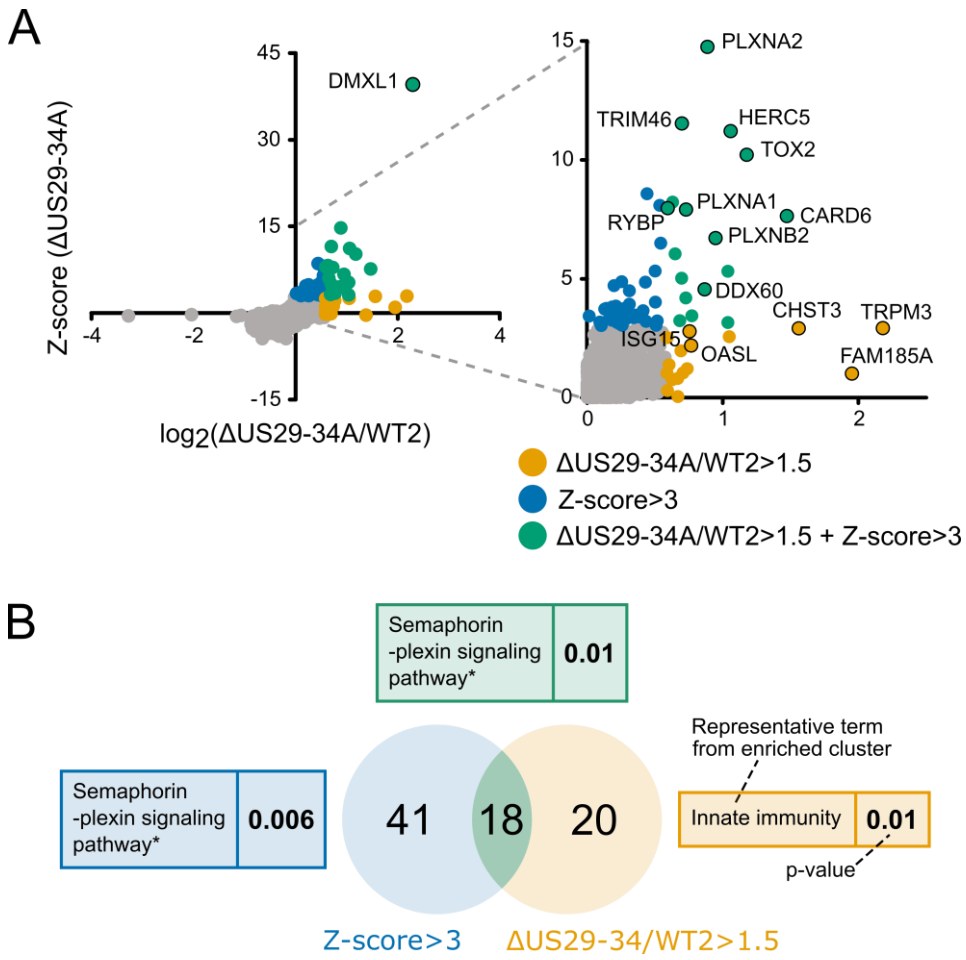

Figure 6.11: Proteins encoded by the US29-34A block are involved in the regulation of innate immunity and the semaphorin-plexin pathway.

These data were previously published in a different format in Nightingale, Lin *et al.* (2018) [62] based on experiments performed by Dr. Katie Nightingale. The raw data were reanalysed and these figures made specifically for this thesis. **(A)** Scatter plot showing Z-score against $\log_2$(FC) for every human protein quantified in at least one of the two experiments performed as explained in Figure 6.2. Where a protein was quantified in both experiments, the average Z-score and FC is presented. WT2 is a ΔUL16/UL18 virus, which was the background upon which the ΔUS29-34A virus generated. A full list of hits from this screen can be found in Appendix V. **(B)** Venn diagram showing the numbers of target proteins satisfying each criteria. DAVID enrichment of GO biological process terms and UniProt keywords was performed on a background of all human proteins quantified, using the default settings for functional annotation clustering [285,286]. DAVID groups enriched terms with similar meanings into clusters. A representative term from each significantly enriched cluster is presented, alongside the Benjamini-Hochberg-adjusted p-value for that term. *Full term: semaphorin-plexin signalling pathway involved in axon guidance (GO:1902287).

Next, data from an unpublished plasma membrane profiling (PMP) screen of cells infected with WT1, WT2 or one of nine block deletion viruses, performed by Dr. Ceri Fielding and Dr. Katie Nightingale, were analysed **(Figure 6.12)**. PMP involves the selective oxidation and aminooxy-biotinylation of sialylated PM proteins prior to cell lysis, followed by affinity enrichment using high capacity streptavidin [190]. Following protein lysis, peptides from each sample were labelled with a different TMT reagent, fractionated and analysed by quantitative tandem MS, as described previously for WCL proteomics **(2.15, 4.3)**. This screen enabled identification of proteins whose presence at the PM was specifically targeted by one or more genes in the US29-34A block. Hits were categorised as for the WCL screen and analysed by DAVID functional enrichment analysis **(Figure 6.12, Appendix V)**. Strikingly, five out of six proteins with a FC relative to WT2 greater than 1.5 and a Z-score greater than 3 were proteins of the plexin family (PLXNA1, B2, A2, B1 and D1).

Plexins are a family of transmembrane receptors that bind semaphorins, a large family of extracellular signalling proteins that play a role in the motility and morphology of an abundance of cell types, and consequently the development and maintenance of many organs and tissues [430]. Semaphorin-plexin signalling has also been implicated in regulation of various aspects of the immune system, including the migration of T cells and dendritic cells (DCs) and communication between cells of the adaptive immune system [431]. Known immune system-related functions of the plexins identified in the WCL and PMP gene block deletion screens are detailed in **Table 6.3**. Plexins, semaphorins and a family of semaphorin co-receptors, the neuropilins, have all been shown to be highly regulated by HCMV infection at the protein and RNA levels in different cell types [86,432]. Data from the ΔUS33A virus time course experiment presented in **6.3.4** can be used to validate results from previous proteomic time course analyses of HCMV infection. As observed in the Weekes *et al.* (2014) quantitative temporal viromics study [86], PLXNA1, B1, B2 and D1 were all downregulated in this experiment, while PLXNA2 levels remained relatively constant **(Figure 6.13)**. Six semaphorins were also quantified **(Figure 6.13)**. SEMA4D and 7A were both dramatically upregulated through infection, while SEMA3A was upregulated specifically at the 48 h time point. In contrast, SEMA3C and 5A were both significantly downregulated. Neuropilins NRP1 and NRP2 were also downregulated over the course of infection **(Figure 6.13)**. Despite evidence for the regulation of these proteins during HCMV infection, the mechanisms of regulation remain uncharacterised.

In the following sections, data from the single-gene-deletion virus screen **(6.3.1)** and the gene expression screen **(6.3.2)** are used to identify potential functions of the viral proteins encoded by the US29-34A block (excluding pUS33A, which was analysed in 6.3) and related to the effects of deleting the entire block on the WCLs and plasma membrane of infected cells.

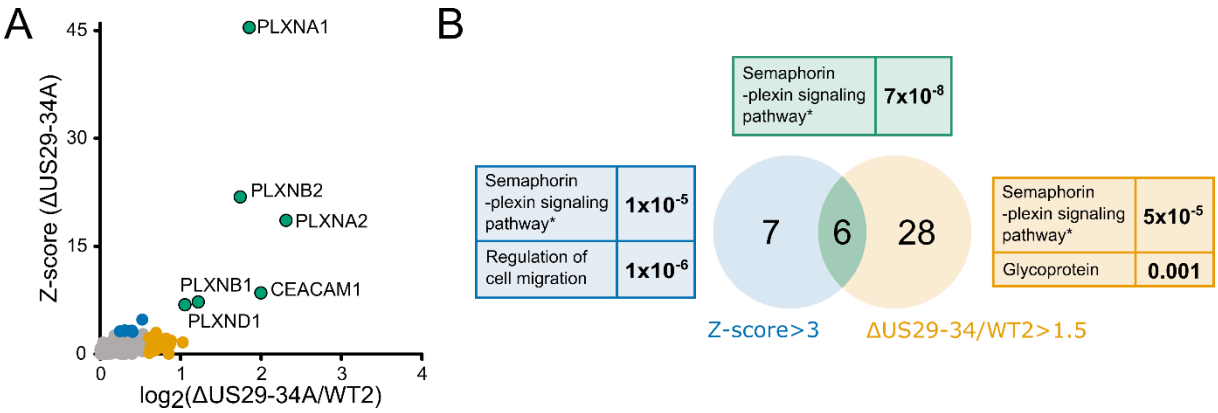

Figure 6.12: Proteins encoded by the US29-34A block are involved in the regulation of plexin abundance at the plasma membrane.

HFFFs were infected with strain Merlin (WT1), WT1 that lacked UL16 and UL18 (WT2), or one of nine block deletion viruses derived from WT1 or WT2 (ΔRL11-UL11, ΔUL2-11, ΔUL22A-25, ΔUS29-34A, ΔUS18-22, ΔRL10-UL1, ΔUS1-11, ΔUS12-17 or ΔUS27-28) (MOI: 10, 72 h infection). Plasma membrane proteins were isolated and lysed as described in Weekes *et al.* 2012 [190] and analysed by quantitative MS. This single repeat experiment was performed by Dr. Ceri Fielding and Dr. Katie Nightingale. These data are unpublished and analysed specifically for this thesis. **(A)** Scatter plot displaying human proteins quantified in the experiment with a FC(ΔUS29-34A/WT2)>1 and Z>0. Proteins with FC>1.5 and Z>3 are listed in Appendix V. **(B)** Venn diagram showing the numbers of target proteins satisfying each criteria. DAVID enrichment of GO biological process terms and UniProt keywords was performed on a background of all human proteins quantified, using the default settings for functional annotation clustering [285,286]. A representative term from each significantly enriched cluster is presented, alongside the Benjamini-Hochberg-adjusted p-value for that term. *Full term: semaphorin-plexin signalling pathway involved in axon guidance (GO:1902287).

Plexin	***Cell type expressing plexin***	***Semaphorin ligand***	***Cell type expressing semaphorin***	***Function***
A1	DCs	Sema3A	Lymphatic endothelial cells	DC trafficking to draining lymph nodes
A1	DCs	Sema6D	T cells, B cells and natural killer (NK) cells	Activation of DCs
B1/2/3		Sema4D	T cells, activated B cells, mature DCs	B cell and T cell activation
D1	$CD4^+/CD8^+$ T cells	Sema3E	Thymic epithelial cortex cells	T-lymphocyte migration and development

Table 6.3: The roles of semaphorin-plexin signalling in immune cell migration and communication.

Based on information from Takamatsu and Kumanogoh [431].

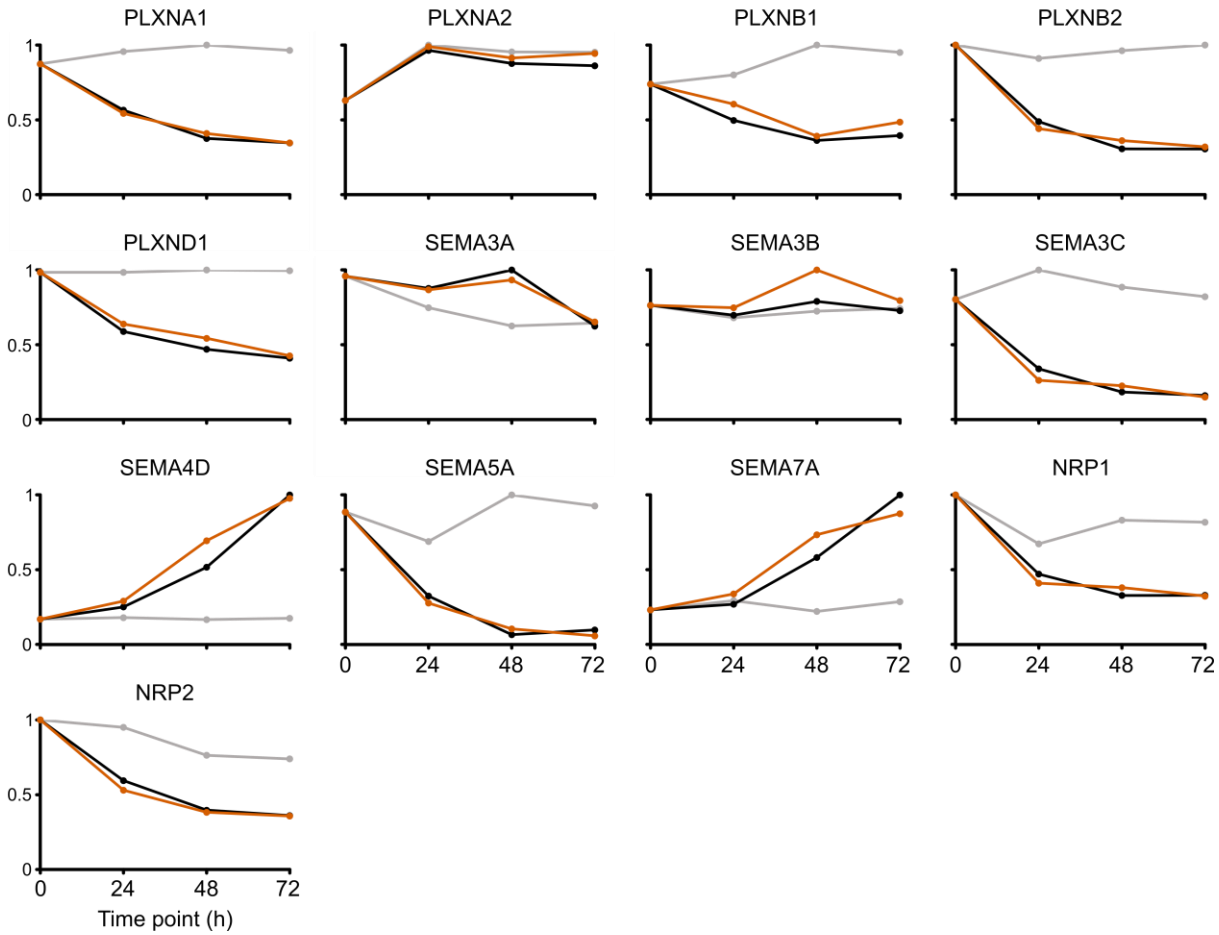

Figure 6.13: Plexins, semaphorins and neuropilins are highly regulated by HCMV infection.
Relative abundance of all quantified plexin, semaphorin and neuropilin family members over the time course, from data introduced in 6.3.4.

6.4.2 Effect of pUS29 on the host cell proteome

As part of the analysis of the single-gene-deletion virus screen, proteins with FC>1.5 and Z>3 relating to deletion of a particular viral gene were subjected to DAVID functional enrichment analysis **(Figure 6.3B)**. This showed that the putative targets for four of the viral proteins - pUS30, pUS31, pUS34 and pUS34A - contained a significantly high proportion of proteins involved in specific cellular processes (**Figure 6.3B** and detailed below). In contrast, deletion of US29 resulted in changes in a number of host proteins that did not share GO biological process terms or UniProt Keywords to a significant extent **(Figure 6.14A)**. Furthermore, none of the proteins significantly rescued (Z>3 and FC>1.5) upon deletion of US29 **(Figure 6.14A, Appendix V)** were identified as targets of the US29-34A block in the WCL block deletion screen **(Figure 6.11)**, meaning further validation would be required to determine if these are true targets of pUS29.

Out of the 54 proteins downregulated more than 1.5-fold with Z<-3 upon expression of any of the V5-tagged genes in the US29-34A block **(6.3.2)**, only 3 were also upregulated more than 1.5-fold with Z>3 in cells infected with the ΔUS29-34A block deletion virus in comparison to WT2 in the WCL block deletion screen **(Figure 6.11, Appendix V)**. One of these proteins was protein O-linked mannose N-acetylglucosaminyltransferase 1 (POMGNT1), which was downregulated four-fold upon expression of pUS29 with a Z-score of five **(Figure 6.14C and D)**.

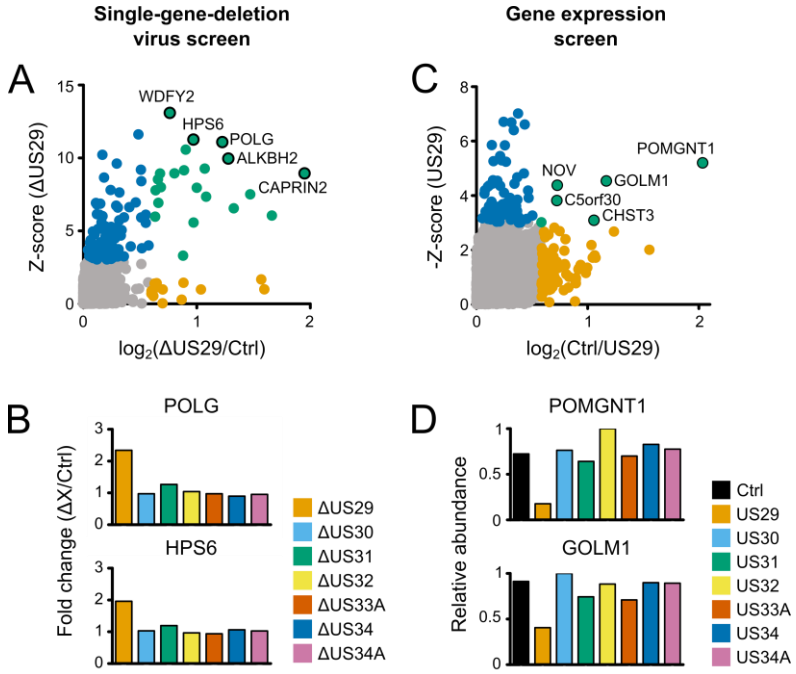

Figure 6.14: Effect of pUS29 on the host cell proteome.
(A-B) Results from the single-gene-deletion virus screen, as described in Figure 6.3. **(C-D)** Results from the gene expression screen, as described in Figure 6.4.

6.4.3 pUS30 is involved in the regulation of antiviral host proteins

DAVID functional enrichment analysis of the proteins significantly rescued upon infection of cells with of ΔUS30 in comparison to those infected with a control virus indicated that pUS30 targets proteins involved in antiviral defence (p: 0.006), including IFN-stimulated gene 20 kDa protein (ISG20), HECT domain and RCC1-like domain-containing protein 5 (HERC5) and DExD/H-box helicase 58 (DDX58, also known as RIG-I) **(Figure 6.15A and B)**. Given that all of these proteins are IFN-stimulated, it could be hypothesised that pUS30 is contributing to suppression of the IFN response. HERC5, which has previously been reported to inhibit HCMV infection [433], was also identified as a target of the US29-34A block in the WCL block deletion screen (Z>3 and FC>1.5) **(Figure 6.11)**, increasing confidence that HERC5 is a true target of US30.

None of the proteins downregulated upon stable expression of US30 (FC>1.5, Z<-3) **(Figure 6.15C and D)** were identified as hits in the WCL block deletion virus screen **(Figure 6.11)**, nor were they rescued by deletion of US30 in the single-gene-deletion virus screen **(Figure 6.15A)**. Further validation would be required to establish whether these are true, direct effects of pUS30 on the cell.

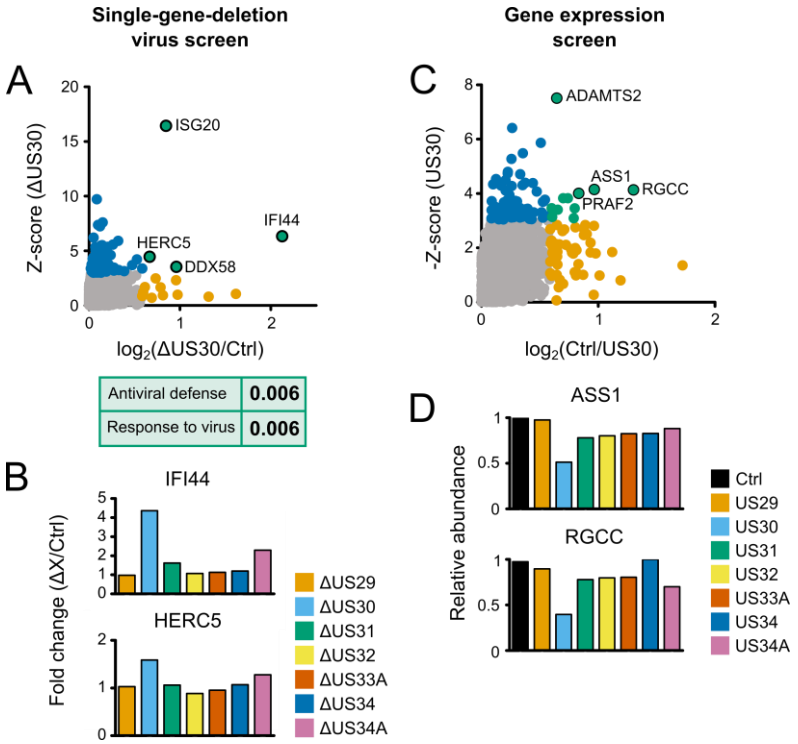

Figure 6.15: Effect of pUS30 on the host cell proteome.

(A-B) Results from the single-gene-deletion virus screen, as described in Figure 6.3. **(C-D)** Results from the gene expression screen, as described in Figure 6.4.

6.4.4 pUS31 is involved in the regulation of plexin signalling

The targets of pUS31 were enriched in proteins involved in mitosis (p: 3×10^{-4}), including kinetochore protein SPC24 and ubiquitin conjugating enzyme E2 C (UBE2C) **(Figure 6.16A)**. pUS31 also appears to target PLXNB2, and although not significant, PLXNA1 and PLXND1 were also slightly rescued in cells infected with ΔUS31 **(Figure 6.17)**. This is particularly intriguing given the proposed role of pUS31 in regulating the differentiation of macrophages and the role of plexins in modulating the activity adaptive immune cell types **(Table 6.1 and Table 6.3)**.

Stable expression of pUS31 led to a downregulation of PLXNA1 by almost two-fold and reduced levels of PLXNB2 and PLXNA2 in comparison to the control **(Figure 6.18)**. These results were validated by Dr. Katie Nightingale, who showed that PLXNA1 and PLXNB2 were downregulated in pUS31-expressing HFFF-TERTs by flow cytometry and immunoblotting, respectively (results not shown).

These results suggest that pUS31 may be the viral protein responsible for the US29-34A-dependent downregulation of plexins in WCLs **(Figure 6.11)** and at the plasma membrane **(Figure 6.12)**.

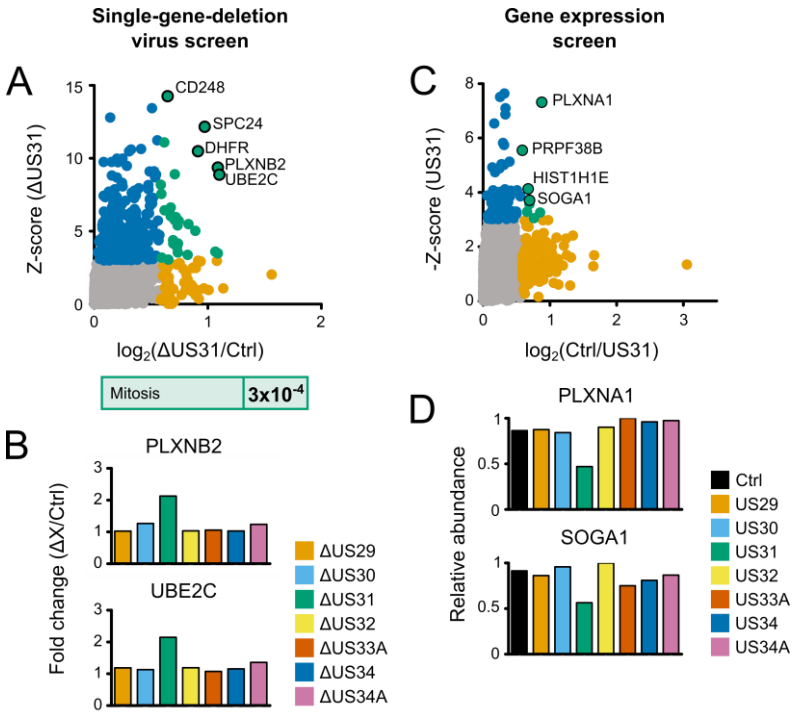

Figure 6.16: Effect of pUS31 on the host cell proteome.

(A-B) Results from the single-gene-deletion virus screen, as described in Figure 6.3. **(C-D)** Results from the gene expression screen, as described in Figure 6.4.

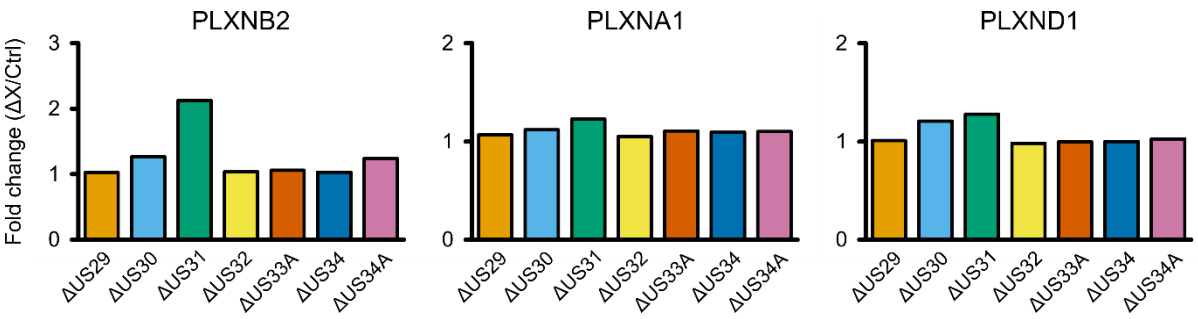

Figure 6.17: Abundance of PLXNB2 is rescued in cells infected with ΔUS31 deletion virus.

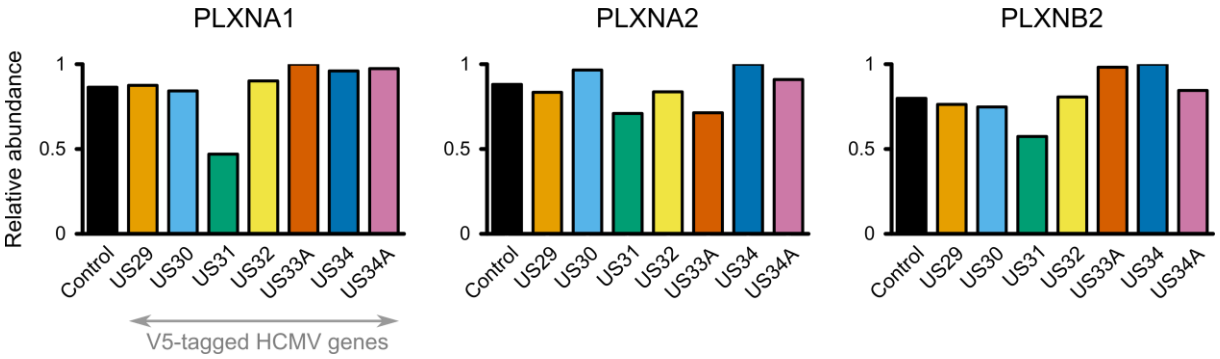

Figure 6.18: Expression of pUS31-V5 is sufficient for the downregulation of PLXNA1.
Protein abundance of plexins in HFFF-TERTs expressing V5-tagged viral genes in the US29-34A block or a control vector, relative to the maximum protein abundance observed across the samples.

6.4.5 Effect of pUS32 on the host cell proteome

Out of the proteins rescued upon deletion of US32 (FC>1.5, Z>3) **(Figure 6.19A)** or downregulated upon expression of pUS32 (FC>1.5, Z<-3), only RING1 and YY1-binding protein (RYBP) was also identified as a target of the US29-34A block in the WCL block deletion screen (Z>3 and FC>1.5) **(Figure 6.11, Appendix V)**. RYBP is involved in the regulation of chromatin remodelling and transcription [434], which is interesting given that pUS32 has been shown to localise to PML nuclear bodies [422].

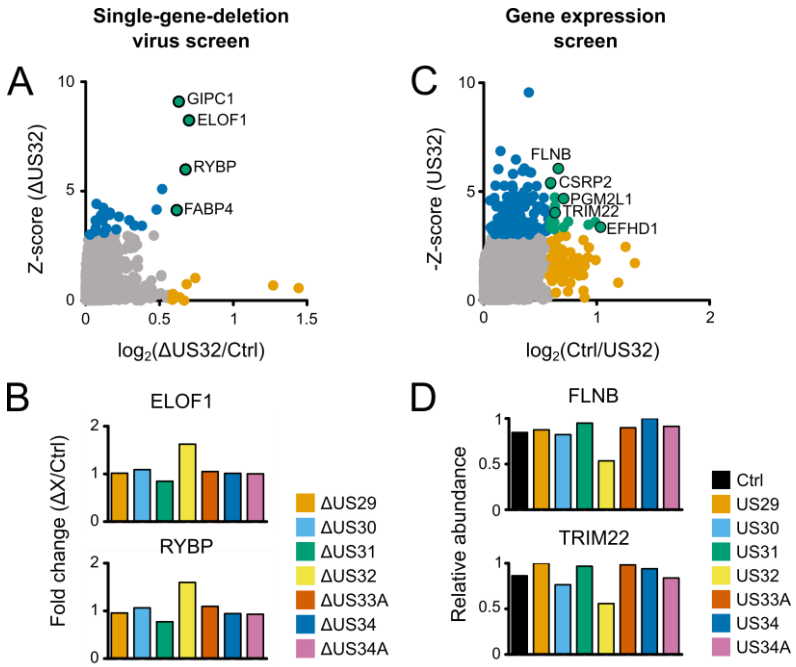

Figure 6.19: Effect of pUS32 on the host cell proteome.
(A-B) Results from the single-gene-deletion virus screen, as described in Figure 6.3. **(C-D)** Results from the gene expression screen, as described in Figure 6.4.

6.4.6 pUS34 affects the abundance of secreted proteins in whole cell lysates

Four out of five proteins rescued upon deletion of US34 were associated with the UniProt keyword 'Secreted' (p: 0.009), which is interesting and perhaps unsurprising given that pUS34 itself is believed to be secreted due to the presence of an N-terminal signal peptide targeting it for the secretory pathway. None of the proteins rescued upon deletion of US34 (FC>1.5, Z>3) **(Figure 6.20A-B)** or downregulated upon expression of pUS34 (FC>1.5, Z<-3) **(Figure 6.20C-D)**, were also identified as a target of the US29-34A block in the WCL block deletion screen (Z>3 and FC>1.5). Furthermore, there was no correspondence between the hits identified in the single-gene-deletion virus and gene expression screens.

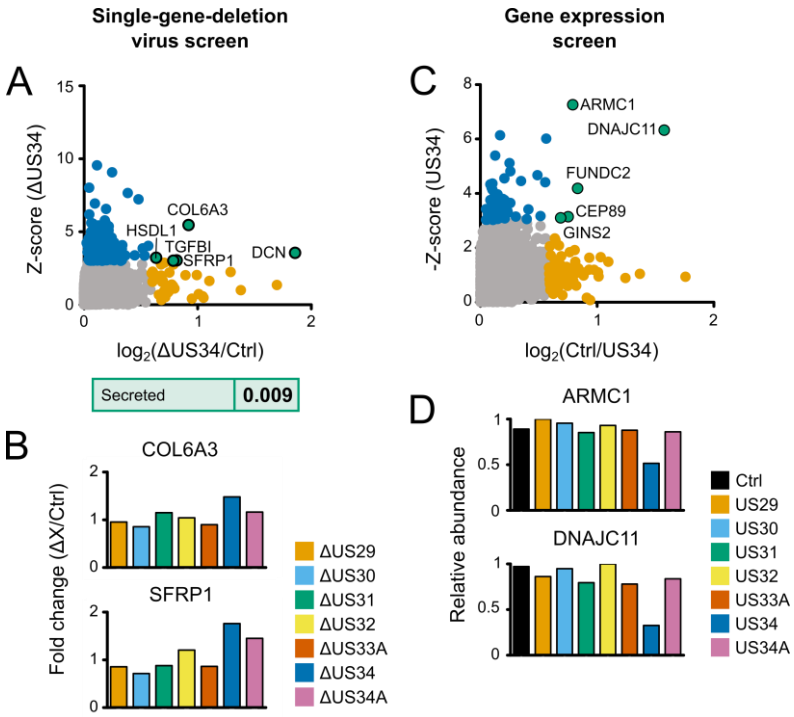

Figure 6.20: Effect of pUS34 on the host cell proteome.

(A-B) Results from the single-gene-deletion virus screen, as described in Figure 6.3. **(C-D)** Results from the gene expression screen, as described in Figure 6.4.

6.4.7 pUS34A is involved in the regulation of IFN signalling pathways

US34A appears to downregulate proteins involved in IFN signalling, including IFIT1, 2 and 3, and HLA-A, B and F **(Figure 6.21A-B)**. It therefore seems that both pUS30 **(6.4.3)** and pUS34A are responsible for the effect of the US29-34A block on innate immunity that was observed in the gene block deletion screen **(6.4.1)**.

No proteins were significantly downregulated upon stable expression of pUS34A-V5 **(Figure 6.21C)**, which may indicate that the V5 tag is hindering the function of pUS34A, as seen with pUS33A. pUS34A is a similarly small viral protein of 8 kDa.

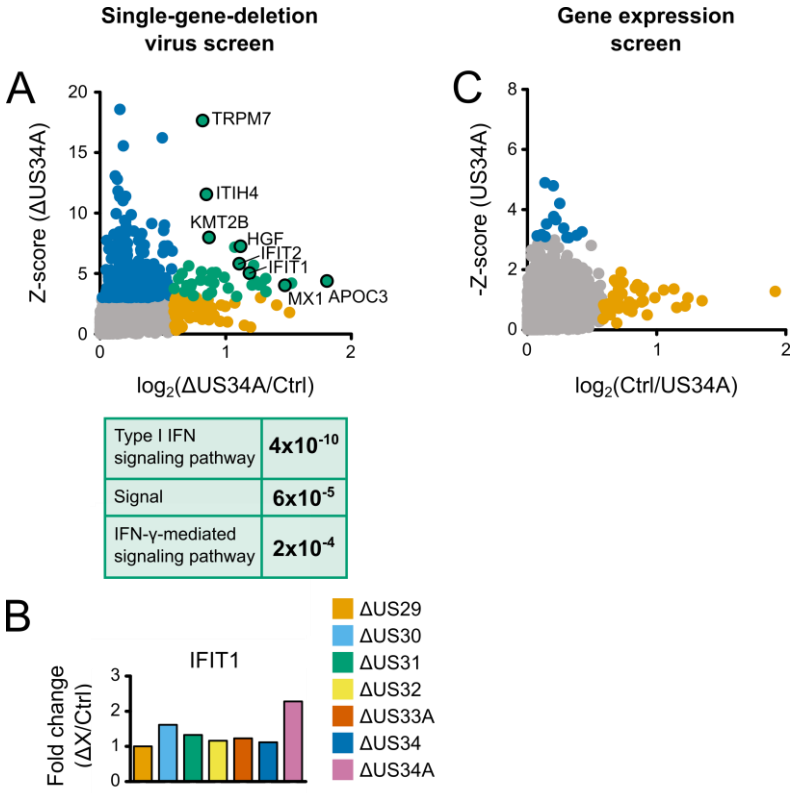

Figure 6.21: Effect of pUS34A on the host cell proteome.
(A-B) Results from the single-gene-deletion virus screen, as described in Figure 6.3. **(C-D)** Results from the gene expression screen, as described in Figure 6.4.

6.4.8 Deletion of genes US30-33A enhances viral late gene expression

Finally, the effect of the US29-34A genes on viral gene expression was studied by analysing the abundance of HCMV proteins in the single-gene-deletion virus screen, described in **(6.3.1)**. Deletion of US30, US31, US32, US33A and US34 resulted in significant differences in the relative expression of viral genes belonging to different temporal protein profile (Tp) classes as defined in Weekes *et al.* 2014 [86] **(Figure 6.22)**. In particular, viral genes assigned Tp5 [86], generally corresponding to the classical 'late' genes, were significantly upregulated in comparison to all other Tp classes in cells infected with ΔUS30, ΔUS31, ΔUS32 and ΔUS33A. Whether this was due to these proteins playing a functional role in the suppression of late gene expression or protein abundance, or an off-target effect of gene deletion on the regulation of late gene transcription, is unknown. In contrast, deletion of US34 led to a decrease in the relative expression of Tp5 genes in comparison to the other Tp classes.

It is also important to note that deletion of some of the genes resulted in significant up or downregulation of other viral proteins. Again, it is unclear whether this is due to true functional effects of the US29-34A proteins or a by-product of viral gene deletion through the disruption of genetics motifs responsible for the regulation of expression of other viral genes. Consequently, any effect of viral gene deletion on the human or viral proteomes presented in this chapter would have to be validated to show that the viral protein in question is sufficient for any change observed. Of particular concern is the finding that the deletion of US29 caused an increase in the abundance of pUS30, whereas deletion of US30 resulted in downregulation of pUS29. The coding sequences of these two genes overlap, and so the primers used to generate the deletion viruses by recombineering (as described in [67]) were designed to leave some sequence up or downstream of the overlapping sequence to minimise disruption to the promoter of US30 and the polyA tail of US29 **(Appendix IV)**. However, avoiding interference cannot be guaranteed, and so deletion of one gene may have modulated expression of the other. It is also possible that read-through from the US29 promoter is causing the upregulation of US30 gene expression in the ΔUS29 virus. This may also be the case in the ΔUS31 virus, where deletion of US31 led to upregulation of pUS32. A protein-protein interaction was identified between US29 and US30 in the HCMV interactome, and so there is a possibility that this regulation occurs at the protein level [269].

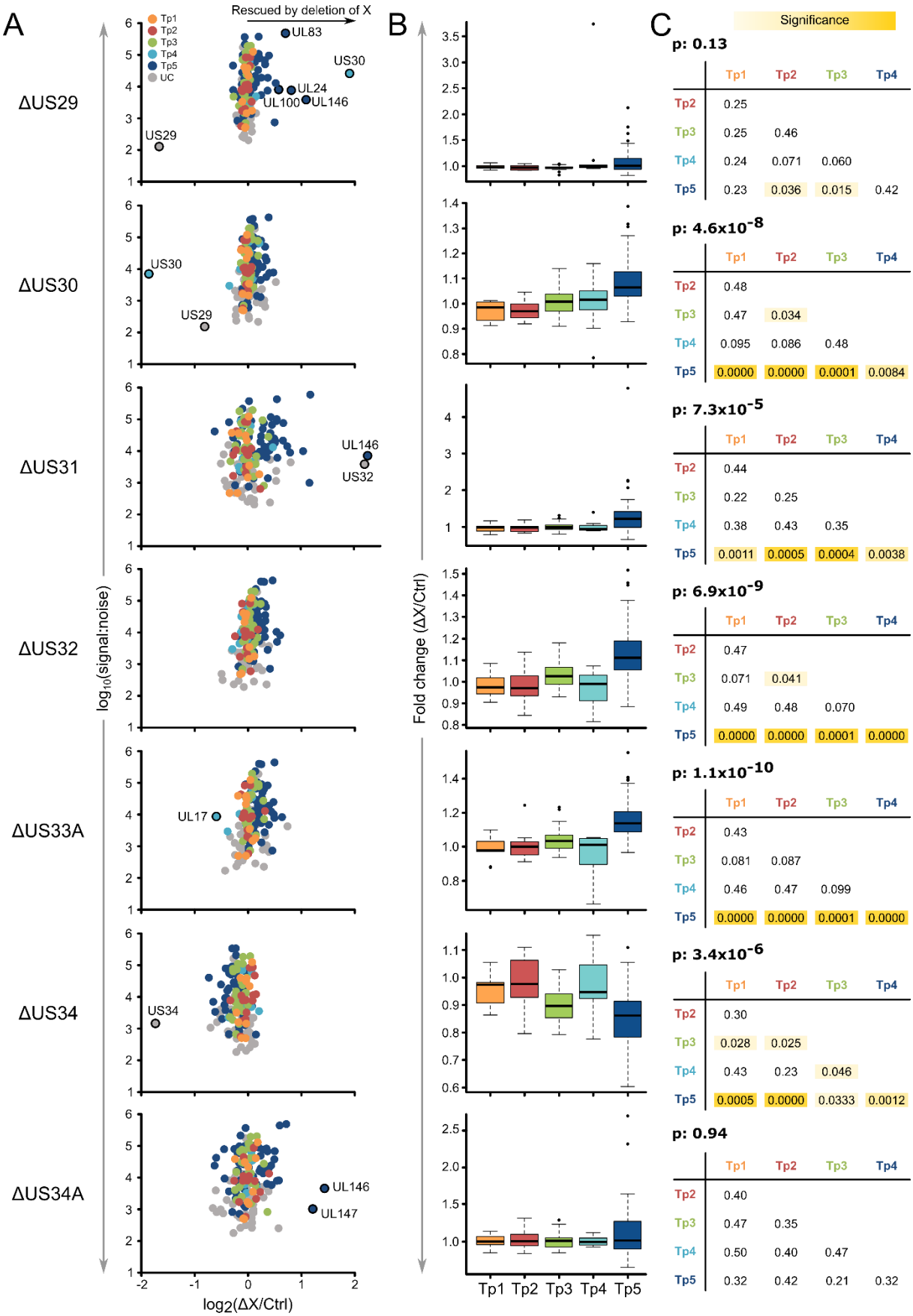
A
B
C
Rescued by deletion of X
Tp1
Tp2
Tp3
Tp4
Tp5
UC
ΔUS29
ΔUS30
ΔUS31
ΔUS32
ΔUS33A
ΔUS34
ΔUS34A
UL83
US30
UL24
UL100
UL146
US29
US32
UL17
US34
UL147
log10(signal:noise)
log2(ΔX/Ctrl)
Fold change (ΔX/Ctrl)
Significance
p: 0.13
p: 4.6x10-8
p: 7.3x10-5
p: 6.9x10-9
p: 1.1x10-10
p: 3.4x10-6
p: 0.94

(Previous page)

Figure 6.22: Deletion of genes US30-33A enhances viral late gene expression.

(A) Scatter plots showing the FC of protein abundance in cells infected with each single-gene-deletion virus vs the control (ΔX/Ctrl, where X is a gene in the US29-34A block) for the 158 viral proteins that were quantified in the experiment. Proteins that were up or downregulated with a significance B p-value of less than 0.0001 are labelled. Each point is coloured according to the temporal profile class (Tp1-5) of the protein, as described in Weekes *et al.* 2014 [86]. US32 was off the scale of the ΔUS32 plot [log_2(FC): -4.6]. UC: uncharacterised. **(B)** Box-and-whisker plots of the ΔX/Ctrl FCs for proteins belonging to each Tp class. **(C)** A Shapiro-Wilk normality test showed that the ΔX/Ctrl FCs for each Tp class did not always exhibit a normal distribution, and so a non-parametric Kruskal-Wallis one-way analysis of variance test was chosen to test the null hypothesis that the mean ΔX/Ctrl FC of each Tp class were the same (p-value shown above each table). Results of a Dunn's post-hoc test, reporting p-values for pairwise comparisons between each Tp class, are shown in the tables.

6.5 Discussion

6.5.1 The mechanism of DMXL1 downregulation

6.5.1.1 pUS33A is necessary and sufficient for DMXL1 downregulation

In this chapter, evidence is provided for the downregulation of DMXL1 by pUS33A, an HCMV protein that is expressed early in the infection time course. pUS33A was both necessary and sufficient for DMXL1 downregulation **(Figure 6.3 and Figure 6.6)**. Tagging pUS33A with V5 at the N- or C-terminus abrogated its effect on DMXL1 levels **(Figure 6.6)**. This is unsurprising, given that the V5 tag is a quarter of the size of 7 kDa pUS33A, and because pUS33A-V5 was not shown to interact with DMXL1 in the HCMV interactome [269].

Deletion of US33A also resulted in a limited increase in the abundance of WDR7 in infected cells **(Figure 6.3).** WDR7 interacts with DMXL1 to form the complex Rabconnectin-3, with both proteins required for the role of Rabconnectin-3 in regulating V-ATPase-dependent organelle acidification. The increase in WDR7 upon US33A deletion suggests that DMXL1 may stabilise WDR7.

A proteomic analysis of a time course of infection showed that in the absence of pUS33A, DMXL1 levels increased substantially over 72 h of infection, while remaining constant in mock-infected cells. This finding is accordant with previous results showing that DMXL1 protein is upregulated in cells infected with irradiated HCMV at 72 hpi, and that the level of DMXL1 transcripts rises through infection **(Figure 1.13)**. Although there are no studies investigating the effect of IFN on DMXL1, DMXL2 levels are not stimulated by IFN [200]. Consequently, it can be hypothesised that expression of DMXL1 is stimulated by infection independently of IFN signalling, a common characteristic of many ARFs **(1.2.1)**.

Confirming whether DMXL1 exhibits antiviral or proviral function should be a priority for further study. Study of DMXL1 will be hindered by the size of the protein, making exogenous expression of native or

tagged DMXL1 near impossible. However, suggestions of experiments that could be performed are described in **Future directions 6.1**.

A. Two-colour restriction assays using siRNA knockdown.

Two-colour restriction assays, as introduced in 3.3, could be used with siRNA instead of shRNA knockdown of DMXL1 to avoid the non-specific effects of shRNA transduction. Recombinant viruses that express early (e.g. UL36) or late genes (e.g. UL32) tagged with fluorescent proteins could be used to observe the impact of DMXL1 on different stages of the replication cycle. Alternatively, a recombinant HCMV expressing mCherry-P2A-UL36 and GFP-UL32 could be used to study both early and late gene expression concomitantly [312]. Introducing the timing of siRNA treatment as a variable could be used to understand the timing of the proviral or antiviral effects of DMXL1.

B. siRNA plaque assay.

Similarly, the plaque assays described in 3.7 could be performed with siRNA-transfected rather than shRNA-transduced cells.

C. CRISPR/Cas9-based upregulation of DMXL1 transcription.

Overexpression of the endogenous protein could be achieved through CRISPR/Cas9-based activation of transcription. sgRNAs can be used to direct the recruitment of an inactive Cas9 protein fused to a transcriptional activators such as VP64 (four tandem copies of viral protein 16) or transactivation domain (TAD) [435]. Drug-inducible versions of this system could be used to study whether the effect of DMXL1 on infection is time-point specific [436].

Future directions 6.1: Is DMXL1 antiviral or proviral?

The role of the V-ATPase in VAC formation, autophagy, TLR signalling, MHC class II presentation and an abundance of other cellular processes suggests that the V-ATPase (and hence, DMXL1) may have both proviral and antiviral roles, potentially acting at different times in the replication cycle. Experiments that could be performed to study the impact of DMXL1 downregulation on these processes are described in **Future directions 6.2**.

It is important to consider the timing of the proviral and/or antiviral effects of the V-ATPase/DMXL1, and the viral countermeasures, through infection. It is likely that viral manipulation of V-ATPase activity is temporally regulated, meaning that attempts to understand the effect of the V-ATPase and DMXL1 on infection through knockdown or chemical inhibition may not effectively recreate the carefully timed situation occurring *in vivo*. For example, miR-US25-1 is thought to downregulate ATP6V0C levels late in infection, yet studies aiming to understand its function have made use of ATP6V0C knockdown prior to infection. While the knockdown of ATP6V0C only impacted the later stages of HCMV replication [222], DMXL1 has been shown to be required for the early stages of HIV-1 infection [417,418].

The effects of viral antagonism of endosomal acidification are also likely to be sensitive to the level of DMXL1 or ATP6V0C downregulation, which may be difficult to mimic in experimental settings. As DMXL1 is stimulated by infection, DMXL1 may only be antiviral at high levels. It could be hypothesised that the virus uses pUS33A to counteract the observed stimulation of DMXL1, but by bringing it down to levels below that in uninfected cells, disrupts some of the canonical function of DMXL1 that is necessary for virus infection.

The impact of DMXL1 downregulation on autophagy and downstream effects on virus replication may be difficult to decipher, as it is thought that HCMV balances the proviral effects of autophagy with its role in viral degradation by temporally regulating autophagic flux throughout the course of infection [336,437]. However, understanding whether the regulation of endosomal acidification through DMXL1 and V-ATPase downregulation contributes to HCMV-mediated modulation of autophagic flux could be key to this story **(Future directions 6.2C)**.

A. Immunofluorescence to study the effect of DMXL1 downregulation on VAC formation.

Pavelin *et al.* [222] used immunofluorescence to observe the distribution of VAC markers upon infection in ATP6V0C knockdown vs control cells. A similar experiment could be performed with DMXL1, to discern whether DMXL1 downregulation has the same impact on VAC formation as disruption of the V-ATPase.

B. PMP to monitor the impact of DMXL1 on the infected cell surface proteome.

As endosomal acidification is necessary for intracellular trafficking, downregulation of DMXL1 in infection may disrupt the cell surface proteome, with implications for innate and adaptive immune signalling. PMP of cells infected with ΔUS33A or the control virus could be used to understand the effect of DMXL1 downregulation on the cell surface proteome.

C. Analysis of the impact of DMXL1 downregulation on read-outs of autophagy.

Lipidated LC3B is required for elongation of the phagophore membrane and is degraded following lysosomal fusion. If DMXL1 is required for autophagic cargo degradation, DMXL1 downregulation should lead to an accumulation of lipidated LC3B, which could be observed by immunoblot. Other read-outs include the observation of LC3B foci formation by microscopy, proteomic or immunoblot analysis of the accumulation of autophagosomal cargo (e.g. p62), or the use of tandem RFP-GFP-tagged LC3 to observe autophagic flux [438].

D. Proteomic analysis of the MHC class II peptidome.

Quantitative proteomics has previously been used to study the endogenous peptide repertoires of MHC class II molecules and could be used to study whether DMXL1 or the V-ATPase has an impact on the MHC class II peptidome (for example, through regulation of peptide loading via the autophagic pathway).

All of these experiments could be performed using WT HCMV and the ΔUS33A virus to rescue DMXL1 levels. Infecting control and DMXL1 siRNA knockdown cells with ΔUS33A would enable attribution of any effects specifically to the level of DMXL1.

Future directions 6.2: What is the function of DMXL1 in infection?

6.5.1.2 pUS33A may hijack the E3 ligase complex KPC to target DMXL1 for degradation

Results from the HCMV interactome revealed that pUS33A interacts with two members of the E3 ligase complex KPC: RNF123 and UBAC1. It was therefore proposed that pUS33A recruits KPC, and/or facilitates substrate recognition of DMXL1, in order to target DMXL1 for proteasomal degradation. An siRNA knockdown of RNF123 and UBAC1 was performed in the context of infection, to observe whether KPC is necessary for DMXL1 downregulation. Unfortunately, the level of DMXL1 downregulation achieved was insufficient to make any confident conclusions, although knockdown of RNF123, UBAC1 and a double knockdown of both proteins did lead to a reduction in the small amount of downregulation that was observed (from 25% downregulation to an average of 7% across the three knockdown cell lines) **(Figure 6.9)**. This experiment requires optimisation to ensure that the effect of KPC is observed under the context of maximal and active DMXL1 degradation, which may be dependent on the time point, percentage of infection and cell density. Furthermore, this experiment was performed prior to the discovery that untagged pUS33A is sufficient for DMXL1 downregulation. Therefore, it would now be possible to study the same effect by performing siRNA knockdown of RNF123 and UBAC1 in the pUS33A-expressing cell lines **(Future directions 6.3A)**.

The Nightingale, Lin *et al.* (2018) study found that DMXL1 downregulation was rescued by the application of the proteasomal inhibitor MG132 at 12 hpi, but not later **(Figure 1.13)**, suggesting that active degradation of DMXL1 may only occur at early time points of infection. However, other experiments performed at 24 h (unpublished, results not shown) and 48 h **(Chapter 4)** have shown rescue of DMXL1 with MG132. MG132 is a broad, non-selective inhibitor that can also inhibit lysosomal cathepsins and calpains in addition to the proteasome [198]. A recent study from our group found that the majority of proteins downregulated at 12 hpi and rescued by MG132 treatment are also rescued by the selective proteasome inhibitor bortezomib [199]. Indeed, although DMXL1 was not strongly downregulated in this experiment, bortezomib did rescue DMXL1 to the same level as with MG132 **(Figure 1.13)**. So far, proteasomal degradation has only been tested in the context of infection. pUS33A cell lines could be treated with MG132 and bortezomib to establish whether pUS33A is sufficient for proteasomal degradation of DMXL1 **(Future directions 6.3B)**.

To define the mechanism of DMXL1 downregulation, interactions between pUS33A and DMXL1, and RNF123 and UBAC1 if their involvement is confirmed, should be characterised. Suggestions of how to achieve this are described in **Future directions 6.3**.

A. siRNA knockdown of RNF123 and UBAC1 in pUS33A-expressing cell lines.

This could be performed to establish whether KPC is necessary for the downregulation of DMXL1 observed in pUS33A-expressing HFFF-TERTs.

B. Use of proteasomal inhibitors to confirm whether DMXL1 is degraded by the proteasome.

pUS33A-expressing cell lines could be treated with MG132 and bortezomib to confirm that pUS33A directs the proteasomal degradation of DMXL1.

C. Confirmation of the interaction between US33A and DMXL1.

The interaction between DMXL1 and US33A could be confirmed in the context of infection or US33A expression by immunoprecipitation MS using antibodies against endogenous DMXL1. However, this may be difficult as over the course of this study there were problems with using antibodies for the identification of DMXL1 by both immunoblot and immunofluorescence. Other methods that can be combined with MS to study interactions include chemical cross-linking, yeast two-hybrid methods, hydrogen/deuterium exchange and proximity-dependent biotin identification (BioID) [179]. Methods that require protein tagging are likely to be challenging given that DMXL1 expression is problematic due to its size, and tagging pUS33A abrogates its function.

D. Characterisation of the interaction between pUS33A and KPC.

If KPC is shown to be involved in DMXL1 downregulation, characterisation of the domains of RNF123 and UBAC1 that interact with pUS33A will enable elucidation of the mechanism of downregulation. This could be achieved through exogenous expression of protein domains followed by immunoprecipitations from cell lysates. Alternatively, protein purification would enable concomitant analysis of structures and interactions, with *in vitro* co-immunoprecipitation, tandem affinity purification, affinity chromatography, isothermal titration calorimetry, surface plasmon resonance, microscale thermophoresis and analytical ultracentrifugation just some examples of techniques that could be used to characterise interactions.

Future directions 6.3: Is KPC necessary for DMXL1 degradation?

6.5.1.3 RNF123 is upregulated during infection

An unexpected finding of the RNF123/UBAC1 knockdown screen was that RNF123 was upregulated in response to infection **(Figure 6.9B)**. This is particularly interesting given the observation that RNF123 can act as a negative regulator of RIG-I and IFIH1, enhancing RNA virus replication [428]. Although there are no studies specifically reporting the detection of HCMV infection by RIG-I-like receptors (RLRs), RLRs have been shown to be stimulated by other herpesvirus infections, and HCMV inhibits signalling via the RLR signalling pathway [439]. The upregulation of RNF123 in infection was suppressed by deletion of US33A, indicating that US33A may be involved in the upregulation of RNF123 **(Figure 6.9D)**. This could be related to the effect of pUS33A on DMXL1, or might represent an unrelated function of pUS33A that pertains to the regulation of RLR signalling. RNA sequencing

(RNA-seq) analysis has shown that levels of RNF123 transcripts increase through infection **(Figure 6.9C)**, indicating that the increase in RNF123 protein levels might be due to increased gene expression.

In the presence of infection, knockdown of RNF123 did not rescue levels of CDKN1B/p27^{Kip1}, the canonical target of KPC-mediated ubiquitination. This suggests that, although RNF123 is upregulated in infection, it is being redirected to carry out a non-canonical and perhaps infection-specific role. Potential experiments that could be performed to decipher the mechanism and function of RNF123 upregulation are detailed in **Future directions 6.4**.

A. RT-qPCR analysis of RNF123 in WT and ΔUS33A HCMV-infected cells.

This would assess whether or not the pUS33A-dependent regulation of RNF123 is transcriptional or post-transcriptional.

B. IFN-β enzyme-linked immunosorbent assay (ELIZA) during infection with WT and ΔUS33A HCMV.

If the interaction between pUS33A and RNF123 is related to the proposed role of RNF123 in regulation of RLR signalling, deletion of pUS33A and the inhibition of RNF123 upregulation should lead to an increase in IFN-β production. That is, if HCMV infection does stimulate RLR signalling.

Future directions 6.4: What is the mechanism and function of RNF123 upregulation?

6.5.2 The function of proteins encoded by the US29-34A gene block

6.5.2.1 pUS31 may be necessary and sufficient for downregulation of plexin family members

Functional enrichment analysis of proteins with increased abundance in cells infected with a virus lacking the US29-34A block of viral genes - in comparison to that in cells infected with a control virus - showed that one or more viral proteins encoded in the US29-34A block specifically target the semaphorin-plexin signalling pathway **(Figure 6.11)**. This enrichment of proteins involved in semaphorin-plexin signalling was even more significant when considering proteins rescued specifically at the PM **(Figure 6.12)**, which was expected as the plexins are a family of transmembrane receptors.

Although the interactions between HCMV and the plexins have not been studied in detail, our and other groups' work has signified a potentially important role for the plexin-semaphorin signalling pathway in HCMV replication [86,432]. The Weekes *et al.* (2014) quantitative temporal viromics study of WCLs and the PM through a time course of HCMV infection showed that the abundance of plexins at the PM is reduced from as early as 12 hpi [86]. For plexins A1, B2 and D1, this is followed by a more gradual decline at the whole cell level [86]. PLXNA2 was downregulated at the PM but not at the whole cell level, while PLXNB1 was only quantified in the PMP screen [86].

Members of the plexin, semaphorin and neuropilin family were well quantified in the ΔUS33A time course presented in this chapter, improving confidence in data from the Weekes *et al.* (2014) paper. In addition to PLXNA1, B2 and D1, PLXNB1 was also downregulated at the WCL level **(Figure 6.13)**. As in Weekes *et al.* (2014), SEMA4D and 7A were significantly upregulated through infection, while SEMA3C, SEMA5A, NRP1 and NRP2 were all downregulated **(Figure 6.13)**. Interestingly, NRP2 is an essential entry receptor for HCMV **(1.1.8.1)** [77,78]. Whether the downregulation of NRP2 is related to its function in virus entry, for example representing a strategy to prevent reinfection of infected cells, is yet to be determined.

The evidence presented in this chapter suggests that the regulation of plexin abundance is mediated by the virus rather than the host. PLXNA1, A2, B1, B2 and D1 were all downregulated from the PM by at least one of the genes in the US29-34A block **(Figure 6.12)**, while PLXNA3 has previously been shown to be a target of the US1-US11 block [62]. Proteomic analysis of whole cell lysates has shown that PLXNB2 was rescued in cells infected with a ΔUS31 deletion virus **(Figure 6.17)** and expression of US31-V5 was sufficient for PLXNA1 downregulation **(Figure 6.18)**. Preliminary work by Dr. Katie Nightingale has confirmed the downregulation of PLXNA1 upon US31-V5 expression by flow cytometry of permeabilised cells, and shown that PLXNB2 was very significantly downregulated by expression of US31-V5 when analysed by immunoblot (results not shown), despite not seeing this effect by proteomics. Although not conclusive, collectively these results suggest that pUS31 is involved in the downregulation of multiple plexins. These experiments should be repeated with specific analysis of the cell surface, as the most significant downregulation of the plexins was seen at the PM **(Future directions 6.5)**.

Preliminary evidence suggests that plexin downregulation might occur via a number of different mechanisms. PLXNA2 transcripts increase during infection [62], and the fact that it is not downregulated in WCLs suggests that the protein is internalised but not degraded. PLXNA1, B1 and D1 RNA levels decrease slightly at 24 h before being upregulated, while PLXNB2 RNA levels remain below that prior to infection, indicating that transcriptional regulation may play a part in PLXNB2 downregulation [62]. Furthermore, some of the plexins, namely A1 and B2, show some evidence of rescue upon treatment of infected cells with the lysosomal protease inhibitor leupeptin [62]. Application of specific proteasomal and lysosomal inhibitors, transcript analysis by RT-qPCR, immunofluorescence-based analysis of protein localisation and knockdown of pUS31 interactors could be used to elucidate the mechanism of plexin downregulation further **(Future directions 6.5)**.

The role of plexin-semaphorin signalling in adaptive immune cell migration and activation is increasingly recognised **(Table 6.3)**. However, nothing is known about the role plexins play in virus-infected cells. Experiments designed to probe the functional role of semaphorin-plexin signalling in HCMV infection are described in **Future directions 6.6**.

A. PMP and RT-qPCR analysis of an infection time course with WT and ΔUS31 HCMV.

To validate the role of pUS31 in plexin downregulation, gain more information about the kinetics of this downregulation, and assess whether the mechanism of downregulation is prior to or following transcription.

B. PMP and RT-qPCR analysis of cells expressing untagged pUS31.

For both A and B, specific inhibitors of the proteasome and lysosome could be implemented to probe the potential mechanism of degradation. Validation of effects seen by proteomics could be achieved by immunoblot or flow cytometry.

C. Analysis of pUS31 and plexin localisation by fluorescent microscopy.

This could be accomplished either by using a virus expressing US31 tagged with a fluorescent protein, or immunofluorescence of V5-tagged US31 in infected cells.

D. siRNA knockdown of pUS31 interactors.

Performed in the context of infection or protein expression to establish whether any pUS31 interactors are necessary for downregulation of the plexins.

Future directions 6.5: Is pUS31 responsible for downregulation of plexin family members?

A. Evaluation of the effect of plexin downregulation on virus replication.

siRNA or CRISPR knockdown of plexins, semaphorins and neuropilins followed by analysis of virus replication via restriction assays, plaque assays and growth curves could be used to determine whether plexin-semaphorin signalling is proviral or antiviral.

B. Analysis of the effect of plexin downregulation on immune cell signalling and activation.

For example, by ELIZA-based analysis of IFNs and cytokines produced by infected cells or co-cultured adaptive immune cells (e.g. T cells or NK cells).

Future directions 6.6: What is the role of plexins in infection?

6.5.2.2 pUS30 and pUS34A are involved in the regulation of innate immunity

Another finding from the analysis of cells infected with gene block deletion viruses was that proteins encoded by the US29-34A gene block are involved in the regulation of host innate immune signalling proteins, including ISG15 and OASL **(Figure 6.11, Appendix V)**. Regulation of these proteins was not unique to the block, as demonstrated by the low Z-scores **(Figure 6.11)**. This high proportion of proteins involved in innate immunity was not observed in the PM-localised targets of the US29-34A block **(Figure 6.12)**, suggesting that the innate immune proteins regulated by US29-34A are predominantly intracellular.

Proteomic analysis of cells infected with single-gene-deletion viruses covering each of the genes in the block revealed that this function is executed by pUS30 and pUS34A **(Figure 6.3)**. Deletion of pUS30 led to rescue of ISG20 and interferon-induced protein 44 (IFI44), and to a lesser extent, HERC5 and RIG-I. ISG20 is an IFN-stimulated RNA exonuclease that has been associated with the restriction of a range of RNA viruses [440]. Upon infection with HCMV, ISG20 is upregulated six-fold by 24 hpi and subsequently downregulated to endogenous levels by 48 hpi [86]. pUS30 exhibits a Tp4 profile, with maximal expression at around 48 hpi, around the time that ISG20 is downregulated. IFI44 is an IFN-induced protein that can aggregate microtubules, and has been shown to inhibit bunyavirus and HIV-1 replication [441,442]. Like ISG20 and other IFN-induced proteins, it is upregulated rapidly during HCMV infection and subsequently downregulated. Neither ISG20 nor IFI44 have been implicated in the restriction of HCMV infection. Furthermore, whether the downregulation of ISG20 and IFI44 by pUS30 is a result of targeted protein downregulation, or due to a more global effect on IFN signalling, remains to be determined.

Deletion of US34A resulted in the rescue of 39 proteins with a FC>1.5 and Z>3 **(Figure 6.3)**. This group of target proteins was enriched in proteins involved in type I and type II IFN signalling, including IFIT1, 2 and 3, and HLA-A, B and F **(Appendix V)**.

6.5.3 Limitations

The US29-34A single-gene-deletion virus screen presented in this chapter provides a useful insight into the function of several uncharacterised HCMV proteins. Sequencing of the virus populations grown up from bacterial artificial chromosome-derived virus seed stocks showed that all of the single-gene-deletion viruses exhibited the desired mutation predicted from the sequences of the primers used for recombineering **(Appendix IV)**. Other than the desired single-gene-deletions, only the ΔUS33A HCMV genomic sequence exhibited a deviation from that of the parental strain (RCMV2582) that was used as a control virus in the experiment. Around 50% of the ΔUS33A HCMV population had a single nucleotide polymorphism at position 22393, causing a leucine to phenylalanine substitution in pUL17. Given that expression of pUS33A was sufficient for DMXL1 downregulation, there can be confidence that the rescue of DMXL1 in cells infected with ΔUS33A was a result of the US33A deletion rather than the mutation in UL17. However, any other observed effect in cells infected with ΔUS33A would have to be validated to rule out the possibility that the mutation in UL17 was responsible.

Another caveat of this screen is that deletion of some genes resulted in off-target effects on the expression of other genes in the block, potentially via the disruption of upstream promoters or regulatory regions or read-through of transcription from the promoters of deleted genes to downstream genes **(Figure 6.22)**. This finding limits the conclusions that can be made without validation of the observed effects.

A final limitation of the work described in this chapter is the lack of correspondence between the single-gene-deletion virus and gene expression screens. One source of this variation is likely to be the presence of V5 tags on the C-terminus of each of the exogenously expressed viral proteins, which may inhibit the folding or function of key protein domains. This was indeed the case for US33A, as there was little correlation in protein abundance between cells expressing pUS33A-V5 or untagged pUS33A. In the future, where virus protein expression is used for screening purposes, untagged, native versions of the proteins could be expressed, with confirmation of transcript expression by qPCR. Alternatively, the disparate results obtained from these two screens may be a result of differential levels of expression achieved through infection vs exogenous expression, or mislocalisation of exogenously expressed proteins in the absence of other viral gene products.

Chapter 7: Concluding remarks

The aim of this project was to identify antiviral factors based on their degradation by HCMV, and then characterise the function and mechanism of degradation. To achieve this, a variety of experimental techniques were used, from classical biochemical approaches to viral replication assays and quantitative proteomic screens.

This project was not conducted without setbacks or difficulties. However, it is hoped that the troubleshooting and method development described in this thesis will provide a solid foundation for those studying antiviral factors using these systems in the future. First, the development of the two-colour restriction assay system, which reduces variability introduced through cell seeding, represents a significant methodological advancement that produced highly reproducible results with known antiviral factors Sp100 and DAXX. Second, quantitative proteomics was shown to be a useful method for quantifying the off-target effects of different methods used to modify cells in culture, and could be used in the future to validate new methods. For example, short hairpin RNA (shRNA) transduction was found to result in global disruption of the cellular proteome, which likely explains the significant phenotypic variability observed by restriction and plaque assays. The same effect was not seen upon small interfering RNA (siRNA) transfection, which is now the method of choice in our group. Finally, this work highlights some of the limitations associated with the use of chemical inhibitors for studying virus-host interactions. MG132 and bortezomib have been instrumental in the discovery of host proteins degraded by HCMV, including HLTF [62], SLFN11 [127], and, likely, DMXL1. However, their ability to disrupt wide-ranging cellular processes via inhibition of the proteasome, such as necroptosis and autophagy, may result in changes in protein abundance that are incorrectly attributed to their effect on the proteasome. Experiments should be designed with these secondary effects in mind, ensuring that a combination of approaches are used to validate any findings.

One of the key discoveries of this thesis is that HCMV protein pUL36 is necessary and sufficient for the inhibition of necroptotic cell death, in addition to its previously established role in the inhibition of apoptosis. It was shown that pUL36 interacts with and downregulates MLKL, the terminal effector of necroptosis. Although the exact mechanism of MLKL downregulation remains uncharacterised, proposals include proteasomal degradation, facilitated by interactions between pUL36 and cellular E3 ligases, or sequestration of MLKL in detergent-resistant membrane complexes. MLKL exhibits many of the common characteristics of an intrinsic antiviral restriction factor: its expression is constitutive and independent of but amplified by IFN, it exhibits signatures of positive selection and is antagonised by a viral protein. However, as it does not inhibit virus replication directly, instead exerting its effect on

HCMV through its ability to execute necroptosis, MLKL would not be considered an antiviral restriction factor. Despite this, the role of MLKL in necroptosis makes it a key component of the cell-intrinsic IFN-independent immune response to HCMV. Pharmacological inhibition of the interaction between pUL36 and MLKL may provide an opportunity to counteract HCMV-mediated suppression of cell death and selectively eliminate infected cells.

HCMV was also found to downregulate DMXL1, a host protein implicated in the regulation of the vacuolar-type H^+-adenosine triphosphatase (V-ATPase) and endosomal acidification. Downregulation of DMXL1 was shown to be dependent on HCMV protein pUS33A, which is proposed to target DMXL1 for proteasomal degradation by recruiting the E3 ligase complex KPC. Although the function of DMXL1 in virus infection remains undefined, the role of the V-ATPase in endosomal trafficking, viral assembly compartment formation, autophagy and immune signalling suggests that HCMV-mediated downregulation of DMXL1 is likely to have diverse impacts on the outcome of viral infection that are highly dependent on the timing of DMXL1 downregulation. DMXL1 is constitutively expressed in many human tissues, stimulated by HCMV infection in the absence of US33A and antagonised by a viral protein, making it a prime candidate for a component of the intrinsic immune response.

In addition to these key findings, this thesis also reports the results of a range of proteomic screens that will enable the identification of additional antiviral host proteins **(Chapter 4)** and the characterisation of virus protein function **(Chapter 6)**. Further details are provided in the individual discussion sections for each chapter, which also provide ideas for further experiments to develop on this work. Many of these experiments are now being taken forward by existing and new members of our group – I look forward to seeing the results.

Alice Fletcher-Etherington

September 2021

Bibliography

1 International Committee on Taxonomy of Viruses. Taxonomy. [Accessed January 8, 2021] Available from: https://talk.ictvonline.org/information/.

2 Davison AJ. Overview of classification. In Human Herpesviruses: Biology, Therapy, and Immunoprophylaxis. Cambridge University Press, 2007; 3-9.

3 Mocarski ES, Shenk T, Griffiths P, *et al.* Cytomegaloviruses. In Knipe DM, Howley PM, eds. Fields Virology. 6th ed. Philadelphia, PA: Lippincott Williams & Wilkins, 2013; 1960-2014.

4 Zuhair M, Smit GSA, Wallis G, *et al.* Estimation of the worldwide seroprevalence of cytomegalovirus: A systematic review and meta-analysis. *Rev Med Virol* 2019; **29**: e2034

5 Stowell JD, Forlin-Passoni D, Din E, *et al.* Cytomegalovirus survival on common environmental surfaces: Opportunities for viral transmission. *J Infect Dis* 2012; **205**: 211-214

6 Britt W. Maternal immunity and the natural history of congenital human cytomegalovirus infection. *Viruses* 2018; **10**: 405

7 Fisher S, Genbacev O, Maidji E, *et al.* Human cytomegalovirus infection of placental cytotrophoblasts in vitro and in utero: implications for transmission and pathogenesis. *J Virol* 2000; **74**: 6808-6820

8 Rafailidis PI, Mourtzoukou EG, Varbobitis IC, *et al.* Severe cytomegalovirus infection in apparently immunocompetent patients: A systematic review. *Virol J* 2008; **5**: 47

9 Britt WJ. Congenital human cytomegalovirus infection and the enigma of maternal immunity. *J Virol* 2017; **91**: e02392-16

10 Springer KL, Weinberg A. Cytomegalovirus infection in the era of HAART: Fewer reactivations and more immunity. *J Antimicrob Chemother* 2004; **54**: 582-586

11 Ford N, Shubber Z, Saranchuk P, *et al.* Burden of HIV-related cytomegalovirus retinitis in resource-limited settings: A systematic review. *Clin Infect Dis* 2013; **57**: 1351-1361

12 Griffiths P, Baraniak I, Reeves M. The pathogenesis of human cytomegalovirus. *J Pathol* 2015; **235**: 288-297

13 Meesing A, Razonable RR. New developments in the management of cytomegalovirus infection after transplantation. *Drugs* 2018; **78**: 1085-1103

14 Kenneson A, Cannon MJ. Review and meta-analysis of the epidemiology of congenital cytomegalovirus (CMV) infection. *Rev Med Virol* 2007; **17**: 253-276

15 Boppana SB, Rivera LB, Fowler KB, *et al.* Intrauterine transmission of cytomegalovirus to infants of women with preconceptional immunity. *N Engl J Med* 2001; **344**: 1366-1371

16 Huang ES, Alford CA, Reynolds DW, *et al.* Molecular epidemiology of cytomegalovirus infections in women and their infants. *N Engl J Med* 1980; **303**: 958-962

17 Du Y, Zhang G, Liu Z. Human cytomegalovirus infection and coronary heart disease: a systematic review. *Virol J* 2018; **15**: 31

18 Lebedeva AM, Shpektor A V, Vasilieva EY, *et al.* Cytomegalovirus infection in cardiovascular

diseases. *Biochem* 2018; **83**: 1437-1447

19 Halenius A, Hengel H. Human cytomegalovirus and autoimmune disease. *Biomed Res Int* 2014: 472978

20 Garrido E. Clinical significance of cytomegalovirus infection in patients with inflammatory bowel disease. *World J Gastroenterol* 2013; **19**: 17

21 Dioverti MV, Razonable RR. Cytomegalovirus. *Microbiol Spectr* 2016; **4**: DMIH2-0022-2015

22 Rahman M, Dastmalchi F, Karachi A, *et al.* The role of CMV in glioblastoma and implications for immunotherapeutic strategies. *https://doi.org/101080/2162402X20181514921* 2018; **8**: e1514921

23 McFaline-Figueroa JR, Wen PY. The viral connection to glioblastoma. *Curr Infect Dis Reports 2017 192* 2017; **19**: 1-5

24 Wang SC, Chen SJ, Chen YC. Potential therapeutic approaches against brain diseases associated with cytomegalovirus infections. *Int J Mol Sci 2020, Vol 21, Page 1376* 2020; **21**: 1376

25 Olsson J, Wikby A, Johansson B, *et al.* Age-related change in peripheral blood T-lymphocyte subpopulations and cytomegalovirus infection in the very old: the Swedish longitudinal OCTO immune study. *Mech Ageing Dev* 2001; **121**: 187-201

26 Wikby A, Johansson B, Olsson J, *et al.* Expansions of peripheral blood CD8 T-lymphocyte subpopulations and an association with cytomegalovirus seropositivity in the elderly: The Swedish NONA immune study. *Exp Gerontol* 2002; **37**: 445-453

27 Pawelec G, Akbar A, Caruso C, *et al.* Is immunosenescence infectious? *Trends Immunol* 2004; **25**: 406-410

28 Trzonkowski P, Myśliwska J, Szmit E, *et al.* Association between cytomegalovirus infection, enhanced proinflammatory response and low level of anti-hemagglutinins during the anti-influenza vaccination—an impact of immunosenescence. *Vaccine* 2003; **21**: 3826-3836

29 Wald A, Selke S, Magaret A, *et al.* Impact of human cytomegalovirus (CMV) infection on immune response to pandemic 2009 H1N1 influenza vaccine in healthy adults. *J Med Virol* 2013; **85**: 1557-1560

30 Den Elzen WPJ, Vossen ACMT, Cools HJM, *et al.* Cytomegalovirus infection and responsiveness to influenza vaccination in elderly residents of long-term care facilities. *Vaccine* 2011; **29**: 4869-4874

31 van den Berg SPH, Warmink K, Borghans JAM, *et al.* Effect of latent cytomegalovirus infection on the antibody response to influenza vaccination: a systematic review and meta-analysis. *Med Microbiol Immunol* 2019; **208**: 305-321

32 Semmes EC, Hurst JH, Walsh KM, *et al.* Cytomegalovirus as an immunomodulator across the lifespan. *Curr Opin Virol* 2020; **44**: 112-120

33 Khan N, Hislop A, Gudgeon N, *et al.* Herpesvirus-specific CD8 T cell immunity in old age: cytomegalovirus impairs the response to a coresident EBV infection. *J Immunol* 2004; **173**: 7481-7489

34 Almanzar G, Schwaiger S, Jenewein B, *et al.* Long-term cytomegalovirus infection leads to significant changes in the composition of the CD8 + T-cell repertoire, which may be the basis for an imbalance in the cytokine production profile in elderly persons. *J Virol* 2005; **79**: 3675-3683

35 Lindau P, Mukherjee R, Gutschow M V., *et al.* Cytomegalovirus exposure in the elderly does

not reduce CD8 T cell repertoire diversity. *J Immunol* 2019; **202**: 476-483

36 De Bourcy CFA, Lopez Angel CJ, Vollmers C, *et al.* Phylogenetic analysis of the human antibody repertoire reveals quantitative signatures of immune senescence and aging. *Proc Natl Acad Sci U S A* 2017; **114**: 1105-1110

37 Hock Tan B. Cytomegalovirus treatment. *Curr Treat Options Infect Dis* 2014; **6**: 256-270

38 Lurain NS, Chou S. Antiviral drug resistance of human cytomegalovirus. *Clin Microbiol Rev* 2010; **23**: 689-712

39 Gagelmannd X, Ljungmand X, Styczynskid X, *et al.* Comparative efficacy and safety of different antiviral agents for cytomegalovirus prophylaxis in allogeneic hematopoietic cell transplantation: A systematic review and meta-analysis. *Biol Blood Marrow Transpl* 2018; **24**: 2101-2109

40 Frange P, Leruez-Ville M. Maribavir, brincidofovir and letermovir: Efficacy and safety of new antiviral drugs for treating cytomegalovirus infections. *Med Mal Infect* 2018; **48**: 495-502

41 Britt WJ, Prichard MN. New therapies for human cytomegalovirus infections. *Antiviral Res* 2018; **159**: 153-174

42 Polachek WS, Moshrif HF, Franti M, *et al.* High-throughput small interfering RNA screening identifies phosphatidylinositol 3-kinase class II alpha as important for production of human cytomegalovirus virions. *J Virol* 2016; **90**: 8360-8371

43 Lin Y-T, Prendergast J, Grey F. The host ubiquitin-dependent segregase VCP/p97 is required for the onset of human cytomegalovirus replication. *PLOS Pathog* 2017; **13**: e1006329

44 McCormick D, Lin YT, Grey F. Identification of host factors involved in human cytomegalovirus replication, assembly, and egress using a two-step small interfering RNA screen. *MBio* 2018; **9**: e00716-18

45 Strang BL. RO0504985 is an inhibitor of CMGC kinase proteins and has anti-human cytomegalovirus activity. *Antiviral Res* 2017; **144**: 21-26

46 Beelontally R, Wilkie GS, Lau B, *et al.* Identification of compounds with anti-human cytomegalovirus activity that inhibit production of IE2 proteins. *Antiviral Res* 2017; **138**: 61-67

47 Strang BL, Asquith CRM, Moshrif HF, *et al.* Identification of lead anti-human cytomegalovirus compounds targeting MAP4K4 via machine learning analysis of kinase inhibitor screening data. *PLoS One* 2018; **13**: e0201321

48 Khan AS, Murray MJ, Ho CMK, *et al.* High-throughput screening of a GlaxoSmithKline protein kinase inhibitor set identifies an inhibitor of human cytomegalovirus replication that prevents CREB and histone H3 post-translational modification. *J Gen Virol* 2017; **98**: 754-768

49 Krishna BA, Wills MR, Sinclair JH. Advances in the treatment of cytomegalovirus. *Br Med Bull* 2019; **131**: 5-17

50 Wills MR, Poole E, Lau B, *et al.* The immunology of human cytomegalovirus latency: Could latent infection be cleared by novel immunotherapeutic strategies? *Cell Mol Immunol* 2015; **12**: 128-138

51 Modlin JF, Arvin AM, Fast P, *et al.* Vaccine development to prevent cytomegalovirus disease: Report from the National Vaccine Advisory Committee. *Clin Infect Dis* 2004; **39**: 233-239

52 Scarpini S, Morigi F, Betti L, *et al.* Development of a vaccine against human cytomegalovirus: advances, barriers, and implications for the clinical practice. *Vaccines 2021, Vol 9, Page 551* 2021; **9**: 551

53 Mocarski ES, Shenk T, Pass RF. Cytomegaloviruses. In Knipe DM, Howley PM, eds. Fields Virology. 5th ed. Philadelphia, PA: Lippincott Williams & Wilkins, 2007; 2701-2772.

54 Gerna G, Kabanova A, Lilleri D. Human cytomegalovirus cell tropism and host cell receptors. *Vaccines* 2019; **7**: 1-18

55 Kalejta RF. Tegument proteins of human cytomegalovirus. *Microbiol Mol Biol Rev* 2008; **72**: 249-265

56 Varnum SM, Streblow DN, Monroe ME, *et al.* Identification of proteins in human cytomegalovirus (HCMV) particles: The HCMV proteome. *J Virol* 2004; **78**: 10960-10966

57 Kalejta RF. Functions of human cytomegalovirus tegument proteins prior to immediate early gene expression. In Shenk T, Stinski MF, eds. Human Cytomegalovirus. Current Topics in Microbiology and Immunology. 325th ed. Berlin, Heidelburg: Springer-Verlag, 2008; 101-115.

58 Gatherer D, Seirafian S, Cunningham C, *et al.* High-resolution human cytomegalovirus transcriptome. *PNAS* 2011; **108**: 19755-19760

59 Davison AJ. Comparative analysis of the genomes. In Human Herpesviruses: Biology, Therapy, and Immunoprophylaxis. Cambridge University Press, 2007; 10-26.

60 Roizman B, Pellett PE. The family Herpesviridae: A brief introduction. In Knipe DM, Howley PM, eds. Fields Virology. 4th ed. Philadelphia, PA: Lippincott Williams & Wilkins, 2001; 2381-2397.

61 Murphy E, Shenk T. HCMV genome. In Shenk T, Stinski MF, eds. Human Cytomegalovirus. Current Topics in Microbiology and Immunology. 325th ed. Berlin, Heidelburg: Springer-Verlag, 2008; 1-19.

62 Nightingale K, Lin K-M, Ravenhill BJ, *et al.* High-definition analysis of host protein stability during human cytomegalovirus infection reveals antiviral factors and viral evasion mechanisms. *Cell Host Microbe* 2018; **24**: 1-14

63 Stern-Ginossar N, Weisburd B, Michalski A, *et al.* Decoding human cytomegalovirus. *Science (80-)* 2012; **338**: 1088-1093

64 Van Damme E, Van Loock M, Nevels M, *et al.* Functional annotation of human cytomegalovirus gene products: An update. *Front Microbiol* 2014; **5**: 218

65 Dunn W, Chou C, Li H, *et al.* Functional profiling of a human cytomegalovirus genome. *Proc Natl Acad Sci U S A* 2003; **100**: 14223-14228

66 Wilkinson GWG, Davison AJ, Tomasec P, *et al.* Human cytomegalovirus: Taking the strain. *Med Microbiol Immunol* 2015; **204**: 273-284

67 Stanton RJ, Baluchova K, Dargan DJ, *et al.* Reconstruction of the complete human cytomegalovirus genome in a BAC reveals RL13 to be a potent inhibitor of replication. *J Clin Invest* 2010; **120**: 3191-3208

68 Dargan DJ, Douglas E, Cunningham C, *et al.* Sequential mutations associated with adaptation of human cytomegalovirus to growth in cell culture. *J Gen Virol* 2010; **91**: 1535-1546

69 Sinzger C, Digel M, Jahn G. Cytomegalovirus cell tropism. In Shenk T, Stinski MF, eds. Human Cytomegalovirus. Current Topics in Microbiology and Immunology. Vol 325. Berlin, Heidelburg: Springer-Verlag, 2008; 63-83.

70 Wang X, Huong SM, Chiu ML, *et al.* Epidermal growth factor receptor is a cellular receptor for human cytomegalovirus. *Nature* 2003; **424**: 456-461

71 Soroceanu L, Akhavan A, Cobbs CS. Platelet-derived growth factor-α receptor activation is

required for human cytomegalovirus infection. *Nature* 2008; **455**: 391-395

72 Feire AL, Koss H, Compton T. Cellular integrins function as entry receptors for human cytomegalovirus via a highly conserved disintegrin-like domain. *Proc Natl Acad Sci U S A* 2004; **101**: 15470-15475

73 Wille PT, Wisner TW, Ryckman B, *et al.* Human cytomegalovirus (HCMV) glycoprotein gB promotes virus entry in Trans acting as the viral fusion protein rather than as a receptor-binding protein. *MBio* 2013; **4**: e00332-13

74 Kari B, Gehrz R. A human cytomegalovirus glycoprotein complex designated gC-II is a major heparin-binding component of the envelope. *J Virol* 1992; **66**: 1761-1764

75 Zhou M, Lanchy J-M, Ryckman BJ. Human cytomegalovirus gH/gL/gO promotes the fusion step of entry into all cell types, whereas gH/gL/UL128-131 broadens virus tropism through a distinct mechanism. *J Virol* 2015; **89**: 8999-9009

76 Kabanova A, Marcandalli J, Zhou T, *et al.* Platelet-derived growth factor-α receptor is the cellular receptor for human cytomegalovirus gHgLgO trimer. *Nat Microbiol* 2016; **1**: 16082

77 Hahn G, Revello MG, Patrone M, *et al.* Human cytomegalovirus UL131-128 genes are indispensable for virus growth in endothelial cells and virus transfer to leukocytes. *J Virol* 2004; **78**: 10023-10033

78 Martinez-Martin N, Marcandalli J, Huang CS, *et al.* An unbiased screen for human cytomegalovirus identifies neuropilin-2 as a central viral receptor. *Cell* 2018; **174**: 1158-1171.e19

79 Compton T, Nepomuceno RR, Nowlin DM. Human cytomegalovirus penetrates host cells by pH-independent fusion at the cell surface. *Virology* 1992; **191**: 387-395

80 Hetzenecker S, Helenius A, Krzyzaniak MA. HCMV induces macropinocytosis for host cell entry in fibroblasts. *Traffic* 2016; **17**: 351-368

81 Ryckman BJ, Jarvis MA, Drummond DD, *et al.* Human cytomegalovirus entry into epithelial and endothelial cells depends on genes UL128 to UL150 and occurs by endocytosis and low-pH fusion. *J Virol* 2006; **80**: 710-722

82 Kahl M, Siegel-Axel D, Stenglein S, *et al.* Efficient lytic infection of human arterial endothelial cells by human cytomegalovirus strains. *J Virol* 2000; **74**: 7628-7635

83 Sinzger C, Kahl M, Laib K, *et al.* Tropism of human cytomegalovirus for endothelial cells is determined by a post-entry step dependent on efficient translocation to the nucleus. *J Gen Virol* 2000; **81**: 3021-3035

84 Strang BL. Viral and cellular subnuclear structures in human cytomegalovirus-infected cells. *J Gen Virol* 2015; **96**: 239-252

85 Kim Y-E, Oh SE, Kwon KM, *et al.* Involvement of the N-terminal deubiquitinating protease domain of human cytomegalovirus UL48 tegument protein in autoubiquitination, virion stability, and virus entry. *J Virol* 2016; **90**: 3229-3242

86 Weekes MP, Tomasec P, Huttlin EL, *et al.* Quantitative temporal viromics: an approach to investigate host-pathogen interaction. *Cell* 2014; **157**: 1460-1472

87 Reeves MB. Chromatin-mediated regulation of cytomegalovirus gene expression. *Virus Res* 2011; **157**: 134-143

88 Sarisky RT, Hayward GS. Evidence that the UL84 gene product of human cytomegalovirus is essential for promoting oriLyt-dependent DNA replication and formation of replication compartments in cotransfection assays. *J Virol* 1996; **70**: 7398-7413

89 Xu Y, Cei SA, Rodriguez Huete A, *et al.* Human cytomegalovirus DNA replication requires transcriptional activation via an IE2- and UL84-responsive bidirectional promoter element within ori Lyt. *J Virol* 2004; **78**: 11664-11677

90 Pari GS, Anders DG. Eleven loci encoding trans-acting factors are required for transient complementation of human cytomegalovirus oriLyt-dependent DNA replication. *J Virol* 1993; **67**: 6979-6988

91 Close WL, Anderson AN, Pellett PE. Betaherpesvirus virion assembly and egress. In Advances in Experimental Medicine and Biology. Vol 1045. Springer New York LLC, 2018; 167-207.

92 Yurochko AD. Human cytomegalovirus modulation of signal transduction. In Shenk T, Stinski MF, eds. Human Cytomegalovirus. Current Topics in Microbiology and Immunology. Vol 325. Berlin, Heidelburg: Springer Verlag, 2008; 205-220.

93 Rodríguez-Sánchez I, Munger J. Meal for two: Human cytomegalovirus-induced activation of cellular metabolism. *Viruses* 2019; **11**: 273

94 Spector DH. Human cytomegalovirus riding the cell cycle. *Med Microbiol Immunol* 2015; **204**: 409-419

95 Alwine JC. Modulation of host cell stress responses by human cytomegalovirus. In Shenk T, Stinski MF, eds. Human Cytomegalovirus. Current Topics in Microbiology and Immunology. Vol 325. Berlin, Heidelburg: Springer Verlag, 2008; 263-279.

96 DeMeritt IB, Milford LE, Yurochko AD. Activation of the NF-κB pathway in human cytomegalovirus-infected cells is necessary for efficient transactivation of the major immediate-early promoter. *J Virol* 2004; **78**: 4498-4507

97 Camozzi D, Pignatelli S, Valvo C, *et al.* Remodelling of the nuclear lamina during human cytomegalovirus infection: Role of the viral proteins pUL50 and pUL53. *J Gen Virol* 2008; **89**: 731-740

98 Alwine JC. The human cytomegalovirus assembly compartment: A masterpiece of viral manipulation of cellular processes that facilitates assembly and egress. *PLoS Pathog* 2012; **8**: e1002878

99 Das S, Pellett PE. Spatial relationships between markers for secretory and endosomal machinery in human cytomegalovirus-infected cells versus those in uninfected cells. *J Virol* 2011; **85**: 5864-5879

100 Das S, Vasanji A, Pellett PE. Three-dimensional structure of the human cytomegalovirus cytoplasmic virion assembly complex includes a reoriented secretory apparatus. *J Virol* 2007; **81**: 11861-11869

101 Shnayder M, Nachshon A, Krishna B, *et al.* Defining the transcriptional landscape during cytomegalovirus latency with single-cell RNA sequencing. *MBio* 2018; **9**: e00013-18

102 Cheng S, Caviness K, Buehler J, *et al.* Transcriptome-wide characterization of human cytomegalovirus in natural infection and experimental latency. *Proc Natl Acad Sci* 2017; **114**: E10586-E10595

103 Elder E, Sinclair J. HCMV latency: What regulates the regulators? *Med Microbiol Immunol* 2019; **208**: 431-438

104 Duggal NK, Emerman M. Evolutionary conflicts between viruses and restriction factors shape immunity. *Nat Rev Immunol* 2012; **12**: 687-695

105 Johnson WE. Rapid adversarial co-evolution of viruses and cellular restriction factors. In Cullen B, ed. Current Topics in Microbiology and Immunology. 371st ed. Springer, Berlin, Heidelberg, 2013; 123-151.

106 Yan N, Chen ZJ. Intrinsic antiviral immunity. *Nat Immunol* 2012; **13**: 214-222

107 Ashley CL, Abendroth A, McSharry BP, *et al.* Interferon-independent innate responses to cytomegalovirus. *Front Immunol* 2019; **10**: 2751

108 Everett RD, Young DF, Randall RE, *et al.* STAT-1- and IRF-3-dependent pathways are not essential for repression of ICP0-null mutant herpes simplex virus type 1 in human fibroblasts. *J Virol* 2008; **82**: 8871-8881

109 Nathans R, Cao H, Sharova N, *et al.* Small-molecule inhibition of HIV-1 Vif. *Nat Biotechnol* 2008; **26**: 1187-1192

110 Cen S, Peng Z-G, Li X-Y, *et al.* Small molecular compounds inhibit HIV-1 replication through specifically stabilizing APOBEC3G. *J Biol Chem* 2010; **285**: 16546-16552

111 Lukashchuk V, McFarlane S, Everett RD, *et al.* Human cytomegalovirus protein pp71 displaces the chromatin-associated factor ATRX from nuclear domain 10 at early stages of infection. *J Virol* 2008; **82**: 12543-12554

112 Tavalai N, Rechter S, Stamminger T. Nuclear domain 10 components promyelocytic leukemia protein and hDaxx independently contribute to an intrinsic antiviral defense against human cytomegalovirus infection. *J Virol* 2008; **82**: 126-137

113 Hwang J, Kalejta RF. Proteasome-dependent, ubiquitin-independent degradation of Daxx by the viral pp71 protein in human cytomegalovirus-infected cells. *Virology* 2007; **367**: 334-338

114 Sloan E, Orr A, Everett RD. MORC3, a component of PML nuclear bodies, has a role in restricting herpes simplex virus 1 and human cytomegalovirus. *J Virol* 2016; **90**: 8621-8633

115 Tavalai N, Rechter S, Leis M, *et al.* Evidence for a role of the cellular ND10 protein PML in mediating intrinsic immunity against human cytomegalovirus infections. *J Virol* 2006; **80**: 8006-8018

116 Schilling E-M, Scherer M, Reuter N, *et al.* The human cytomegalovirus IE1 protein antagonizes PML nuclear body-mediated intrinsic immunity via the inhibition of PML de novo SUMOylation. *J Virol* 2017; **91**: e02049-16

117 Adler M, Tavalai N, Mü R, *et al.* Human cytomegalovirus immediate-early gene expression is restricted by the nuclear domain 10 component Sp100. *J Gen Virol* 2011; **92**: 1532-1538

118 Kim Y-E, Lee J-H, Kim ET, *et al.* Human cytomegalovirus infection causes degradation of Sp100 proteins that suppress viral gene expression. *J Virol* 2011; **85**: 11928-11937

119 Weisblum Y, Oiknine-Djian E, Zakay-Rones Z, *et al.* APOBEC3A is upregulated by human cytomegalovirus (HCMV) in the maternal-fetal interface, acting as an innate anti-HCMV effector. *J Virol* 2017; **91**: e01296-17

120 Lee SH, Kalejta RF, Kerry J, *et al.* BclAF1 restriction factor is neutralized by proteasomal degradation and microRNA repression during human cytomegalovirus infection. *Proc Natl Acad Sci U S A* 2012; **109**: 9575-9580

121 Martinez FP, Cruz R, Lu F, *et al.* CTCF binding to the first intron of the major immediate early (MIE) gene of human cytomegalovirus (HCMV) negatively regulates MIE gene expression and HCMV replication. *J Virol* 2014; **88**: 7389-7401

122 Machala EA, Avdic S, Stern L, *et al.* Restriction of human cytomegalovirus infection by galectin-9. *J Virol* 2018; **93**: e01746-18

123 Zhang L, Wang B, Li L, *et al.* Antiviral effects of IFIT1 in human cytomegalovirus-infected fetal astrocytes. *J Med Virol* 2017; **89**: 672-684

124 Schilling M, Bulli L, Weigang S, *et al.* Human MxB protein is a pan-herpesvirus restriction factor. *J Virol* 2018; **92**: e01056-18

125 Kim ET, Roche KL, Kulej K, *et al.* SAMHD1 modulates early steps during human cytomegalovirus infection by limiting NF-κB activation. *Cell Rep* 2019; **28**: 434-448

126 Businger R, Deutschmann J, Gruska I, *et al.* Human cytomegalovirus overcomes SAMHD1 restriction in macrophages via pUL97. *Nat Microbiol* 2019; **4**: 2260-2272

127 Nightingale K, Fielding CA, Zerbe C, *et al.* Human cytomegalovirus protein RL1 degrades the antiviral factor SLFN11 via recruitment of the CRL4 E3 ubiquitin ligase complex. *bioRxiv* 2021

128 Reichel A, Stilp A-C, Scherer M, *et al.* Chromatin remodeling factor SPOC1 acts as a cellular restriction factor against human cytomegalovirus by repressing the major immediate-early promoter. *J Virol* 2018; **92**: e00342-18

129 Rauwel B, Jang SM, Cassano M, *et al.* Release of human cytomegalovirus from latency by a KAP1/TRIM28 phosphorylation switch. *Elife* 2015; **4**: e06068

130 Full F, van Gent M, Sparrer KMJ, *et al.* Centrosomal protein TRIM43 restricts herpesvirus infection by regulating nuclear lamina integrity. *Nat Microbiol* 2019; **4**: 164-176

131 Chin KC, Cresswell P. Viperin (cig5), an IFN-inducible antiviral protein directly induced by human cytomegalovirus. *Proc Natl Acad Sci U S A* 2001; **98**: 15125-15130

132 Seo J-Y, Cresswell P. Viperin regulates cellular lipid metabolism during human cytomegalovirus infection. Früh K, ed. *PLoS Pathog* 2013; **9**: e1003497

133 Lin Y-T, Chiweshe S, McCormick D, *et al.* Human cytomegalovirus evades ZAP detection by suppressing CpG dinucleotides in the major immediate early 1 gene. *PLOS Pathog* 2020; **16**: e1008844

134 Gonzalez-Perez AC, Stempel M, Wyler E, *et al.* The zinc finger antiviral protein ZAP restricts human cytomegalovirus and selectively binds and destabilizes viral UL4/UL5 transcripts. *MBio* 2021; **12**: 1-23

135 Boehme KW, Guerrero M, Compton T. Human cytomegalovirus envelope glycoproteins B and H are necessary for TLR2 activation in permissive cells. *J Immunol* 2006; **177**: 7094-7102

136 Compton T, Kurt-Jones EA, Boehme KW, *et al.* Human cytomegalovirus activates inflammatory cytokine responses via CD14 and Toll-like receptor 2. *J Virol* 2003; **77**: 4588-4596

137 Biolatti M, Gugliesi F, Dell'Oste V, *et al.* Modulation of the innate immune response by human cytomegalovirus. *Infect Genet Evol* 2018; **64**: 105-114

138 Paijo J, Döring M, Spanier J, *et al.* cGAS senses human cytomegalovirus and induces type I interferon responses in human monocyte-derived cells. *PLoS Pathog* 2016; **12**: e1005546

139 Isaacson MK, Juckem LK, Compton T. Virus entry and innate immune activation. In Shenk T, Stinski MF, eds. Human Cytomegalovirus. Current Topics in Microbiology and Immunology. 325th ed. Berlin, Heidelburg: Springer-Verlag, 2008; 85-100.

140 Paulus C, Nevels M. The human cytomegalovirus major immediate-early proteins as antagonists of intrinsic and innate antiviral host responses. *Viruses* 2009; **1**: 760-779

141 Biron CA, Byron KS, Sullivan JL. Severe herpesvirus infections in an adolescent without natural killer cells. *N Engl J Med* 1989; **320**: 1731-1735

142 Wu Z, Sinzger C, Reichel JJ, *et al.* Natural killer cells can inhibit the transmission of human

cytomegalovirus in cell culture by using mechanisms from innate and adaptive immune responses. *J Virol* 2015; **89**: 2906-2917

143 Iversen A-C, Norris PS, Ware CF, *et al.* Human NK cells inhibit cytomegalovirus replication through a noncytolytic mechanism involving lymphotoxin-dependent induction of IFN-β. *J Immunol* 2005; **175**: 7568-7574

144 Jackson SE, Mason GM, Wills MR. Human cytomegalovirus immunity and immune evasion. *Virus Res* 2010; **157**: 151-160

145 Fielding CA, Aicheler R, Stanton RJ, *et al.* Two novel human cytomegalovirus NK cell evasion functions target MICA for lysosomal degradation. *PLoS Pathog* 2014; **10**: e1004058

146 Fielding CA, Weekes MP, Nobre L V, *et al.* Control of immune ligands by members of a cytomegalovirus gene expansion suppresses natural killer cell activation. *Elife* 2017; **6**: e22206

147 Macagno A, Bernasconi NL, Vanzetta F, *et al.* Isolation of human monoclonal antibodies that potently neutralize human cytomegalovirus infection by targeting different epitopes on the gH/gL/UL128-131A complex. *J Virol* 2010; **84**: 1005-1013

148 Manandhar T, Hò GGT, Pump WC, *et al.* Battle between host immune cellular responses and HCMV immune evasion. *Int J Mol Sci* 2019; **20**: 3626

149 Sylwester AW, Mitchell BL, Edgar JB, *et al.* Broadly targeted human cytomegalovirus-specific CD4 and CD8 T cells dominate the memory compartments of exposed subjects. *J Exp Med* 2005; **202**: 673-685

150 Sellar RS, Peggs KS. Therapeutic strategies for cytomegalovirus infection in haematopoietic transplant recipients: A focused update. *Expert Opin Biol Ther* 2014; **14**: 1121-1126

151 Berry R, Watson GM, Jonjic S, *et al.* Modulation of innate and adaptive immunity by cytomegaloviruses. *Nat Rev Immunol* 2020; **20**: 113-127

152 Khairallah C, Déchanet-Merville J, Capone M. γδ T cell-mediated immunity to cytomegalovirus infection. *Front Immunol* 2017; **8**: 105

153 Jones TR, Hanson LK, Sun L, *et al.* Multiple independent loci within the human cytomegalovirus unique short region down-regulate expression of major histocompatibility complex class I heavy chains. *J Virol* 1995; **69**: 4830-4841

154 Wiertz EJHJ, Jones TR, Sun L, *et al.* The human cytomegalovirus US11 gene product dislocates MHC class I heavy chains from the endoplasmic reticulum to the cytosol. *Cell* 1996; **84**: 769-779

155 Jones TR, Wiertz EJHJ, Sun L, *et al.* Human cytomegalovirus US3 impairs transport and maturation of major histocompatibility complex class I heavy chains. *Proc Natl Acad Sci U S A* 1996; **93**: 11327-11333

156 Ahn K, Gruhler A, Galocha B, *et al.* The ER-luminal domain of the HCMV glypcoprotein US6 inhibits peptide translocation by TAP. *Immunity* 1997; **6**: 613-621

157 Mason GM, Jackson S, Okecha G, *et al.* Human cytomegalovirus latency-associated proteins elicit immune-suppressive IL-10 producing CD4+ T cells. Rooney CM, ed. *PLoS Pathog* 2013; **9**: e1003635

158 Cheung AKL, Gottlieb DJ, Plachter B, *et al.* The role of the human cytomegalovirus UL111A gene in down-regulating CD4+T-cell recognition of latently infected cells: Implications for virus elimination during latency. *Blood* 2009; **114**: 4128-4137

159 Dikic I. Proteasomal and autophagic degradation systems. *Annu Rev Biochem* 2017; **86**: 193-224

160 Hanna J, Guerra-Moreno A, Ang J, *et al.* Protein degradation and the pathologic basis of disease. *Am J Pathol* 2019; **189**: 94-103

161 Morreale FE, Walden H. Types of ubiquitin ligases. *Cell* 2016; **165**: 248

162 Kwon YT, Ciechanover A. The ubiquitin code in the ubiquitin-proteasome system and autophagy. *Trends Biochem Sci* 2017; **42**: 873-886

163 Livneh I, Kravtsova-Ivantsiv Y, Braten O, *et al.* Monoubiquitination joins polyubiquitination as an esteemed proteasomal targeting signal. *BioEssays* 2017; **39**: 1700027

164 Sun L, Chen ZJ. The novel functions of ubiquitination in signaling. *Curr Opin Cell Biol* 2004; **16**: 119-126

165 Gu H, Fada BJ. Specificity in ubiquitination triggered by virus infection. *Int J Mol Sci* 2020; **21**: 1-19

166 Luo H. Interplay between the virus and the ubiquitin–proteasome system: Molecular mechanism of viral pathogenesis. *Curr Opin Virol* 2016; **17**: 1-10

167 Le-Trilling VTK, Trilling M. Ub to no good: How cytomegaloviruses exploit the ubiquitin proteasome system. *Virus Res* 2020; **281**: 197938

168 Luzio JP, Pryor PR, Bright NA. Lysosomes: Fusion and function. *Nat Rev Mol Cell Biol* 2007; **8**: 622-632

169 Feher J. Cell Structure. In Quantitative Human Physiology. 2nd ed. Academic Press, 2017; 101-119.

170 Lamb CA, Yoshimori T, Tooze SA. The autophagosome: Origins unknown, biogenesis complex. *Nat Rev Mol Cell Biol* 2013; **14**: 759-774

171 Tognarelli EI, Reyes A, Corrales N, *et al.* Modulation of endosome function, vesicle trafficking and autophagy by human herpesviruses. *Cells* 2021; **10**: 542

172 Chaumorcel M, Lussignol M, Mouna L, *et al.* The human cytomegalovirus protein TRS1 inhibits autophagy via its interaction with Beclin 1. *J Virol* 2012; **86**: 2571-2584

173 Belzile J-P, Sabalza M, Craig M, *et al.* Trehalose, an mTOR-independent inducer of autophagy, inhibits human cytomegalovirus infection in multiple cell types. *J Virol* 2016; **90**: 1259-1277

174 Taisne C, Lussignol M, Hernandez E, *et al.* Human cytomegalovirus hijacks the autophagic machinery and LC3 homologs in order to optimize cytoplasmic envelopment of mature infectious particles. *Sci Rep* 2019; **9**: 4560

175 McFarlane S, Aitken J, Sutherland JS, *et al.* Early induction of autophagy in human fibroblasts after infection with human cytomegalovirus or herpes simplex virus 1. *J Virol* 2011; **85**: 4212-4221

176 Dr Michael Weekes | Cambridge Institute for Medical Research. [Accessed August 22, 2021] Available from: https://www.cimr.cam.ac.uk/staff/dr-michael-weekes.

177 Zhang Y, Fonslow BR, Shan B, *et al.* Protein analysis by shotgun/bottom-up proteomics. *Chem Rev* 2013; **113**: 2343

178 Yang F, Shen Y, Camp DG, *et al.* High pH reversed-phase chromatography with fraction concatenation as an alternative to strong-cation exchange chromatography for two-dimensional proteomic analysis. *Expert Rev Proteomics* 2012; **9**: 129

179 Fletcher-Etherington A, Weekes MP. Quantitative temporal viromics. *Annu Rev Virol* 2021; **8**: 159-181

180 Röst HL, Rosenberger G, Navarro P, *et al.* OpenSWATH enables automated, targeted analysis of data-independent acquisition MS data. *Nat Biotechnol* 2014; **32**: 219-223

181 Krasny L, Huang PH. Data-independent acquisition mass spectrometry (DIA-MS) for proteomic applications in oncology. *Mol Omi* 2020; **17**: 29-42

182 Chen X, Wei S, Ji Y, *et al.* Quantitative proteomics using SILAC: Principles, applications, and developments. *Proteomics* 2015; **15**: 3175-3192

183 Thompson A, Scha R, Kuhn K, *et al.* Tandem mass tags: A novel quantification strategy for comparative analysis of complex protein mixtures by MS/MS. *Anal Chem* 2003; **75**: 1895-1904

184 Ting L, Rad R, Gygi SP, *et al.* MS3 eliminates ratio distortion in isobaric labeling-based multiplexed quantitative proteomics. *Nat Methods* 2012; **8**: 937-940

185 Thompson A, Wö N, Koncarevic S, *et al.* TMTpro: Design, synthesis, and initial evaluation of a proline-based isobaric 16-plex tandem mass tag reagent set. *Anal Chem* 2019; **91**: 15941-15950

186 Jia S, Wang R, Wu K, *et al.* Elucidation of the mechanism of action for metal based anticancer drugs by mass spectrometry-based quantitative proteomics. *Mol 2019, Vol 24, Page 581* 2019; **24**: 581

187 Matheson NJ, Sumner J, Wals K, *et al.* Cell surface proteomic map of HIV infection reveals antagonism of amino acid metabolism by Vpu and Nef. *Cell Host Microbe* 2015; **18**: 409-423

188 Hsu JL, van den Boomen DJH, Tomasec P, *et al.* Plasma membrane profiling defines an expanded class of cell surface proteins selectively targeted for degradation by HCMV US2 in cooperation with UL141. *PLoS Pathog* 2015; **11**: e1004811

189 Li Y, Qin H, Ye M. An overview on enrichment methods for cell surface proteome profiling. *J Sep Sci* 2020; **43**: 292-312

190 Weekes MP, Antrobus R, Talbot S, *et al.* Proteomic plasma membrane profiling reveals an essential role for gp96 in the cell surface expression of LDLR family members, including the LDL receptor and LRP6. *J Proteome Res* 2012; **11**: 1475-1484

191 Weekes MP, Antrobus R, Lill JR, *et al.* Comparative analysis of techniques to purify plasma membrane proteins. *J Biomol Tech* 2010; **21**: 108-115

192 Wang LW, Shen H, Nobre L, *et al.* Epstein-Barr-virus-induced one-carbon metabolism drives B cell transformation. *Cell Metab* 2019; **30**: 539-555

193 Ersing I, Nobre L, Wang LW, *et al.* A temporal proteomic map of Epstein-Barr virus lytic replication in B cells. *Cell Rep* 2017; **19**: 1479-1493

194 Soh TK, Davies CTR, Muenzner J, *et al.* Temporal proteomic analysis of herpes simplex virus 1 infection reveals cell-surface remodeling via pUL56-mediated GOPC degradation. *Cell Rep* 2020; **33**: 108235

195 Caller LG, Davies CTR, Antrobus R, *et al.* Temporal proteomic analysis of BK polyomavirus infection reveals virus-induced G2 arrest and highly effective evasion of innate immune sensing. *J Virol* 2019; **93**: e00595-19

196 Soday L, Lu Y, Albarnaz JD, *et al.* Quantitative temporal proteomic analysis of vaccinia virus infection reveals regulation of histone deacetylases by an interferon antagonist. *Cell Rep* 2019; **27**: 1920-1933

197 Turnbull ML, Wise HM, Nicol MQ, *et al.* Role of the B allele of influenza A virus segment 8 in setting mammalian host range and pathogenicity. *J Virol* 2016; **90**: 9263-9284

198 Kisselev AF, Goldberg AL. Proteasome inhibitors: From research tools to drug candidates. *Chem Biol* 2001; **8**: 739-758

199 Lin K-M, Nightingale K, Soday L, *et al.* Rapid degradation pathways of host proteins during HCMV infection revealed by quantitative proteomics. *Front Cell Infect Microbiol* 2020; **10**: 578259

200 Rusinova I, Forster S, Yu S, *et al.* INTERFEROME v2.0: An updated database of annotated interferon-regulated genes. *Nucleic Acids Res* 2012; **41**: D1040-D1046

201 Murphy JM. The killer pseudokinase mixed lineage kinase domain-like protein (MLKL). *Cold Spring Harb Perspect Biol* 2020; **12**: a036376

202 Taylor RC, Cullen SP, Martin SJ. Apoptosis: Controlled demolition at the cellular level. *Nat Rev Mol Cell Biol* 2008; **9**: 231-241

203 Oberst A, Dillon C, Weinlich R, *et al.* Catalytic activity of the caspase-8-FLIP(L) complex inhibits RIPK3-dependent necrosis. *Nature* 2011; **471**: 363-368

204 Newton K, Wickliffe KE, Dugger DL, *et al.* Cleavage of RIPK1 by caspase-8 is crucial for limiting apoptosis and necroptosis. *Nature* 2019; **574**: 428-431

205 Zhang J, Yang Y, He W, *et al.* Necrosome core machinery: MLKL. *Cell Mol Life Sci* 2016; **73**: 2153-2163

206 Chen X, Li W, Ren J, *et al.* Translocation of mixed lineage kinase domain-like protein to plasma membrane leads to necrotic cell death. *Cell Res* 2014; **24**: 105-121

207 Sun L, Wang H, Wang Z, *et al.* Mixed lineage kinase domain-like protein mediates necrosis signaling downstream of RIP3 kinase. *Cell* 2012; **148**: 213-227

208 Petrie EJ, Czabotar PE, Murphy JM. The structural basis of necroptotic cell death signaling. *Trends Biochem Sci* 2019; **44**: 53-63

209 Skaletskaya A, Bartle LM, Chittenden T, *et al.* A cytomegalovirus-encoded inhibitor of apoptosis that suppresses caspase-8 activation. *Proc Natl Acad Sci U S A* 2001; **98**: 7829-7834

210 Upton JW, Kaiser WJ, Mocarski ES. DAI/ZBP1/DLM-1 complexes with RIP3 to mediate virus-induced programmed necrosis that is targeted by murine cytomegalovirus vIRA. *Cell Host Microbe* 2012; **11**: 290-297

211 Guo H, Omoto S, Harris PA, *et al.* Herpes simplex virus suppresses necroptosis in human cells. *Cell Host Microbe* 2015; **17**: 243-251

212 Upton J, Kaiser W, Mocarski E. Cytomegalovirus M45 cell death suppression requires receptor-interacting protein (RIP) homotypic interaction motif (RHIM)-dependent interaction with RIP1. *J Biol Chem* 2008; **283**: 16966-16970

213 Omoto S, Guo H, Talekar GR, *et al.* Suppression of RIP3-dependent necroptosis by human cytomegalovirus. *J Biol Chem* 2015; **290**: 11635-11648

214 Fletcher-Etherington A, Nobre L, Nightingale K, *et al.* Human cytomegalovirus protein pUL36: A dual cell death pathway inhibitor. *Proc Natl Acad Sci U S A* 2020; **117**: 18771-18779

215 Dutta N, Lashmit P, Yuan J, *et al.* The human cytomegalovirus UL133-138 gene locus attenuates the lytic viral cycle in fibroblasts. *PLoS One* 2015; **10**: e0120946

216 Gabaev I, Williamson JC, Crozier TWM, *et al.* Quantitative proteomics analysis of lytic KSHV infection in human endothelial cells reveals targets of viral immune modulation. *Cell Rep* 2020; **33**: 108249

217 Kraemer C, Enklaar T, Zabel B, *et al.* Mapping and structure of DMXL1, a human homologue of the DmX gene from Drosophila melanogaster coding for a WD repeat protein. *Genomics* 2000; **64**: 97-101

218 Jaskolka MC, Winkley SR, Kane PM. RAVE and rabconnectin-3 complexes as signal dependent regulators of organelle acidification. *Front Cell Dev Biol* 2021; **9**: 698190

219 Merkulova M, Păunescu TG, Azroyan A, *et al.* Mapping the H + (V)-ATPase interactome: Identification of proteins involved in trafficking, folding, assembly and phosphorylation. *Nat Publ Gr* 2015; **5**: 14827

220 Huttlin EL, Bruckner RJ, Navarrete-Perea J, *et al.* Dual proteome-scale networks reveal cell-specific remodeling of the human interactome. *Cell* 2021; **184**: 3022-3040.e28

221 Pavelin J, Reynolds N, Chiweshe S, *et al.* Systematic microRNA analysis identifies ATP6V0C as an essential host factor for human cytomegalovirus replication. *PLoS Pathog* 2013; **9**: e1003820

222 Pavelin J, Mccormick D, Chiweshe S, *et al.* Cellular v-ATPase is required for virion assembly compartment formation in human cytomegalovirus infection. *Open Biol* 2017; **7**: 160298

223 Leclercs S, Palaniswamis R, Xie B, *et al.* Molecular cloning and characterization of a factor that binds the human glucocorticoid receptor gene and represses its expression. *J Biol Chem* 1991; **266**: 17333-17340

224 Inoue-Toyoda M, Kato K, Nagata K, *et al.* Glucocorticoids facilitate the transcription from the human cytomegalovirus major immediate early promoter in glucocorticoid receptor- and nuclear factor-I-like protein-dependent manner. *Biochem Biophys Res Commun* 2015; **458**: 180-185

225 Tanaka J, Ogura T, Kamiya S, *et al.* Enhanced replication of human cytomegalovirus in human fibroblasts treated with dexamethasone. *J gen Virol* 1984; **65**: 1759-1767

226 Van Damme E, Sauviller S, Lau B, *et al.* Glucocorticosteroids trigger reactivation of human cytomegalovirus from latently infected myeloid cells and increase the risk for HCMV infection in D+R+ liver transplant patients. *J Gen Virol* 2015; **96**: 131-143

227 Arthur WT, Burridge K. RhoA inactivation by p190RhoGAP regulates cell spreading and migration by promoting membrane protrusion and polarity. *Mol Biol Cell* 2001; **12**: 2711-2720

228 Todorovic B, Nichols AC, Chitilian JM, *et al.* The human papillomavirus E7 proteins associate with p190RhoGAP and alter its function. *J Virol* 2014; **88**: 3653-3663

229 Zerenturk EJ, Sharpe LJ, Ikonen E, *et al.* Desmosterol and DHCR24: Unexpected new directions for a terminal step in cholesterol synthesis. *Prog Lipid Res* 2013; **52**: 666-680

230 Waterham HR, Koster J, Romeijn GJ, *et al.* Mutations in the 3b-hydroxysterol D 24-reductase gene cause desmosterolosis, an autosomal recessive disorder of cholesterol biosynthesis. *Am J Hum Genet* 2001; **69**: 685-694

231 Greeve I, Hermans-Borgmeyer I, Brellinger C, *et al.* The human DIMINUTO/DWARF1 homolog seladin-1 confers resistance to Alzheimer's disease-associated neurodegeneration and oxidative stress. *J Neurosci* 2000; **20**: 7345-7352

232 Róg T, Vattulainen I, Jansen M, *et al.* Comparison of cholesterol and its direct precursors along the biosynthetic pathway: Effects of cholesterol, desmosterol and 7-dehydrocholesterol on saturated and unsaturated lipid bilayers. *J Chem Phys* 2008; **129**: 6335

233 Vainio S, Jansen M, Koivusalo M, *et al.* Significance of sterol structural specificity. Desmosterol cannot replace cholesterol in lipid rafts. *J Biol Chem* 2005; **281**: 348-355

234 Tallorin L, Villareal V, Hsia C, *et al.* Hepatitis C virus NS3-4A protease regulates the lipid environment for RNA replication by cleaving host enzyme 24-dehydrocholesterol reductase. *J Biol Chem* 2020; **295**: 12426-12436

235 Sanchez V, Dong JJ. Alteration of lipid metabolism in cells infected with human cytomegalovirus. *Virology* 2010; **404**: 71-77

236 Low H, Mukhamedova N, Cui HL, *et al.* Cytomegalovirus restructures lipid rafts via US28/CDC42 mediated pathway enhancing cholesterol efflux from host cells. *Cell Rep* 2016; **16**: 186-200

237 Gunn-Moore FJ, Welsh GI, Herron LR, *et al.* A novel 4.1 ezrin radixin moesin (FERM)-containing protein, 'Willin'. *FEBS Lett* 2005; **579**: 5089-5094

238 Angus L, Moleirinho S, Herron L, *et al.* Willin/FRMD6 expression activates the Hippo signaling pathway kinases in mammals and antagonizes oncogenic YAP. *Oncogene* 2012; **31**: 238-250

239 Visser-Grieve S, Hao Y, Yang X. Human homolog of Drosophila expanded, hEx, functions as a putative tumor suppressor in human cancer cell lines independently of the Hippo pathway. *Oncogene* 2012; **31**: 1189-1195

240 Moleirinho S, Patrick C, Tilston-Lü Nel AM, *et al.* Willin, an upstream component of the Hippo signaling pathway, orchestrates mammalian peripheral nerve fibroblasts. *PLoS One* 2013; **8**: e60028

241 Xu Y, Wang K, Yu Q, *et al.* FRMD6 inhibits human glioblastoma growth and progression by negatively regulating activity of receptor tyrosine kinases. *Oncotarget* 2016; **7**: 70080-70091

242 Daigle D, Gradoville L, Tuck D, *et al.* Valproic acid antagonizes the capacity of other histone deacetylase inhibitors to activate the Epstein-Barr virus lytic cycle. *J Virol* 2011; **85**: 5628-5643

243 Zhang T, Zhang J, You X, *et al.* Hepatitis B virus X protein modulates oncogene yes-associated protein by CREB to promote growth of hepatoma cells. *Hepatology* 2012; **56**: 2051-2059

244 Liu G, Yu F-X, Kim Y, *et al.* Kaposi sarcoma-associated herpesvirus promotes tumorigenesis by modulating the Hippo pathway. *Oncogene* 2015; **34**: 3536–3546

245 Vladimer GI, Górna MW, Superti-Furga G, *et al.* IFITs: Emerging roles as key anti-viral proteins. *Front Immunol* 2014; **5**: 94

246 Yang Z, Liang H, Zhou Q, *et al.* Crystal structure of ISG54 reveals a novel RNA binding structure and potential functional mechanisms. *Cell Res* 2012; **22**: 1328-1338

247 Terenzi F, Hui DJ, Merrick WC, *et al.* Distinct induction patterns and functions of two closely related interferon-inducible human genes, ISG54 and ISG56. *J Biol Chem* 2006; **281**: 34064-34071

248 Pei R, Qin B, Zhang X, *et al.* Interferon-induced proteins with tetratricopeptide repeats 1 and 2 are cellular factors that limit hepatitis B virus replication. *J Innate Immun* 2014; **6**: 182-191

249 Liu R, Moss B. Vaccinia virus C9 ankyrin repeat/F-box protein is a newly identified antagonist of the type I interferon-induced antiviral state. *J Virol* 2018; **92**: 53-71

250 Li D, Swaminathan S. Human IFIT proteins inhibit lytic replication of KSHV: A new feed-forward loop in the innate immune system. *PLOS Pathog* 2019; **15**: e1007609

251 Navarro L, Mowen K, Rodems S, *et al.* Cytomegalovirus activates interferon immediate-early response gene expression and an interferon regulatory factor 3-containing interferon-stimulated

response element-binding complex. *Mol Cell Biol* 1998; **18**: 3796-3802

252 Zhu H, Cong J-P, Shenk T. Use of differential display analysis to assess the effect of human cytomegalovirus infection on the accumulation of cellular RNAs: Induction of interferon-responsive RNAs. *Microbiology* 1997; **94**: 13985-13990

253 Boyle KA, Pietropaolo RL, Compton T. Engagement of the cellular receptor for glycoprotein B of human cytomegalovirus activates the interferon-responsive pathway. *Mol Cell Biol* 1999; **19**: 3607-3613

254 Preston CM, Harman AN, Nicholl MJ. Activation of interferon response factor-3 in human cells infected with herpes simplex virus type 1 or human cytomegalovirus. *J Virol* 2001; **75**: 8909-8916

255 Neve EPA, Svensson K, Fuxe J, *et al.* VIPL, a VIP36-like membrane protein with a putative function in the export of glycoproteins from the endoplasmic reticulum. *Exp Cell Res* 2003; **288**: 70-83

256 Yamaguchi D, Kawasaki N, Matsuo I, *et al.* VIPL has sugar-binding activity specific for high-mannose-type N-glycans, and glucosylation of the α1,2 mannotriosyl branch blocks its binding. *Glycobiology* 2007; **17**: 1061-1069

257 Kamiya Y, Kamiya D, Yamamoto K, *et al.* Molecular basis of sugar recognition by the human L-type lectins ERGIC-53, VIPL, and VIP36. *J Biol Chem* 2008; **283**: 1857-1861

258 Zhang YC, Zhou Y, Yang CZ XD. A review of ERGIC-53: Its structure, functions, regulation and relations with diseases. *Histol Histopathol* 2009; **24**: 1193-1204

259 Zhang B, Cunningham MA, Nichols WC, *et al.* Bleeding due to disruption of a cargo-specific ER-to-Golgi transport complex. *Nat Genet* 2003; **34**: 220-225

260 Nufer O, Mitrovic S, Hauri H-P. Profile-based data base scanning for animal L-type lectins and characterization of VIPL, a novel VIP36-like endoplasmic reticulum protein. *J Biol Chem* 2003; **278**: 15886-15896

261 Hara-Kuge S, Ohkura T, Ideo H, *et al.* Involvement of VIP36 in intracellular transport and secretion of glycoproteins in polarized Madin-Darby canine kidney (MDCK) cells. *J Biol Chem* 2002; **277**: 16332-16339

262 McSharry BP, Jones CJ, Skinner JW, *et al.* Human telomerase reverse transcriptase-immortalized MRC-5 and HCA2 human fibroblasts are fully permissive for human cytomegalovirus. *J Gen Virol* 2001; **82**: 855-863

263 Allison R, Edgar JR, Pearson G, *et al.* Defects in ER-endosome contacts impact lysosome function in hereditary spastic paraplegia. *J Cell Biol* 2017; **216**: 1337-1355

264 GENEWIZ. [Accessed August 22, 2021] Available from: https://www.genewiz.com/en-GB.

265 Madeira F, Park YM, Lee J, *et al.* The EMBL-EBI search and sequence analysis tools APIs in 2019. *Nucleic Acids Res* 2019; **47**: W636-W641

266 DNASTAR Lasergene | Bioinformatics Software. [Accessed August 22, 2021] Available from: https://www.dnastar.com/software/lasergene/.

267 SnapGene | Software for everyday molecular biology. [Accessed August 22, 2021] Available from: https://www.snapgene.com/.

268 Hartley JL, Temple GF, Brasch MA. DNA cloning using in vitro site-specific recombination. *Genome Res* 2000; **10**: 1788-1795

269 Nobre L V, Nightingale K, Ravenhill BJ, *et al.* Human cytomegalovirus interactome analysis

identifies degradation hubs, domain associations and viral protein functions. *Elife* 2019; **8**: e49894

270 Glass M, Everett RD. Components of promyelocytic leukemia nuclear bodies (ND10) act cooperatively to repress herpesvirus infection. *J Virol* 2013; **87**: 2174-2185

271 Sanjana NE, Shalem O, Zhang F. Improved vectors and genome-wide libraries for CRISPR screening. *Nat Methods* 2014; **11**: 783-784

272 Shalem O, Sanjana NE, Hartenian E, *et al.* Genome-scale CRISPR-Cas9 knockout screening in human cells. *Science (80-)* 2014; **343**: 84-87

273 Wang T, Birsoy K, Hughes NW, *et al.* Identification and characterization of essential genes in the human genome. *Science (80-)* 2015; **350**: 1096-1101

274 Koike-Yusa H, Li Y, Tan EP, *et al.* Genome-wide recessive genetic screening in mammalian cells with a lentiviral CRISPR-guide RNA library. *Nat Biotechnol* 2014; **32**: 267-273

275 Ran FA, Hsu PD, Wright J, *et al.* Genome engineering using the CRISPR-Cas9 system. *Nat Protoc* 2013; **8143**: 2281-2308

276 Dolan A, Cunningham C, Hector RD, *et al.* Genetic content of wild-type human cytomegalovirus. *J Gen Virol* 2004; **85**: 1301-1312

277 Stanton RJ, McSharry BP, Rickards CR, *et al.* Cytomegalovirus destruction of focal adhesions revealed in a high-throughput western blot analysis of cellular protein expression. *J Virol* 2007; **81**: 7860-7872

278 FlowJo, LLC. [Accessed August 23, 2021] Available from: https://www.flowjo.com/.

279 Tandem Mass Tag Systems | Thermo Fisher Scientific - UK. [Accessed August 23, 2021] Available from: https://www.thermofisher.com/uk/en/home/life-science/protein-biology/protein-mass-spectrometry-analysis/protein-quantitation-mass-spectrometry/tandem-mass-tag-systems.html.

280 McAlister GC, Huttlin EL, Haas W, *et al.* Increasing the multiplexing capacity of TMT using reporter ion isotopologues with isobaric masses. *Anal Chem* 2012; **84**: 7469-7478

281 McAlister GC, Nusinow DP, Jedrychowski MP, *et al.* MultiNotch MS3 enables accurate, sensitive, and multiplexed detection of differential expression across cancer cell line proteomes. *Anal Chem* 2014; **86**: 7150-7158

282 Huttlin EL, Jedrychowski MP, Elias JE, *et al.* A tissue-specific atlas of mouse protein phosphorylation and expression. *Cell* 2010; **143**: 1174-1189

283 Käll L, Canterbury JD, Weston J, *et al.* Semi-supervised learning for peptide identification from shotgun proteomics datasets. *Nat Methods* 2007; **4**: 923-925

284 Saldanha AJ. Java Treeview—extensible visualization of microarray data. *Bioinformatics* 2004; **20**: 3246-3248

285 Huang DW, Sherman BT, Lempicki RA. Systematic and integrative analysis of large gene lists using DAVID bioinformatics resources. *Nat Protoc* 2008; **4**: 44-57

286 Huang DW, Sherman BT, Lempicki RA. Bioinformatics enrichment tools: Paths toward the comprehensive functional analysis of large gene lists. *Nucleic Acids Res* 2009; **37**: 1-13

287 Vizcaíno JA, Csordas A, del-Toro N, *et al.* 2016 update of the PRIDE database and its related tools. *Nucleic Acids Res* 2016; **44**: D447-D456

288 Deutsch EW, Csordas A, Sun Z, *et al.* The ProteomeXchange consortium in 2017: Supporting the cultural change in proteomics public data deposition. *Nucleic Acids Res* 2017; **45**: D1100-

D1106

289 Proux E, Studer RA, Bastien Moretti S, *et al.* Selectome: A database of positive selection. *Nucleic Acids Res* 2009; **37**: D404-7

290 Bastien Moretti S, Laurenczy B, Gharib WH, *et al.* Selectome update: Quality control and computational improvements to a database of positive selection. *Nucleic Acids Res* 2014; **42**: D917-21

291 Sievers F, Wilm A, Dineen D, *et al.* Fast, scalable generation of high-quality protein multiple sequence alignments using Clustal Omega. *Mol Syst Biol* 2011; **7**: 539

292 Clustal Omega < Multiple Sequence Alignment < EMBL-EBI. [Accessed August 23, 2021] Available from: https://www.ebi.ac.uk/Tools/msa/clustalo/.

293 Hildebrand A, Remmert M, Biegert A, *et al.* Fast and accurate automatic structure prediction with HHpred. *Proteins Struct Funct Bioinforma* 2009; **77**: 128-132

294 Kelley LA, Mezulis S, Yates CM, *et al.* The Phyre2 web portal for protein modeling, prediction and analysis. *Nat Protoc* 2015; **10**: 845-858

295 Roy A, Kucukural A, Zhang Y. I-TASSER: A unified platform for automated protein structure and function prediction. *Nat Protoc* 2010; **5**: 725-738

296 Yang J, Anishchenko I, Park H, *et al.* Improved protein structure prediction using predicted interresidue orientations. *Proc Natl Acad Sci U S A* 2020; **117**: 1496-1503

297 Goddard TD, Huang CC, Meng EC, *et al.* UCSF ChimeraX: Meeting modern challenges in visualization and analysis. *Protein Sci* 2018; **27**: 14-25

298 R Core Team. R: A language and environment for statistical computing. 2018. [Accessed August 30, 2021] Available from: https://www.r-project.org/.

299 Inkscape. [Accessed August 23, 2021] Available from: https://inkscape.org/.

300 Shannon P, Markiel A, Ozier O, *et al.* Cytoscape: A software environment for integrated models of biomolecular interaction networks. *Genome Res* 2003; **13**: 2498-2504

301 Cox J, Mann M. MaxQuant enables high peptide identification rates, individualized p.p.b.-range mass accuracies and proteome-wide protein quantification. *Nat Biotechnol* 2008; **26**: 1367-1372

302 Singhania R, Pavey S, Payne E, *et al.* Short interfering RNA induced generation and translation of stable 5′ mRNA cleavage intermediates. *Biochim Biophys Acta* 2016; **1859**: 1034-1042

303 Zhang J, Nielsen R, Yangà Z. Evaluation of an improved branch-site likelihood method for detecting positive selection at the molecular level. *Mol Biol Evol* 2005; **22**: 2472-2479

304 Clark E, Spector DH. Studies on the contribution of human cytomegalovirus UL21a and UL97 to viral growth and inactivation of the anaphase-promoting complex/cyclosome (APC/C) E3 ubiquitin ligase reveal a unique cellular mechanism for downmodulation of the APC/C subunits APC... *J Virol* 2015; **89**: 6928-6939

305 Kosar M, Giannattasio M, Piccini D, *et al.* The human nucleoporin Tpr protects cells from RNA-mediated replication stress. *Nat Commun* 2021; **12**: 3937

306 Jin Y, Li R, Zhang Z, *et al.* ZBED1/DREF: A transcription factor that regulates cell proliferation. *Oncol Lett* 2020; **20**: 137

307 Radko S, Koleva M, James K, *et al.* Adenovirus E1A targets the DREF nuclear factor to regulate virus gene expression, DNA replication, and growth. *J Virol* 2014; **88**: 13469-13481

308 Hao T, Xu J, Fang S, *et al.* Overexpression of ZNF460 predicts worse survival and promotes metastasis through JAK2/STAT3 signaling pathway in patient with colon cancer. *J Cancer* 2021; **12**: 3198-3208

309 Lo H-F, Tsai C-Y, Chen C-P, *et al.* Association of dysfunctional synapse defective 1 (SYDE1) with restricted fetal growth – SYDE1 regulates placental cell migration and invasion. *J Pathol* 2017; **241**: 324-336

310 Zhuma T, Tyrrell R, Sekkali B, *et al.* Human HMG box transcription factor HBP1: A role in hCD2 LCR function. *EMBO J* 1999; **18**: 6396-6406

311 Yoshimura S, Gerondopoulos A, Linford A, *et al.* Family-wide characterization of the DENN domain Rab GDP-GTP exchange factors. *J Cell Biol* 2010; **191**: 367-381

312 Houldcroft CJ, Jackson SE, Lim EY, *et al.* Assessing anti-HCMV cell mediated immune responses in transplant recipients and healthy controls using a novel functional assay. *Front Cell Infect Microbiol* 2020; **10**: 275

313 Sun X, Yin J, Starovasnik MA, *et al.* Identification of a novel homotypic interaction motif required for the phosphorylation of receptor-interacting protein (RIP) by RIP3. *J Biol Chem* 2002; **277**: 9505-9511

314 Murphy JM, Czabotar PE, Hildebrand JM, *et al.* The pseudokinase MLKL mediates necroptosis via a molecular switch mechanism. *Immunity* 2013; **39**: 443-453

315 Petrie EJ, Sandow JJ, Jacobsen A V, *et al.* Conformational switching of the pseudokinase domain promotes human MLKL tetramerization and cell death by necroptosis. *Nat Commun* 2018; **9**: 2422

316 Hildebrand JM, Tanzer MC, Lucet IS, *et al.* Activation of the pseudokinase MLKL unleashes the four-helix bundle domain to induce membrane localization and necroptotic cell death. *Proc Natl Acad Sci* 2014; **111**: 15072-15077

317 Samson AL, Zhang Y, Geoghegan ND, *et al.* MLKL trafficking and accumulation at the plasma membrane control the kinetics and threshold for necroptosis. *Nat Commun* 2020; **11**: 1-17

318 Quarato G, Guy CS, Grace CR, *et al.* Sequential engagement of distinct MLKL phosphatidylinositol-binding sites executes necroptosis. *Mol Cell* 2016; **61**: 589-601

319 Tanzer M, Matti I, Hildebrand J, *et al.* Evolutionary divergence of the necroptosis effector MLKL. *Cell Death Differ* 2016; **23**: 1185-1197

320 Wang H, Sun L, Su L, *et al.* Mixed lineage kinase domain-like protein MLKL causes necrotic membrane disruption upon phosphorylation by RIP3. *Mol Cell* 2014; **54**: 133-146

321 Yoon S, Bogdanov K, Kovalenko A, *et al.* Necroptosis is preceded by nuclear translocation of the signaling proteins that induce it. *Cell Death Differ* 2016; **23**: 253-260

322 He S, Wang L, Miao L, *et al.* Receptor interacting protein kinase-3 determines cellular necrotic response to TNF-α. *Cell* 2009; **137**: 1100-1111

323 Feng S, Yang Y, Mei Y, *et al.* Cleavage of RIP3 inactivates its caspase-independent apoptosis pathway by removal of kinase domain. *Cell Signal* 2007; **19**: 2056-2067

324 Kaiser WJ, Upton JW, Long AB, *et al.* RIP3 mediates the embryonic lethality of caspase-8-deficient mice. *Nature* 2011; **471**: 368-373

325 Holler N, Zaru R, Micheau O, *et al.* Fas triggers an alternative, caspase-8-independent cell death pathway using the kinase RIP as effector molecule. *Nat Immunol* 2000; **1**: 489-495

326 El-Mesery M, Shaker ME, Elgaml A. The SMAC mimetic BV6 induces cell death and sensitizes different cell lines to TNF-α and TRAIL-induced apoptosis. *Exp Biol Med* 2016; **241**: 2015-2022

327 Feoktistova M, Geserick P, Kellert B, *et al.* cIAPs block Ripoptosome formation, a RIP1/caspase-8 containing intracellular cell death complex differentially regulated by cFLIP isoforms. *Mol Cell* 2011; **43**: 449-463

328 Jacobsen A V, Lowes KN, Tanzer MC, *et al.* HSP90 activity is required for MLKL oligomerisation and membrane translocation and the induction of necroptotic cell death. *Cell Death Dis* 2016; **7**: e2051-e2051

329 Najafov A, Mookhtiar AK, Luu HS, *et al.* TAM kinases promote necroptosis by regulating oligomerization of MLKL. *Mol Cell* 2019; **75**: 457-468.e4

330 Dovey CM, Diep J, Clarke BP, *et al.* MLKL requires the inositol phosphate code to execute necroptosis. *Mol Cell* 2018; **70**: 936-948.e7

331 Zargarian S, Shlomovitz I, Erlich Z, *et al.* Phosphatidylserine externalization, "necroptotic bodies" release, and phagocytosis during necroptosis. *PLOS Biol* 2017; **15**: e2002711

332 Yoon S, Kovalenko A, Bogdanov K, *et al.* MLKL, the protein that mediates necroptosis, also regulates endosomal trafficking and extracellular vesicle generation. *Immunity* 2017; **47**: 51-65

333 Gong Y-N, Guy C, Olauson H, *et al.* ESCRT-III acts downstream of MLKL to regulate necroptotic cell death and its consequences. *Cell* 2017; **169**: 286-300.e16

334 Zhan C, Huang M, Yang X, *et al.* MLKL: Functions beyond serving as the executioner of necroptosis. *Theranostics* 2021; **11**: 4759

335 Bell BD, Leverrier S, Weist BM, *et al.* FADD and caspase-8 control the outcome of autophagic signaling in proliferating T cells. *Proc Natl Acad Sci U S A* 2008; **105**: 16677-16682

336 Altman AM, Miller MJ, Mahmud J, *et al.* Human cytomegalovirus-induced autophagy prevents necroptosis of infected monocytes. *J Virol* 2020; **94**: e01022-20

337 Nikoletopoulou V, Markaki M, Palikaras K, *et al.* Crosstalk between apoptosis, necrosis and autophagy. *Biochim Biophys Acta* 2013; **1833**: 3448-3459

338 Degterev A, Huang Z, Boyce M, *et al.* Chemical inhibitor of nonapoptotic cell death with therapeutic potential for ischemic brain injury. *Nat Chem Biol* 2005; **1**: 112-119

339 Ye YC, Yu L, Wang HJ, *et al.* TNFα-induced necroptosis and autophagy via supression of the p38–NF-κB survival pathway in L929 cells. *J Pharmacol Sci* 2011; **117**: 160-169

340 Frank D, Vaux DL, Murphy JM, *et al.* Activated MLKL attenuates autophagy following its translocation to intracellular membranes. *J Cell Sci* 2019; **132**: jcs220996

341 Conos SA, Chen KW, De Nardo D, *et al.* Active MLKL triggers the NLRP3 inflammasome in a cell-intrinsic manner. *Proc Natl Acad Sci U S A* 2017; **114**: E961-E969

342 Vince JE, Silke J. The intersection of cell death and inflammasome activation. *Cell Mol Life Sci* 2016; **73**: 2349-2367

343 Dai J, Zhang C, Guo L, *et al.* A necroptotic-independent function of MLKL in regulating endothelial cell adhesion molecule expression. *Cell Death Dis* 2020; **11**: 282

344 DeFilippis VR, Sali T, Alvarado D, *et al.* Activation of the interferon response by human cytomegalovirus occurs via cytoplasmic double-stranded DNA but not glycoprotein B. *J Virol* 2010; **84**: 8913-8925

345 DeFilippis VR, Alvarado D, Sali T, *et al.* Human cytomegalovirus induces the interferon

response via the DNA sensor ZBP1. *J Virol* 2010; **84**: 585-598

346 Tabeta K, Georgel P, Janssen E, *et al.* Toll-like receptors 9 and 3 as essential components of innate immune defense against mouse cytomegalovirus infection. *Proc Natl Acad Sci U S A* 2004; **101**: 3516-3521

347 Marshall E, Bierle C, Brune W, *et al.* Essential role for either TRS1 or IRS1 in human cytomegalovirus replication. *J Virol* 2009; **83**: 4112-4120

348 Balachandran S, Kim CN, Yeh WC, *et al.* Activation of the dsRNA-dependent protein kinase, PKR, induces apoptosis through FADD-mediated death signaling. *EMBO J* 1998; **17**: 6888

349 Brune W, Andoniou C. Die another day: Inhibition of cell death pathways by cytomegalovirus. *Viruses* 2017; **9**: 249

350 Arnoult D, Bartle LM, Skaletskaya A, *et al.* Cytomegalovirus cell death suppressor vMIA blocks Bax- but not Bak-mediated apoptosis by binding and sequestering Bax at mitochondria. *Proc Natl Acad Sci* 2004; **101**: 7988-7993

351 Xuan B, Qian Z, Torigoi E, *et al.* Human cytomegalovirus protein pUL38 induces ATF4 expression, inhibits persistent JNK phosphorylation, and suppresses endoplasmic reticulum stress-induced cell death. *J Virol* 2009; **83**: 3463-3474

352 Sun Y, Bao Q, Xuan B, *et al.* Human cytomegalovirus protein pUL38 prevents premature cell death by binding to ubiquitin-specific protease 24 and regulating iron metabolism. *J Virol* 2018; **92**: e00191-18

353 Zhu H, Shen Y, Shenk T. Human cytomegalovirus IE1 and IE2 proteins block apoptosis. *J Virol* 1995; **69**: 7960-7970

354 Patterson CE, Shenk T. Human cytomegalovirus UL36 protein is dispensable for viral replication in cultured cells. *J Virol* 1999; **73**: 7126-7131

355 McCormick AL, Skaletskaya A, Barry PA, *et al.* Differential function and expression of the viral inhibitor of caspase 8-induced apoptosis (vICA) and the viral mitochondria-localized inhibitor of apoptosis (vMIA) cell death suppressors conserved in primate and rodent cytomegaloviruses. *Virology* 2003; **316**: 221-233

356 Louise McCormick A, Roback L, Livingston-Rosanoff D, *et al.* The human cytomegalovirus UL36 gene controls caspase-dependent and-independent cell death programs activated by infection of monocytes differentiating to macrophages. *J Virol* 2010; **84**: 5108-5123

357 Chan G, Nogalski MT, Stevenson E V., *et al.* Human cytomegalovirus induction of a unique signalsome during viral entry into monocytes mediates distinct functional changes: a strategy for viral dissemination. *J Leukoc Biol* 2012; **92**: 743-752

358 Smith MS, Bentz GL, Alexander JS, *et al.* Human cytomegalovirus induces monocyte differentiation and migration as a strategy for dissemination and persistence. *J Virol* 2004; **78**: 4444-4453

359 Dufour F, Sasseville AM-J, Chabaud S, *et al.* The ribonucleotide reductase R1 subunits of herpes simplex virus types 1 and 2 protect cells against TNFα- and FasL-induced apoptosis by interacting with caspase-8. *Apoptosis* 2011; **16**: 256-271

360 Patrone M, Percivalle E, Secchi M, *et al.* The human cytomegalovirus UL45 gene product is a late, virion-associated protein and influences virus growth at low multiplicities of infection. *J Gen Virol* 2003; **84**: 3359-3370

361 Valyi-Nagy T, Bandi Z, Albrecht T. Hydrolysis of inositol lipids: an early signal of human cytomegalovirus infection. *Arch Virol* 1988; **101**: 199-207

362 Bradley AJ, Lurain NS, Ghazal P, *et al.* High-throughput sequence analysis of variants of human cytomegalovirus strains Towne and AD169. *J Gen Virol* 2009; **90**: 2375-2380

363 Dephoure N, Zhou C, Villé J, *et al.* A quantitative atlas of mitotic phosphorylation. *Proc Natl Acad Sci U S A* 2008; **105**: 10762-10767

364 Daub H, Olsen J V, Bairlein M, *et al.* Kinase-selective enrichment enables quantitative phosphoproteomics of the kinome across the cell cycle. *Mol Cell* 2008; **31**: 438-448

365 McComb S, Shutinoski B, Thurston S, *et al.* Cathepsins limit macrophage necroptosis through cleavage of RIP1 kinase. *J Immunol* 2014; **192**: 5671-5678

366 De Vasconcelos NM, Opdenbosch N Van, Van Gorp H, *et al.* Single-cell analysis of pyroptosis dynamics reveals conserved GSDMD-mediated subcellular events that precede plasma membrane rupture. *Cell Death Differ* 2019; **26**: 146-161

367 Kaiser WJ, Sridharan H, Huang C, *et al.* Toll-like receptor 3-mediated necrosis via TRIF, RIP3, and MLKL. *J Biol Chem* 2013; **288**: 31268-31279

368 Mandal P, Berger SB, Pillay S, *et al.* RIP3 induces apoptosis independent of pro-necrotic kinase activity. *Mol Cell* 2014; **56**: 481-495

369 Liu S, Liu H, Johnston A, *et al.* MLKL forms disulfide bond-dependent amyloid-like polymers to induce necroptosis. *Proc Natl Acad Sci U S A* 2017; **114**: E7450-E7459

370 Zhang D-W, Zheng M, Zhao J, *et al.* Multiple death pathways in TNF-treated fibroblasts: RIP3- and RIP1-dependent and independent routes. *Cell Res* 2011; **21**: 368-371

371 Christofferson DE, Li Y, Yuan J. Control of life-or-death decisions by RIP1 kinase. *Annu Rev Physiol* 2014; **76**: 129-150

372 Ros U, Peña-Blanco A, Hänggi K, *et al.* Necroptosis execution is mediated by plasma membrane nanopores independent of calcium. *Cell Rep* 2017; **19**: 175-187

373 Andoniou CE, Degli-Esposti MA. Insights into the mechanisms of CMV-mediated interference with cellular apoptosis. *Immunol Cell Biol* 2006; **84**: 99-106

374 Terhune S, Torigoi E, Moorman N, *et al.* Human cytomegalovirus UL38 protein blocks apoptosis. *J Virol* 2007; **81**: 3109-3123

375 Yu L, Alva A, Su H, *et al.* Regulation of an ATG7-beclin 1 program of autophagic cell death by caspase-8. *Science (80-)* 2004; **304**: 1500-1502

376 Sarikas A, Hartmann T, Pan ZQ. The cullin protein family. *Genome Biol* 2011; **12**: 220

377 Li D, Xie P, Zhao F, *et al.* F-box protein FBXO3 targets SMURF1 ubiquitin ligase for ubiquitination and degradation. *Biochem Biophys Res Commun* 2015; **458**: 941-945

378 Shao W, Zumer K, Fujinaga K, *et al.* FBXO3 protein promotes ubiquitylation and transcriptional activity of AIRE (Autoimmune Regulator). *J Biol Chem* 2016; **291**: 17953-17963

379 Shima Y, Shima T, Chiba T, *et al.* PML activates transcription by protecting HIPK2 and p300 from SCF FBX3-mediated degradation. *Mol Cell Biol* 2008; **28**: 7126-7138

380 Kainulainen M, Habjan M, Hubel P, *et al.* Virulence factor NSs of Rift Valley fever virus recruits the F-Box protein FBXO3 to degrade subunit p62 of general transcription factor TFIIH. *J Virol* 2014; **88**: 3464-3473

381 Behrends C, Sowa ME, Gygi SP, *et al.* Network organization of the human autophagy system. *Nature* 2010; **466**: 68-76

382 Sowa ME, Bennett EJ, Gygi SP, *et al.* Defining the human deubiquitinating enzyme interaction landscape. *Cell* 2009; **138**: 389-403

383 Huttlin EL, Ting L, Bruckner RJ, *et al.* The BioPlex network: A systematic exploration of the human interactome. *Cell* 2015; **162**: 425-440

384 Efstathiou S, Lawrence GL, Brown CM, *et al.* Identification of homologues to the human cytomegalovirus US22 gene family in human herpesvirus 6. *J Gen Virol* 1992; **73**: 1661-1671

385 Zhang D, Iyer LM, Aravind L. A novel immunity system for bacterial nucleic acid degrading toxins and its recruitment in various eukaryotic and DNA viral systems. *Nucleic Acids Res* 2011; **39**: 4532-4552

386 Shearer RF, Iconomou M, Watts CKW, *et al.* Functional roles of the E3 ubiquitin ligase UBR5 in cancer. *Mol Cancer Res* 2015; **13**: 1523-1532

387 Liu F, Cao L, Zhang T, *et al.* CRL4B(RBBP7) targets HUWE1 for ubiquitination and proteasomal degradation. *Biochem Biophys Res Commun* 2018; **501**: 440-447

388 Li M, Beg AA. Induction of necrotic-like cell death by tumor necrosis factor alpha and caspase inhibitors: Novel mechanism for killing virus-infected cells. *J Virol* 2000; **74**: 7470-7477

389 Moriwaki K, Chan FK-M. The inflammatory signal adaptor RIPK3: Functions beyond necroptosis. *Int Rev Cell Mol Biol* 2017; **328**: 253-275

390 Viswanathan K, Früh K, DeFilippis V. Viral hijacking of the host ubiquitin system to evade interferon responses. *Curr Opin Microbiol* 2010; **13**: 517-523

391 Liu X, Salokas K, Weldatsadik RG, *et al.* Combined proximity labeling and affinity purification−mass spectrometry workflow for mapping and visualizing protein interaction networks. *Nat Protoc* 2020; **15**: 3182-3211

392 Menzies SA, Volkmar N, van den Boomen DJH, *et al.* The sterol-responsive RNF145 E3 ubiquitin ligase mediates the degradation of HMG-CoA reductase together with gp78 and hrd1. *Elife* 2018; **7**: e40009

393 Ali M, Mocarski ES. Proteasome inhibition blocks necroptosis by attenuating death complex aggregation. *Cell Death Dis* 2018; **9**: 346

394 Ali M, Roback L, Mocarski ES. Herpes simplex virus 1 ICP6 impedes TNF receptor 1–induced necrosome assembly during compartmentalization to detergent-resistant membrane vesicles. *J Biol Chem* 2019; **294**: 991-1004

395 Lim J, Park H, Heisler J, *et al.* Autophagy regulates inflammatory programmed cell death via turnover of RHIM-domain proteins. *Elife* 2019; **8**: e44452

396 Ding W-X, Ni H-M, Gao W, *et al.* Linking of autophagy to ubiquitin-proteasome system is important for the regulation of endoplasmic reticulum stress and cell viability. *Am J Pathol* 2007; **171**: 513

397 Sun-Wada GH, Wada Y, Futai M. Diverse and essential roles of mammalian vacuolar-type proton pump ATPase: Toward the physiological understanding of inside acidic compartments. *Biochim Biophys Acta - Bioenerg* 2004; **1658**: 106-114

398 Futai M, Oka T, Sun-Wada G, *et al.* Luminal acidification of diverse organelles by V-ATPase in animal cells. *J Exp Biol* 2000; **203**: 107-116

399 Yoshimori T, Yamamoto A, Moriyama Y, *et al.* Bafilomycin A1, a specific inhibitor of vacuolar-type H(+)-ATPase, inhibits acidification and protein degradation in lysosomes of cultured cells. *J Biol Chem* 1991; **266**: 17707-17712

400 Mauvezin C, Nagy P, Juhász G, *et al.* Autophagosome-lysosome fusion is independent of V-ATPase-mediated acidification. *Nat Commun* 2015; **6**: 7007

401 Brown D, Paunescu TG, Breton S, *et al.* Regulation of the V-ATPase in kidney epithelial cells: Dual role in acid-base homeostasis and vesicle trafficking. *J Exp Biol* 2009; **212**: 1762-1772

402 Hurtado-Lorenzo A, Skinner M, El Annan J, *et al.* V-ATPase interacts with ARNO and Arf6 in early endosomes and regulates the protein degradative pathway. *Nat Cell Biol* 2006; **8**: 124-136

403 Schwartz JH, Li G, Yang Q, *et al.* Role of SNAREs and H + -ATPase in the targeting of proton pump-coated vesicles to collecting duct cell apical membrane. *Kidney Int* 2007; **72**: 1310-1315

404 Marshansky V, Rubinstein JL, Grüber G. Eukaryotic V-ATPase: Novel structural findings and functional insights. *Biochim Biophys Acta* 2014; **1837**: 857-879

405 Sethi N, Yan Y, Quek D, *et al.* Rabconnectin-3 is a functional regulator of mammalian notch signaling. *J Biol Chem* 2010; **285**: 34757-34764

406 Mangieri LR, Mader BJ, Thomas CE, *et al.* ATP6V0C knockdown in neuroblastoma cells alters autophagy-lysosome pathway function and metabolism of proteins that accumulate in neurodegenerative disease. *PLoS One* 2014; **9**: e93257

407 Pamarthy S, Kulshrestha A, Katara GK, *et al.* The curious case of vacuolar ATPase: Regulation of signaling pathways. *Mol Cancer* 2018; **17**: 41

408 Macfarlane D, Manzel L. Antagonism of immunostimulatory CpG-oligodeoxynucleotides by quinacrine, chloroquine, and structurally related compounds. *J Immunol* 1998; **160**: 1122-1131

409 Bénaroch P, Yilla M, Raposo G, *et al.* How MHC class II molecules reach the endocytic pathway. *EMBO J* 1995; **14**: 37

410 Marshansky V, Futai M. The V-type H+-ATPase in vesicular trafficking: Targeting, regulation and function. *Curr Opin Cell Biol* 2008; **20**: 415-426

411 Kawabe H, Sakisaka T, Yasumi M, *et al.* A novel rabconnectin-3-binding protein that directly binds a GDP/GTP exchange protein for Rab3A small G protein implicated in Ca2+-dependent exocytosis of neurotransmitter. *Genes to Cells* 2003; **8**: 537-546

412 Sakisaka T, Takai Y. Purification and properties of rabconnectin-3. *Methods Enzymol* 2005; **403**: 401-407

413 Yan Y, Denef N, Schüpbach T. The vacuolar proton pump (V-ATPase) is required for Notch signaling and endosomal trafficking in Drosophila. *Dev Cell* 2009; **17**: 387

414 Kane PM. Targeting reversible disassembly as a mechanism of controlling V-ATPase activity. *Curr Protein Pept Sci* 2012; **13**: 117-123

415 Li B, Clohisey SM, Shao Chia B, *et al.* Genome-wide CRISPR screen identifies host dependency factors for influenza A virus infection. *Nat Commun* 2020; **11**: 164

416 Mandic R, Fackler OT, Geyer M, *et al.* Negative factor from SIV binds to the catalytic subunit of the V-ATPase to internalize CD4 and to increase viral infectivity. *Mol Biol Cell* 2001; **12**: 463-473

417 König R, Zhou Y, Elleder D, *et al.* Global analysis of host-pathogen interactions that regulate early stage HIV-1 replication. *Cell Oct* 2008; **3**: 49-60

418 Brass AL, Dykxhoorn DM, Benita Y, *et al.* Identification of host proteins required for HIV infection through a functional genomic screen. *Science (80-)* 2008; **319**: 921-926

419 Weekes MP, Tan SYL, Poole E, *et al.* Latency-associated degradation of the MRP1 drug transporter during latent human cytomegalovirus infection. *Science* 2013; **340**: 199-202

420 Guo G, Ye S, Xie S, *et al.* The cytomegalovirus protein US31 induces inflammation through mono-macrophages in systemic lupus erythematosus by promoting NF-κB2 activation. *Cell Death Dis* 2018; **9**: 104

421 Goodrum FD, Jordan CT, High K, *et al.* Human cytomegalovirus gene expression during infection of primary hematopoietic progenitor cells: A model for latency. *Proc Natl Acad Sci U S A* 2002; **99**: 16255-16260

422 Salsman J, Zimmerman N, Chen T, *et al.* Genome-wide screen of three herpesviruses for protein subcellular localization and alteration of PML nuclear bodies. *PLOS Pathog* 2008; **4**: e1000100

423 Haller O, Staeheli P, Schwemmle M, *et al.* Mx GTPases: Dynamin-like antiviral machines of innate immunity. *Trends Microbiol* 2015; **23**: 154-163

424 Lee H-C, Lee E-S, Uddin MB, *et al.* Released tryptophanyl-tRNA synthetase stimulates innate immune responses against viral infection. *J Virol* 2019; **93**: e01291-18

425 Kamura T, Hara T, Matsumoto M, *et al.* Cytoplasmic ubiquitin ligase KPC regulates proteolysis of p27Kip1 at G1 phase. *Nat Cell Biol* 2004; **6**: 1229-1235

426 Kravtsova-Ivantsiv Y, Shomer I, Cohen-Kaplan V, *et al.* KPC1-mediated ubiquitination and proteasomal processing of NF-κB1 p105 to p50 restricts tumor growth. *Cell* 2015; **161**: 333-347

427 Yuan Y, Wang Y, Liu X, *et al.* KPC1 alleviates hypoxia/reoxygenation-induced apoptosis in rat cardiomyocyte cells though BAX degradation. *J Cell Physiol* 2019; **234**: 22921-22934

428 Wang S, Yang Y, Chen T, *et al.* RNF123 has an E3 ligase-independent function in RIG-I-like receptor-mediated antiviral signaling. *EMBO Rep* 2016; **17**: 1155-1168

429 Hara T, Kamura T, Kotoshiba S, *et al.* Role of the UBL-UBA protein KPC2 in degradation of p27 at G1 phase of the cell cycle. *Mol Cell Biol* 2005; **25**: 9292

430 Alto LT, Terman JR. Semaphorins and their signaling mechanisms. *Methods Mol Biol* 2017; **1493**: 1-25

431 Takamatsu H, Kumanogoh A. Diverse roles for semaphorin-plexin signaling in the immune system. *Trends Immunol* 2012; **33**: 127-135

432 Luo MH, Hannemann H, Kulkarni AS, *et al.* Human cytomegalovirus infection causes premature and abnormal differentiation of human neural progenitor cells. *J Virol* 2010; **84**: 3528

433 Kim YJ, Kim ET, Kim Y-E, *et al.* Consecutive inhibition of ISG15 expression and ISGylation by cytomegalovirus regulators. *PLOS Pathog* 2016; **12**: e1005850

434 Simoes da Silva CJ, Simón R, Busturia A. Epigenetic and non-epigenetic functions of the RYBP protein in development and disease. *Mech Ageing Dev* 2018; **174**: 111-120

435 Didovyk A, Borek B, Tsimring L, *et al.* Transcriptional regulation with CRISPR-Cas9: Principles, advances, and applications. *Curr Opin Biotechnol* 2016; **40**: 177

436 Lu J, Zhao C, Zhao Y, *et al.* Multimode drug inducible CRISPR/Cas9 devices for transcriptional activation and genome editing. *Nucleic Acids Res* 2018; **46**: e25-e25

437 Lussignol M, Esclatine A. Herpesvirus and autophagy: 'All right, everybody be cool, this is a robbery!' *Viruses* 2017; **9**: 372

438 Kimura S, Noda T, Yoshimori T. Dissection of the autophagosome maturation process by a novel reporter protein, tandem fluorescent-tagged LC3. *Autophagy* 2007; **3**: 452-460

439 Marques M, Ferreira A, Ribeiro D, *et al.* The interplay between human cytomegalovirus and pathogen recognition receptor signaling. *Viruses* 2018; **10**: 514

440 Wu N, Nguyen X-N, Wang L, *et al.* The interferon stimulated gene 20 protein (ISG20) is an innate defense antiviral factor that discriminates self versus non-self translation. *PLoS Pathog* 2019; **15**: e1008093

441 Power D, Santoso N, Dieringer M, *et al.* IFI44 suppresses HIV-1 LTR promoter activity and facilitates its latency. *Virology* 2015; **481**: 142-150

442 Carlton-Smith C, Elliott RM. Viperin, MTAP44, and protein kinase R contribute to the interferon-induced inhibition of bunyamwera orthobunyavirus replication. *J Virol* 2012; **86**: 11548-11557

443 Landolfo S, De Andrea M, Dell'Oste V, *et al.* Intrinsic host restriction factors of human cytomegalovirus replication and mechanisms of viral escape. *World J Virol* 2016; **5**: 87-96

444 Chemudupati M, Kenney AD, Bonifati S, *et al.* From APOBEC to ZAP: Diverse mechanisms used by cellular restriction factors to inhibit virus infections. *Biochim Biophys Acta Mol Cell Res* 2019; **1866**: 382-394

445 Kluge SF, Sauter D, Kirchhoff F. SnapShot: Antiviral restriction factors. *Cell* 2015; **163**: 774

446 Schilling EM, Scherer M, Stamminger T. Intrinsic immune mechanisms restricting human cytomegalovirus replication. *Viruses* 2021; **13**: 179

Appendix I: Primers and oligonucleotides

Appendix Table I: Primer sequences for cloning proteins for overexpression

Primer	*Sequence 5' → 3'*
Candidate antiviral restriction factors	
MLKL fwd	ggggacaagtttgtacaaaaaagcaggctatggaaaatttgaagcatattatc
MLKL rev	ggggaccactttgtacaagaaagctgggtctacttagaaaaggtggag
IFIT2 fwd	ggggacaagtttgtacaaaaaagcaggctatgagtgagaacaataagaattcc
IFIT2 rev	ggggaccactttgtacaagaaagctgggttcattccccattccagcttg
FRMD6 fwd	ggggacaagtttgtacaaaaaagcaggctatgaacaaattgaattttcataac
FRMD6 rev	ggggaccactttgtacaagaaagctgggtttacacaacaaactctggaac
UL36-V5	
UL36 fwd	ggggacaagtttgtacaaaaaagcaggctatggacgacctacgggacacgctgatggcc
UL36 V5 rev	ggggaccactttgtacaagaaagctgggtttattacgtagaatcaagacctaggagcgggttagggattgg
UL36-1 V5 rev	ggggaccactttgtacaagaaagctgggtttattacgtagaatcaagacctaggagcgggttagggattggcttaccagcgct gtggaagtggtcgcagtgacgaaagc
UL36-2/5 V5 rev	ggggaccactttgtacaagaaagctgggtttattacgtagaatcaagacctaggagcgggttagggattggcttaccagcgct gtggtttcggtgtcccttctttcccatg
UL36-3 V5 rev	ggggaccactttgtacaagaaagctgggtttattacgtagaatcaagacctaggagcgggttagggattggcttaccagcgct catgatcatggggtcaggggtttttttgggg
UL36-4/5 fwd	ggggacaagtttgtacaaaaaagcaggctactatgcgcgactaccagcg
UL36-4/6 V5 rev	ggggaccactttgtacaagaaagctgggtttattacgtagaatcaagacctaggagcgggttagggattggcttaccagcgct gttgttcatgtaggcgtgtggcg
UL36-6 fwd	ggggacaagtttgtacaaaaaagcaggctcctgaccccatgatcatgtttgacg
MLKL-HA	
MLKL fwd	ggggacaagtttgtacaaaaaagcaggctatggaaaatttgaagcatattatc
MLKL HA rev	ggggaccactttgtacaagaaagctgggtctaggcgtagtcgggcacgtcgtaggggtaagcgctcttagaaaaggtggag ag
MLKL-1/2 fwd	ggggacaagtttgtacaaaaaagcaggctgaaaatttgaagcatattatcaccc
MLKL-1 HA rev	ggggaccactttgtacaagaaagctgggtctaggcgtagtcgggcacgtcgtaggggtaagcgctatctcttcttagcatctg g
MLKL-2 HA rev	ggggaccactttgtacaagaaagctgggtctaggcgtagtcgggcacgtcgtaggggtaagcgctcttgatttgctcttgcgg
MLKL-3 fwd	ggggacaagtttgtacaaaaaagcaggctcaagagcaaatcaaggagatc
MLKL-3/4 HA rev	ggggaccactttgtacaagaaagctgggtctaggcgtagtcgggcacgtcgtaggggtaagcgctcttagaaaaggtggag agtttc
MLKL-4 fwd	ggggacaagtttgtacaaaaaagcaggctctaagaagagataatgaaaaaatagaagc
US33A-V5	
US33A fwd	ggggacaagtttgtacaaaaaagcaggctatgagcctcaggttccccg
US33A rev	ggggaccactttgtacaagaaagctgggtttaggaccgcggcacgtaaaac
V5-SA-US33A fwd	ggggacaagtttgtacaaaaaagcaggctatgggtaagccaatccctaacccgctcctaggtcttgattctacgagcgctagc ctcaggttccccgag
V5-GGGS-US33A fwd	ggggacaagtttgtacaaaaaagcaggctatgggtaagccaatccctaacccgctcctaggtcttgattctacgggaggtgg atcaagcctcaggttccccgag
US33A-GGGS-V5 rev	ggggaccactttgtacaagaaagctgggtttacgtagaatcaagacctaggagcgggttagggattggcttacctgatccac ctccggaccgcggcacgtaaaac

Appendix Table II: Primer combinations for cloning UL36-V5 and MLKL-HA domains

Construct	*Amino acids*	*Forward primer*	*Reverse primer*
UL36-V5 full-length	1-476	UL36 fwd	UL36 V5 rev
UL36-V5 #1	1-135	UL36 fwd	UL36-1 V5 rev
UL36-V5 #2	1-295	UL36 fwd	UL36-2/5 V5 rev
UL36-V5 #3	1-325	UL36 fwd	UL36-3 V5 rev
UL36-V5 #4	136-476	UL36-4/5 fwd	UL36-4/6 V5 rev
UL36-V5 #5	136-295	UL36-4/5 fwd	UL36-2/5 V5 rev
UL36-V5 #6	320-476	UL36-6 fwd	UL36-4/6 V5 rev
MLKL-HA full-length	1-471	MLKL fwd	MLKL HA rev
MLKL 4HB HA	2-154	MLKL-1/2 fwd	MLKL-1 HA rev
MLKL 4HB+Br HA	2-194	MLKL-1/2 fwd	MLKL-2 HA rev
MLKL PsKD HA	190-471	MLKL-3 fwd	MLKL-3/4 HA rev
MLKL PsKD+Br HA	151-471	MLKL-4 fwd	MLKL-3/4 HA rev

Appendix Table III: shRNA oligonucleotides

shRNA oligo	*Sequence 5' → 3'*
Control sh1 top	gatccgttataggctcgcaaaaggttcaagagacctttgcgagcctataacttttttg
Control sh1 bottom	aattcaaaaaagttataggctcgcaaaaggtctcttgaacctttgcgagcctataacg
Control sh2 top	gatccggcatataactatttaggtatttcaagagaatacctaaatagttatatgccttttttg
Control sh2 bottom	aattcaaaaaaggcatataactatttaggtattctcttgaaatacctaaatagttatatgccg
Control sh3 top	gatcccgtgatcttcaccgacaagatttcaagagaatcttgtcggtgaagatcacgtttttg
Control sh3 bottom	aattcaaaaaacgtgatcttcaccgacaagattctcttgaaatcttgtcggtgaagatcacgg
Control sh4 (DHCR24 sh2 scramble) top	gatccgacatatctcgcgtagaactgttcaagagacagttctacgcgagatatgtctttttg
Control sh4 bottom	aattcaaaaaagacatatctcgcgtagaactgtctcttgaacagttctacgcgagatatgtcg
Control sh5 (IFIT2 sh2 scramble) top	gatccaggtcgcgcttatacattccattcaagagatggaatgtataagcgcgacctttttttg
Control sh5 bottom	aattcaaaaaaaggtcgcgcttatacattccatctcttgaatggaatgtataagcgcgacctg
Control sh6 (DMXL1 sh1 scramble)	gatccatggtagtacgtatgaaccacttcaagagagtggttcatacgtactaccatttttttg
Control sh6 bottom	aattcaaaaaaatggtagtacgtatgaaccactctcttgaagtggttcatacgtactaccatg
ARHGAP35 sh1 top	gatccgcccttattctgaaacacattttcaagagaaatgtgtttcagaataagggctttttg
ARHGAP35 sh1 bottom	aattcaaaaaagcccttattctgaaacacatttctcttgaaaatgtgtttcagaataagggcg
ARHGAP35 sh2 top	gatcccataatcgaggctactcatatttcaagagaatatgagtagcctcgattatgttttttg
ARHGAP35 sh2 bottom	aattcaaaaaacataatcgaggctactcatattctcttgaaatatgagtagcctcgattatgg
DHCR24 sh1 top	gatccgctctcgcttatcttcgatatttcaagagaatatcgaagataagcgagagctttttttg
DHCR24 sh1 bottom	aattcaaaaaagctctcgcttatcttcgatattctcttgaaatatcgaagataagcgagagcg
DHCR24 sh2 top	gatccccgcgtgtgaaacactttgaattcaagagattcaaagtgtttcacacgcggttttttg
DHCR24 sh2 bottom	aattcaaaaaaccgcgtgtgaaacactttgaatctcttgaattcaaagtgtttcacacgcggg
DMXL1 sh1 top	gatccgcttccagtaaagaacgagttttcaagagaaactcgttctttactggaagctttttttg
DMXL1 sh1 bottom	aattcaaaaaagcttccagtaaagaacgagtttctcttgaaaactcgttctttactggaagcg
DMXL1 sh2 top	gatccgacattcagttggctcttgtattcaagagatacaagagccaactgaatgtctttttttg
DMXL1 sh2 bottom	aattcaaaaaagacattcagttggctcttgtatctcttgaatacaagagccaactgaatgtcg
DMXL1 sh3 top	gatccggaattaggctgtgataaattcaagagatttatcacagcctaattccttttttg
DMXL1 sh3 bottom	aattcaaaaaaggaattaggctgtgataaatctcttgaatttatcacagcctaattccg
DMXL1 sh4 top	gatccgggatatcctggaggtaaattcaagagatttacctccaggatatccctttttttg
DMXL1 sh4 bottom	aattcaaaaaagggatatcctggaggtaaatctcttgaatttacctccaggatatcccg
FRMD6 sh1 top	gatccgatgaagttccagagtttgttttcaagagaaacaaactctggaacttcatctttttttg
FRMD6 sh1 bottom	aattcaaaaaagatgaagttccagagtttgtttctcttgaaaacaaactctggaacttcatcg
FRMD6 sh2 top	gatccgccatgattctcaacactgattcaagagatcagtgttgagaatcatggctttttttg
FRMD6 sh2 bottom	aattcaaaaaagccatgattctcaacactgatctcttgaatcagtgttgagaatcatggcg
FRMD6 sh3 top	gatccgcacattccaaacatgcacaattcaagagattgtgcatgtttggaatgtgctttttttg
FRMD6 sh3 bottom	aattcaaaaaagcacattccaaacatgcacaatctcttgaattgtgcatgtttggaatgtgcg
IFIT2 sh1 top	gatccgcaacctactggcctatctaattcaagagattagataggccagtaggttgctttttttg
IFIT2 sh1 bottom	aattcaaaaaagcaacctactggcctatctaatctcttgaattagataggccagtaggttgcg
IFIT2 sh2 top	gatcccgactctcagacgttcagattttcaagagaaatctgaacgtctgagagtcgttttttg
IFIT2 sh2 bottom	aattcaaaaaacgactctcagacgttcagatttctcttgaaaatctgaacgtctgagagtcgg
LMAN2L sh1 top	gatccgaatctgcatggggatggcttttcaagagaaagccatccccatgcagattctttttttg
LMAN2L sh1 bottom	aattcaaaaaagaatctgcatggggatggctttctcttgaaaagccatccccatgcagattcg
LMAN2L sh2 top	gatccgccctcagtggacaatatgaattcaagagattcatattgtccactgagggctttttttg
LMAN2L sh2 bottom	aattcaaaaaagccctcagtggacaatatgaatctcttgaattcatattgtccactgagggcg
MLKL sh1 top	gatcccctctgacagtaactttgatattcaagagatatcaaagttactgtcagaggttttttg
MLKL sh1 bottom	aattcaaaaaacctctgacagtaactttgatatctcttgaatatcaaagttactgtcagaggg
MLKL sh2 top	gatccgaagcttcactgagacgattattcaagagataatcgtctcagtgaagcttctttttttg
MLKL sh2 bottom	aattcaaaaaagaagcttcactgagacgattatctcttgaataatcgtctcagtgaagcttcg

Appendix Table IV: CRISPR oligonucleotides

gRNA oligo	*Sequence 5' → 3'*	*gRNA oligo*	*Sequence 5' → 3'*
sgDHCR24_1_Fwd	caccggcacacggccagcgacacgg	sgDMXL_3_Fwd	caccgaaggcatataaaggaagtgg
sgDHCR24_1_Rev	aaacccgtgtcgctggccgtgtgcc	sgDMXL_3_Rev	aaacccacttcctttatatgccttc
sgDHCR24_2_Fwd	caccgggggagagtccagccaatgg	sgDMXL_4_Fwd	caccggaaagccgagacagaagcca
sgDHCR24_2_Rev	aaacccattggctggactctccccc	sgDMXL_4_Rev	aaactggcttctgtctcggctttcc
sgDHCR24_3_Fwd	caccgggcacacgaacacccagcgc	sgFRMD6_1_Fwd	caccgggaactgctgtggctggcgg
sgDHCR24_3_Rev	aaacgcgctgggtgttcgtgtgccc	sgFRMD6_1_Rev	aaacccgccagccacagcagttccc
sgDHCR24_4_Fwd	caccgtgagcttgatgacctcacag	sgFRMD6_2_Fwd	caccggaagaggacttacaggacga
sgDHCR24_4_Rev	aaacctgtgaggtcatcaagctcac	sgFRMD6_2_Rev	aaactcgtcctgtaagtcctcttcc
sgMLKL_1_Fwd	caccgtgatcaggccgaggacgcgg	sgFRMD6_3_Fwd	caccgtgtttctgaagagctcgagg
sgMLKL_1_Rev	aaacccgcgtcctcggcctgatcac	sgFRMD6_3_Rev	aaaccctcgagctcttcagaaacac
sgMLKL_2_Fwd	caccggaagggcagtcttcacccag	sgFRMD6_4_Fwd	caccgtggcagctcccacacctcag
sgMLKL_2_Rev	aaacctgggtgaagactgcccttcc	sgFRMD6_4_Rev	aaacctgaggtgtgggagctgccac
sgMLKL_3_Fwd	caccgaagaaccctaccatccacag	sgARHGAP35_1_Fwd	caccggattggagacaaacttgagc
sgMLKL_3_Rev	aaacctgtggatggtagggttcttc	sgARHGAP35_1_Rev	aaacgctcaagtttgtctccaatcc
sgMLKL_4_Fwd	caccgaatactgcaagaaacagtgc	sgARHGAP35_2_Fwd	caccggtatagctgctctgcaggga
sgMLKL_4_Rev	aaacgcactgtttcttgcagtattc	sgARHGAP35_2_Rev	aaactccctgcagagcagctatacc
sgLMAN2L_1_Fwd	caccggcaggggccacagcaagtcg	sgARHGAP35_3_Fwd	caccggtaaaggcagagacagccgt
sgLMAN2L_1_Rev	aaaccgacttgctgtggcccctgcc	sgARHGAP35_3_Rev	aaacacggctgtctctgcctttacc
sgLMAN2L_2_Fwd	caccggaatctgatgggcaatgcca	sgARHGAP35_4_Fwd	caccgggaatcgctatcctatgtag
sgLMAN2L_2_Rev	aaactggcattgcccatcagattcc	sgARHGAP35_4_Rev	aaacctacataggatagcgattccc
sgLMAN2L_3_Fwd	caccgaagaagaatctgcatgggga	sgIFIT2_1_Fwd	caccggacccaggcatagtttcccc
sgLMAN2L_3_Rev	aaactccccatgcagattcttcttc	sgIFIT2_1_Rev	aaacggggaaactatgcctgggtcc
sgLMAN2L_4_Fwd	caccggaagttgtttgaactgacag	sgIFIT2_2_Fwd	caccgtatgaagcttcagagccagg
sgLMAN2L_4_Rev	aaacctgtcagttcaaacaacttcc	sgIFIT2_2_Rev	aaaccctggctctgaagcttcatac
sgDMXL_1_Fwd	caccggagagagtttgcatcacctg	sgIFIT2_3_Fwd	caccggaagttagttgaagaagcct
sgDMXL_1_Rev	aaaccaggtgatgcaaactctctcc	sgIFIT2_3_Rev	aaacaggcttcttcaactaacttcc
sgDMXL_2_Fwd	caccggtggctggtcagttttgccg	sgIFIT2_4_Fwd	caccggaagccttggagaaagcccc
sgDMXL_2_Rev	aaaccggcaaaactgaccagccacc	sgIFIT2_4_Rev	aaacggggctttctccaaggcttcc

Appendix Table V: Synthesised DNA sequence for blasticidin resistance (BSR)

Sequence 5' → 3'	*Features*
cgggtacccattgtatgggatctgatctggggcctcggtgcacatgctttacatgtgtttagtcgaggttaaaaaaacgtctaggc cccccgaaccacggggacgtggttttcctttgaaaaacacgatgataatatggccacaaccATGAAAACATTTAAC ATTTCTCAACAAGATCTAGAATTAGTAGAAGTAGCGACAGAGAAGATTACAAT GCTTTATGAGGATAATAAACATCATGTGGGAGCGGCAATTCGTACGAAAACA GGAGAAATCATTTCGGCAGTACATATTGAAGCGTATATAGGACGAGTAACTGT TTGTGCAGAAGCCATTGCGATTGGTAGTGCAGTTTCGAATGGACAAAAGGATT TTGACACGATTGTAGCTGTTAGACACCCTTATTCTGACGAAGTAGATAGAAGT ATTCGAGTGGTAAGTCCTTGTGGTATGTGTAGGGAGTTGATTTCAGACTATGC ACCAGATTGTTTTGTGTTAATAGAAATGAATGGCAAGTTAGTCAAAACTACGA TTGAAGAACTCATTCCACTCAAATATACCCGAAATTAAtgcatcgatgg	KpnI and ClaI restriction enzyme sites Part of IRES BSR coding sequence

Appendix Table VI: Sequencing primers

Primer	*Direction*	*Primer sequence 5' → 3'*	*For sequencing inserts in…*
M13F-20	Fwd	gtaaaacgacggccag	pDONR221 and pDONR223
M1326-Rev	Rev	caggaaacagctatgac	
M13-40FOR	Fwd	gttttcccagtcacgac	pDONR225
SFFVp	Fwd	cgcgccagtcctccgattg	pHAGE-pSFFV
pHAGE-Rev	Rev	gcttcggccagtaacgtta	pHAGE-pSFFV
ARHGAP35_attL_REV	Rev	ccgtggaaacggatgaagg	pDONR225-ARHGAP35 and pHAGE-pSFFV-puroR-ARHGAP35
ARHGAP35 int 1	Rev	ctcctctttcttccggatgg	
ARHGAP35 int 2	Rev	agtgctacaagctgaatagg	
ARHGAP35 int 3	Rev	tttctgattccggtcagacg	
U6P	Fwd	gggcaggaagagggcctat	pHR-SIREN

Appendix Table VII: Site-directed mutagenesis primers

Amino acid mutation	*Codon mutation*	*Primer*	*Sequence 5' → 3'*	*Combined with*
UL36 I113V	ATC → GTC	Fwd	gcgcgactgcgtctacgagctggcgcccacc	UL36 V5 attB2 rev
		Rev	ccagctcgtagacgcagtcgcgcaggtcatcg	UL36 attB1 fwd
UL36 H126N	CAT→ AAT	Fwd	ttttctgcggaatggctttcgtcactgcgaccac	UL36 V5 attB2 rev
		Rev	gacgaaagccattccgcagaaaatccttcatg	UL36 attB1 fwd
UL36 C131R	TGC → CGC	Fwd	ctttcgtcaccgcgaccacttccacactatgcg	UL36 V5 attB2 rev
		Rev	ggaagtggtcgcggtgacgaaagccatgccgc	UL36 attB1 fwd
UL36 S177T	AGC → ACC	Fwd	cgcttcctacaccatcgacgacccttttcgatg	UL36 V5 attB2 rev
		Rev	ggtcgtcgatggtgtaggaagcgtagccccgc	UL36 attB1 fwd
UL36 A472V	GCC → GTC	Fwd	cccgccacacgtctacatgaacaacagcgctgg	UL36 V5 attB2 rev
		Rev	tgttcatgtagacgtgtggcggggtgaggggcg	UL36 attB1 fwd

Appendix Table VIII: TOPO cloning primers

Primer	*Direction*	*Primer sequence 5' → 3'*	*For TOPO cloning of*
D1 + D3	Fwd	cagaggttaccgccaggttt	Regions targeted by DHCR24 guides 1 and 3
D1 + D3	Rev	ggacatccagaagcaggtga	

Appendix Table IX: ON-TARGETplus SMARTPool siRNA sequences

Gene target	*siRNA sequences*
FBXO3	gcaagcuuccugacgauua gggaugaucucaagaaaua guuaguggguuccuggguua gagaccaaauuuucagaua
CUL1	caacgaagaguucagguuu cgaggaagaccgcaaacua agacagugcuugauguuca cauagaagacaaagacgua
UBR5	gcacuuauauacuggauua gauuguagguuacuuagaa gaucaauccuaacugaauu ggucgaagaugugcuacua
HUWE1	gcuuugggcuggccuaaua gcaguuggcggcuuucuua gagcccagaugacuaagua uaacaucaauuguccacuu
RBBP7	ccacuggucuccacauaau cggauaagaccguagcuuu gaaguaaaccgugcucguu auacaccguuucuauauga
DMXL1	aguaaugagaguacguuaa ccucaaaauuauaucgcaa gggauuauauagagcugaa cauaugagccuaacaggaa
RNF123	ggugaagcuucuagguaua gcacauggcggaccuccua caacugggccuucucugaa gcgcuacuauugggaugaa
UBAC1	gcuaauugaacacgcagaa gcacguagguggcguuguu cagaaugccgcgugcgagu agagaugagcugacggaaa
Non-targeting pool (control)	uggguuacaugucgacuaa uggguuacauguuguguga uggguuacauguuuucuga uggguuacauguuuuccua

Appendix Table X: SYBR Green qPCR primers

Primer	*Sequence 5' → 3'*
US33A qPCR fwd	gggttacgagaaactgggatac
US33A qPCR rev	aacggaaaagtgaacggcaa
GAPDH qPCR fwd	gaaatcccatcaccatcttccagg
GAPDH qPCR rev	gagccccagccttctccatg

Appendix II: Vectors

All vector maps were created with SnapGene [267].

Appendix Figure I: pDONR223

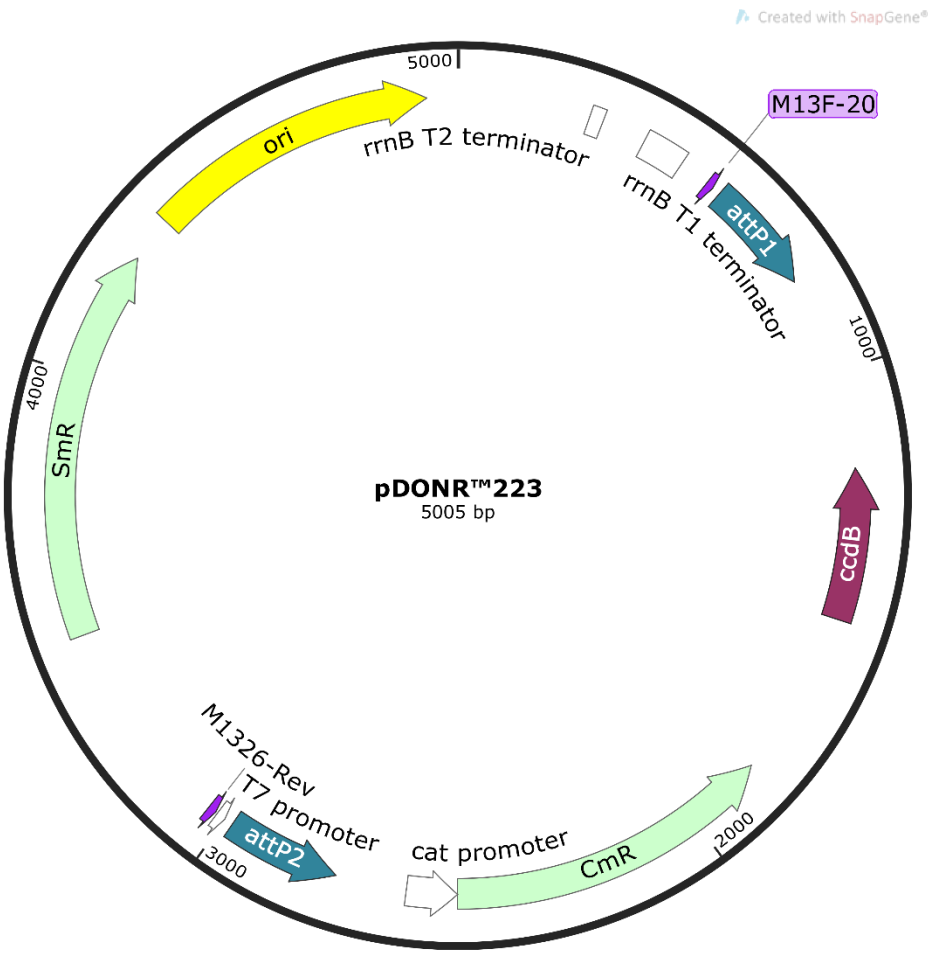

A Gateway BP recombination reaction between an *att*B-flanked DNA fragment and *att*P-containing pDONR vector leads to replacement of the ccdB toxin coding sequence and the chloramphenicol acetyltransferase resistance marker (cat/CmR) with the desired DNA sequence [268]. SmR, spectinomycin resistance; ori, pBR322 origin of replication.

Appendix Figure II: pHAGE-SFFV-puroR

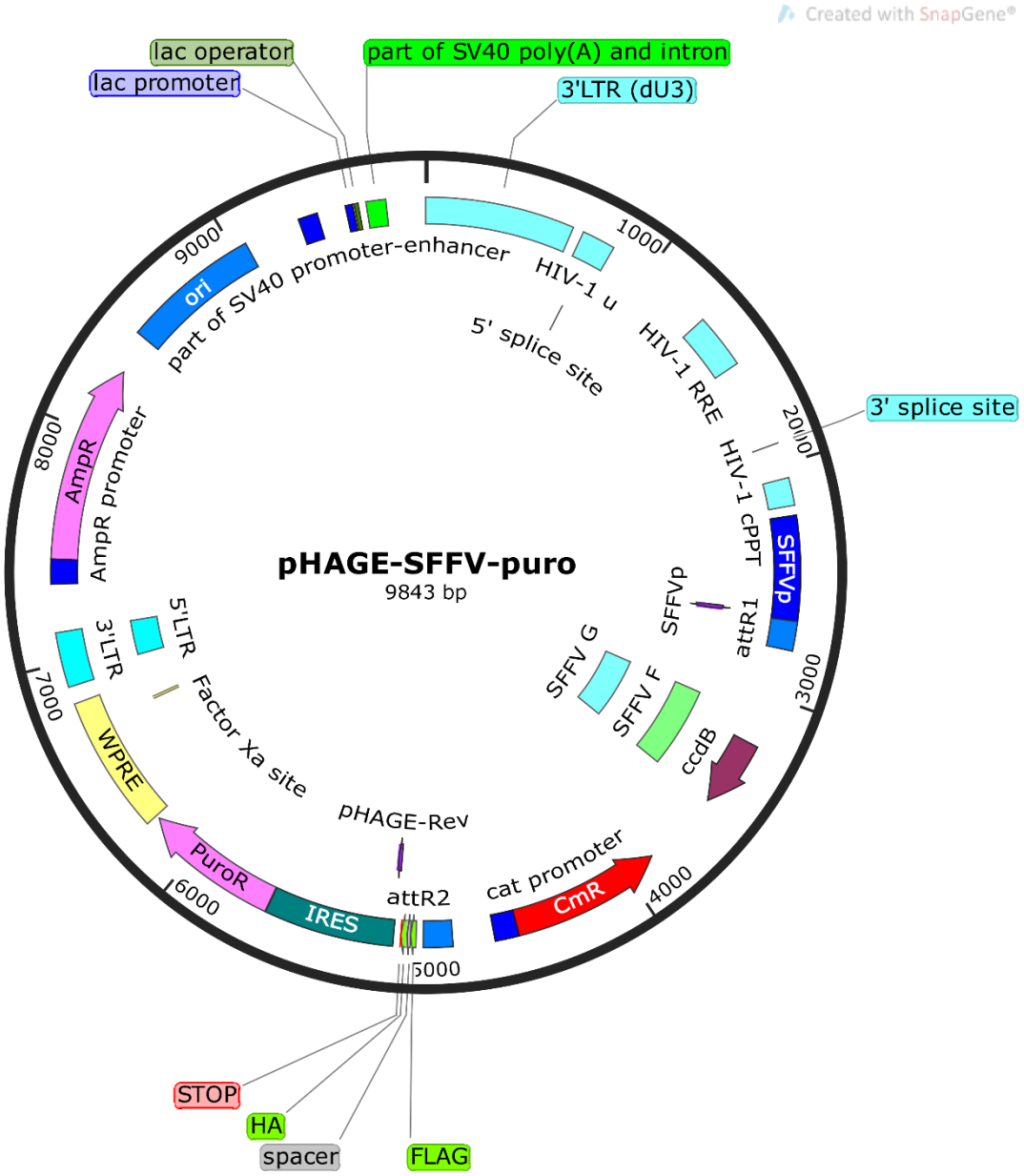

An LR recombination reaction between an entry clone (pDONR encoding the desired DNA sequence) and an *att*R-containing destination vector (e.g. pHAGE) generates an expression clone [268]. The ccdB coding sequence and the CmR are replaced by the sequence to be expressed. Expression of the insert is driven by the SFFV promoter. The coding region contains FLAG and HA sequences at the C-terminal end, unless a stop codon is placed at the 3' end of the insert. AmpR, ampicillin resistance; CAT/CmR, chloramphenicol acetyltransferase resistance; cPPT, central polypurine tract; HA, hemagglutinin; IRES, internal ribosome entry site; lac, lactose; LTR, long terminal repeat; ori, origin; PuroR, puromycin resistance; RRE, Rev response element; SFFVp, spleen focus forming virus promoter; SV40, simian vacuolating virus 40; WPRE, woodchuck hepatitis virus post-transcriptional regulatory element.

Appendix Figure III: pHR-SIREN

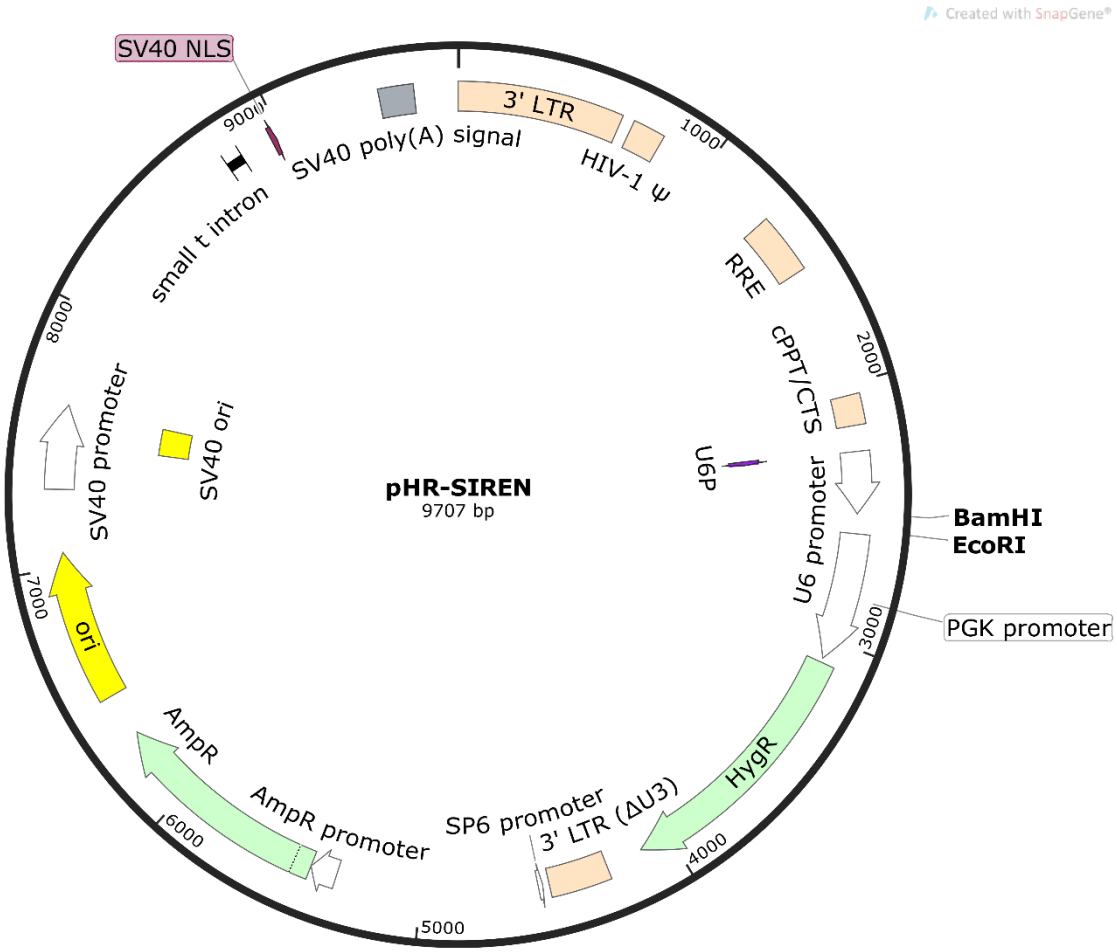

The desired shRNA sequence is inserted into the vector by restriction digestion (using enzymes BamHI and EcoRI) and ligation. AmpR, ampicillin resistance; cPPT, central polypurine tract; HygR, hygromycin resistance; LTR, long terminal repeat; ori, origin; PGK, phosphoglycerate kinase; RRE, Rev response element; SV40, simian vacuolating virus 40.

Appendix III: Solutions

Appendix Table XI: Solutions

200 mM HEPES buffer	8 ml 1 M HEPES stock (Sigma) was diluted with 32 ml HPLC grade water (VWR). pH was adjusted to 8.5 with the necessary amount of 1 M sodium hydroxide (Sigma).
2 × DMEM	2× MEM (Thermo), 20% (v/v) FBS, 0.45% (v/v) sodium bicarbonate (Thermo), 200 U/ml penicillin, 200 µg/ml streptomycin, 4 mM glutamine (Sigma) in sterile water (Sigma).
Digestion buffer for SILAC IP	50 mM Tris-HCl pH 8.5, 10% (v/v) AcN (Sigma), 1 mM DTT (Thermo), 10 µg/ml trypsin (Promega).
DTT	1 M stock solution was made by dissolving 1 g of DTT in 6.5 ml of HPLC grade water. The stock solution was diluted to 100 mM with 200 mM HEPES pH 8.5.
Guanidine lysis buffer	9 ml of 8 M guanidine HCl (Thermo) was diluted with 3 ml 200 mM HEPES pH 8.5 to give a final solution of 6 M guanidine/50 mM HEPES pH 8.5.
Hydroxlamine	50% stock solution (Thermo) was diluted to 5% hydroxylamine in 200 mM HEPES pH 8.5.
Iodoacetamide	Iodoacetamide (Sigma) was dissolved in 200 mM HEPES pH 8.5 to a final concentration of 500 mM.
LysC	2 U of LysC (Wako) was dissolved in 800 µl of HPLC grade water.
MCLB lysis buffer	50 mM Tris-HCl pH 7.5 (Sigma), NaCl (300 mM or 50 mM, as specified in the methods, Sigma), 0.5% v/v NP40 (Sigma), 1 mM DTT and cOmplete EDTA-free Protease Inhibitor Cocktail (Roche) (1 tablet/10 ml).
Protein Loading Dye (6×)	375 mM Tris-HCl pH 6.8, 12% (w/v) SDS (Fisher Chemical), 30% (v/v) glycerol (Fisher Chemical), 0.6 M DTT, 0.06% (w/v) bromophenol blue (Sigma).
RIPA buffer	10× stock (CST) was diluted to 1× with distilled water. The 1× working solution contains 20 mM Tris-HCl (pH 7.5), 150 mM NaCl, 1 mM sodium calcium edetate, 1 mM egtazic acid, 1 % v/v NP-40, 1% v/v sodium deoxycholate, 2.5 mM sodium pyrophosphate, 1 mM β-glycerophosphate, 1 mM sodium orthovanadate, 1 µg/ml leupeptin. One cOmplete EDTA-free Protease Inhibitor Cocktail tablet (Roche) was added to 10 ml of 1× RIPA buffer.
Running buffer for immunoblot	25 mM Trizma® base (Sigma), 192 mM glycine (Fisher Chemical), 0.1% (w/v) SDS (Fisher Chemical) in water.
Transfer buffer for immunoblot	25 mM Trizma® base, 192 mM glycine, 10 or 20% methanol, as indicated, in water.
Trypsin for proteomics	100 µg trypsin (Promega) was dissolved in 3 ml 200 mM HEPES pH 8.5.

(Previous page) AcN, acetonitrile; DMEM, Dulbecco's Modified Eagle's Medium; DTT, dithiothreitol; EDTA, ethylenediaminetetraacetic acid; FBS, fetal bovine serum; HCl, hydrochloride; HEPES, 4-(2-hydroxyethyl)-1-piperazineethanesulfonic acid; HPLC, high-performance liquid chromatography; IP, immunoprecipitation; MCLB, mammalian cell lysis buffer; MEM, Minimum Essential Media; NaCl, sodium chloride; RIPA, radioimmunoprecipitation assay; SDS, sodium dodecyl sulphate; SILAC, stable isotope labelling using amino acids in cell culture

Appendix IV: Virus sequences

Appendix Table XII: Sequences deleted in the US29-34A single-gene-deletion viruses

Whole-genome consensus sequences of passage 1 of each recombinant virus were confirmed using the Illumina platform by Jenna Nichols and Professor Andrew Davison.

Deletion	***Sequence*** *(lowercase: deleted)*	***Confirmed by sequencing?***
ΔUS29	atgcggtgtttccgatggtggctctacagtgggtggtggtggctcacgtttggatgtgctcggaccgtgacggtgggtttcg tcgcgcccacggtccgggcacaatcaaccgtggtccgctctgagccggctccgccgtcggaaacccgacgagacaac aatgacacgtcttacttcagcagcacctctttccattcttccgtgtcccctgccacctcagtggaccgtcaatttcgacggac cacgtacgaccgttgggacggtcgacgttggctgcgtacccgctacgggaacgccagcgcctgcgtgacgggcaccc aatggagcaccaacttttttttctctcagtgtgagcactatcctagtttcgtgaaactcaacggggtgcagcgctggacacct gttcggagacctatgggcgaggttgcctactacgggggttgttgtatggtgggcgggggtaatcgtgcgtacgtgatactc gtgagcggttacgggaccgccagctacggcaacgctttacgcgtggattttgggcgcggcaactgcacggcgccaaaa cgcacctaccctcggcgcttagaactgcacgatggccgcacagaccctagccgttgcgatccctaccaagtgtatttctac ggtctacagtgtcctgagcaactggttatcaccgcccacggcggcgtgggtatgcgccgctgccctaccggctctcgtcc caccccgtcccggccccaccggcatgacttggagaacgagctacatggtctgtgtggtgatcttctggtgtgcgtccttta ttagctctgctgctgttggagctcgttcccatggaagccgtgcgtcacccgctgcttttctggcgacgcgtggcgttatcgc cgtccacttccaaggtggatcgcgccgtcaagctgtgtcttcggcgcatg/TTGGGTCTGCCGCCGCCAC CGTCAGTCGCACCACCTGGGGAAAAGAAGGAGCTACCGGCTCAGGCGGC CTTGTCGCCGCCACTGACCACCTGGTCACTACCGCCGTTTCCGTCCACGC GGATACCTGACAGTCCGCCGCCACCGTACCAGCTTCGTCACGCCACGTCA CTAGTGACGGTACCCACGCTGCTGTTATATACGTCATCCGACATCGGTGA CACAGCTTCAGAAACAACGTGTGTGGCGCACGCTACTTATGGGGAACCC CCGGAGCCCGCTCGATCGACGGCTACGGTTCAGGAATGTACCGTTCTTAC CGCCCCGAATTGCGGCATCGTCAACAACGACGGCGCGGTCTCTGAAGGC CAAGACCATGGAGATGCGGTTCACCATAGCCTGGATGTGGTTTCCCAGTG TGCTGCTGATACTGGGGTTGTTGACACCTCCGAGTAA	Yes
ΔUS30	ATGGGGAACCCCCGGAGCCCGCTCGATCGACGGCTACGGTTCAGGAATG TACCGTTCTTACCGCCCCGAATTGCGGCATCGTCAACAACGACGGCGCGG TCTCTGAAGGCCAAGACCATGGAGATGCGGTTCACCATAGCCTGGATGTG GTTTCCCAGTGTGCTGCTGATACTGGGGTTGTTGACACCTCCGAGTAACG GGTGCACCGTCGATGTTGGACGAAACGTATCCATTCGAGAACAGTGCCG CCTTCGAAACGGTGCGACGTTCTCCAAGGGAGACATCGAAGGTAACTTC AGTGGGCCCGTCGTC/gtggagttggactacgaagacatcgatattactggcgaacggcagcgacttcggtt ccatctcagcggactcgggtgtcctacaaaggaaaatataagaaaagacaatgaaagcgacgtcaacggtggaattcgc tgggctctatatatacaaaccggcgacgccaagtacggtattcgtaaccagcatttgagtatacggttaatgtatcctgggg aaaaaaatacacaacagctgttgggttctgatttcagttgcgaacgtcaccggagaccgtccacgccgttgggaaagaac gccgaagtgcctcccgcgacccgcacgtcttctacatacggcgtcctcagcgcttttgtagtgtggatcggatccggcctc aatatcatctggtggaccggcatcgtgcttctggcggcggacgctctcggacttggcgagcgttggctgaggttggcact gtcccaccgggataaacatcacgcatcgagaaccgcggcgctccagtgtcaacgcgacatgttacttcggcaacgtcga cgggctcggcggctgcacgccgtttctgaaggcaaactgcaggaagagaagaaacgacagtctgctctggtctggaac gttgaggcgcgacccttccgtccacacatcagctgattgtgctgccccctcctgtagcgtcagctcctcctgcggttccct cgcagccccccgagtattcgtctgtgtttccgcctgtataa	Yes
ΔUS31	atgtcgctcttggagcgcgaagagagttggcgtcgcgtagtcgactactcgcacaacctgtggtgtacgtgcggtaactg gcaaagccacgttgagattcaggacgaggagcccaactgcgagcagccggagcccgcacactggctagaatacgtgg cggtccagtggcaggcccgggttcgcgattctcacgatcgctggtgtctctgcaacgcctggcgtgatcacgccttgcgc ggccgttggggtacggcgtattcctcgggttcctcggcctcttcctccggtttcgtcgcggagagcaagttcacctggtgg aaacgactgcgccacagtacccggcgctggttgtttcgccgccggcgagctcgatacactccgtctaactgtggggaaa gtagcactagcagcggccagagtagcggtgacgaga/GTAACTGCAGTCTACGCACCCACGGC GTGTACACACGGGGTGAACAACACTAA	Yes

ΔUS32	atggctatgtacacatccgaatccgaacgcgactggcgtcgtgtaatccacgactcgcacggcctgtggtgcgattgcgg cgactggcgagagcacctctattgtgtgtacgacagccatttttcagcgacgacccacgacccgagccgaacggagggc cgccaattggcggcgacagatgcggcggttacaccgtctgtggtgtttttgtcaggactggaagtgtcacgcgttatacgc cgagtgggacggcaaagaatccgacgacgagtcgtcggcgtcttcctcgggcgaagcgccagagcaacaggtccccg cttggaagaccgtgcgagccttctcgcgggcctaccaccaccgcattaaccggggtctgcggggcacgcccccaccgc gcaacttgccgggatacgagcacgcttccgagggctggcggttttgcaatcgacgggaacggcgagaggacgatcttc gcacgcgggctgagccggaccgcgtggtgttccagttagggggagtacctcctcgccgtcaccgggaaacttacgtgta a	Yes
ΔUS33A	atgagcctcaggttccccgagagggcgggttacgagaaactgggataccgcccgcatgccaaacgcgtgtgggtgcat gacccgttgggattgacgcggtttatcatgaggcaactcatgatgtacccgctggtgttgccgttcacttttccgttttacgtg ccgcggtcctag	Yes. 50% of population has a single nucleotide polymorphism at 22393 (L to F in UL17).
ΔUS34	atgaacttagagcaactcatcaacgtccttggtctgctcgtctggattgccgctcgtgctgtcagccgcgttggtccgcatg gctccggactcgtttatcgtgagcttcatgatttctacgggtatctgcagctggaccttctgggaccagtggtggcggggaa tcgctcagtccggacctggagagagcaggcggaccgagccagagggaccttcgttcggcgttcaggccttaatactagc cacatcttacctgtcggcggcctgtctgggggctccggtaccttacccgccggcctgtatcgtcccgaagaagaggtgttc ctcctcttgaaccgctgccatgggccactgtcaacgccgaaaagcgcttgtctggctgag/GTTGGTGTCGCT AATGCCAGTTTTTTATCTCGCTTCAATGTCGGTGATTTTCACGGAGCGTCA TGGGAAAACGGTACCGCTCCCGATGGAGAGCCCGGGGTATGCTGA	Yes
ΔUS34A	ATGCTGA/aattcttcttaaaattacgtaaacgacgtcgtccagtcgttgtgccgcgattcgtacggttcatcgtctacg tcgttttgttcaccgtcgctgtgcaacgcgtgaaacaagagcgtgatgcgcaccttcggcggtatgaagaacgattgcaga aaaaccgtgcacggcgtcggcagagttttccgtga	Yes

Appendix V: Proteomics results

Appendix Table XIII: 48 h degradation screen data

Data for the 52 proteins with a fold downregulation and rescue of >2 and p<0.05 for both ratios at 48 hpi. Downregulation: Mock/HCMV. Rescue: HCMV+MG132/HCMV. Significance B was calculated using Perseus and corrected for multiple hypothesis testing. Medium confidence and high confidence shortlists refer to the early degradation screens performed by Nightingale and colleagues [62].

Gene Symbol	***48h fold downregulation***	***48h fold rescue***	***48h downregulation significance B***	***48h rescue significance B***	***Medium confidence hit in*** [62]***?***	***High confidence hit in*** [62]***?***
MLKL	21.9	30.3	1E-09	1E-12	YES	YES
PCDHGB5	9.1	6.0	5E-05	4E-04	YES	YES
SUGP2	5.4	2.1	6E-05	9E-04	YES	YES
ANAPC1	5.6	2.8	2E-04	3E-03	YES	YES
HLTF	3.3	4.0	3E-03	4E-05	YES	YES
ZBED1	3.7	3.2	8E-03	4E-03	YES	YES
ANAPC5	2.4	2.4	2E-02	2E-03	YES	YES
EFNB2	10.6	2.9	4E-08	2E-06	YES	
CDC42EP3	8.1	2.1	9E-07	1E-03	YES	
LMAN2L	9.1	3.6	1E-05	1E-03	YES	
GJA1	4.1	2.1	5E-04	3E-02	YES	
MBD4	4.3	10.0	3E-03	3E-06	YES	
STAT2	2.9	2.1	7E-03	9E-05	YES	
BCAR1	2.7	2.2	1E-02	4E-04	YES	
LRP12	2.9	4.5	3E-02	1E-04	YES	
ASPN	10.9	3.0	2E-06	4E-02		
GADD45A	13.4	368.0	2E-06	8E-56		
COL2A1	6.5	2.5	1E-05	7E-05		
IER5	7.8	77.3	4E-05	6E-20		
PDCD4	5.0	2.3	1E-04	2E-04		
CRIM1	4.3	2.1	3E-04	8E-03		
TXNIP	4.4	2.8	3E-04	4E-06		
TCP11L2	10.6	11.5	4E-04	4E-03		
CEP112	5.8	3.0	4E-04	2E-02		
CATSPERG	5.2	5.6	8E-04	1E-04		
FAM92A1	5.2	3.2	8E-04	1E-02		
CDC42EP2	5.0	2.8	1E-03	3E-02		
ANKRD1	5.7	105.3	1E-03	1E-22		

INHBA	4.8	3.0	1E-03	4E-02
ID2	4.3	18.4	2E-03	2E-13
HBP1	3.0	13.1	5E-03	1E-14
HLA-A	2.8	2.3	7E-03	4E-06
TWIST2	3.5	3.6	8E-03	6E-03
SERPINE1	2.8	2.8	1E-02	7E-08
TCEAL9	3.2	34.7	1E-02	3E-26
DLC1	3.2	2.4	1E-02	1E-02
KANSL1L	5.2	22.2	1E-02	1E-04
GEM	3.4	5.1	1E-02	3E-04
FOSL1	2.6	2.9	1E-02	1E-04
PLIN2	2.6	5.0	1E-02	4E-09
RND3	2.6	6.5	2E-02	4E-17
HSPB6	2.9	2.0	2E-02	4E-02
MAGEF1	4.2	101.0	3E-02	5E-09
ZMYND11	2.7	2.0	3E-02	4E-02
SYDE1	2.9	2.6	3E-02	2E-02
HLA-A	2.3	2.5	3E-02	2E-06
LRP10	3.8	5.8	4E-02	5E-02
ZFAND2A	2.3	178.0	4E-02	8E-120
DENND5A	2.6	3.5	4E-02	3E-03
ZNF460	2.6	6.1	4E-02	6E-05
PHLDA1	2.6	8.5	5E-02	2E-05
SKA2	2.5	4.0	5E-02	9E-04

Appendix Table XIV: US29-34A single-gene-deletion virus screen

HFFF-TERTs were infected with a control (Ctrl) virus or one of seven single-gene-deletion viruses (ΔUS29, ΔUS30, ΔUS31, ΔUS32, ΔUS33A, ΔUS34 or ΔUS34A) and harvested for whole cell lysate proteomic analysis after 60 h of infection. Data for proteins that were rescued by deletion of any of the genes when their abundance was compared to that in control HCMV-infected cells, with a FC (ΔX/Ctrl) greater than 1.5 and a Z-score greater than 3, are shown.

Viral gene (X)	*Target (Gene symbol)*	*ΔX/Ctrl*	*Z-score*
US29	WDFY2	1.7	13.1
US29	HPS6	2.0	11.3
US29	POLG	2.3	11.1
US29	SLC35B3	1.9	10.6
US29	ALKBH2	2.4	10.0
US29	PBX1	2.1	9.3
US29	PPP4C	1.9	9.2
US29	CAPRIN2	3.9	8.9
US29	POLL	1.7	8.9
US29	KANSL2	1.6	8.9
US29	MPC2	1.6	8.5
US29	SPIN4	1.6	8.0
US29	PCDH1	2.0	8.0
US29	UNC13B	1.6	7.8
US29	GFPT2	2.8	7.5
US29	FXR1	2.1	7.3
US29	EPB41L1	1.6	6.9
US29	MGME1	2.5	6.5
US29	COL5A2	3.2	6.1
US29	SMYD4	1.6	6.0
US29	RBM23	2.0	5.6
US29	GPC4	1.8	3.3
US30	ISG20	1.8	16.4
US30	IFI44	4.4	6.3
US30	HERC5	1.6	4.5
US30	DDX58	1.9	3.5
US31	CD248	1.6	14.3
US31	SPC24	2.0	12.2
US31	PPDPF	1.5	11.1
US31	DHFR	1.9	10.5
US31	PLXNB2	2.1	9.4
US31	SULT1A1	1.6	8.9
US31	UBE2C	2.1	8.9
US31	ANLN	1.5	8.2
US31	TACC3	1.5	7.6

US31	BIRC5	1.6	6.6
US31	BCL2L12	1.5	6.4
US31	NRGN	1.6	6.4
US31	SHCBP1	1.6	6.0
US31	LAMA1	1.6	6.0
US31	CDCA8	1.6	5.8
US31	CYGB	1.7	5.7
US31	SKA1	1.8	5.5
US31	SDC4	1.7	5.4
US31	SKP2	1.9	5.0
US31	KIAA0101	1.6	4.4
US31	SPC25	1.7	4.2
US31	GPC1	1.6	4.2
US31	GTSE1	1.7	3.9
US31	COL7A1	2.1	3.6
US31	APOE	1.7	3.5
US31	RNF4	2.1	3.5
US31	CTSK	1.8	3.4
US31	GNG5	1.5	3.2
US31	CYB5R1	1.6	3.1
US32	GIPC1	1.5	9.1
US32	ELOF1	1.6	8.2
US32	RYBP	1.6	6.0
US32	FABP4	1.5	4.1
US33A	DMXL1	3.7	24.6
US33A	WDR7	1.5	9.2
US34	COL6A3	1.9	5.5
US34	DCN	3.6	3.5
US34	HSDL1	1.6	3.2
US34	SFRP1	1.8	3.0
US34	TGFBI	1.7	3.0
US34A	TRPM7	1.8	17.6
US34A	ITIH4	1.8	11.5
US34A	KMT2B	1.8	8.0
US34A	HGF	2.2	7.2
US34A	SOD2	2.1	7.2
US34A	PLG	2.2	5.8
US34A	IFIT2	2.2	5.8
US34A	PCDHGB7	2.3	5.7
US34A	COMP	1.6	5.6
US34A	CMPK2	1.7	5.1
US34A	OAS3	1.9	5.1
US34A	PLSCR1	1.9	5.1
US34A	IFIT1	2.3	5.0
US34A	TAPBP	1.6	5.0
US34A	CD82	2.0	4.7

US34A	GREM1	2.5	4.6
US34A	ITIH3	1.5	4.6
US34A	HLA-B	1.7	4.4
US34A	RNF220	1.8	4.4
US34A	APOC3	3.5	4.4
US34A	PTGIS	3.5	4.3
US34A	USP18	2.4	4.3
US34A	VTN	1.9	4.2
US34A	TMEM8A	2.9	4.2
US34A	SERPINE2	2.4	4.2
US34A	HLA-A	1.7	4.1
US34A	HLA-F	2.4	4.1
US34A	IFIT3	2.3	4.0
US34A	MX1	2.8	4.0
US34A	NLRX1	1.6	4.0
US34A	PARP9	1.6	3.9
US34A	CNTRL	2.0	3.8
US34A	PLGRKT	1.5	3.7
US34A	HELZ2	1.6	3.5
US34A	CFAP54	2.5	3.5
US34A	OASL	1.8	3.4
US34A	SLC35A1	1.8	3.2
US34A	MT2A	1.7	3.2
US34A	TUBAL3	2.1	3.1

Appendix Table XV: US29-34A gene expression screen

Whole cell lysates of eight HFFF-TERT cell lines each expressing one of the genes in the US29-34A gene block (tagged with V5) or an empty control vector (Ctrl) were analysed by mass spectrometry. Fifty-four proteins were downregulated more than 1.5-fold with Z<-3 by expression of one of the viral genes (X). The data for these proteins is shown below.

Viral gene (X)	*Target (Gene Symbol)*	*Ctrl/X*	*Z-score*
US29	POMGNT1	4.1	5.2
US29	GOLM1	2.2	4.5
US29	NOV	1.7	4.4
US29	C5orf30	1.7	3.8
US29	CHST3	2.1	3.1
US29	CCDC102B	1.5	3.0
US30	ADAMTS2	1.6	7.5
US30	ASS1	2.0	4.1
US30	RGCC	2.5	4.1
US30	PRAF2	1.8	4.0
US30	COL6A1	1.6	3.8
US30	THSD4	1.7	3.8
US30	NID2	1.5	3.5
US30	IGDCC4	1.7	3.5
US30	HNMT	1.6	3.4
US30	FRMD8	1.5	3.1
US30	CRABP2	1.7	3.1
US31	PLXNA1	1.8	7.3
US31	PRPF38B	1.5	5.5
US31	HIST1H1E	1.6	4.1
US31	SOGA1	1.6	3.7
US31	TTYH3	1.6	3.6
US31	GMEB1	1.6	3.3
US31	SLC30A1	1.8	3.3
US31	ILF3	1.7	3.0
US32	FLNB	1.6	6.0
US32	CSRP2	1.5	5.4
US32	UBASH3B	1.5	5.3
US32	GPT2	1.5	4.7
US32	PGM2L1	1.6	4.7
US32	NAT1	1.5	4.3
US32	TRIM22	1.5	4.0
US32	FAP	1.5	3.6
US32	CA13	1.7	3.6
US32	EPHA5	2.0	3.6
US32	TRIM41	1.5	3.6

US32	PSAT1	1.9	3.5
US32	KCNAB2	1.5	3.4
US32	MLPH	1.6	3.4
US32	EFHD1	2.0	3.4
US32	TRAF5	1.5	3.3
US33A	PLAUR	1.5	4.3
US33A	REST	1.7	4.1
US33A	SLC37A4	1.7	3.7
US33A	CSPG4	1.6	3.4
US33A	GLIPR1	2.2	3.3
US33A	OLFML2B	1.8	3.2
US33A	MELK	2.1	3.2
US33A	NFATC3	1.8	3.0
US34	ARMC1	1.7	7.3
US34	DNAJC11	3.0	6.3
US34	FUNDC2	1.8	4.2
US34	CEP89	1.7	3.1
US34	GINS2	1.6	3.1

Appendix Table XVI: Whole cell lysate gene block deletion virus screen

These data were previously published in Nightingale, Lin *et al.* (2018) [62] based on experiments performed by Dr. Katie Nightingale. The raw data were reanalysed specifically for this thesis. Data for proteins that were rescued by deletion of the US29-34A block when their abundance was compared to that in WT2 (ΔUL16/18) HCMV-infected cells, with a fold change (FC) (ΔUS29-34A/WT2) greater than 1.5 or a Z-score greater than 3, are shown.

Gene Symbol	*ΔUS29-34A/WT2*	*Z-score*	*FC>1.5*	*Z>3*	*Hit in single-gene-deletion virus screen?*	*Hit in gene expression screen?*
DMXL1	4.9	39.6	Y	Y	US33A	US33A
PLXNA2	1.8	14.8	Y	Y		
TRIM46	1.6	11.5	Y	Y		
HERC5	2.1	11.2	Y	Y	US30	
TOX2	2.3	10.2	Y	Y		
DUSP11	1.5	8.2	Y	Y		
RYBP	1.5	8.0	Y	Y	US32	
PLXNA1	1.7	7.9	Y	Y		US31-V5
CARD6	2.8	7.6	Y	Y		
PLXNB2	1.9	6.7	Y	Y	US31	
THAP11	1.6	6.1	Y	Y		
RNF216	2.1	5.3	Y	Y		
ARL6IP6	1.6	5.0	Y	Y		
DDX60	1.8	4.6	Y	Y		
MIER3	1.7	4.2	Y	Y		
POMGNT1	1.7	3.4	Y	Y		US29-V5
PLAUR	1.6	3.2	Y	Y		US33A-V5
LRP6	2.1	3.2	Y	Y		
TRPM3	4.5	2.9	Y			
CHST3	2.9	2.9	Y			
ISG15	1.7	2.8	Y			
TADA2B	2.1	2.6	Y			
PEX16	1.5	2.5	Y			
OASL	1.7	2.2	Y			
CD14	1.6	2.0	Y			
CD82	1.5	1.4	Y			
POLH	1.7	1.2	Y			
SLC22A4	1.5	1.0	Y			
FAM185A	3.9	1.0	Y			
APOH	1.6	1.0	Y			
GSG2	1.5	0.8	Y			
FAM168B	1.6	0.8	Y			
GOLM1	1.5	0.3	Y			
TMEM200B	1.6	0.1	Y			
TMEM173	1.6	-0.1	Y			

RAD51	1.6	-0.1	Y	
SP140L	1.5	-0.2	Y	
ZNF503	2.6	-0.3	Y	
WBSCR22	1.4	8.6		Y
WDR7	1.5	8.1		Y
CDC42EP1	1.5	6.5		Y
MTF2	1.4	5.3		Y
ERI1	1.2	4.9		Y
FRG1	1.3	4.9		Y
ESRRA	1.1	4.7		Y
CSNK1E	1.2	4.5		Y
ETFRF1	1.4	4.0		Y
SNX11	1.2	3.9		Y
SHB	1.2	3.9		Y
SFXN2	1.2	3.8		Y
AKAP13	1.1	3.8		Y
TICAM1	1.1	3.8		Y
CCDC85B	1.2	3.8		Y
FAM83H	1.1	3.7		Y
NPAT	1.2	3.7		Y
ST7	1.2	3.7		Y
GIPC1	1.3	3.7		Y
COBLL1	1.2	3.6		Y
MYO5A	1.1	3.6		Y
ZNF444	1.3	3.5		Y
FAR2	1.3	3.5		Y
LPXN	1.0	3.4		Y
RPGRIP1L	1.3	3.4		Y
MTFR2	1.3	3.4		Y
PNMAL1	1.3	3.4		Y
DAZAP1	1.1	3.4		Y
SECISBP2	1.2	3.4		Y
PAXBP1	1.2	3.3		Y
ANKRD13C	1.1	3.3		Y
PARP12	1.1	3.3		Y
SLC12A2	1.4	3.2		Y
SPRY4	1.4	3.2		Y
TEP1	1.2	3.2		Y
SRP14	1.1	3.2		Y
NOP9	1.2	3.2		Y
STXBP3	1.2	3.1		Y
LETMD1	1.2	3.0		Y
PLXND1	1.4	3.0		Y
SRP9	1.1	3.0		Y

Appendix Table XVII: Plasma membrane gene block deletion virus screen

These data are from an unpublished plasma membrane profiling screen of cells infected with WT1, WT2 or one of nine block deletion viruses, performed by Dr. Ceri Fielding and Dr. Katie Nightingale. The raw data were analysed specifically for this thesis. Data for proteins that were rescued by deletion of the US29-34A block when their abundance was compared to that in WT2 HCMV-infected cells, with a fold change (FC) (ΔUS29-34A/WT2) greater than 1.5 or a Z-score greater than 3, are shown.

Gene Symbol	*ΔUS29-34A/WT2*	*Z-score*	*FC>1.5*	*Z>3*	*Hit in single-gene-deletion virus screen?*	*Hit in gene expression screen?*
PLXNA1	3.6	45.5	Y	Y		US31-V5
PLXNB2	3.3	21.9	Y	Y		
PLXNA2	5.0	18.6	Y	Y		
CEACAM1	4.0	8.5	Y	Y		
PLXNB1	2.3	7.3	Y	Y	US31	
PLXND1	2.1	6.9	Y	Y		
ORAI1	1.6	3.0	Y			
HLA-DRB1	1.5	2.3	Y			
PRNP	1.8	2.2	Y			
LRP8	1.8	1.9	Y			
VTN	2.0	1.7	Y			
RTN4RL2	1.6	1.6	Y			
ABCC3	1.7	1.4	Y			
HLA-DRA	1.6	1.4	Y			
NECTIN3	1.8	1.3	Y			
CD46	1.6	1.2	Y			
MYO19	1.8	1.1	Y			
FLT4	1.5	1.0	Y			
HBG1	1.7	1.0	Y			
SLC22A4	1.6	1.0	Y			
RALB	1.7	0.9	Y			
NUCB2	1.5	0.9	Y			
ATP6AP1	1.6	0.9	Y			
S1PR1	1.6	0.8	Y			
SON	1.6	0.6	Y			
EMP3	1.6	0.5	Y			
ITGB2	1.5	0.4	Y			
ITGAM	1.5	0.2	Y			
PLXNA3	1.8	0.1	Y			
PANX1	1.5	-0.1	Y			
HLA-B	1.5	-0.1	Y			
IFIT2	10.1	-0.1	Y			
FN1	2.0	-0.1	Y			
QSOX2	1.7	-0.1	Y			

SLC12A2	1.4	4.8	Y
GNA13	1.2	3.3	Y
ENPP1	1.3	3.3	Y
SLC4A2	1.3	3.3	Y
MME	1.2	3.2	Y
CNNM3	1.2	3.2	Y
PTGFRN	1.3	3.1	Y